CUKUROVA UNIVERSITY
INSTITUTE OF NATURAL AND APPLIED SCIENCES

PhD THESIS

A Comparative Analysis of Energy and Exergy Performance of Different PVT Collector Configurations

Umutcan OLMUŞ

Department of Mechanical Engineering

December, 2025

CUKUROVA UNIVERSITY
INSTITUTE OF NATURAL AND APPLIED SCIENCES

PhD THESIS APPROVAL

A Comparative Analysis of Energy and Exergy Performance of Different PVT Collector Configurations

Umutcan OLMUŞ

Department of Mechanical Engineering

This Doctorate Thesis was evaluated by the following Jury Members on 22/12/2025 and was approved by unanimity.

Jury : Prof. Dr. Orhan BÜYÜKALACA (Advisor) …………

: Prof. Dr. Ertaç HÜRDOĞAN …………

: Prof. Dr. Arif ÖZBEK …………

: Assoc. Prof. Dr. Göktürk Memduh ÖZKAN …………

: Asst. Prof. Dr. Kamil Neyfel ÇERÇİ …………

This Thesis was written in the Department of Mechanical Engineering, Institute of Natural and Applied Sciences.

Thesis Number:

Prof. Dr. Sadık DİNÇER
Director
Institute of Natural and Applied Sciences

This work was supported by the Scientific Research Project Unit of Çukurova University.
Project ID: FDK-2023-15516

CONTENTS

CUKUROVA UNIVERSITY
INSTITUTE OF NATURAL AND APPLIED SCIENCES

PhD THESIS

A Comparative Analysis of Energy and Exergy Performance of Different PVT Collector Configurations

Umutcan OLMUŞ

Advisor: Prof. Dr. Orhan BÜYÜKALACA

Department of Mechanical Engineering

ABSTRACT

Photovoltaic thermal (PVT) collectors have emerged as promising hybrid systems capable of simultaneously generating both electrical and thermal energy from solar radiation. Compared to standalone photovoltaic panels or thermal collectors, PVT systems offer higher energy efficiency per unit area and improved cost-effectiveness, while also reducing PV cell temperature-related efficiency losses. However, the performance of PVT collectors is highly sensitive to a range of design and operational parameters, including absorber geometry, flow configurations, and inlet-outlet arrangements. This study presents a comprehensive numerical investigation of 47 different PVT collector configurations derived from 26 absorber designs, categorized into three main groups: parallel, serpentine and spiral tube geometries. All configurations were modeled in 3-D using COMSOL Multiphysics software based on the finite element method, under steady-state, laminar, and incompressible flow assumptions, and a total of 1615 simulations were performed, each requiring approximately two hours of computational time on the workstation. Each design was standardized to ensure equal absorber surface areas and tube lengths, enabling fair comparison across all configurations. A detailed performance analysis was conducted using a combination of energy and exergy-based metrics such as thermal and electrical power output, overall and primary energy saving efficiency, pressure drop, thermal energy per unit pressure drop (TEPD), and exergy efficiency. Additionally, the effects of key operating parameters including fluid flow rate, solar irradiance, fluid inlet temperature, ambient temperature, and wind velocity were systematically examined. Among all configurations, the highest thermal energy output was achieved by the parallel tube design coded as Config E (949.83 W), while the serpentine tube Config R1 delivered the highest electrical output (255.95 W) and exergetic performance. Config E demonstrated the highest overall (0.7564) and primary energy saving efficiency (0.9941), while parallel tube Config F achieved the top TEPD value of 74.91 W/Pa at 5 L/h flow rate. Config R1 recorded the maximum exergy efficiency with 0.1498, followed by serpentine tube Config H at 0.1496 and Config E at 0.1494.

Keywords: Solar energy, Photovoltaic thermal collector, Collector design, Numerical simulation, Finite element method

ÇUKUROVA ÜNİVERSİTESİ
FEN BİLİMLERİ ENSTİTÜSÜ

DOKTORA TEZİ

Farklı PVT Kollektör Konfigürasyonlarının Enerji ve Ekserji Performansının Karşılaştırmalı Analizi

Umutcan OLMUŞ

Danışman: Prof. Dr. Orhan BÜYÜKALACA

Makine Mühendisliği Anabilim Dalı

ÖZ

Fotovoltaik termal (PVT) kolektörler, güneş ışınımından aynı anda hem elektrik hem de ısıl enerji üretebilen hibrit sistemler olarak öne çıkmaktadır. Geleneksel fotovoltaik paneller veya termal kolektörlerle karşılaştırıldığında, PVT sistemleri birim alan başına daha yüksek enerji verimi ve maliyet etkinliği sunmakta, aynı zamanda fotovoltaik (PV) hücre sıcaklığına bağlı verim kayıplarını da azaltmaktadır. Ancak, PVT kolektörlerin performansı, yutucu geometrisi, akış konfigürasyonları ve giriş-çıkış düzenlemeleri gibi birçok tasarım ve işletme parametresine yüksek derecede duyarlıdır. Bu çalışmada, paralel, serpantin ve spiral boru geometrileri olmak üzere üç ana grupta sınıflandırılan 26 yutucu tasarımından türetilen toplam 47 farklı PVT kolektör konfigürasyonunun kapsamlı bir sayısal incelemesi sunulmuştur. Tüm konfigürasyonlar, kararlı, laminer ve sıkıştırılamaz akış varsayımları altında, sonlu elemanlar yöntemine dayalı COMSOL Multiphysics yazılımı kullanılarak üç boyutlu olarak modellenmiş; bu kapsamda toplam 1615 adet analiz gerçekleştirilmiş ve her bir analiz iş istasyonunda yaklaşık iki saat sürmüştür. Her bir tasarım, eşit yutucu yüzey alanı ve boru uzunluğuna sahip olacak şekilde standartlaştırılmış, böylece konfigürasyonlar arası adil karşılaştırma sağlanmıştır. Performans değerlendirmesi; ısıl enerji ve elektrik üretimi, toplam ve birincil enerji tasarrufu verimi, basınç kaybı, birim basınç başına ısıl enerji üretimi (TEPD) ve ekserji verimliliği gibi enerji ve ekserji tabanlı ölçütler üzerinden gerçekleştirilmiştir. Ayrıca, akışkan debisi, güneş ışınımı, akışkan giriş sıcaklığı, ortam sıcaklığı ve rüzgâr hızı gibi temel işletme parametrelerinin etkileri sistematik olarak incelenmiştir. Tüm konfigürasyonlar arasında, en yüksek ısıl enerji üretimi paralel borulu Config E (949.83 W), en yüksek elektriksel güç ve ekserji performansı ise serpantin borulu Config R1 tarafından elde edilmiştir. Config E, en yüksek genel (0.7564) ve birincil enerji tasarrufu verimi (0.9941) değerlerine ulaşırken, paralel borulu Config F, 5 L/saat debide 74.91 W/Pa ile en yüksek TEPD değerini elde etmiştir. Ekserji verimliliğinde ise en yüksek değer 0.1498 ile Config R1'de gözlemlenmiş, onu serpantin borulu Config H (0.1496) ve Config E (0.1494) takip etmiştir.

Anahtar Kelimeler: Güneş enerjisi, Fotovoltaik termal kollektör, Kolektör tasarımı, Sayısal simülasyon, Sonlu elemanlar yöntemi

GENİŞLETİLMİŞ ÖZET

Enerji, modern toplumların gelişmişlik düzeyini belirleyen en temel unsurlardan biri olarak kabul edilmektedir. Artan dünya nüfusu, sanayileşme sürecinin hızlanması ve teknolojik ilerlemeler, küresel enerji talebinin her geçen yıl daha da artmasına neden olmaktadır. Mevcut durumda bu talebin büyük bir bölümü fosil yakıtlar aracılığıyla karşılanmakta; ancak kömür, petrol ve doğalgaz gibi kaynakların sınırlı rezervlere sahip olması, bu kaynakların uzun vadede sürdürülebilir olmadığını göstermektedir. Ayrıca fosil yakıtların kullanımıyla birlikte ortaya çıkan sera gazı emisyonları, iklim değişikliği ve çevresel bozulma gibi küresel sorunları da beraberinde getirmektedir. Bu nedenle, enerji üretiminde çevre dostu, yenilenebilir ve sürdürülebilir alternatiflerin geliştirilmesi kritik bir ihtiyaç haline gelmiştir.

Bu bağlamda, yenilenebilir enerji kaynakları arasında yer alan güneş enerjisi, sürdürülebilirliği, çevreye zararsız oluşu, erişilebilirliği ve tükenmez yapısı sayesinde ön plana çıkmaktadır. Güneş enerjisi sistemleri temel olarak iki ana kategoride değerlendirilmektedir: elektrik enerjisi üretimi için kullanılan fotovoltaik (PV) paneller ve ısıl enerji elde etmeye yönelik geliştirilen termal güneş kolektörleri. Ancak bu iki sistemin ayrı ayrı kullanılması hem alan ihtiyacını artırmakta hem de kurulum maliyetlerini yükseltmektedir.

Son yıllarda geliştirilen fotovoltaik termal (PVT) kolektörler, aynı anda hem elektrik hem de ısıl enerji üretimi yapabilmeleri sayesinde bu dezavantajları ortadan kaldırmakta ve birim alandan elde edilen toplam enerji verimini artırmaktadır. Bu sistemler, yalnızca enerji üretimini optimize etmekle kalmayıp, aynı zamanda PV hücrelerin aşırı ısınmasına bağlı verim kayıplarını da azaltarak sistem ömrünü uzatmaktadır. Tüm bu özellikleriyle PVT kolektörler, sürdürülebilir enerji çözümleri içerisinde giderek daha fazla önem kazanmaktadır.

Fotovoltaik termal kolektörler, güneş enerjisini hem elektrik hem de ısıl enerjiye dönüştürebilen hibrit sistemlerdir. Bu sistemler, klasik fotovoltaik panellerde sıkça karşılaşılan verim kaybı problemini, bütünleşmiş bir ısı değişim mekanizması sayesinde aşarak hücre sıcaklıklarını düşürmekte ve böylece elektrik üretim verimini artırmaktadır. Ayrıca aynı sistemde ısıl enerji de üretilebilmesi, toplam enerji verimliliğini ciddi oranda yükseltmekte ve sistemin çok amaçlı kullanılabilirliğini desteklemektedir.

Ancak PVT kolektörlerin performansı, yalnızca yapısal bütünlüklerine değil, aynı zamanda tasarım ve işletme parametrelerine de son derece duyarlıdır. Yutucu geometrisi, akışkan giriş-çıkış konfigürasyonları, boru yerleşimi, akışkan tipi, akış yönü gibi birçok faktör, sistemin hem elektrik hem de ısıl enerji çıktıları üzerinde doğrudan etkilidir. Bu nedenle, literatürde yapılan çalışmaların çoğu tek bir konfigürasyonun analizine odaklanmış, çok sayıda konfigürasyonun sistematik ve eşit koşullarda karşılaştırıldığı kapsamlı analizlere ise nadiren rastlanmıştır. Ayrıca boru yerleşimi yönünden dikey ve yatay düzenlemelerin karşılaştırılması, çift ya da çoklu girişli yapıların etkilerinin değerlendirilmesi gibi önemli konular ya eksik bırakılmış ya da yalnızca sınırlı parametreler göz önüne alınarak incelenmiştir.

Bu tez çalışması, literatürdeki bu eksiklikleri gidermek ve PVT sistem tasarımı konusunda detaylı ve kapsamlı bir referans sunmak amacıyla hazırlanmıştır. Çalışmada, aynı geometrik yüzey alanına ve eşit boru uzunluklarına sahip toplam yirmi altı farklı absorber tasarımı geliştirilmiş ve bu tasarımlardan kırk yedi farklı akış konfigürasyonu elde edilmiştir. Tasarımlar paralel, serpantin ve spiral boru yapıları olmak üzere üç ana kategoride sınıflandırılmıştır. Her bir konfigürasyon, COMSOL Multiphysics yazılımı kullanılarak üç boyutlu sayısal modellerle analiz edilmiş ve sonlu elemanlar yöntemi yardımıyla simülasyonlar gerçekleştirilmiştir. Bu kapsamda toplam 1615 adet analiz yürütülmüş olup her bir simülasyon 40 çekirdek işlemcili bir iş istasyonunda yaklaşık iki saat sürmüştür.

Bu kapsamda yalnızca enerji performans parametreleri değil; aynı zamanda ekserji verimi, basınç kayıpları, TEPD (birim basınç düşüşü başına termal enerji üretimi), yüzey ve yutucu sıcaklığı dağılımları gibi parametreler de analiz edilmiştir. Ayrıca sistemin farklı çalışma koşullarındaki (akışkan debisi, güneş ışınımı, ortam sıcaklığı, rüzgâr hızı, akışkan giriş sıcaklığı) tepkileri de kapsamlı şekilde incelenmiştir. Böylece yalnızca ideal değil, gerçek saha koşullarında da sistem performansını değerlendiren çok boyutlu bir analiz gerçekleştirilmiştir.

Bu tez çalışmasında, farklı geometrik yapılara sahip fotovoltaik termal kolektörlerin enerji ve ekserji performansları detaylı bir şekilde karşılaştırmalı olarak incelenmiştir. Çalışmada kullanılan tüm konfigürasyonlar, aynı kolektör yüzey alanına ve eşit boru uzunluklarına sahip olacak şekilde tasarlanmış, böylece her tasarımın performansı eşit geometrik koşullar altında değerlendirilmiştir. Bu yaklaşım, adil ve karşılaştırılabilir bir analiz yapılmasını mümkün kılmıştır.

Modellenen sistemlerde kararlı durum, sıkıştırılamaz akış ve laminer rejim varsayımları geçerli kabul edilmiştir. PVT kolektörün katmanları tüm konfigürasyonlarda sabit tutulmuş ve sırasıyla cam yüzey, EVA katmanları, PV hücresi, tedlar tabakası, absorber plaka ve bu plakalara bağlı akışkan borularından oluşmuştur. Tüm katmanların termo-fiziksel özellikleri sabit kabul edilmiştir. Soğutucu akışkan olarak su kullanılmıştır.

Paralel borulu konfigürasyonlar (A-F) arasında, boruların dikey ya da yatay şekilde yerleştirildiği, tekli, ikili ya da çoklu giriş-çıkış yapıları içeren toplam on farklı akış modeli incelenmiştir. A ve B yapılandırmaları literatürde sıkça kullanılan klasik tasarımlar olup, tek giriş ve çıkışa sahiptir. C ve D grupları, çift girişli yapılardan oluşmakta, E ve F konfigürasyonları ise çok girişli olup kolektör içerisinde herhangi bir iç bağlantı noktasına sahip değildir. Bu sayede, akışın daha geniş bir alana yayılması sağlanarak daha homojen bir sıcaklık dağılımı hedeflenmiştir.

Serpantin borulu konfigürasyonlar (G-S), tek, çift ve üç girişli sistemlerden oluşmakta olup boru dizilimlerinin yatay ve dikey yerleşimlerine göre farklı gruplara ayrılmıştır. G ve H yapıları tek girişli klasik modellerdir. I, J, M, O ve P yapılandırmaları çift girişli olup dikey boru dizilimine sahiptir; K, L, N ve R yapılandırmaları ise boruların yatay olarak yerleştirdiği çift girişlidir. Q ve S ise üç girişli tasarımlardır. Bu konfigürasyonlar arasında, giriş noktalarının konumu, akış yönü ve iç boru düzeni gibi değişkenler detaylı şekilde analiz edilmiştir. Spiral borulu konfigürasyonlar (T-Z), helisel yapı sayısına, giriş tipi (tek veya çift), akış yönü ve giriş konumuna göre sınıflandırılmış toplam on iki farklı akış modelini içermektedir. T, U, V ve W konfigürasyonları tek girişli sistemlerdir; bunlar arasında helisel yapı sayısı ve iç düzen farklılık göstermektedir. V konfigürasyonunda dört helisel yapı varken T ve W modellerinde tek helis yer almaktadır. X, Y ve Z konfigürasyonları ise sırasıyla T, U ve V konfigürasyonlarının çift girişli versiyonlarıdır. Bu çift girişli sistemlerde de giriş yönü ve akış karakteristikleri farklılaştırılmıştır.

Tüm bu yapılandırmalar, yalnızca enerji verimi (ısıl enerji ve elektrik üretimi) açısından değil, aynı zamanda ekserji performansı açısından da değerlendirilmiştir. Her bir yapı için hücre sıcaklığı dağılımı, çıkış sıcaklığı, ısıl ve elektrik güç çıktısı, toplam enerji verimi, birincil enerji tasarruf oranı, basınç düşüşü, birim basınç başına termal enerji üretimi, termal ve elektriksel ekserji üretimi, ekserji verimi ve ekserji kayıpları hesaplanmıştır. Ek olarak, her konfigürasyon, farklı işletme koşullarında da incelenmiş; giriş suyu sıcaklığı (10-40 °C), akışkan debisi (5-50 L/saat), güneş ışınımı (200-1200 W/m^2), ortam sıcaklığı (15-40 °C) ve rüzgâr hızı (1-5 m/s) gibi parametrelerin sistem performansına etkisi ayrı ayrı analiz edilmiştir. Bu detaylı parametre analizinin bir arada bulunduğu, literatürde sınırlı sayıda çalışmada bulunmaktadır. Çalışma kapsamında paralel, serpantin ve spiral konfigürasyonlar her bir bölümde ayrıntılı olarak incelenmiştir. Daha sonra paralel, serpantin ve spiral konfigürasyonlar içinden en iyi üçer konfigürasyon detaylı olarak karşılaştırılmıştır. Son olarak her tasarım grubu içerisinden en iyi üç konfigürasyon olmak üzere toplamda dokuz konfigürasyon, aynı boyutlardaki konvansiyonel bir PV panel ile çeşitli performans göstergeleri açısından kıyaslanmıştır. Böylece, geliştirilen PVT konfigürasyonlarının geleneksel PV panele göre avantajları somut şekilde ortaya konulmuştur.

Bu çalışmada incelenen 47 farklı PVT konfigürasyonunun performansları, enerji ve ekserjetik temelli ölçütlerle kapsamlı biçimde değerlendirilmiştir. Paralel borulu tasarım grubunda E, F ve A konfigürasyonları; serpantin borulu tasarım grubunda H, R1 ve Q konfigürasyonları, spiral borulu tasarım grubunda W, X1 ve Z1 konfigürasyonları ön plana çıkmıştır. Paralel tüp konfigürasyonlar arasında temel durum koşullarında en iyi performans, ısıl enerji ve elektrik parametrelerde konfigürasyon E, ekserjetik performans parametrelerinde ise konfigürasyon A tarafından sağlanmıştır. Basınç düşüşü ve TEPD'de ise konfigürasyon F ön plana çıkmaktadır. Çeşitli operasyon parametrelerinin etkisine bakıldığında, en yüksek ısıl enerji üretimi (949.83 W) ve ısıl verim (0.6107) 50 L/saat akışkan debisinde konfigürasyon E'de elde edilmiştir. Elektrik enerjisi üretimi (255.66 W) ise en fazla yine aynı konfigürasyonda, güneş ışınımının maksimum olduğu durumda elde edilmiştir. Aynı zamanda genel verim (0.7564) ve birincil enerji tasarrufu verimi (0.9941) açısından en yüksek değerler akışkan debisinin maksimum olduğu durumda konfigürasyon E'de gözlemlenmiştir. Config F, basınç kaybı ve TEPD değerleri açısından ön plana çıkmıştır. Düşük akış rejiminde (5 L/saat) 74.91 W/Pa değerine ulaşarak, düşük basınç kaybı ve yüksek ısıl enerji üretimi sunmuştur. Ekserji performans parametrelerine bakıldığında güneş ışınımının en fazla olduğu durumda, konfigürasyon E en yüksek ısıl enerji (73.52 W), elektrik (255.66 W) ve toplam çıkış ekserjisini (329.18 W) üretmiştir. En yüksek ekserji verimliliğine ise 10 °C akışkan giriş sıcaklığında (0.1494) konfigürasyon E'de ulaşılmıştır.

Serpantin kolektörler arasında, temel durum koşulları altında en iyi ısıl ve elektrik performansta konfigürasyon R1 ön plan çıkmış, onu konfigürasyon H ve Q takip etmiştir. Serpantin tasarımlarda ısıl enerji üretiminin en yüksek olduğu durum (945 W) ve ısıl verim (0.6079) 50 L/saat debide konfigürasyon H ve R1'de elde edilmiştir. 1200 W/m^2 güneş ışınımında en yüksek elektrik gücü (255.95 W) ve toplam verim (0.7536) konfigürasyon R1'de elde edilmiştir. En yüksek birincil enerji tasarrufu verimi (0.9941) de yine konfigürasyon R1'de görülmüştür. Basınç kaybı ve TEPD değerlerine bakıldığında ise konfigürasyon Q ön plana çıkmaktadır. TEPD parametresi en yüksek değerine 5 L/saat akışkan debisinde 5.55 W/Pa ile konfigürasyon Q'da ulaşmıştır. Ekserji performansı açısından bakıldığında en yüksek ısıl, elektrik, toplam çıkış ekserjisi ve ekserji verimliliği (sırasıyla 73.95 W, 255.95 W, 329.90 W, 0.1498) konfigürasyon R1'de görülmüştür.

Spiral tüp konfigürasyon arasında temel durum koşullarında en iyi performans, ısıl, elektrik ve ekserji performans parametrelerinde konfigürasyon W, X1 ve Z1 ön plana çıkmaktadır. Basınç düşüşünde konfigürasyon X2 en iyi performansı sergilerken, TEPD'de ise konfigürasyon X1 ve X3 ön plana çıkmaktadır. İşletme parametrelerinin performanslara etkisi incelendiğinde, en yüksek ısıl güç (900 W) ve ısıl verim (0.5787), X1 tarafından 50 L/saat debide elde edilmiştir. Elektrik enerjisi üretimi, toplam ve birincil enerji tasarrufu verimleri (sırasıyla 252.69 W, 0.7234 ve 0.9595) en yüksek değerlerine konfigürasyon X1'de ulaşmıştır. TEPD değerine bakıldığında ise, konfigürasyon Z1, düşük akışta (5 L/saat) en yüksek değer olan 3.65 W/Pa'ya ulaşmıştır. Spiral konfigürasyonların ekserji performans parametreleri incelendiğinde konfigürasyon X1, güneş ışınımının1200 W/m^2 olduğu durumda en yüksek ısıl, elektrik ve toplam çıkış ekserjisi (sırasıyla 60.25 W, 252.69 W, 312.94 W) ve en yüksek ekserji verimine (0.1414) sahip olmuştur.

İncelenen 47 konfigürasyon içinde, en yüksek ısıl enerji üretimi paralel tüp konfigürasyon E'de (949.83 W) görülürken, onu serpantin tüp konfigürasyon H ve R1 (945 W) takip etmiştir. Isıl verimde en iyi performansı konfigürasyon E (0.6107) sergilerken, onu konfigürasyon H ve R1 (0.6079) izlemiştir. Elektrik üretimine bakıldığında ise konfigürasyon R1 (255.95 W) ön plana çıkmıştır. Toplam verim parametresi incelendiğinde en yüksek değer konfigürasyon E'de (0.7564) görülmüş, konfigürasyon H ve R1 (0.7536) hemen ardından gelmiştir. Birincil enerji tasarrufu verimi açısından en iyi performansı konfigürasyon E (0.9941) göstermiş, R1 ve H (sırasıyla 0.9915 ve 0.9914) yakın performans göstermiştir. Ekserji performans parametrelerinde en yüksek ısıl ekserji R1'de (73.95 W) bulunmuş, ardından E ve H gelmiştir. Elektrik ve toplam ekserjide konfigürasyon R1 (sırasıyla 255.95 W ve 329.90 W) ön plana çıkmıştır. Ekserji verimliliğine bakıldığında ise en iyi sonuç Config R1 (0.1498), H (0.1496) ve E (0.1494) tarafından elde edilmiştir.

ACKNOWLEDGEMENTS

First and foremost, I would like to express my sincere gratitude to my supervisor Prof. Dr. Orhan BÜYÜKALACA for his invaluable guidance, knowledge, and continuous support throughout my doctoral studies. His constructive feedback, patience, and encouragement have played a crucial role in the successful completion of this thesis.

In addition, I would like to extend my gratitude to my thesis committee members Prof. Dr. Ertaç HÜRDOĞAN and Prof. Dr. Arif ÖZBEK, and to my jury members Assoc. Prof. Dr. Göktürk Memduh ÖZKAN and Assist. Prof. Dr. Kamil Neyfel ÇERÇİ for their insightful comments and valuable contributions.

I would also like to express my heartfelt appreciation to our department head and Vice Rector of Çukurova University, Prof. Dr. Hüseyin AKILLI, whose exemplary leadership, visionary perspective, and sincere support have always been a source of inspiration for me.

I am also deeply grateful to my colleague and invaluable friend Res. Asst. Yunus Emre GÜZELEL for his constant encouragement, collaboration, and motivation during this process. I would like to express my sincere thanks to Assoc. Prof. Dr. Çağrı UZAY and Dr. Durmuş Can ACER for their collaboration, invaluable friendship and continuous support throughout the years.

I am also grateful to the 1.5 Adana Technology Teams family, of which I have been proud to be a part both as a student and later as one of the advisors since my undergraduate years. Being a member of this great family has taught me the true value of teamwork, collaboration, and shared achievement. Moreover, I would like to express my heartfelt thanks to my colleagues Res. Asst. Muhammet Batuhan KÜLTÜR, Res. Asst. Mehmet Burak İBEKCİ and Res. Asst. Hasan ÇELİK, with whom I had the privilege to work shoulder to shoulder during this demanding journey, for their dedication, sincerity, and selfless efforts. I would also like to thank Res. Asst. Alperen Burak GÜRÜK and Res. Asst. İbrahim DİKER for his valuable support. I gratefully acknowledge the financial support provided by the Çukurova University Scientific Research Projects (BAP) Coordination Unit.

I would like to express my deepest gratitude to my wife Sevil, my daughter Feyza, and my family, who have always stood by my side with their endless love, patience, and encouragement. The PhD journey is not only an academic pursuit but also a life experience that requires perseverance, sacrifice, and understanding. During this long and intense process, my family has been my greatest source of motivation and strength. The patience, understanding, and unwavering support of my beloved wife Sevil, together with the joy and inspiration brought by my precious daughter Feyza, have made this journey profoundly meaningful for me. I would also like to extend my sincere thanks to all members of my family for their love, prayers, and constant support. This thesis has been completed thanks to their faith, patience, and affection. Without their support, this success would not have been possible.

LIST OF TABLES

LIST OF FIGURES

SYMBOLS AND ABBREVIATIONS

A_{PVT} : PVT surface area (m^2)

c_p : specific heat at constant pressure (J/kgK)

$\dot{E}$: electrical power (W)

h : convective heat transfer coefficient (W/m^2K)

I : solar radiation (W/m^2)

k : thermal conductivity (W/mK)

$\dot{m}$: mass flow rate (kg/s)

n : surface normal

P : pressure (Pa)

p_c : packing factor

PES : primary energy saving

PV : photovoltaic

PVT : photovoltaic thermal

q : heat flux vector

$\dot{Q}_{th}$: thermal energy rate (W)

T : temperature (K, °C)

TEPD : thermal energy produced per pressure drop (W/Pa)

U : heat transfer coefficient (W/m^2K)

V : velocity (m/s)

$\dot{V}$: volume flow rate (L/h)

$\dot{X}$: exergy rate (W)

Greek Symbols

α : absorptivity

ε : emissivity

σ : Stefan-Boltzmann constant, (W/m^2K^4)

τ : transmissivity

η : efficiency (%)

μ : dynamic viscosity (Ns/m^2)

ρ : density (kg/m^3)

Subscripts

abs : absorbed

amb : ambient

c : cell

con	: convection
el	: electrical
ex	: exergy
f	: fluid
g	: glass
in	: inlet
out	: outlet
ov	: overall
pl	: plate
rad	: radiation
ref	: reference
td	: tedlar
th	: thermal
tu	: tube
w	: water

1. INTRODUCTION

Energy has a crucial role in determining the quality of life and progress of societies. It is predicted that one of the most serious problems that humanity will face in the future is the problem of energy scarcity in the world. Global energy demand has increased significantly and will continue to increase due to population growth, technological advances and rapid industrial development (Olmuş et al., 2025a). Currently, this increasing demand is primarily met by fossil fuels such as coal, oil and natural gas. However, the depletion of these finite resources, combined with their significant contribution to global warming and environmental degradation, has intensified the search for sustainable renewable energy sources and technologies that can replace fossil fuels (Çerçi et al., 2024; Rajamony et al., 2024)

As of today, global energy demand is around 640 x 10^{18} joules. By 2035, this is expected to increase to 680 x 10^{18} joules in the STEPS scenario (which reflects current policies and measures already in place or officially announced by governments), with the increase in energy demand coming from emerging markets and developing economies. Fossil fuels play an important role in meeting energy demand in all three scenarios, with the demand for fossil fuels reaching a peak by 2030. The share of fossil fuels in total energy supply is around 80% in the STEPS scenario starting from 2000, then drops to 75% in 2030 and below 60% in 2050. In the APS scenario (which assumes that all announced national energy and climate pledges are fully achieved on time), the share of fossil fuels drops to approximately 35% in 2050. In the NZE scenario (which outlines a pathway to achieve net zero emissions globally by 2050) fossil fuel use gradually decreases, making up less than 65% of total energy supply by 2030 and about 15% by 2050 (Figure 1.1). Clean energy will grow more than total energy demand between 2023 and 2035 (IEA, 2024a).

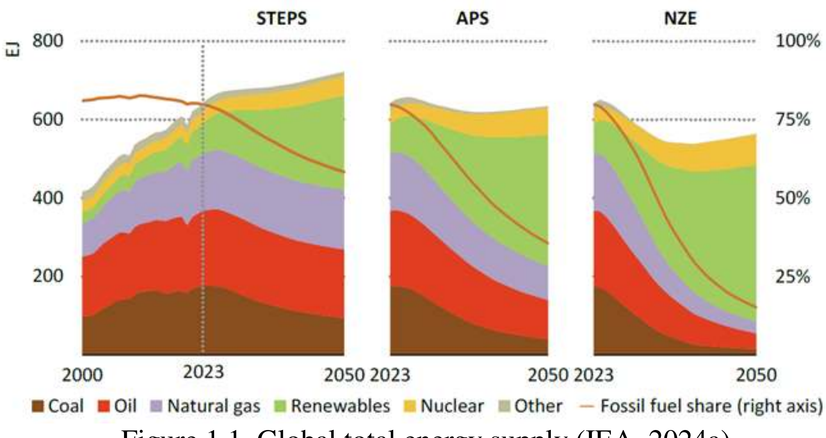

Figure 1.1. Global total energy supply (IEA, 2024a)

Figure 1.2 presents the energy consumption in end-use sectors in 2023 and the expectations for 2030 and 2050. Total energy consumption in end-use sectors increased by 1.7% in 2023 compared to the previous year, reaching 445 x 10^{18} J. When examined on a sectoral basis, the sector with the highest consumption is the industry sector with a consumption of over 170 x 10^{18} J, while consumption in buildings is 125 x 10^{18} J, consumption in transportation is 120 x 10^{18} J, and consumption in agriculture and other sectors is 25 x 10^{18} J. Considering the STEPS scenario, consumption is expected to increase by 1.3% annually over the next ten years, which is in line with the growth rate of total final consumption seen in the last decade. While total final consumption is expected to reach 500 x 10^{18} J by 2035, it is seen that most of this increase is due to the industry sector, especially in developing economies. According to the APS scenario, the increase in energy consumption is expected to increase slightly with efficiency gains and then decrease in 2050. When the NZE scenario is evaluated, improvements in energy efficiency and reductions in energy consumption will occur by 2030 and will decrease significantly by 2050.

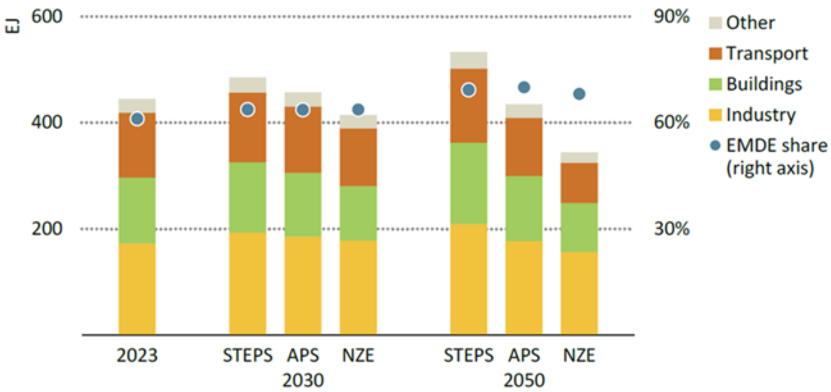

Figure 1.2. Total final consumption by end-use sector, 2023, 2030 and 2050 (IEA, 2024a)

Energy efficiency and increasing electrification rates are the main factors in reducing the share of fossil fuels in final consumption, and this varies by sector. Figure 1.3 shows the energy consumption in the buildings sector by fuel and scenario in 2023, 2030 and 2050. While electricity consumption constituted 31% of total energy demand in 2010, this rate increased to 37% in 2023 in the building sector. Electricity use in the buildings sector is expected to increase further in 2030 and 2050. In the STEPS scenario, the share of electricity in building energy consumption is expected to exceed 40% by 2030 and 50% by 2050, with most of this growth driven by rising demand for cooling and the expansion of data centers, particularly in emerging market and developing economies (IEA, 2024a).

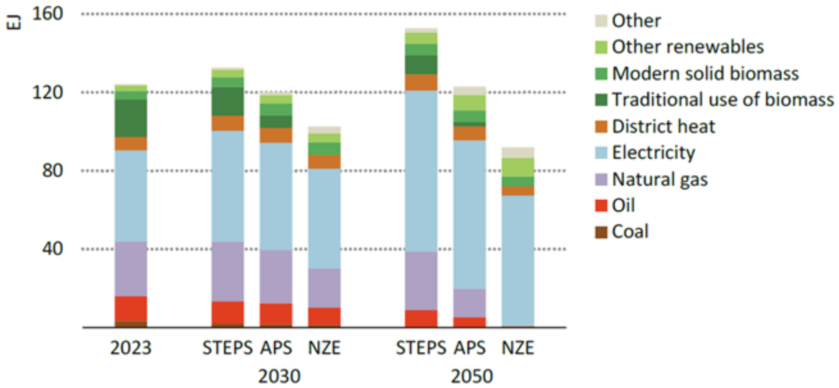

Figure 1.3. Energy consumption in buildings by fuel and scenario, 2023-2050 (IEA, 2024a)

Energy demand and usage in the industrial sector for 2023, 2030 and 2050 are shown in Figure 1.4. According to the STEPS scenario, fossil fuels play an important role in the industrial sector. They are widely used especially in coal, steel and cement production. In addition, while electricity use in industry was at 22% in 2023, it increases to 25% in 2030 according to the STEPS scenario and to 27% in the APS scenario. Technologies that can replace fossil fuels in applications requiring high temperatures in industry have not yet been put into practice. Direct electrification is more suitable for industries that are not energy intensive and this energy can be provided through heat pumps. In addition, there are alternative solutions such as resistance heating, bioenergy and low-emission hydrogen. With the increase in their use, the use of fossil fuels in 2050 in the APS scenario may decrease to 20% (IEA, 2024a).

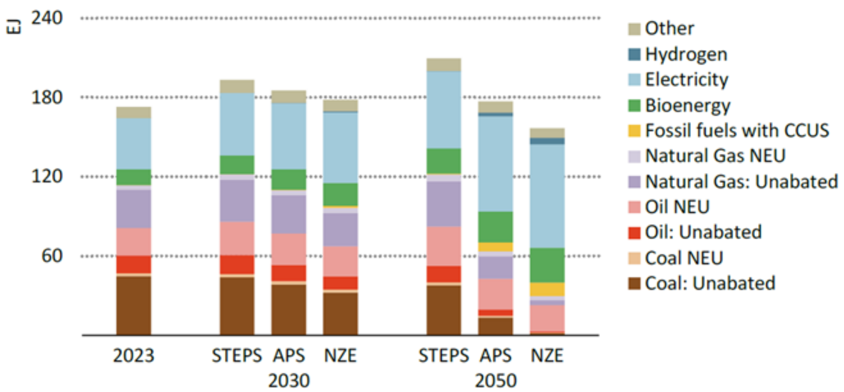

Figure 1.4. Energy demand in industry by fuel and scenario, 2023-2050 (IEA, 2024a)

The electricity sector will account for approximately 36% of global energy-related CO_2 emissions in 2023, making it the world's largest emitter. Electricity demand has increased almost twice as fast as overall energy demand over the past decade and is expected to increase further. While photovoltaic and wind technologies have continued to grow in recent years, coal is still the most important source of electricity generation at 36%, followed by natural gas at 22%. Fossil fuels account for 60% of global electricity supply, the lowest rate in the last 50 years. For the first time, renewable energy sources are responsible for generating 30% of global electricity. As can be seen from Figure 1.5, renewable energy sources, especially solar photovoltaic and wind technologies, will play a very large role in electricity generation by 2050. According to the STEPS scenario, these two clean energy sources will almost triple from 2023 to 2030, leaving coal behind. Coal is expected to peak in 2025 and then decline steadily. By 2035, solar photovoltaic and wind technologies are expected to provide more than 40% of electricity generation. While the general trend in hydroelectricity production is slow growth, nuclear energy is expected to increase steadily. In the APS scenario, wind and photovoltaic technologies will grow faster than in STEPS. In the NZE scenario, the electricity sector will be completely decarbonized by 2040, with the development of carbon capture technologies and low-emission hydrogen, and the use of natural gas will be completely phased out by 80% (IEA, 2024a).

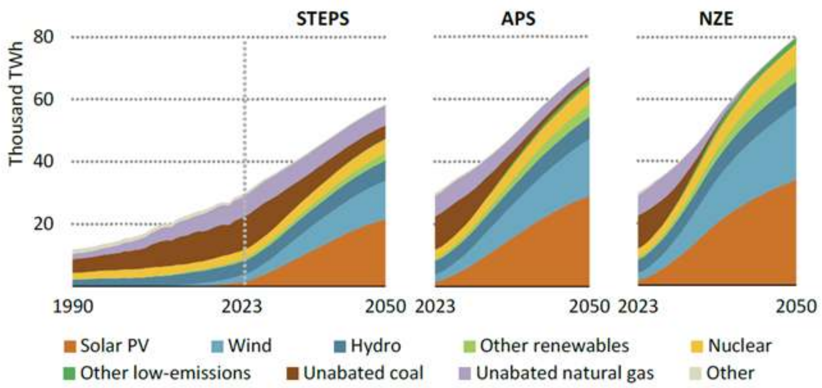

Figure 1.5. Global electricity generation by source and scenario, 1990-2050 (IEA, 2024a)

Electricity generation from renewable energy sources is expected to increase from 666 GW in 2024 to approximately 935 GW in 2030 (Figure 1.6). Photovoltaic and wind technologies are expected to account for 95% of all renewable energy capacity additions by 2030, as their production costs are lower in most countries than both fossil and other alternative sources, and with policy support. Global renewable capacity is expected to exceed 5520 GW between 2024 and 2030, which is 2.6 times higher than in the last six years. While solar photovoltaic technology currently provides approximately 5% of total electricity generation, this is projected to increase to 17% in 2030. By 2035, photovoltaic technology will overtake coal and natural gas to become the main source of electricity (IEA, 2024b).

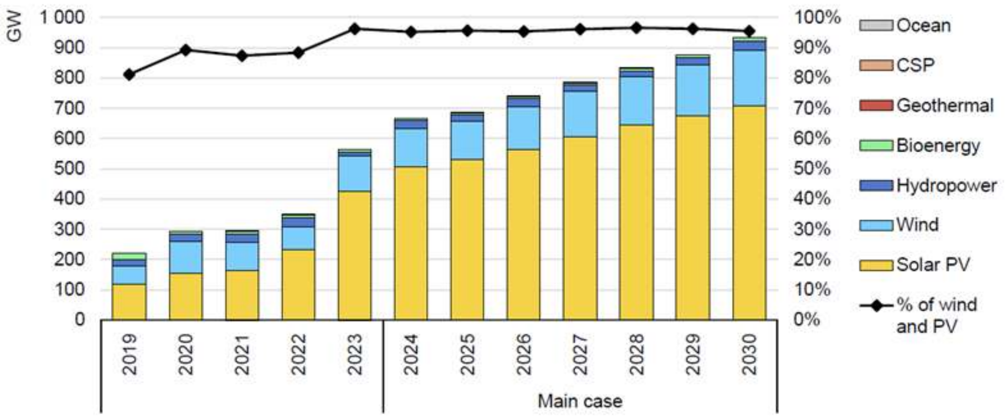

Figure 1.6. Renewable electricity capacity additions, 2019-2030 (IEA, 2024b)

Among these renewable resources, solar energy stands out due to its abundance, pollution-free, inexhaustible, sustainability and accessibility (Ahmadinejad et al., 2022; Olmuş et al., 2025b). Solar energy is used in various applications (Figure 1.7). The two most common applications of solar energy are thermal collectors, which provide thermal energy, and photovoltaic (PV) panels, which convert solar irradiance into electrical energy (Çerçi et al., 2024).

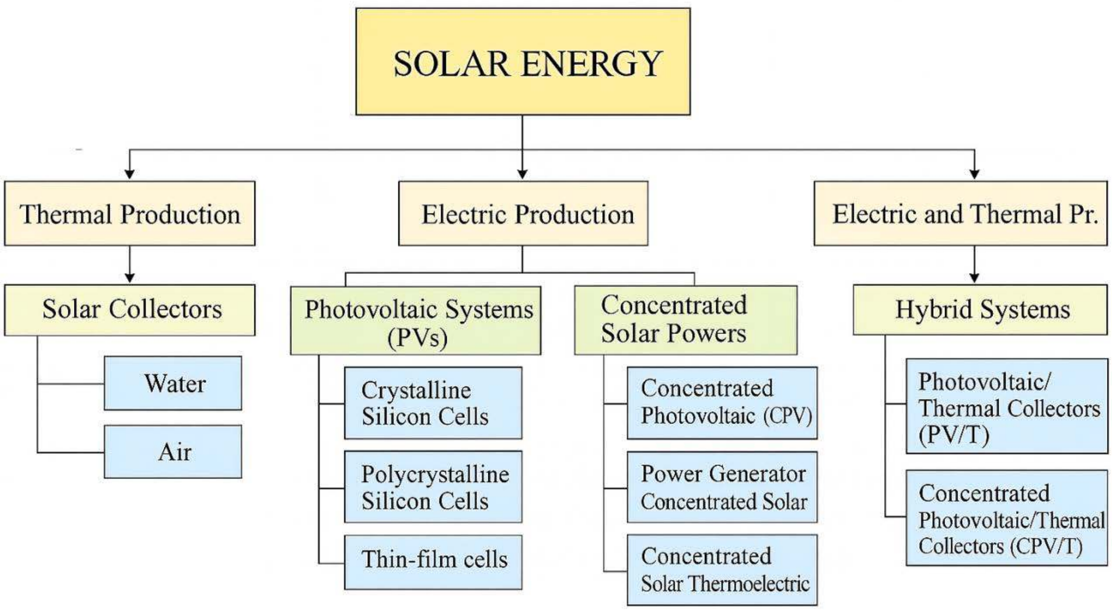

Figure 1.7. Classification of energy production systems from solar energy (Bayrak et al., 2017)

Solar thermal collectors can be utilized across low, medium, and high-temperature applications, with common uses including hot water supply, space heating, and drying processes. Solar collectors used for heating purposes are generally classified based on the working fluid either water or air and by collector type, such as flat-plate and vacuum-tube solar collectors. Flat-plate collectors, which are commonly used, typically consist of a transparent glass cover, an absorber plate where the energy is collected, tubes behind the absorber, and insulation material. Solar radiation passes through the glass surface and is absorbed by the absorber plate, and the collected energy is transferred to the tubes located behind the absorber. Air-based collectors, meanwhile, are generally employed in air conditioning of buildings and drying applications. Since the thermophysical properties of air are not as good as water, air collectors generally exhibit lower efficiencies compared to water-based collectors.

The use of photovoltaic panels, which convert sunlight into electrical energy, is becoming increasingly widespread. Photovoltaic panels consist of numerous solar cells assembled together. These solar cells combine to form modules, and modules then connect to create panels. Solar cells convert sunlight directly into electrical energy, and silicon, a semiconductor material, is commonly used in the production of solar cells. The most widely used cell types are crystalline silicon solar cells and thin-film solar cells. Among these, crystalline silicon panels are the dominant technology in current PV markets. The schematic representation of the crystalline silicon solar cell and thin-film solar cell manufacturing are illustrated in Figure 1.8. Silicon-based PV technology accounts for 90% of photovoltaic panel sales due to their high efficiency and decreasing prices.

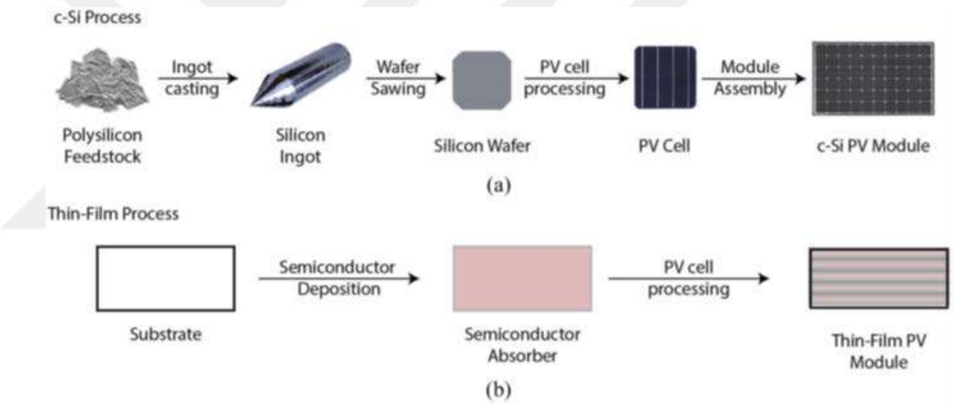

Figure 1.8. Schematic representation of the crystalline silicon and thin-film solar cell manufacturing (Herrando et al., 2023)

PV panels convert approximately 10% to 20% of solar irradiance into electrical energy, while the rest is converted into heat (Zou et al., 2024). However, high levels of solar irradiance can cause temperatures in PV panels to increase, leading to reduced efficiency and potential cell degradation. Specifically, for every 1°C increase in PV cell temperature above 25°C, efficiency can decrease by 0.3% to 0.5% (Shen et al., 2021a). The electrical efficiency of PV panels can be increased by effective cooling strategies. One of the most effective solutions identified is to cool the panels using different methods. By integrating a PV panel with a thermal collector, systems known as photovoltaic-thermal (PVT) collectors have been developed and the temperature of the PV panel has been reduced (Si et al., 2023). This hybrid system not only reduces the PV panel temperature but also produces both electrical and thermal energy from a single system. The thermal energy produced can be used in a variety of applications, making PVT collectors more versatile.

Moreover, PVT collectors provide higher energy efficiency per square meter and lower installation costs compared to using separate PV panels and thermal collectors together (Maseer et al., 2024; Zou et al., 2024). PVT collectors can produce both electrical and thermal energy through a single system (Figure 1.9). This is economical in terms of both the area it covers and the installation cost. In addition, the electrical energy produced in PVT collectors is more than a conventional PV panel. PVT collectors can be classified based on various factors such as collector cover, PV cell type, cooling method, cooling fluid and collector structure (Figure 1.10). Flat plate collectors are the most common design. The working fluid in the collector plays an important role in improving the efficiency of PVT collectors. Air and water are widely used as cooling fluids in PVT collectors. Moreover, in recent years, the effect of nanofluids on PVT collector performance has been intensively investigated.

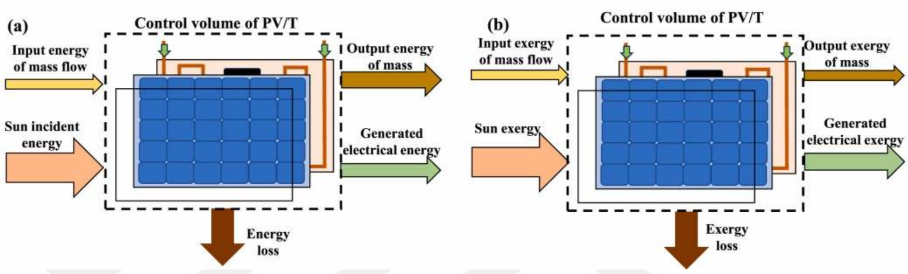

Figure 1.9. Illustration of (a) energetic and (b) exergetic flow analysis (Tyagi and Kumar, 2024)

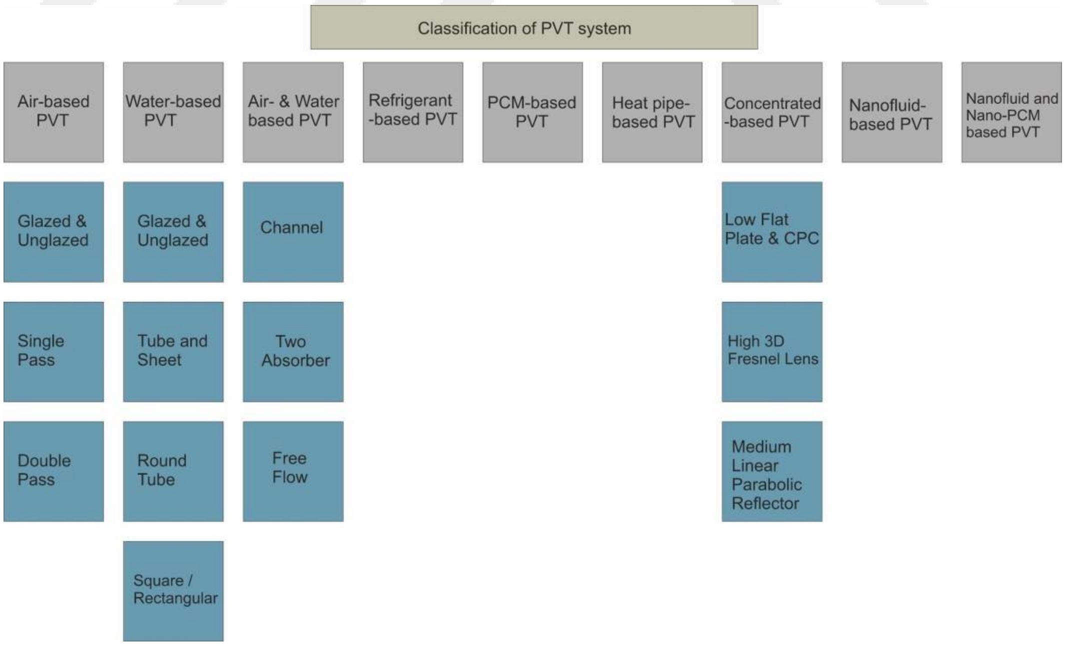

Figure 1.10. Classification of PVT systems (Kazem et al., 2020)

In air-based PVT collectors, the temperature of the PV cell is reduced by airflow, and the heated air can be directed to specific locations via air channels positioned behind the PV panels. Air-based PVT collectors can be classified according to whether the air flow is natural or forced circulation. They can also be categorized according to whether the air channel is above or below the PV cell and according to single or double pass design as shown in Figure 1.11.

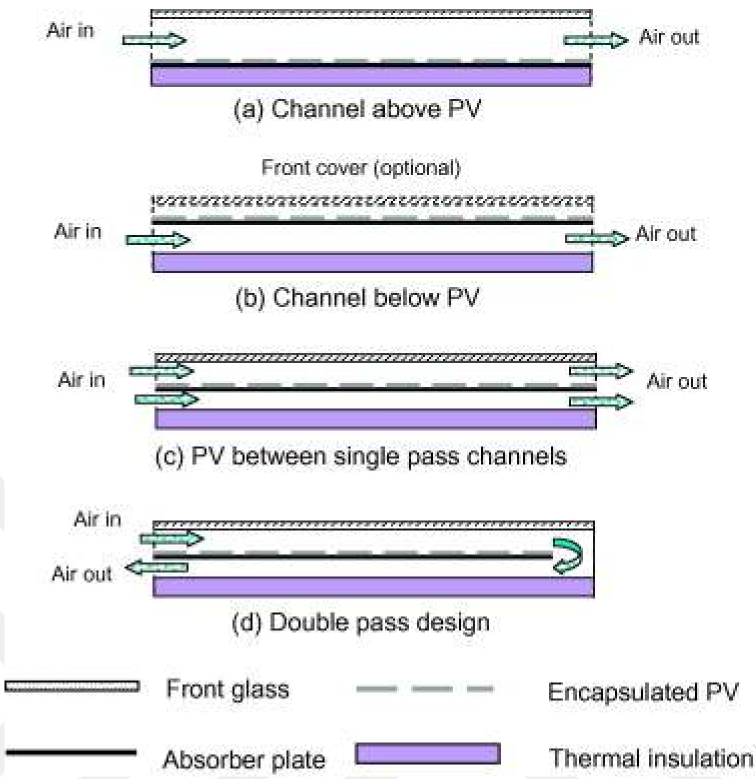

Figure 1.11. Cross section of common air-based PVT collector designs (Chow, 2010)

In water-based PVT collectors, tubes or channels are placed just below the absorber located under the PV panel through which the water will pass. Thus, while the water passing through the tube or channel cools the PV panel, the hot water coming out can be utilized for hot water requirements. A primary challenge with water-based PVT collectors is the risk of freezing in cold climates, which limits their usage in such regions. The most common water-based PVT collector designs are illustrated in Figure 1.12.

When comparing air and water-based PVT collectors, although the operating and maintenance costs of air-based PVT collectors are low, the efficiency of water-based PVT collectors is higher since the thermophysical properties of water are better than those of air.

PVT collectors can be produced with or without glass. The main reason for using glass in PVT collectors is to increase their thermal efficiency by reducing thermal losses. On the other hand, since this also reduces losses, it causes the temperature of the PV cells to be higher and their efficiency to decrease.

PVT collector performance is influenced by a wide range of design, operational and climate-related parameters, each contributing differently to thermal and electrical outputs (Figure 1.13). Design parameters such as the type of PV module, absorber plate material and thickness, tube configuration and presence of fins determine the structural and thermal characteristics of system, while multi-inlet designs and optimal tube placement can enhance fluid distribution and heat extraction. Operational parameters, including the packing factor, fluid inlet temperature and thermal resistance, govern the heat transfer efficiency within the system, whereas the use of fans can further assist cooling and airflow management. Meanwhile, climatic conditions, notably wind speed, ambient temperature, solar radiation, relative humidity and accumulated dust play a critical role in determining the efficiency of the collector, affecting both convective heat losses and irradiance received by the PV surface.

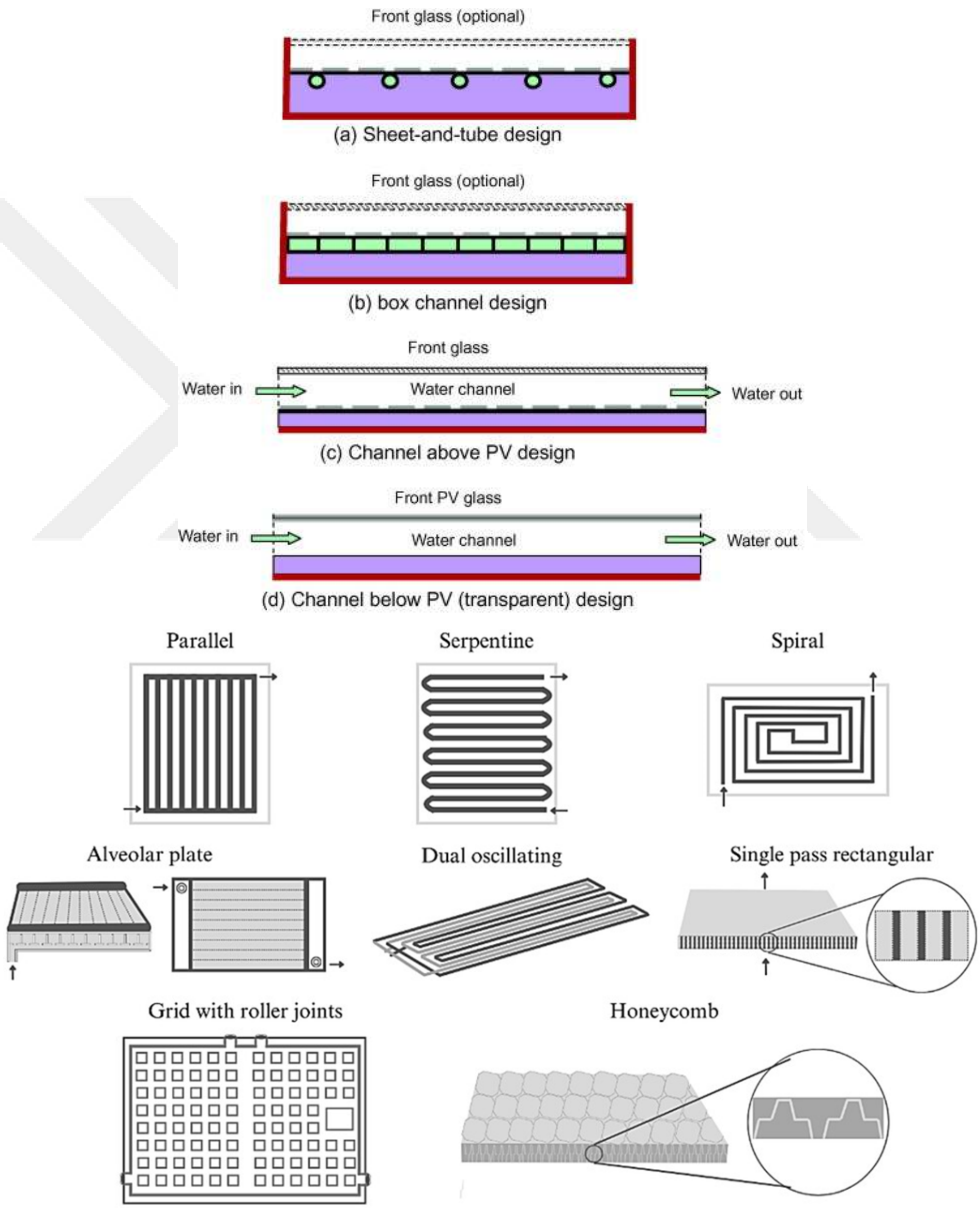

Figure 1.12. Common water-based PVT collector designs (Chow, 2010; Bonilla et al., 2025)

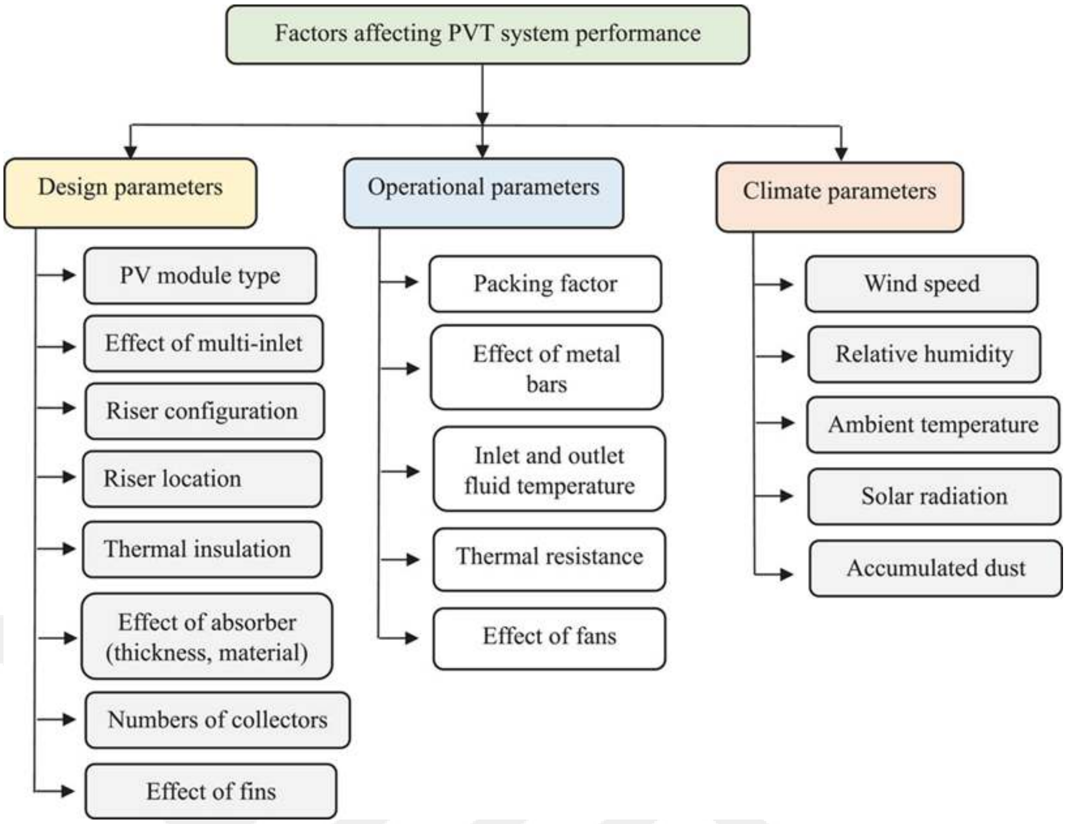

Figure 1.13. Parameters affecting PVT collector performance (El Alami et al., 2025)

Numerous experimental (Dong et al., 2024; Hamada et., 2024), analytical (Dubey et al., 2009; Shyam et al., 2015) and numerical (Nasrin et al., 2018a; Rubbi et al., 2020) studies have been conducted on PVT collectors, focusing on various designs (Olmuş et al., 2025a; Olmuş et al., 2025b; Poredos et al., 2020; Shen et al., 2021b; Sheshpoli et al., 2021), dimensions (Mosa et al., 2019; Teymori-omran et al., 2021), materials (Herrando et al., 2019; Kazemian et al., 2024), fluid types (Alhamayani, 2024; Sreekumar et al., 2022) and application areas (Olmuş et al., 2022; Olmuş et al., 2023) that affect both electrical and thermal performance. Commonly studied designs include parallel, serpentine and spiral tube PVT collectors.

2. PRELIMINARY WORK

Photovoltaic thermal collectors have been widely investigated in recent decades due to their ability to simultaneously produce electrical and thermal energy from solar radiation, thereby improving overall energy utilization. Numerous studies have focused on enhancing the performance of PVT collectors through various design modifications, fluid flow arrangements and cooling fluids. In particular, absorber geometries such as parallel, serpentine and spiral tube designs are among the most widely adopted configurations in the literature. Furthermore, operating conditions including solar irradiance, fluid flow rate, fluid inlet temperature, and ambient conditions significantly affect system behavior and optimization.

To provide a comprehensive overview of current developments in PVT technology, this chapter offers a categorized review of recent research. The review is structured under five main sections, parallel tube configurations, serpentine tube configurations, spiral tube configurations, channel-type designs and comparative studies involving different PVT configurations. Finally, the last section synthesizes the key insights derived from the literature and outlines the motivation and research gap addressed in the present study.

2.1. Parallel Tube Configurations

Parallel tube absorber configurations are among the most extensively studied designs in PVT collectors due to their relatively simple geometry, ease of manufacturing and effective thermal management capabilities. In these systems, the working fluid flows through a set of straight tubes arranged parallel to each other beneath the PV panel, enabling efficient heat extraction from the PV cells. The number of tubes, their arrangement (vertical or horizontal), and the inlet-outlet configurations (single, double or multi-inlet) can significantly influence the thermal and electrical performance of the collector. A wide range of research has investigated the effects of operational parameters such as solar irradiance, fluid flow rate and cooling strategies on the efficiency of parallel tube PVT collectors. This section reviews experimental, numerical and analytical studies that focus on optimizing the performance of PVT systems utilizing parallel tube geometries.

Among the early attempts to research on modelling PVT collectors, Kalogirou (2001) performed modeling and simulation of a PVT collector using TRNSYS software. While Type 49 PVT collector was used in TRNSYS software, electrical and thermal performance of parallel tube PVT collector was investigated using meteorological data in Cyprus (Figure 2.1). While electricity and thermal energy production, overall efficiency were determined as performance parameters, water flow rate, solar irradiance depending on meteorological conditions of Cyprus, ambient temperature were taken as operational parameters. Four PV panels were connected in series and the dimensions of the newly developed panel were 2.12x1.2 m in modeling. Water was used as the fluid in modeling and the flow rate was changed between 0 and 150 L/h. The results revealed that the optimum flow rate is 25 L/h. Furthermore, the performance of a conventional PV panel and the developed PVT collector were compared, while the average annual electrical efficiency of the PV panel was 2.8%, the electrical efficiency of the PVT collector was calculated as 7.7%. Additionally, when thermal efficiency was also taken into account, the overall efficiency of the PVT collector was found to be 31.7%.

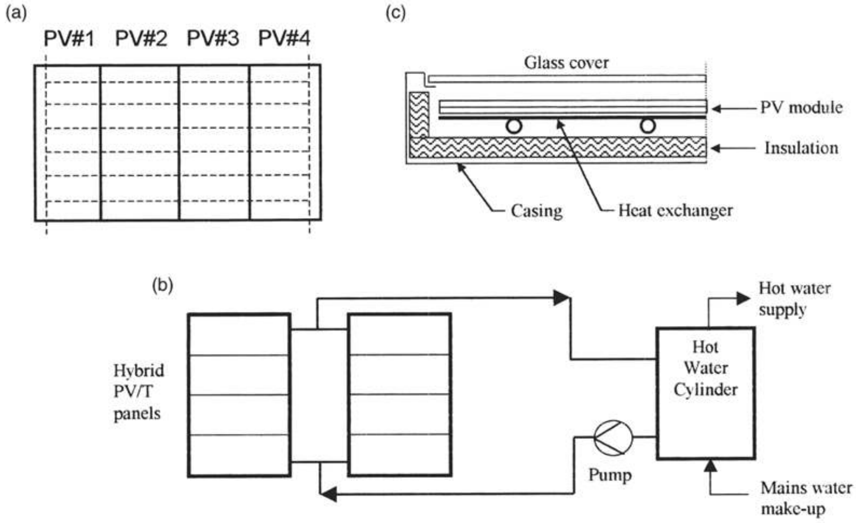

Figure 2.1. Schematic representation of the PVT system analyzed in the study by Kalogirou (2001)

Expanding upon the comparative potential of different working fluids, Tripanagnostopoulos et al. (2002) conducted an experimental study where air and water-based PVT collectors, and glazed PVT collectors and unglazed PVT collectors were tested on their thermal and electrical efficiency for outdoor conditions (Figure 2.2). It was observed that water-based PVT collectors were more efficient than air-based PVT collectors. The findings showed that glazed PVT collector provided 30% more thermal efficiency than unglazed PVT collector, while the electrical efficiency decreased by approximately 16%.

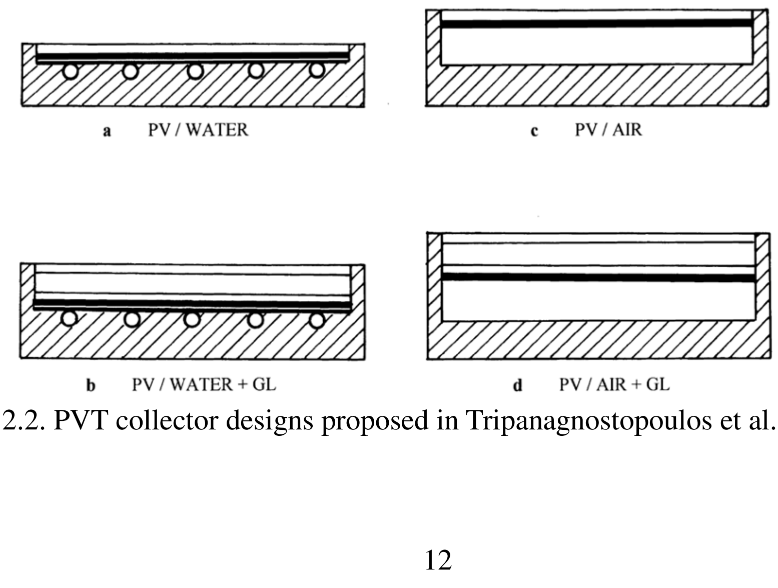

Figure 2.2. PVT collector designs proposed in Tripanagnostopoulos et al. (2002)

In a subsequent study focusing on environmental conditions, Rahman et al. (2015) fabricated an experimental setup to investigate the effects of solar irradiance, flow rate and dust on PV panel and parallel tube designed PVT collector (Figure 2.3). The solar irradiance ranged between 400 W/m^2 and 1000 W/m^2, flow rate between 40 L/h and 160 L/h, and PV cell temperature, electrical efficiency and output power was determined as performance metrics. A conventional PV panel was also used for comparison in the study. The results showed that the surface temperature of the PV panel without cooling increased up to 56 °C, while the electrical efficiency and output power decreased to 3.13% and 20.47 W at solar irradiance with 1000 W/m^2. It was also seen that with every 1 °C increase in PV cell temperature, the output power decreased by 0.37 W and the electrical efficiency decreased by 0.06%. With every 100 W/m^2 increase in solar irradiance, the cell temperature and output power of the PV panel increased by 4.93 °C and 2.94 W, respectively, while in the case where parallel tubes were integrated with the PV panel, they increased by 2.64 °C and 4.35 W. At 800 W/m^2 solar irradiance, in the case of without dust on the PV panel surface, the output power reached 25.31 W, and the electrical efficiency was 4.84%, while in the case of dust on the PV panel, the output power reached 17.61 W, and the electrical efficiency reached 3.37%. The presence of pollution on the PV panel surface reduced performance by approximately 30%.

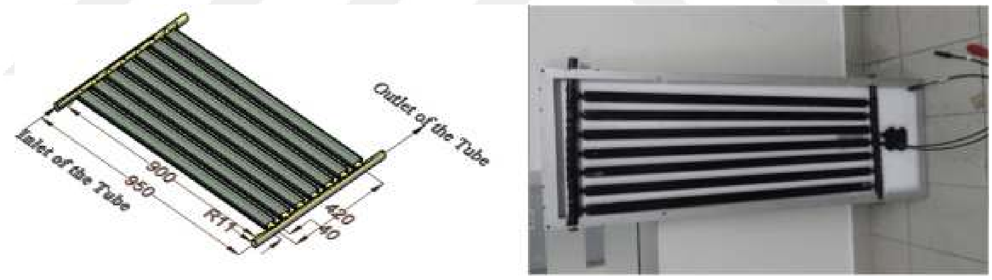

Figure 2.3. Configuration of the PVT collector investigated in Rahman et al. (2015)

While many studies focused on conventional fluids, Khanjari et al. (2016) numerically investigated the effect of using nanofluids on the performance of parallel tube designed PVT collectors using CFD method (Figure 2.4). The study investigated the effect of pure water, Ag/water and Alumina/water nanofluids and nanoparticle volume fraction, fluid inlet velocity on the efficiency metrics and heat transfer. As the fluid inlet velocity increases from 0.04 m/s to 0.23 m/s, the effect of the investigated nanofluid and pure water decreases the outlet temperature, while the thermal and overall efficiency decreases, the electrical efficiency increases. In all three efficiencies, Ag/water nanofluid exhibited the best performance, and it was followed by Alumina/water nanofluid. While the heat transfer coefficient was very close to each other when all three fluids were used at low fluid velocities, Ag/water nanofluid clearly differed from the other two fluids and increased sharply as the fluid velocity increases. Moreover, the findings showed that the thermal, electrical, overall and exergy efficiencies enhanced with increase in nanoparticle volume fraction.

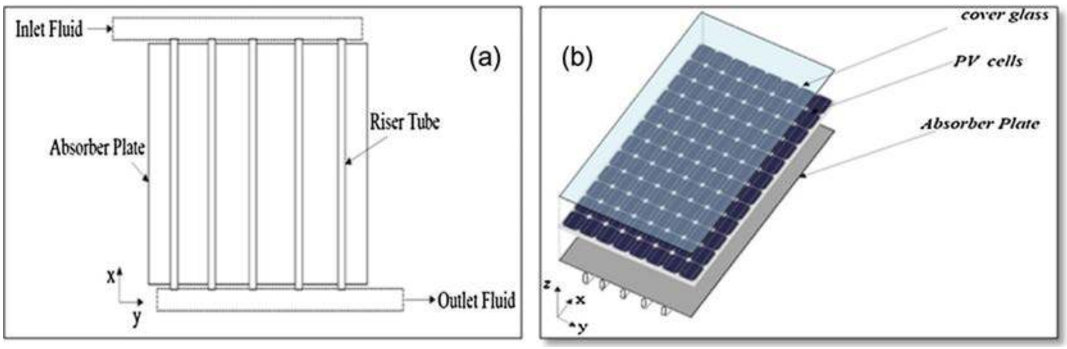

Figure 2.4. PVT collector analyzed in the study by Khanjari et al. (2016)

Preet et al. (2017) designed, manufactured and tested a PV panel, a parallel tube designed PVT collector and a PCM supported PVT collector for one day under outdoor conditions (Figure 2.5). Surface temperature, electrical and thermal efficiency were determined as performance metrics, water was used as fluid and the effect on performance of PVT collector was investigated by taking the water flow rate as 0.013 kg/s, 0.023 kg/s and 0.031 kg/s. While two absorber plates were used in PVT collectors, one plate was connected behind the PV panel and the other under the copper tubes. Paraffin wax RT-30 was used as PCM material. The results showed that the efficiencies increased with the increase in fluid flow rate. Water-based PVT collector reduced the temperature by 47% compared to the PV panel, and the PCM supported PVT collector reduced the temperature by 53% at 0.031 kg/s flow rate. This phenomenon increased electrical efficiency by 230% and 300%, respectively. At the same flow rate, thermal efficiencies were obtained as 62.37% for the water-based PVT collector and 35.4% for the PCM-based PVT collector.


Figure 2.5. PVT collector analyzed in the study by Preet et al. (2017)

A similar experimental and simulation approach was employed by Shi et al. (2017), who experimentally tested a PVT collector providing cooling with copper tubes and simulated it in MATLAB software using the experimental data. The experiments were carried out using a solar simulator in a laboratory. While solar irradiance intensity (508.41 W/m^2 and 364.81 W/m^2) and circulating water velocity (0.13 L/min and 0.25 L/min) were considered as operational parameters, electrical, thermal and overall efficiency and primary energy economic ratio were determined as performance parameters. The findings showed that at high solar irradiance, the thermal efficiency, overall efficiency and primary energy economic ratio of the collector were obtained as 51.4%, 62.3% and 82.5%, respectively. At lower solar irradiance, these parameters were found as 37.2%, 46.5% and 67.6%, respectively.

To compare the effect of glazing, Chen et al. (2018) performed a numerical and experimental study including a parallel tube designed glazed PVT collector, an unglazed PVT collector, a PV panel and a flat plate solar collector (Figure 2.6). The performance of the PVT collector was experimentally tested, and the results were used to validate the numerical simulations. The length of the PVT collectors used was 2 m, the width with 1 m, the distance between the tubes and the tube diameter was 10 cm and 10 mm, respectively. Numerical modeling was carried out using MATLAB and TRNSYS software. While the water inlet temperature, fluid flow rate, solar irradiance and wind speed were taken as operation parameters, thermal, electrical and primary energy saving efficiency were evaluated as performance parameters. The fluid inlet temperature was changed between 20 and 55 °C, solar irradiance between 200 and 1000 W/m^2 and the fluid flow rate between 0.0085 and 0.011 kg/s. The results showed that the thermal efficiency of the glazed PVT collector was 51.3% and that of the unglazed PVT collector was 43.9%. From the electrical efficiency perspective, the efficiency of the glazed PVT collector was 12.7%, while that of the unglazed PVT collector was 14.2%.

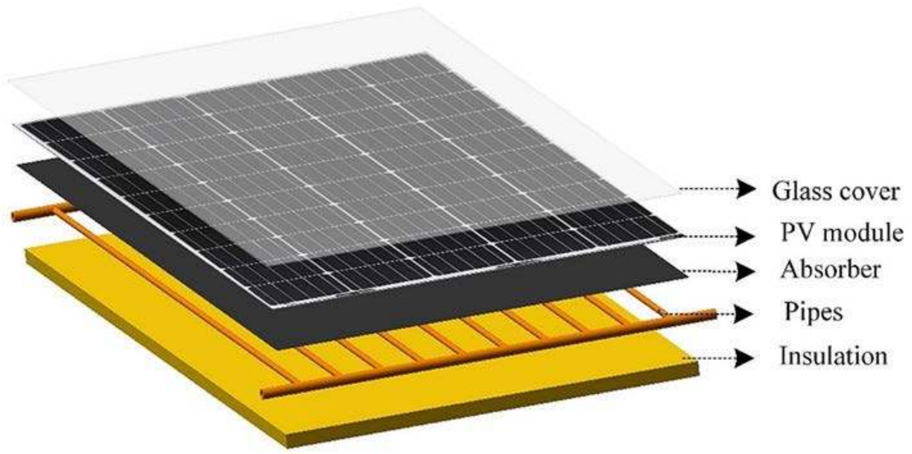

Figure 2.6. Design structure of the integrated PVT collector in Chen et al. (2018)

From a geometric optimization perspective, a numerical study was carried out using Fluent software with variation of different channel numbers and flow arrangements to investigate thermal performance in parallel designed PVT collectors by Shen et al. (2021b). Since the Reynolds number was arranged below 2000, laminar three-dimensional steady model was used in numerical analysis (Figure 2.7). Temperature and velocity distribution, PV cell temperature and pressure drop were presented for different channel numbers and flow arrangements. The study resulted in showing that the increment in channel number up to 10 reduced the value of pressure drop, and further increase beyond 10 increased the value of pressure drop gradually. It was also observed that the increase in the number of channels was associated with a further decrease in the temperature of the PV panel and more uniform temperature distribution.

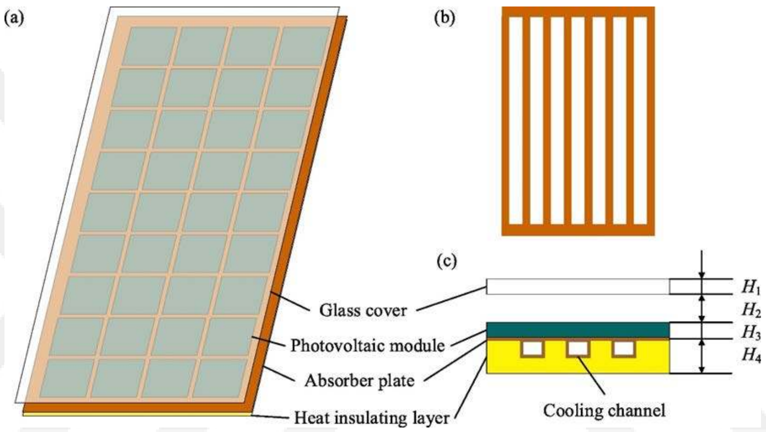

Figure 2.7. Layout of the PVT collector investigated in the study by Shen et al. (2021b)

Parthiban et al. (2020) numerically simulated the effects of various operational and environmental parameters on PVT collector. A parallel tube PVT collector was used in the study, and a single tube was modeled to reduce computational time (Figure 2.8). The operational parameters in the study included a fluid flow rate ranging from 6 to 44 L/h and a fluid inlet temperature between 25°C and 35°C. Environmental parameters were also varied, with solar irradiance levels adjusted between 600 and 1000 W/m², wind speed between 1 and 5 m/s, and ambient temperature set between 25 and 35°C. An increase in flow rate resulted in enhancement of thermal and electrical efficiency. At the maximum flow rate of 44 L/h, thermal efficiency reached the highest values of 45.54% and electrical efficiency reached 18.04%.

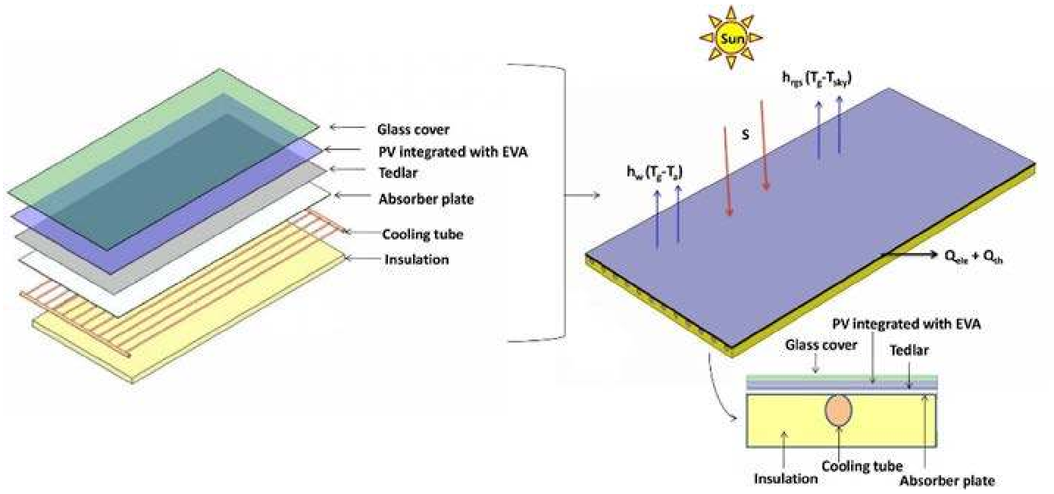

Figure 2.8. Simulation geometry and boundary conditions in the study by Parthiban et al. (2020)

Nanofluid-based enhancement was explored by Sreekumar et al. (2022), who performed a numerical analysis using finite volume method for PVT collectors using MXene/water nanofluid. Parallel tube configuration was used in PVT collector and only one tube was modeled to shorten the computational time (Figure 2.9). In the study, the effect of thermal and electrical efficiency, pressure drop, PV cell temperature was investigated by changing the fluid flow rate between 30 and 90 kg/h and nanofluid mass fraction as 0.01wt%, 0.1wt% and 0.2wt%. It was observed that MXene/water nanofluid enhanced thermal efficiency between 4.6% and 17% and electrical efficiency between 1.9% and 3.5% according to nanofluid mass fraction compared to pure water. The highest overall efficiency was obtained as 83% at 90 kg/h flow rate and 0.2wt% nanofluid mass fraction. Although the pressure drop of the nanofluid was 88% higher than that of water, the pumping power was very small.

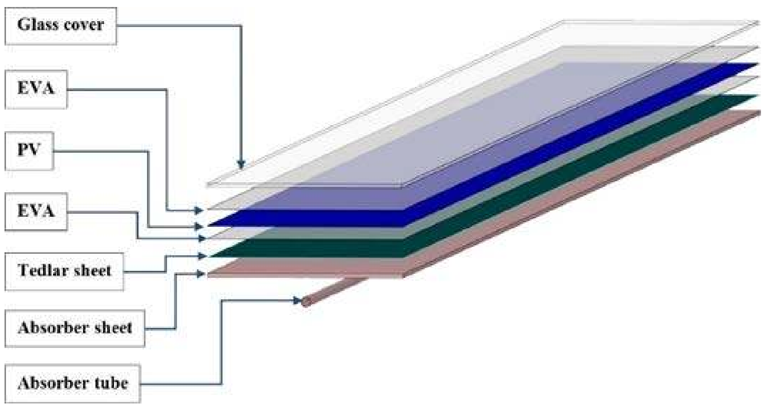

Figure 2.9. Schematic diagram of the PVT collector in the study by Sreekumar et al. (2022)

In another study examining different fluids and operating parameters, Büyükalaca et al. (2023) explored the use of hexagonal boron nitride (hBN) and water nanofluid in a photovoltaic thermal (PVT) collector featuring a horizontally arranged tube geometry (Figure 2.10). The study investigated the effects of various parameters including nanoparticle diameter, nanoparticle volume fraction, flow rate and solar irradiance on the system performance through numerical simulations and artificial neural network models. The performance metrics considered were thermal, electrical, and overall efficiency, along with an evaluation of exergy performance. Additionally, an enviro-economic analysis was conducted. The results showed that when the volume fraction of hBN nanoparticles was varied between 0% and 0.22%, thermal efficiency increased up to 0.18% before declining, while electrical efficiency exhibited a continuous improvement. With the use of 20 nm hBN nanoparticles, the system achieved a 0.7% increase in electrical efficiency, a 3.01% increase in thermal efficiency, a 2.71% rise in overall efficiency, and a 1.80% improvement in exergy efficiency compared to water alone. Furthermore, the hBN/water nanofluid demonstrated better performance than graphene/water nanofluid, which is commonly studied in the literature, though the difference in performance was relatively small.

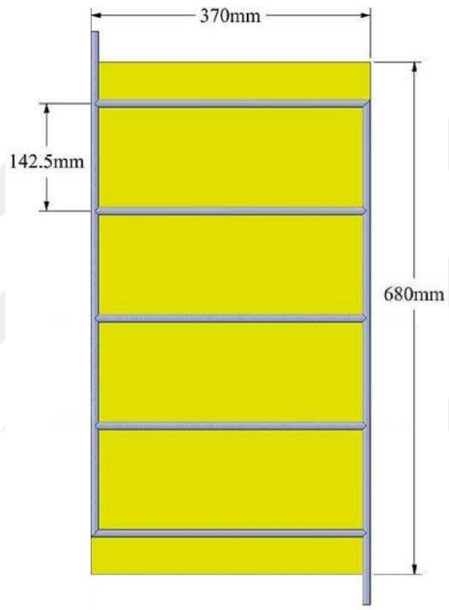

Figure 2.10. Configuration of the parallel tube design in the study by Büyükalaca et al. (2023)

2.2. Serpentine Tube Configurations

Serpentine tube configurations are another widely explored design in PVT collectors, known for their ability to enhance heat transfer due to extended flow paths and increased contact surface area. In this design, the working fluid follows a continuous winding path through the absorber, resulting in longer residence time and improved thermal exchange with the PV surface. Serpentine configurations are typically implemented with single, double or even triple inlet-outlet arrangements, and can be oriented either vertically or horizontally depending on the application. The complex flow dynamics inherent to serpentine geometries can lead to increased thermal efficiency but may also result in higher pressure drops. This section reviews key studies in the literature that have investigated the thermal, electrical and hydraulic performance of serpentine tube PVT collectors under various geometric and operating conditions.

The performance benefits of nanofluid use in serpentine configurations have been explored experimentally by Al-Shamani et al. (2016), who fabricated and tested the performance of a rectangular tube designed PVT collector operating with nanofluids in their experimental study (Figure 2.11). In the study, the operating parameter fluid mass flow rate was changed between 0.068 and 0.170 kg/s, solar irradiance between 400 and 1000 W/m^2, and the effects of SiO_2, TiO_2 and SiC nanofluids on the electrical, thermal and total efficiency of the PVT collector were investigated. The best results in terms of performance parameters were obtained in the case where SiC nanofluid was used. SiC nanofluid based PVT collector reduced the PV cell temperature below 54 °C at 0.170 kg/s flow rate and 1000 W/m^2 solar irradiance, while the electrical efficiency was calculated as 13.52%, thermal efficiency as 68.21% and total efficiency as 81.73%. Likewise, electrical, thermal and total power productions were 116 W, 698 W and 814 W, respectively.

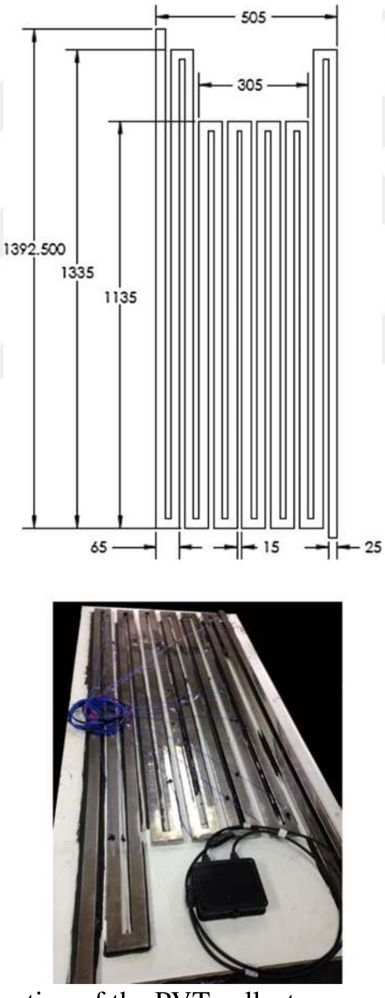

Figure 2.11. Outdoor test configuration of the PVT collector presented by Al-Shamani et al. (2016)

Effect of different fluids on PVT collector performance was investigated by Hosseinzadeh et al. (2018). They numerically compared the effect of ZnO/water nanofluid and pure water on the performance of a serpentine designed PVT collector using ANSYS Fluent software (Figure 2.12). Taguchi method was employed to determine the optimum performance of ZnO/water nanofluid based PVT collector. Solar irradiance, ambient temperature, wind velocity, fluid inlet temperature, fluid mass flow rate and mass fraction of ZnO/water nanofluid were taken as operating parameters. Solar irradiance was ranged between 200 and 1000 W/m^2, wind speed from 1 m/s to 9 m/s, ambient temperature from 20 to 40 °C, fluid inlet temperature from 20 to 40 °C, fluid mass flow rate from 30 kg/h to 70 kg/h and nanoparticle mass fraction from 0wt% to 12wt%. While one of these parameters was changed, the others were taken according to the base-case conditions; solar irradiance was set to 600 W/m^2, wind speed to 5 m/s, ambient and inlet temperature to 30 °C, fluid flow rate to 50 kg/h and ZnO nanoparticle mass fraction to 6wt% in the base-case conditions. According to Taguchi method, the most important parameter affecting the PVT collector efficiency was the fluid inlet temperature. While the fluid inlet temperature was decreased from 40 to 20 °C, the thermal efficiency was improved by about 16%. Moreover, the thermal efficiency was enhanced with the increase of solar irradiance, fluid flow rate, nanoparticle mass fraction and ambient temperature. With the increase of nanofluid mass fraction, the thermal efficiency increased up to approximately 12.78% compared to pure water. Moreover, according to Taguchi analysis, the optimal operating conditions were 1000 W/m^2 for solar irradiance, wind speed of 1 m/s, ambient temperature of 40 °C, fluid inlet temperature of 20 °C, fluid flow rate of 70 kg/h and ZnO nanoparticles mass fraction of 12wt%.

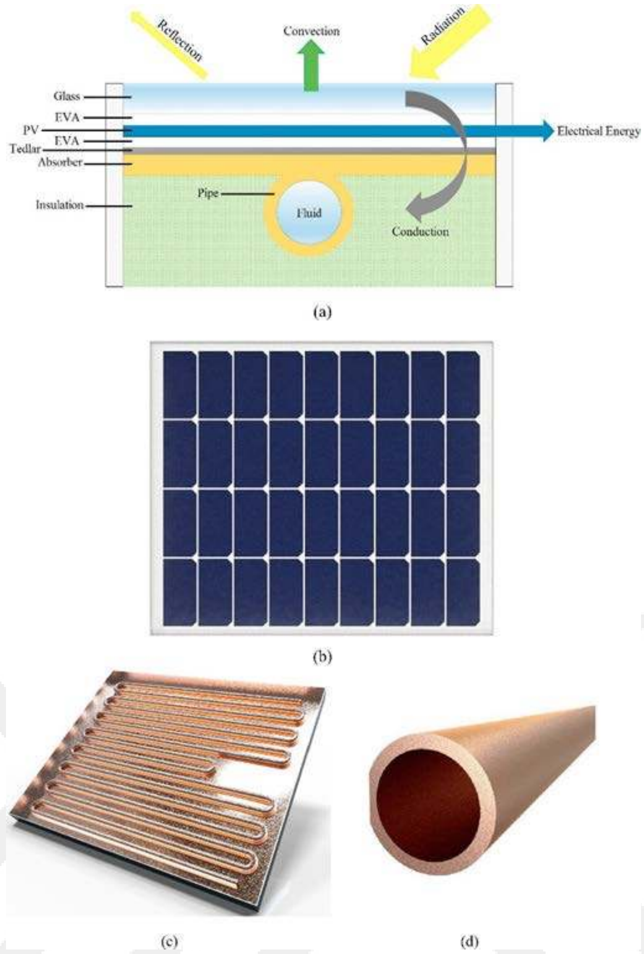

Figure 2.12. Details of the absorber design and heat transfer components used in Hosseinzadeh et al. (2018)

Another serpentine based PVT collector was investigated with numerical and experimental methods by Zhou et al. (2018). The effects of fluid inlet velocity, tube spacing, absorber materials, horizontally and vertically arranged tubes were evaluated on temperature distribution. In the study, three tube spacings (70 mm, 150 mm, 159 mm), two absorber materials (copper and aluminum) were tested and the fluid inlet velocity was varied between 0.3 m/s and 0.9 m/s. The findings showed that the most uniform temperature distribution was obtained with reduced tube spacing. Furthermore, it was observed that using copper as the absorber material improved the temperature distribution, the plate temperature decreased with the increase of the fluid inlet temperature, and the horizontally arranged serpentine tubes provided lower plate temperature due to the increased number of bends.

From a design optimization perspective, Park et al. (2022) performed numerical analysis of water-based PVT collectors with serpentine design using ANSYS Fluent software. In their study, the authors examined the effects of changing the fluid inlet position and pitch size between 40 and 120 mm on the produced thermal energy, water outlet temperature, pressure drop and thermal energy produced per unit pressure drop (Figure 2.13). As the pitch size increased from 40 mm to 80 mm, thermal energy produced per unit pressure drop (TEPD) increased from 0.1357 to 0.1411

W/Pa, while TEPD decreased to 0.1326 W/Pa as the pitch size increased from 80 to 120 mm. The results indicated that the optimum pitch size, considering the thermal energy produced per unit pressure drop, was 80 mm. Additionally, with the increase of pitch size, the water outlet temperature decreased from 306.51 K to 299.81 K, the thermal efficiency decreased from 80.87% to 27.64% and the pressure drop decreased from 12053 Pa to 4217 Pa.

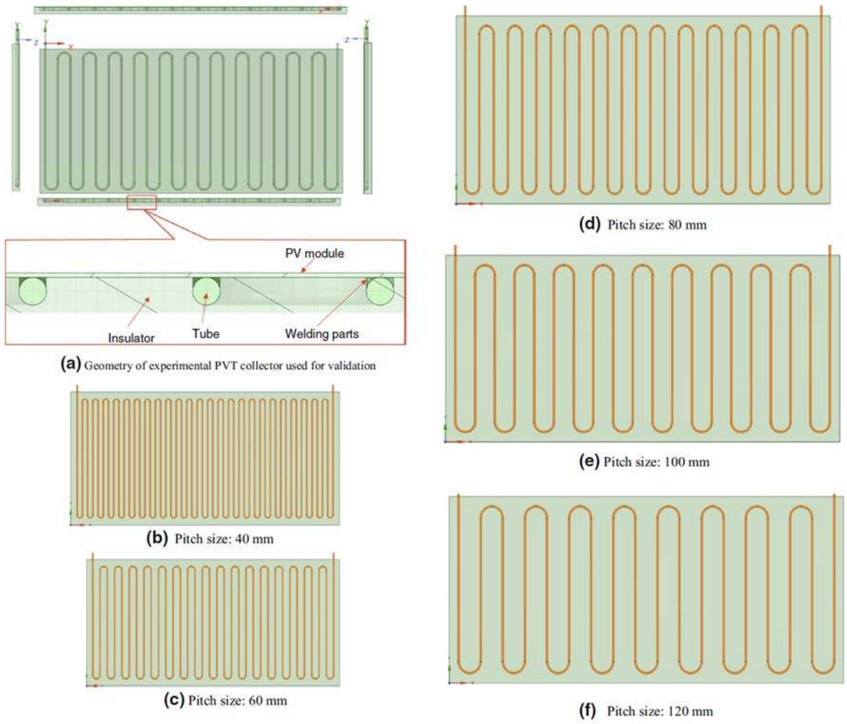

Figure 2.13. Configuration of the serpentine tube design the study by Park et al. (2022)

A more geometrically comprehensive analysis was conducted by Aghakhani et al. (2022), who investigated the cooling performance of a water-based PVT collector using COMSOL Multiphysics software with serpentine tube design (Figure 2.14). The study analyzed the effects of varying tube diameter, the number of loops, and water flow rate on system performance. In the study, a 60 W solar panel was used, tube diameters were 9.53 mm, 12.70 mm and 15.88 mm, loop numbers were 3, 7 and 11, and the water flow rate was changed between 0.5 and 2.5 L/min. The results indicated that increasing the flow rate and number of loops effectively reduced the maximum temperature of the PV cells, although the pressure drop increased with additional loops. The study also revealed that the optimal combination of parameters, highest flow rate, smallest tube diameter, and longest tube length, resulted in the lowest PV surface temperature and the most uniform temperature distribution across the surface.

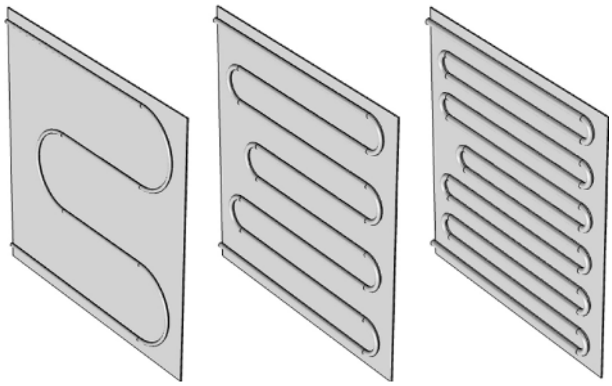

Figure 2.14. Comparison of serpentine tube configurations based on the number of loops used in Aghakhani et al. (2022)

Another contribution to the understanding of operation parameters on serpentine tube PVT collectors came from Yan et al. (2022). The authors carried out both numerical and experimental investigations of a serpentine designed PVT collector. They used water as a coolant and the influence of flow rate, solar irradiance, fluid inlet and ambient temperatures on temperature distribution (Figure 2.15), PV cell temperature, fluid outlet temperature, thermal and electrical efficiency of PVT collector were investigated. The results demonstrated that the overall efficiency decreased 22% with the increasing fluid inlet temperature from 19 to 34 °C. Moreover, thermal efficiency enhanced approximately 8% with the increasing flow rate minimum to maximum, while electrical efficiency improved by %0.047 for each 40 l/h increment in flow rate.

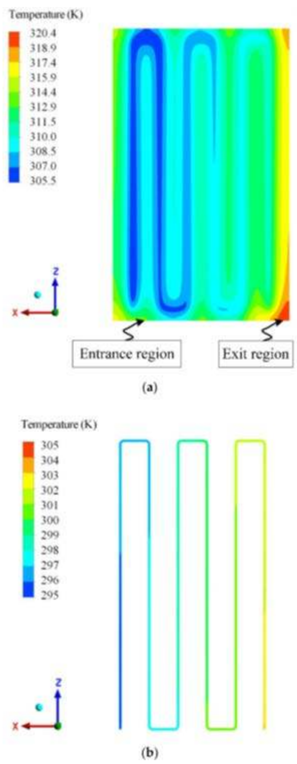

Figure 2.15. Temperature distribution of (a) PVT collector surface, and (b) the tube in the study by Yan et al. (2022)

Unlike many earlier studies that focused primarily on either individual operational parameters or geometric configurations, Alsharifi et al. (2024) adopted a more integrated optimization perspective by developing a comprehensive 3D mathematical model using COMSOL Multiphysics (Figure 2.16). In their study, four key design parameters such as panel aspect ratio, serpentine tube pitch, solar irradiance and coolant flow rate were optimized to enhance the electrical and thermal efficiency of the collector. These analyses were carried out numerically using COMSOL Multiphysics software. The results showed that increasing the panel aspect ratio from 0.125 to 8 led to improvements in both electrical and thermal efficiency, by 1.99% and 12.10%, respectively. Conversely, increasing the serpentine tube pitch resulted in a reduction in both efficiencies. A rise in solar irradiance from 200 W/m^2 to 1000 W/m^2 decreased electrical efficiency by 8.36%, while boosting thermal efficiency by 75.33%. Additionally, increasing the coolant flow rate from 0.1 L/min to 1.4 L/min enhanced electrical efficiency by 12.4% and thermal efficiency by 167.8%.

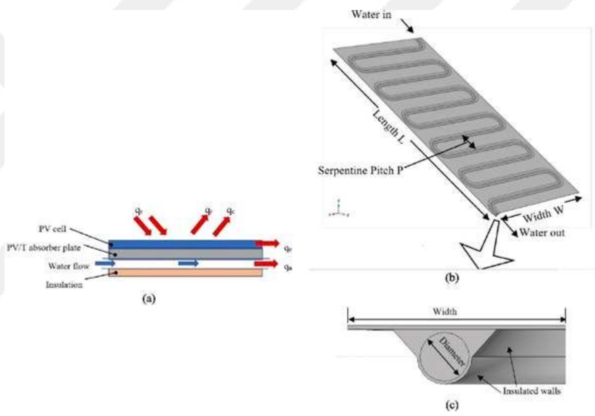

Figure 2.16. Schematic representation of the PVT collector, (a) energy balance of the system, (b) 3D view of the PVT, and (c) cross-sectional view of the cooling tube presented by Alsharifi et al. (2024)

2.3. Spiral Tube Configurations

Spiral tube configurations have gained increasing attention due to their compact design and potential for uniform temperature distribution across the absorber surface. Depending on the design, spiral tube configurations can feature single or double inlets, and may vary in terms of the number of helical turns, the direction of fluid flow and the positioning of the inlet and outlet. While the extended fluid path improves thermal contact and heat absorption, it also introduces higher pressure drops, which can increase pumping power requirements of the system and reduce hydraulic efficiency. These trade-offs influence not only thermal and electrical output but also the overall performance of the system. This section presents an overview of recent studies investigating the thermal, electrical and hydraulic behavior of spiral tube PVT collectors under various geometric and operational conditions.

One of the experimental investigations into spiral tube PVT collectors was carried out by Ceylan et al. (2014). The authors conducted an experimental study to reduce the temperature of the PV panel by attaching spiral tubes behind the PV panels (Figure 2.17). Water was used as the coolant, the cooling water temperature was set as 45 °C and 55 °C and the effect on electrical efficiency, electrical power generation, thermal efficiency and thermal energy generation was investigated. The study was also compared with a PV panel under the same conditions. While the PVT collector electrical efficiency varied between 12% and 16%, the PV panel electrical efficiency was calculated as 10%.

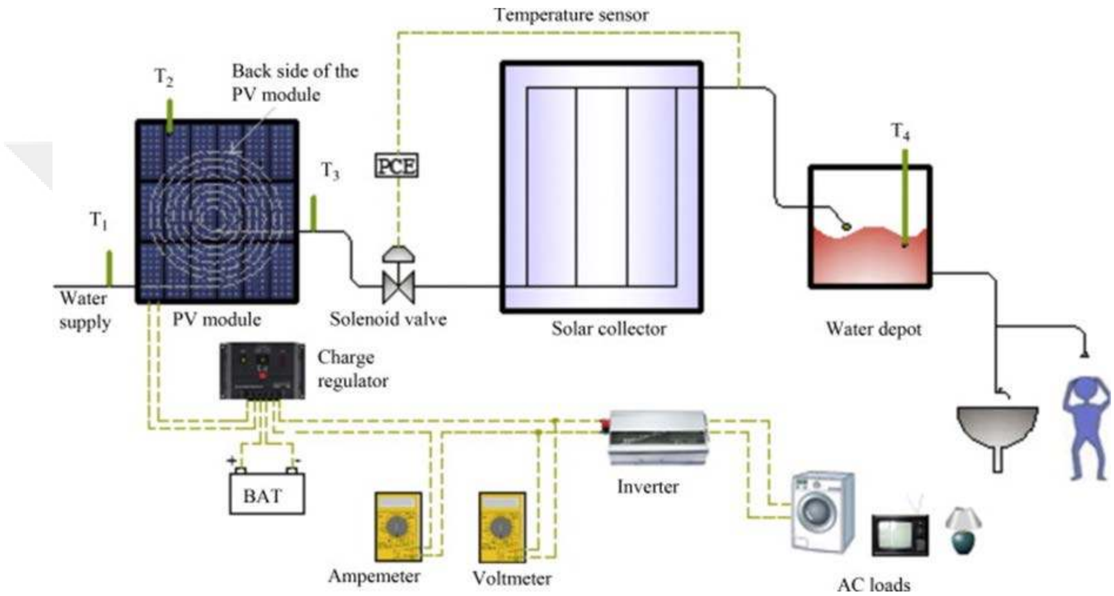

Figure 2.17. PVT collector system used in Ceylan et al. (2014)

Another experimental study, supported by numerical analysis, was carried out by Nasrin et al. (2018b) to enhance the performance of spiral tube PVT collectors using a water/MWCNT nanofluid (Figure 2.18). The variable parameters used in the experimental and numerical parts were solar irradiance, weight fraction, while the mass flow rate and fluid inlet temperature were kept constant at 0.5 L/min and 32 °C, respectively. The effects of these parameters were investigated on temperature distribution, PV cell temperature, electrical efficiency, electrical power, fluid outlet temperature, thermal efficiency, thermal energy production and overall efficiency. The results demonstrated that thermal energy production enhanced approximately 114 W with each 100 W/m^2 solar irradiance increment. The authors also compared the water and water/MWCNT nanofluid on the performance parameters. The findings showed that the thermal, electrical and overall efficiency was higher in water/MWCNT nanofluid approximately 0.14%, 3.67% and 4.11% respectively.

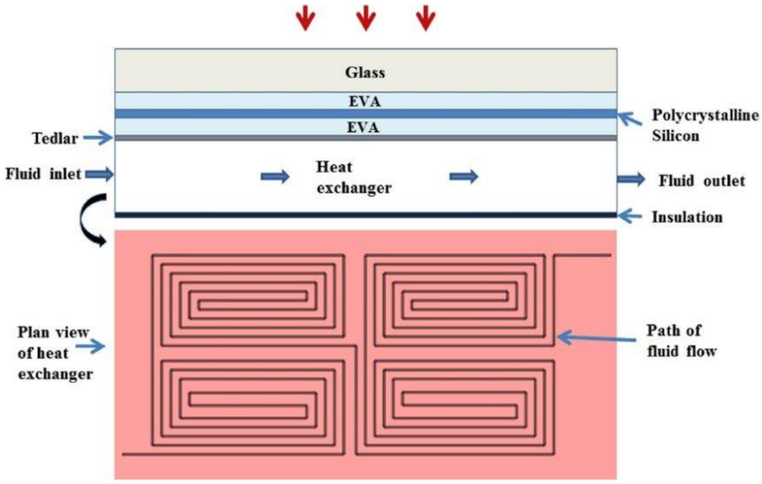

Figure 2.18. Schematic representation spiral tube configuration in the study by Nasrin et al. (2018b)

In another experimental and numerical study, Fayaz et al. (2019) compared the PV panel, water-based PVT collector with spiral design and PVT-PCM system (Figure 2.19). The numerical analysis was performed with COMSOL Multiphysics software at a flow rate 0.5 L/min, water inlet temperature with 32 °C and varying solar irradiance between 200 W/m^2 and 1000 W/m^2. The results indicated that the maximum PV cell temperatures were 75.6 °C, 67.0 °C, 63.0°C for PV panel, PVT collector, PVT-PCM system, respectively. The electrical efficiency of PV, PVT ve PVT-PCM were 13.72%, 13.85% and 14.01% in the numerical simulations. It was also reported that the enhancement of electrical efficiency was 6.2% for PVT collector and 7.2% for PVT-PCM system compared to the PV panel. Furthermore, while the overall efficiency of the PVT collector was 89.9%, it was 85.88% for PVT-PCM system.

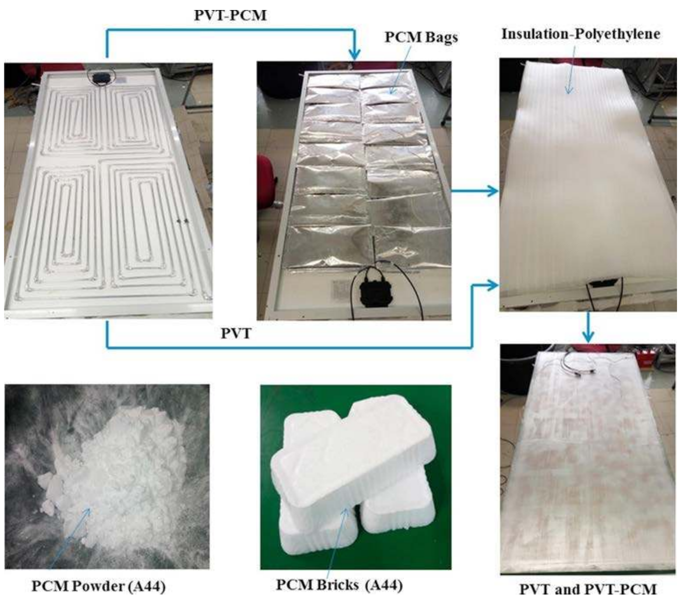

Figure 2.19. Outdoor test configuration of the PVT collector used in Fayaz et al. (2019)

Building upon these investigations, recent studies have increasingly incorporated exergy analysis and economic performance alongside energy performance evaluations to provide a more comprehensive assessment of spiral tube PVT collectors. Tian et al. (2021) investigated numerically the energy, exergy, and economic performance of a spiral designed PVT collector cooled with a nanofluid composed of magnesium oxide (MgO) and water and a PV panel (Figure 2.20). In the study, nanoparticle volume fractions were varied between 0% and 1%, while the fluid flow rate was adjusted between 0.5 and 4 L/min. The results indicated that increasing the flow rate reduced the panel temperature but also lowered the exergy output. In contrast, the addition of nanoparticles, particularly at lower flow rates, enhanced exergy efficiency. Specifically, the inclusion of 1% MgO at a flow rate of 0.5 L/min resulted in a 0.45% improvement in exergy efficiency. However, as the flow rate increased from its minimum to maximum value, exergy efficiency decreased by 2.03%. The economic analysis revealed that the payback period for the PVT collector was 4 years, while the payback period for the conventional PV system was calculated to be 6 years.

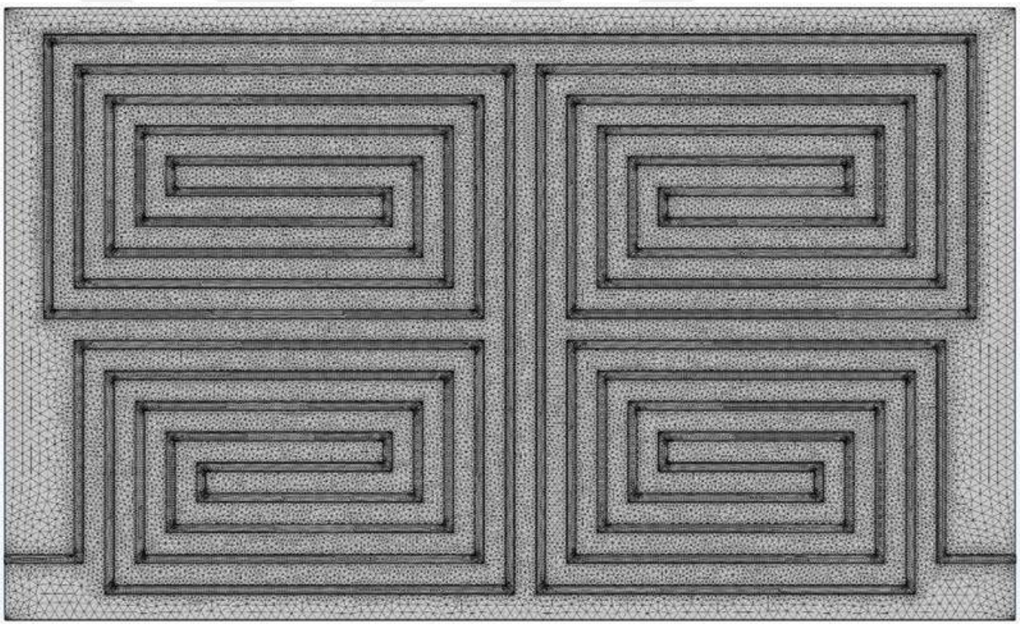

Figure 2.20. Mesh structure of spiral tube configuration presented by Tian et al. (2021)

2.4. Channel Type Configurations

In addition to tube-based absorbers, channel-type configurations have also been explored in literature as alternative geometries for PVT collectors. These systems typically employ rectangular or triangular channels. Although not as commonly studied as parallel, serpentine or spiral tubes, several recent investigations have focused on this configuration type due to its potential to enhance thermal efficiency and improve heat transfer uniformity. This section highlights selected studies in which channel-based PVT collectors were designed, modeled, or tested under varying operating and geometric conditions.

One of the numerical studies in this field was carried out by Nahar et al. (2019), who analyzed a PVT collector with a channel geometry without an absorber using COMSOL Multiphysics software (Figure 2.21). They investigated the effect of Reynolds and Prandtl numbers on the electrical and thermal efficiency of the PVT collector. An increase in the Reynolds number from its lower to upper limits resulted in heat transfer enhancement of approximately 25%, subsequently improving both the thermal and electrical efficiencies. In addition, the channel depth was changed between 10 and 20 mm and the impact on the PV cell temperature was investigated. When the channel depth was increased from 10 to 20 mm, the PV cell temperature decreased by 10.2 °C. The results also showed that every 1 °C decrease in the PV cell temperature increased the electrical efficiency by 0.05%. Moreover, the solar irradiance was also changed between 200 and 1000 W/m^2 and the effect on electrical efficiency and output power was investigated. The findings showed that output power increased by 4.98 W, while electrical efficiency decreased by 0.06% with every 100 W/m^2 increase in solar irradiance.

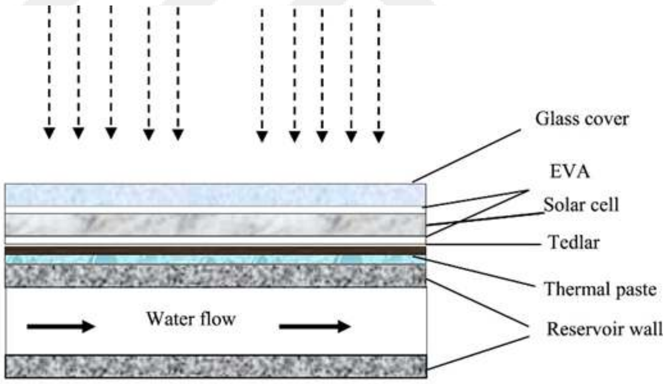

Figure 2.21. Schematic representation of PVT collector layers in the study by Nahar et al. (2019)

Seeking further improvements in the performance of PVT collector, Shen et al. (2021a) numerically examined how modified cooling channel shapes could boost the overall efficiency of PVT collectors (Figure 2.22). The investigation focused on two different cooling channel designs, shark dorsal fin type sawtooth and regular type sawtooth, to enhance the heat transfer between the cooling water and PV modules. Simulations were performed using COMSOL Multiphysics software, and the solar irradiance was varied from 300 to 1200 W/m^2, and the cooling water mass flow rate was varied from 0.0018 to 0.018 kg/s. The results showed that the shark fin design reduced the average cell temperature by 6.05°C compared to conventional straight channels, leading to a 0.3% increase in electrical efficiency and a 3.9% improvement in thermal efficiency. The optimal performance was achieved with a channel depth of 0.03-0.05 m, a sawtooth height of 0.02 m, and a tooth width of 0.01 m. The study demonstrated that these specially designed cooling channels are particularly effective in improving the efficiency of PVT collectors under conditions of high solar irradiance.

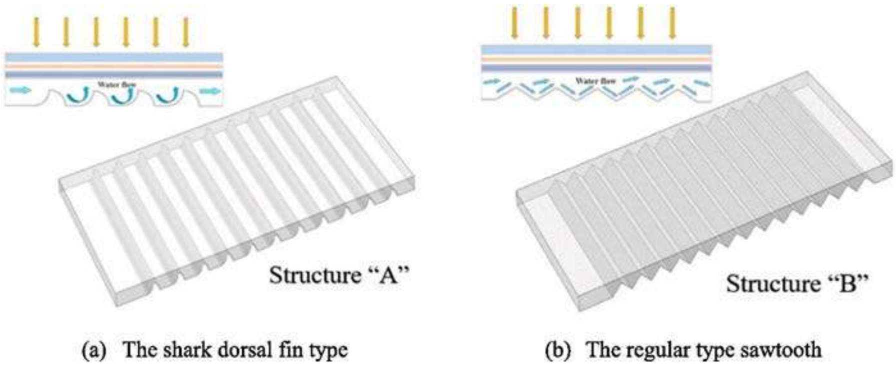

Figure 2.22. Schematic diagram of the PVT system proposed by Shen et al. (2021a)

In line with recent efforts to systematically compare cooling strategies, Attia et al. (2024) numerically examined the performance of serpentine channels with both single and multiple inlets using air and water as working fluids. The authors conducted a numerical study to investigate the performance of two different PVT collectors with tube cooling channels using ANSYS Fluent software. One of the developed designs featured a single inlet and outlet with a serpentine channel design, while the other design had three inlets and three outlets, which are equally divided into the collector, following a serpentine pattern (Figure 2.23). The study investigated the use of both water and air as cooling fluids, varying solar irradiance between 200 and 1000 W/m^2 and fluid flow rates from 0.001 to 0.005 kg/s. Temperature and velocity distributions, fluid outlet temperature, thermal efficiency, PV cell temperature and electrical efficiency were determined as performance metrics. The results showed that thermal and electrical efficiencies improved by 7.23% and 4%, respectively, in the water-based three-inlet collector compared to the single-inlet design. It was observed that increasing the fluid flow rate led to a decrease in fluid outlet temperature but an improvement in thermal efficiency. Additionally, as solar radiation intensified, both the fluid outlet temperature and PV cell temperature increased, resulting in higher thermal efficiency but a decline in electrical efficiency. When the cases where air and water fluids were used in the single-inlet design were compared with the cases where air and water fluids were used in the multi-inlet design, the case where multiple inlets and water fluid were used yielded the best results for all performance parameters.

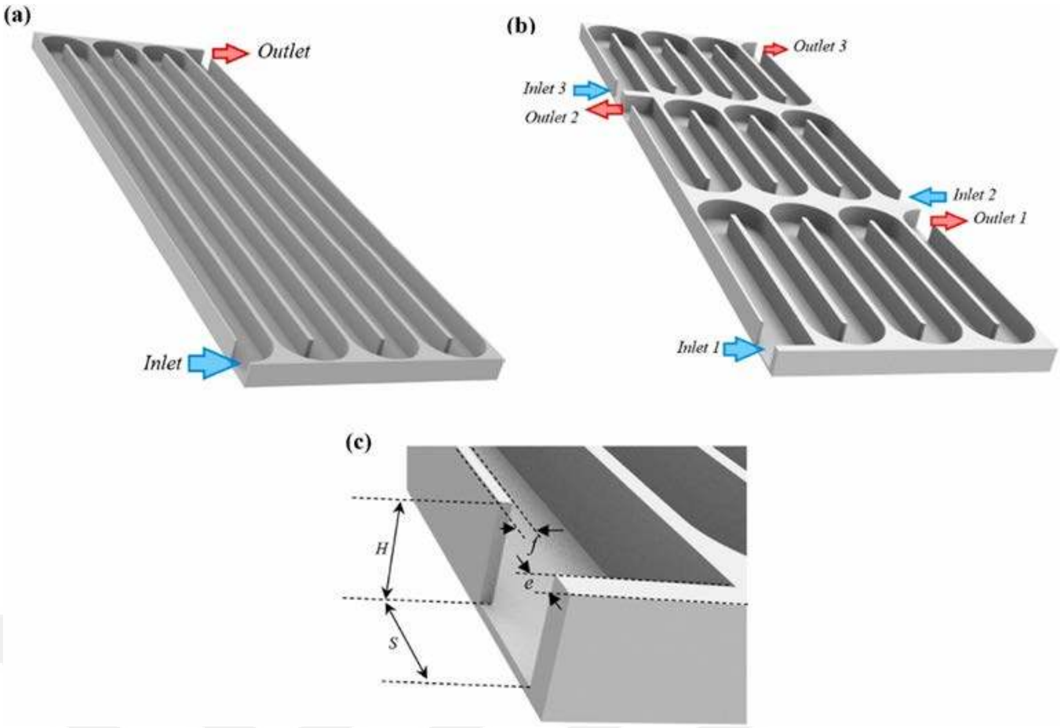

Figure 2.23. Layout of the solar PVT collector investigated in the study by Attia et al. (2024)

Building on previous research, Abo-Zahhad et al. (2024) conducted a comprehensive numerical comparison of multiple PVT configurations, differing in channel width and inlet-outlet arrangements, to assess their thermal and exergy performance. A comprehensive comparison of a PV panel and serpentine channel designed six PVT collector configurations was carried out using ANSYS Fluent software. Six different PVT collector configurations (Figure 2.24) separated from each other based on the number of inlets and outlets, and channel width. PV cell temperature, electrical efficiency, electrical power, pressure drop, thermal, electrical and total exergy, exergy loss, and different exergy efficiencies were selected as performance parameters. The developed PVT collectors showed an improvement of around 28% in electrical power output compared to the PV panel. Configurations with four and six inputs showed superior performance compared to other configurations. These two designs reduced the PV cell temperature by approximately 18 °C. Furthermore, the entropy production of PVT collector configurations was compared in this study. The PVT collector with four inputs stands out in this case by showing a 7% decrease in entropy production.

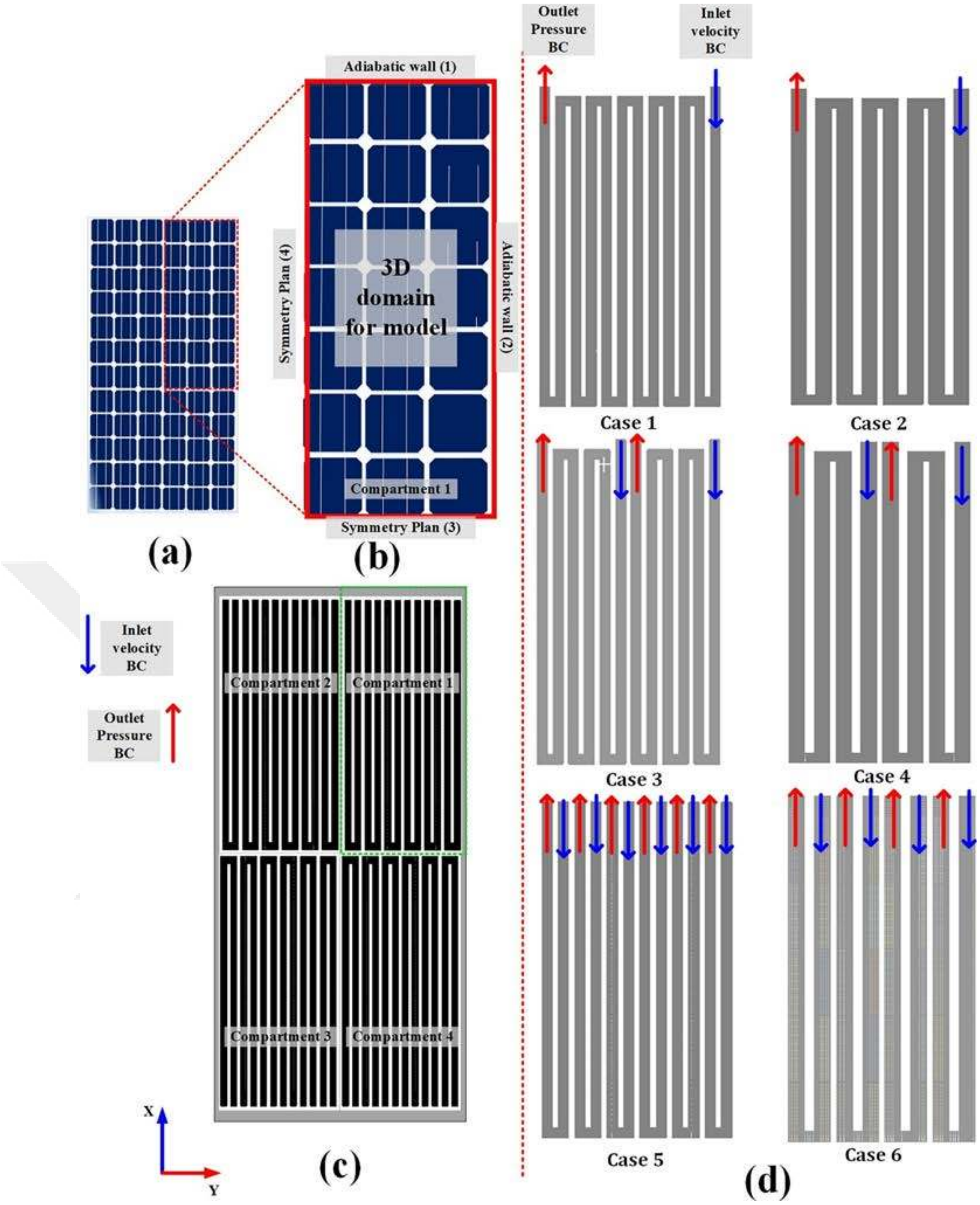

Figure 2.24. Schematic of the serpentine channel configuration used in Abo-Zahhad et al. (2024)

2.5. Comparison of Different Configurations

While numerous studies in the literature focus on a single type of absorber design, a growing body of research has undertaken comparative analyses involving multiple PVT configurations, particularly parallel, serpentine and spiral tube layouts. These comparative studies are highly valuable, as they provide insights into how various geometries perform under identical or controlled conditions in terms of thermal and electrical efficiency, pressure drop and overall system effectiveness. Some works also evaluate the performance trade-offs among configurations based on specific operation conditions. This section reviews key studies that perform side-by-side assessments of different PVT collector geometries, often employing numerical modeling, experimental setups or both of them.

To highlight the impact of flow path geometry on PVT performance, Kazem et al. (2020) experimentally tested and numerically investigated three PVT collectors with web flow (Figure 2.25c), direct (Figure 2.25a) and spiral designs (Figure 2.25b). Numerical analyzes were performed using COMSOL Multiphysics software, and water was used as a coolant. A conventional PV panel was also used for comparison in the study. During the numerical analysis, the fluid mass flow rate was changed between 10 kg/h and 40 kg/h, while solar irradiance was adjusted between 200 W/m^2 and 1000 W/m^2. The water inlet temperature was taken as 25 °C, and the convection heat transfer coefficient was set at 11.8 W/m^{2}K. The numerical results revealed that, the PV cell surface temperature was found to be the highest at 68 °C with 10 kg/h flow rate in the web flow design, whereas the lowest surface temperature was found to be 45.2 °C with 40 kg/h flow rate in the spiral flow design. While the PV panel electrical efficiency was 7.8%, the overall efficiencies of web, direct and spiral designed PVT collectors were 18.5%, 28% and 35% respectively. Furthermore, the highest electrical and thermal efficiency were found for the spiral based design with 9.1% and 26% respectively. The findings showed that the spiral-based PVT collector was the most efficient design.

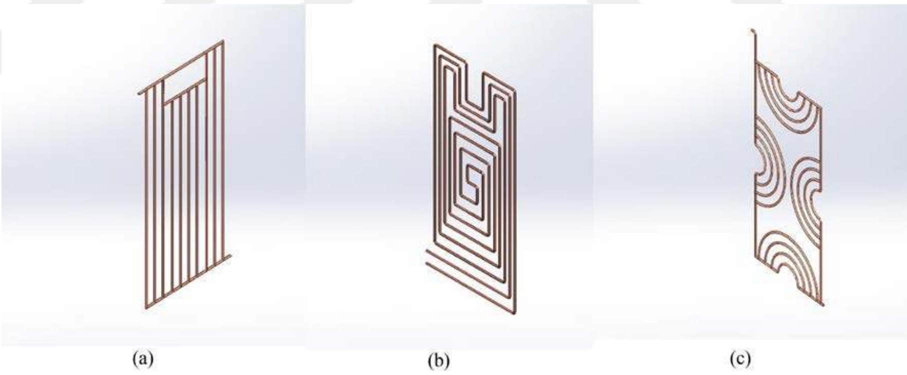

Figure 2.25. Design variations of the PVT collectors evaluated for thermal and electrical performance by Kazem et al. (2020)

In a follow-up study, Kazem et al. (2021) developed and tested direct (Figure 2.26b), oscillating (Figure 2.26c), web flow (Figure 2.25a) and hybrid PVT collectors where spiral and direct (Figure 2.26d) are used together (Figure 2.26). The developed PVT collectors were compared with a conventional PV panel based on thermal and electrical performance parameters. In the study, PV cell temperature, fluid outlet temperature, thermal, electrical and overall efficiencies were taken as performance parameters, while solar irradiance, ambient temperature and water flow rate used were taken as operational parameters. The developed and produced PVT collectors were tested for approximately 16 hours. Since the experiments were carried out in outdoor conditions, solar irradiance and ambient temperature changed depending on time. Water was used as the coolant and the water flow rate was taken as 0.02 kg/s. The results showed that the highest voltage, power generation and efficiencies were provided in the PVT collector called hybrid design. The electrical efficiency for hybrid, oscillating, direct and web flow design PVT collectors were found to be 12.7%, 11.94%, 11.13% and 11.16%, respectively, while the thermal efficiency was 60.7%, 53.3%, 37% and 18.7%, respectively. In terms of overall efficiency, the hybrid design showed 9% to 15% higher performance than the oscillating, direct and web flow design. The surface temperature of the hybrid design PVT collector, which produced the best result, was approximately 20°C lower than a conventional PV panel.

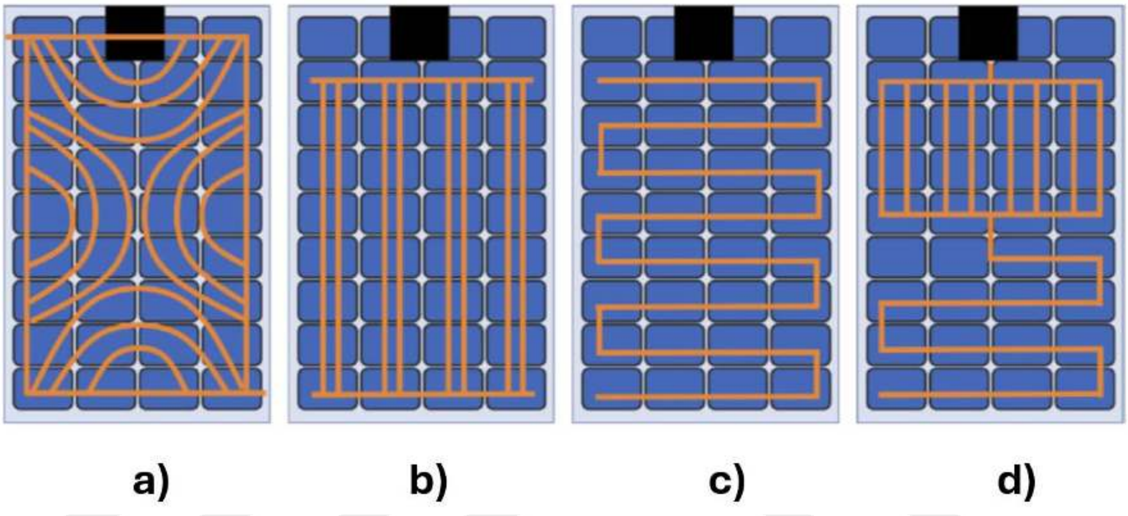

Figure 2.26. Comparative illustration of seven PVT collector designs analyzed by Kazem et al. (2021)

A more controlled comparison was implemented by Sheshpoli et al. (2021), focusing on the influence of tube geometry while keeping tube length constant. The comparison of four different configurations with the identical tube length using experimental and numerical methods was carried out. The authors determined the output power, fluid outlet temperature, pressure drop, plate temperature and temperature distribution as performance parameters while performing the numerical analyses in the ANSYS Fluent software. In the simulations, the constant heat flux was taken as 1000 W/m^2 and the fluid inlet temperature was 300 K, while the Reynolds number varied between 200 and 800. The numerical simulation and experimental results showed that the surface temperature and fluid outlet temperature decrease with the increase of the Reynolds number. In addition, although the pressure drop increases 7 times as the Reynolds number increases from 200 to 800, since these Reynolds numbers represent very low flow rates, the pump consumption was neglected in the efficiency calculations since it remains below 0.1 W.

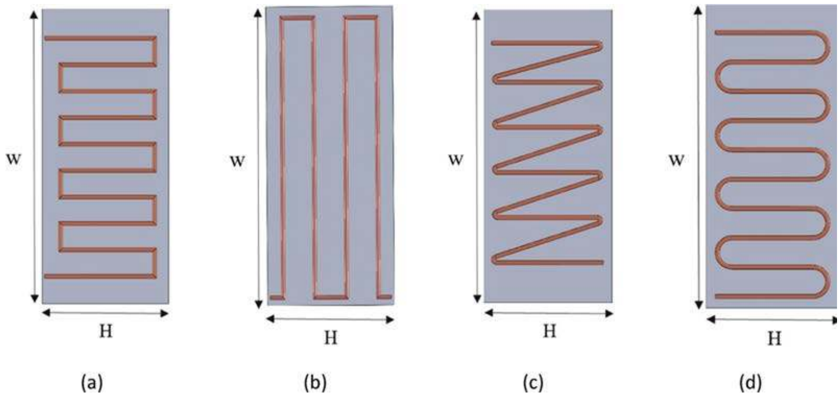

Figure 2.27. Design variations of the PVT collectors in the study by Sheshpoli et al. (2021)

A detailed parametric study by Teymori-omran et al. (2021) further examined how tube arrangement, diameter and flow rate influence system performance. A water-based PVT collector was numerically analyzed using ANSYS Fluent software to determine the optimum tube arrangement. In the study, the effects of three different tube arrangements (Figure 2.28), five different tube diameters in the range of 6-14 mm and seven different flow rates in the range of 1.5-3 L/min on thermal and electrical efficiency, pumping power and overall efficiency were investigated. The best thermal efficiency for different tube arrangements, tube diameters and flow rates were obtained in the transverse arrangement, reaching a value of 65.71% at a tube diameter of 10 mm and a flow rate of 3 L/min. On the contrary, the lowest thermal efficiency was obtained in the continuous tube arrangement, reaching a value of 44% at a pipe diameter of 6 mm and a flow rate of 1.5 L/min. On the other hand, the lowest electrical efficiency was observed in the longitudinal arrangement, reaching a value of 11.73% at a tube diameter of 14 mm and a flow rate of 1.5 L/min, while the highest efficiency was achieved with a value of 11.88% at a diameter of 14 mm and a flow rate of 3 L/min.

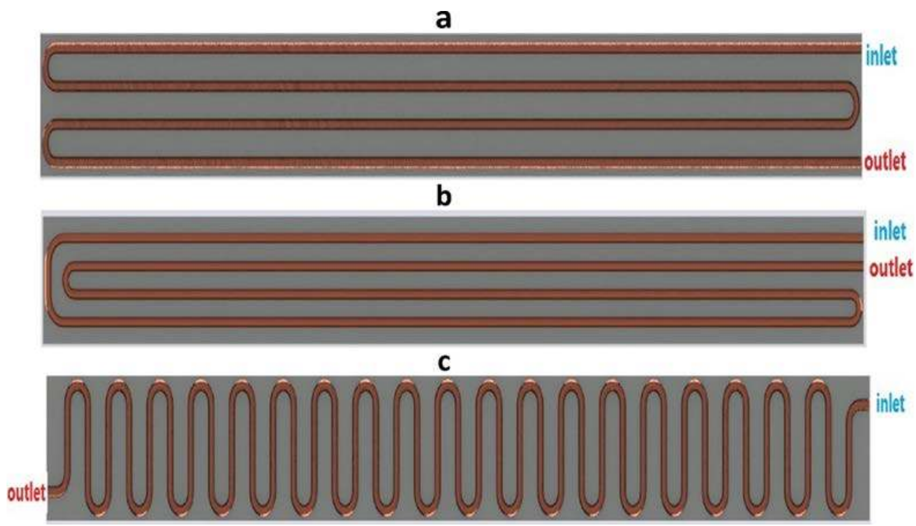

Figure 2.28. Schematic representation of PVT collector designs in Teymori-omran et al. (2021)

In a full-scale experimental evaluation, Hamada et al. (2024) carried out an experimental study to investigate the effect of different absorber tube designs which were spiral from edge-to-edge, spiral from center-to-edge and serpentine (Figure 2.29). The tube length was fixed as 1600 mm, the flow rate was changed between 1.5 L/min and 3 L/min with using water as the coolant. The findings showed that the lowest PV cell temperature was observed at the maximum flow rate of 3 L/min. At this flow rate, compared to a conventional PV panel, the PV cell temperature was lower by 3.6°C to 4.8°C for the three configurations. Also, compared to a conventional PV panel in power generation, an improvement of from 10% to 11% was observed for three configurations investigated. The overall efficiency was again maximum at the flow rate of 3 L/min for all three configurations, being 69.6% for the spiral from edge-to-edge design, 64.6% for the spiral from center-to-edge design, and 63.5% for the serpentine design. The pressure drops for these three configurations were calculated as 29.5 kPa, 29.33 kPa, and 24.79 kPa, respectively.

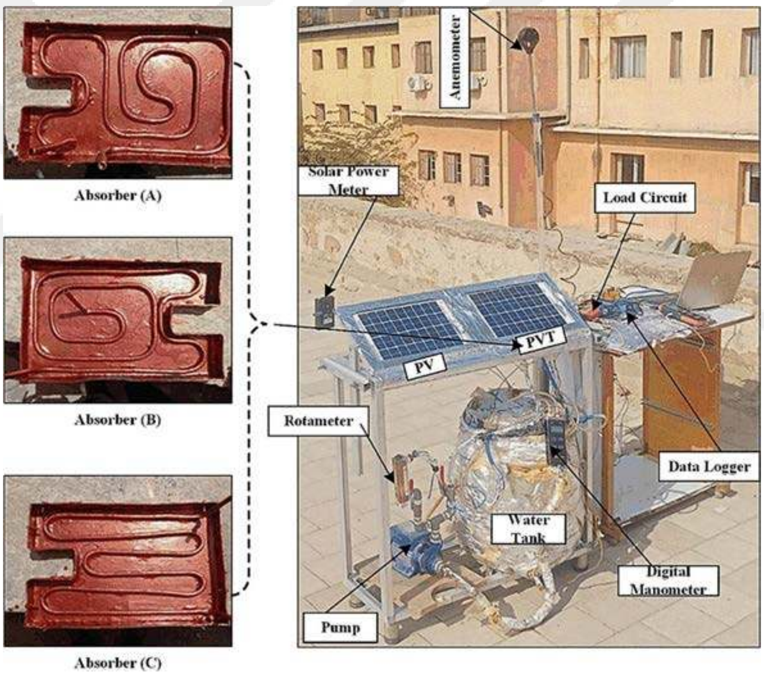

Figure 2.29. Experimental test setup and different PVT configurations used in Hamada et al. (2024)

Taking a comprehensive approach, Kazemian et al. (2024) systematically compared a wide variety of designs based on performance and economic criteria. The authors conducted a numerical comparison of 12 different PVT collector designs, including parallel, parallel without connection, spiral, multi-path serpentine, connected multi-path serpentine, two-sided serpentine, U-shaped, wavy, split-flow, and grid configurations (Figure 2.30). The designs were evaluated under base-case conditions, with consistent wetted surface area and tube length using ANSYS Fluent 18.2 software. The investigation considered several key performance indicators, such as absorber temperature distribution, thermal and electrical power output, thermal exergy, pressure drop, PV surface temperature, payback time, and cost savings. The results indicated that the multi-path serpentine design achieved the highest overall power output. However, the study also noted that two-sided serpentine configurations could lead to efficiency losses due to higher pressure drops, while the parallel design exhibited the highest surface temperature, potentially diminishing electrical efficiency. For the three best-performing geometries, absorber and tube materials (copper, aluminum, steel, and brass) were compared in terms of collector length, weight, cost savings, and thermal performance. Aluminum was found to offer the best balance between performance and weight. Ultimately, the multi-path serpentine design was identified as the most efficient when considering energy and exergy performance, weight, payback time, and cost savings.

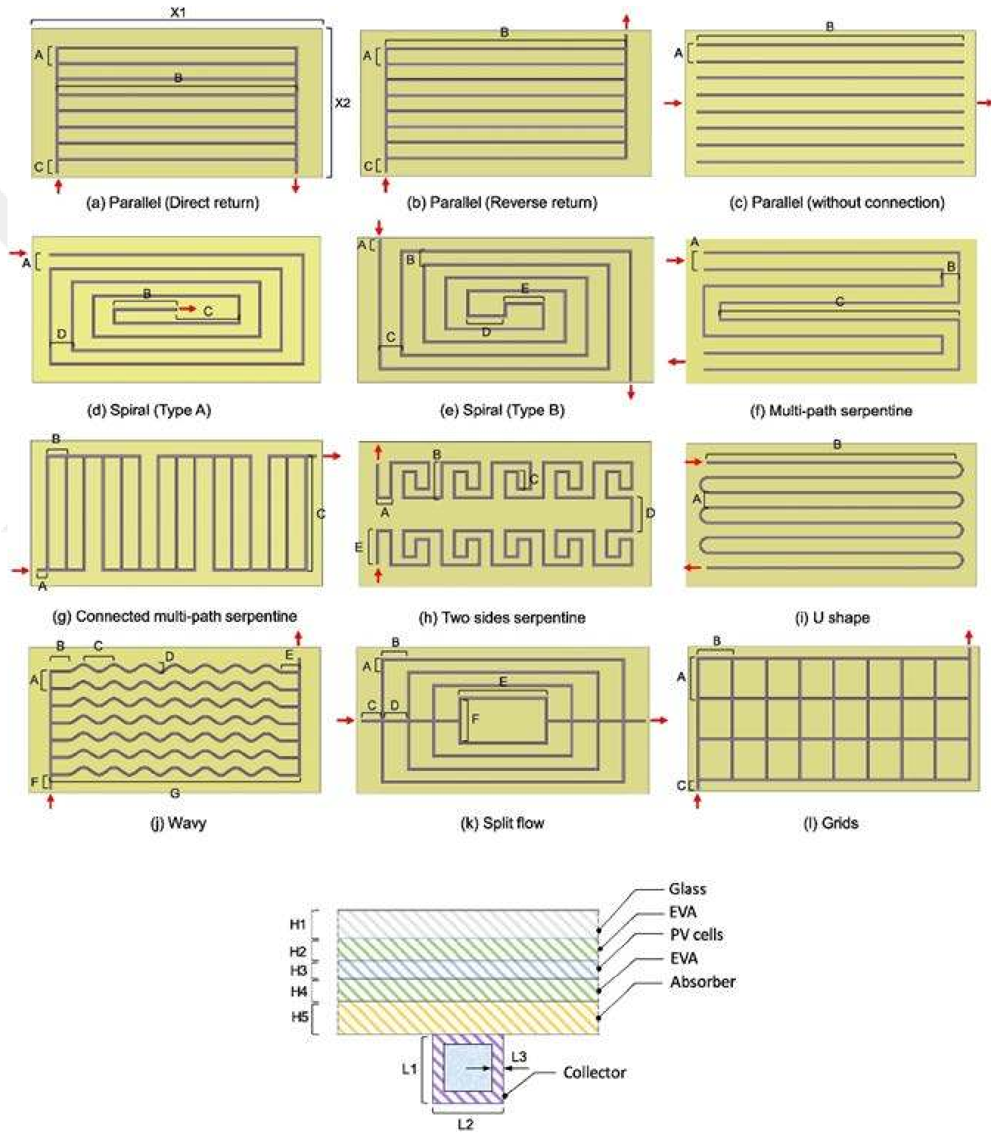

Figure 2.30. Different PVT collector configurations of PVT system in the study by Kazemian et al. (2024)

2.6. Significance and Goal of the Study

Photovoltaic thermal (PVT) collectors are hybrid systems capable of simultaneously generating both electrical and thermal energy from solar radiation. These systems address the efficiency reduction problem commonly encountered in conventional photovoltaic (PV) panels, while also enhancing the overall energy output by producing usable thermal energy. The performance of PVT collectors is influenced by numerous design and operational parameters, such as the geometry of the absorber, flow configuration, physical properties of the working fluid, inlet/outlet arrangements. Therefore, to ensure fair and reliable comparisons among different PVT collector configurations, it is crucial to maintain geometric consistency between the compared designs and conduct systematic analyses.

Although there are numerous experimental, analytical, and numerical studies on PVT collectors in the literature, most of these investigations focus on a single collector type. Even when multiple configurations are compared, consistency in key variables such as geometric dimensions, material properties or operating conditions is often lacking. This limits the direct comparability and generalizability of the findings. In particular, important parameters such as pressure drop, which significantly affects the hydraulic performance of the collectors, are frequently overlooked in many studies.

In addition, the literature rarely provides systematic and detailed comparisons of vertically and horizontally arranged tube configurations, and configurations with dual or multiple inlets are almost entirely overlooked. However, these configurations play a critical role in determining flow distribution, which directly influences thermal uniformity and PV cell temperature. Therefore, a comprehensive investigation into the effects of such inlet variations on collector performance is of significant value for both academic research and industrial applications.

The research conducted within the scope of this thesis aims to address the aforementioned gaps and provide a comprehensive contribution to literature. To this end, various PVT collector configurations were designed with equal tube lengths, identical absorber surface areas, and uniform material properties. Three-dimensional numerical models of these configurations were developed using the COMSOL Multiphysics software. The numerical analyses were carried out using the finite element method under the assumptions of steady-state, incompressible, and laminar flow conditions.

In the first part of this study, six parallel tube absorber designs (A, B, C, D, E and F) and ten different flow configurations were investigated. These configurations included single-inlet, double-inlet, and multi-inlet designs, with both vertical and horizontal tube arrangements. In the second part, thirteen different serpentine tube absorber designs (G, H, I, J, K, L, M, N, O, P, Q, R and S) and twenty-five flow configurations were analyzed. These configurations featured single, double, and triple inlets, along with vertical and horizontal tube layouts. In the third part, seven distinct spiral tube absorber designs (T, U, V, W, X, Y and Z) and twelve flow configurations were examined. Spiral tube designs were categorized based on single- or double-inlet arrangements, as well as the number of helical turns, inlet position, and flow direction of the working fluid.

All configurations were evaluated not only in terms of energy performance but also through exergy-based assessments. A wide range of performance metrics was comprehensively analyzed, including temperature distribution, PVT cell temperature, fluid outlet temperature, thermal and electrical power output, overall energy and primary energy saving efficiency, pressure drop, thermal energy per unit pressure drop (TEPD), thermal and electrical exergy generation, exergy output, exergy destruction and exergy efficiency. In this regard, the study stands out as one of the few comprehensive works that offers a holistic evaluation of PVT collectors in terms of both energy conversion efficiency and hydraulic performance.

The effects of key operational parameters including fluid flow rate, solar irradiance, fluid inlet temperature, ambient temperature and wind velocity on various performance indicators of the investigated configurations were comprehensively analyzed. In the existing literature, studies examining such a wide range of operational parameters in conjunction are notably limited. Furthermore, the three best-performing configurations from each design category (parallel, serpentine and spiral tubes) were compared in detail. In the final stage of the study, the performance enhancements of the top nine configurations were assessed against a conventional PV panel of the same size across multiple performance metrics. These analyses provide valuable insights into how system performance may vary under real operating conditions. The findings of this study not only contribute to theoretical understanding of PVT systems but also offer practical guidance for engineering design and field implementation.

In conclusion, this thesis distinguishes itself as an original and comprehensive study that goes beyond the limitations of previous research by systematically evaluating a large number of PVT collector configurations with diverse design characteristics under fair and consistent conditions. The detailed comparisons conducted under fixed geometric and thermophysical parameters provide a robust reference for future PVT collector absorber designs, offering guidance for performance optimization and energy efficiency improvements. Additionally, identifying configurations that simultaneously deliver high thermal and electrical efficiency with minimal pressure drop contributes to the development of more sustainable and cost-effective solar energy systems.

3. MATERIAL AND METHOD

3.1. Model Geometry

This study conducts a comprehensive comparative analysis of various parallel, serpentine and spiral tube PVT collectors. A total of twenty-six absorber designs are examined, consisting of six parallel, thirteen serpentine and seven spiral tube absorber designs. Each group is further differentiated by various flow configurations defined by whether the tubes are vertical or horizontal, the number of fluid inlets, and the fluid inlet positions and directions. Collectively, forty-seven distinct flow configurations are derived from these twenty-six absorber designs and evaluated in this study. While determining the configurations, commonly used designs from the literature were selected, additionally, some novel designs were also proposed to enhance performance. These configurations were systematically examined to evaluate their thermal and electrical performance using Computational Fluid Dynamics (CFD) simulations. The three-dimensional PVT collector configurations examined in this study were numerically modeled with finite element method using COMSOL Multiphysics software. Within the scope of this study, a total of 1615 simulations were performed, each requiring approximately two hours of computational time on the workstation. All simulations were executed on a workstation equipped with 192 GB RAM and 40 core CPU.

In parallel with the analysis of PVT configurations, a conventional PV panel which was identical in size to the PVT collectors was modeled as a reference system. This allowed for a direct comparison of energetic and exergetic performance metrics across all configurations, highlighting the relative advantages of the PVT collectors.

A schematic representation of the PVT collector was shown in Figure 3.1, and all PVT collector configurations were designed with the standardized tube lengths and PVT collector areas to ensure a fair comparison. The layers forming the PVT collector in all configurations were the same and consist of glass at the top, two EVA layers encapsulating the PV cells, PV cell, tedlar, an absorber plate and tubes attached to the plate. Thermophysical properties of the components comprising the PVT collector are presented in Table 3.1, with the properties of the solid components assumed constant. Water was used as the coolant in the PVT collectors investigated. The dimension of the collectors was 2000 mm x 1000 mm and the geometric properties of the components forming the collector are presented in Table 3.2.

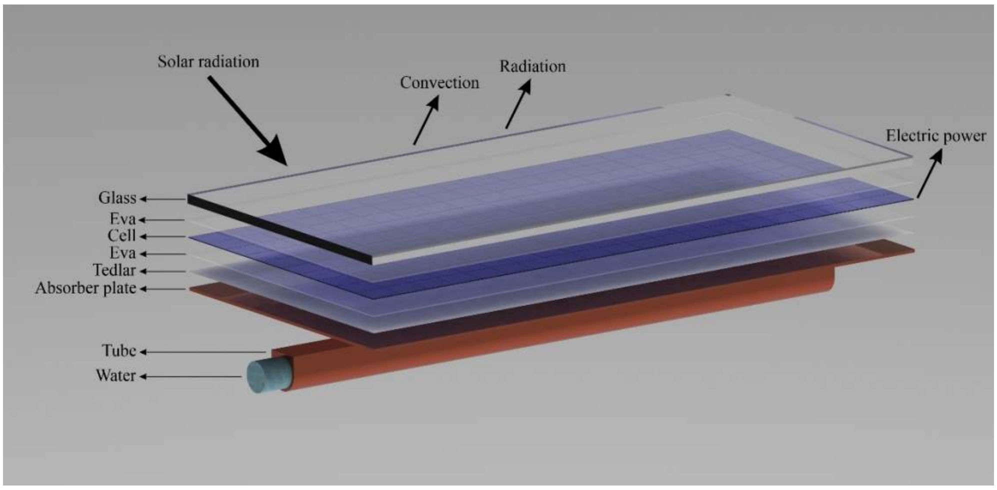

Figure 3.1. Schematic diagram of photovoltaic thermal collector

3.1.1. Parallel Tube PVT Collector Designs

Within the scope of this study, six parallel tube absorber designs (A, B, C, D, E and F) and ten different flow configurations were examined, as illustrated in Figure 3.2.

In configurations A, C1, C2, C3, and E, the tubes are arranged vertically, whereas in configurations B, D1, D2, D3 and F the tubes are arranged horizontally. Among these configurations, Config A and Config B are the commonly utilized designs in the literature, both featuring a single inlet and outlet. In contrast, configurations C1, C2, C3, D1, D2 and D3 incorporated double fluid inlets, positioned in vertical or horizontal arrangements, allowing for enhanced fluid distribution. The key differences between these configurations arise from the position and direction of the fluid inlet, in addition to the vertical or horizontal tube arrangement. Configurations E and F are distinct in that they feature multiple inlets without any internal connection points, resulting in a different flow distribution compared to the other configurations.

Table 3.1. Thermophysical properties of PVT collector components (Aghakhani et al., 2022; Kazemian et al., 2021; Maadi et al., 2020; Michael et al., 2016; Yu et al., 2019)

Material	ρ (kg/m^3)	k (W/mK)	c_p (J/kgK)
Glass	2450	2	500
EVA	960	0.35	2090
PV cell	2329	148	700
Tedlar	1200	0.20	1250
Copper absorber plate	8978	387.6	381
Copper tube	8978	387.6	381

Table 3.2. Dimensions of PVT collector components (Eisapour et al., 2020; Hosseinzadeh et al., 2018; Khanjari et al., 2016; Nahar et al., 2017; Nasrin et al., 2018b)

Component	Dimensions (mm)
Glass	2000 x 1000 x 3
EVA	2000 x 1000 x 0.5
PV Cell	2000 x 1000 x 0.3
Tedlar	2000 x 1000 x 0.1
Copper absorber plate	2000 x 1000 x 1
Inner and outer diameter of copper tubes	10-12

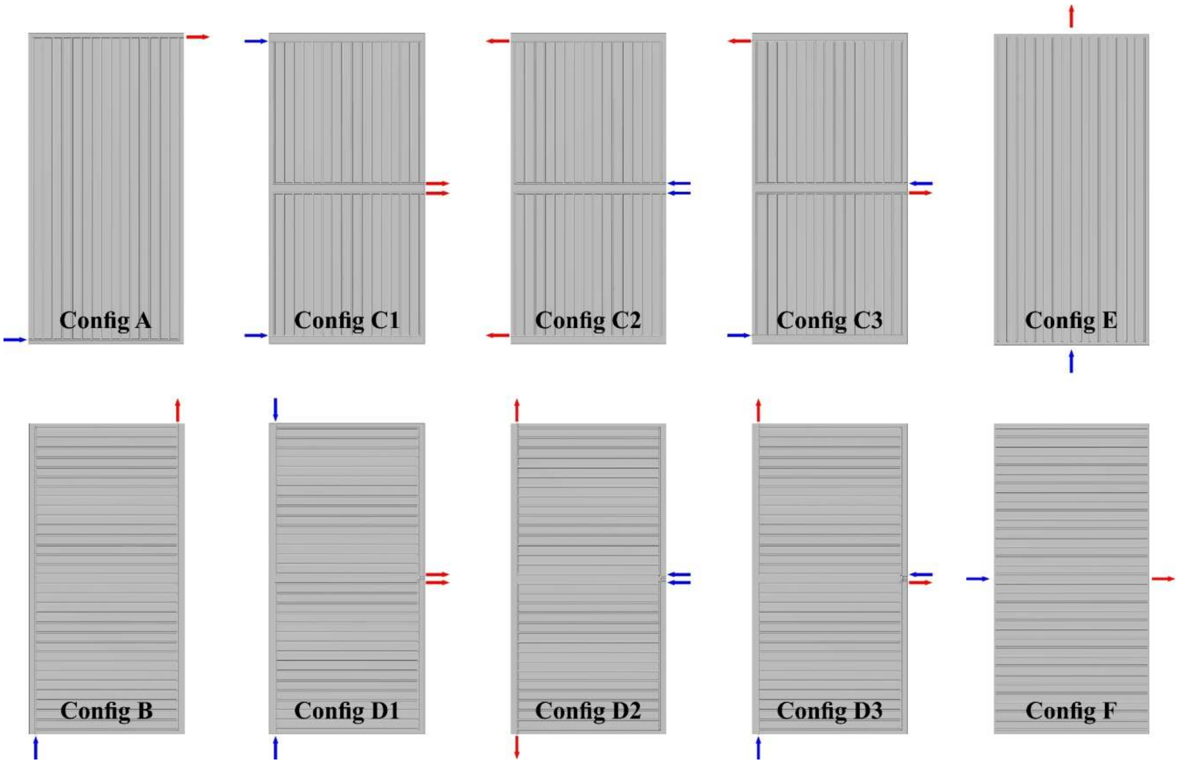

Figure 3.2. Different parallel tube PVT collector configurations

3.1.2. Serpentine Tube PVT Collector Designs

One of the commonly utilized designs for PVTs in literature is serpentine tube geometry. In this study, thirteen different serpentine-tube absorber designs (G, H, I, J, K, L, M, N, O, P, Q, R and S) and twenty-five flow configurations were compared.

The serpentine tube configurations presented in Figure 3.3 are categorized with their horizontal and vertical arrangement, single-inlet, double-inlet and triple-inlet arrangements, as well as their flow directions.

Configurations G and H are single-inlet absorber designs, arranged vertically and horizontally, respectively. Configurations I, J, M, O and P are double-inlet absorber designs, arranged vertically, and these flow configurations are distinguished from each other depending on the location and direction of the fluid inlet. On the other hand, configurations K, L, N and R are horizontally arranged absorber designs with double-inlet. Configurations S and Q are triple-inlet absorber designs, arranged vertically and horizontally, respectively.

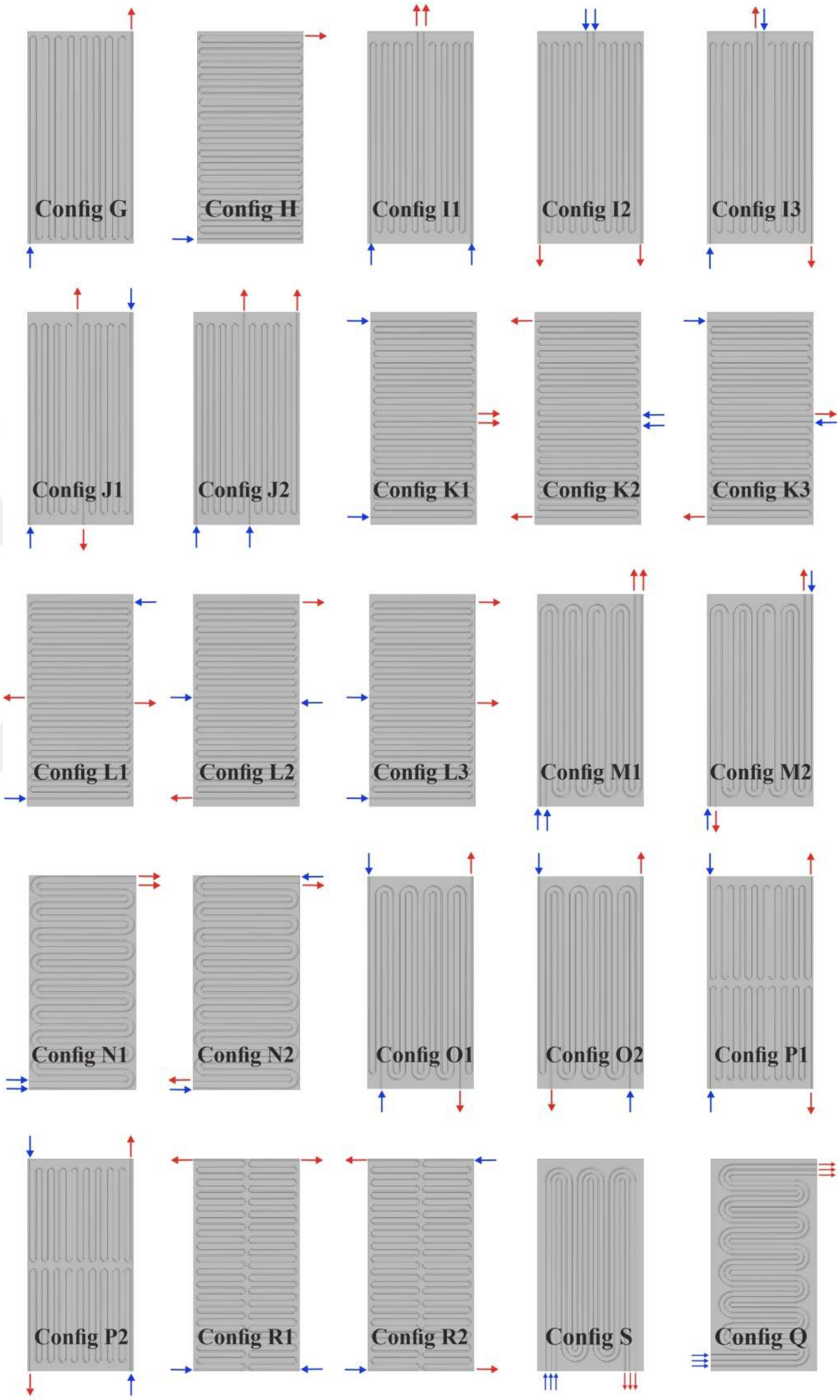

Figure 3.3. Different serpentine tube PVT collector configurations

3.1.3. Spiral Tube PVT Collector Designs

In addition to parallel and serpentine absorber designs, the spiral tube absorber designs are another commonly utilized geometry for PVTs. A total of seven distinct absorber designs (T, U, V, W, X, Y and Z) and twelve different flow configurations were analyzed. The spiral tube flow configurations, illustrated in Figure 3.4, are classified based on their single-inlet and double-inlet arrangements, as well as the number of helical structure, position and flow direction of the working fluid. Configurations T, U, V and W are single-inlet configurations, with their primary distinction arising from the helical structure within their internal design. Specifically, T and W configurations feature a single helical structure, whereas the U configuration incorporates a double helical structure. The V configuration, in contrast, employs four helical structures.

While double-helical designs include configurations X (X1, X2, X3), Y (Y1, Y2, Y3) and Z (Z1, Z2), X configurations serve as the double-helical counterpart of configuration T, with variations in the positioning and direction of fluid inlets. Similarly, configuration Y corresponds to the double-helical version of configuration U, while configuration Z represents the double-helical adaptation of configuration V.

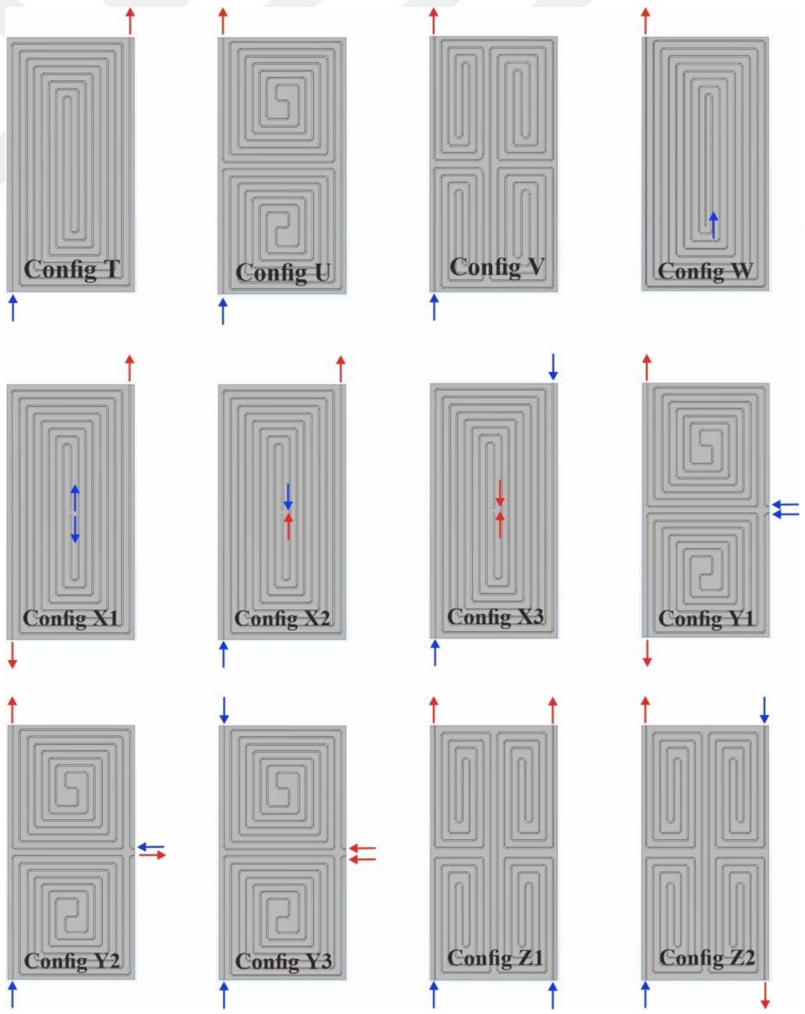

Figure 3.4. Different spiral tube PVT collector configurations

3.2. Numerical Procedure

The numerical modeling of the configurations developed in the study was carried out using the finite element method in COMSOL Multiphysics software version 6.2. The flow regime in the modeling is assumed to be laminar, the flow is incompressible and steady. For the analysis in COMSOL Multiphysics software, the *Laminar flow* and *Heat Transfer in Solids and Fluids* physics were used and combined in *Nonisothermal Multiphysics* model. The main assumptions in the numerical modeling were as follows (Olmuş et al., 2025a; Olmuş et al., 2025b):

- The surface of the PVT collector is completely clean, free of dust or any substances that might affect the absorption and reflection of solar radiation.
- Water is used as coolant.
- The transmissivity of EVA is approximately 100%.
- Thermophysical properties of water are temperature-dependent.
- Thermophysical properties of solid components are assumed to be independent of temperature. Given that temperature variations within the system are relatively small, the thermal properties of solid components, including density, thermal conductivity and specific heat are considered constant.
- The side and bottom surfaces of the PVT collector are fully insulated.
- Absorbed solar radiation is considered as the primary energy source for PV cells.
- The total flow rate through the tubes is constant across all configurations. In multi-inlet designs, the coolant flow is evenly distributed among the inlets, with the total flow rate being divided by the number of inlets.

Based on these assumptions, the governing equations were presented in this section. Conduction and convection heat transfer mechanisms were evaluated throughout all areas of the PVT collector. The heat transfer equations and laminar flow equations for the layers of the PVT collector (Figure 3.5) are presented in Eqs. 3.1-3.9 (Aghakhani et al., 2022; Nahar et al., 2019; Nasrin et al., 2018a; Sardarabadi and Passandideh-Fard, 2016). Left side of Eqs. 3.1-3.4 represents the heat conduction within the layer volume and the resulting thermal gradient, while the right side of the equation represents the thermal gains and losses acting on various surfaces of the related layer. Since the side and bottom surfaces of the PVT collector are assumed to be completely insulated, heat transfer occurs from the upper glass surface to the coolant below.

For the glass;

The first term on the right side of Eq. 3.1 is the absorbed solar irradiance by the glass layer, the second term is the convective heat transfer between the top surface of the glass layer and the ambient environment, the third term is the radiative heat transfer between the top surface of the glass layer and the surroundings, and the last term is the heat transfer from the glass layer to the PV cell (Olmuş et al., 2025a; Olmuş et al., 2025b).

$$-\left(\frac{k}{\rho c_p}\right)_g\left(\frac{\partial^2 T_g}{\partial x^2}+\frac{\partial^2 T_g}{\partial y^2}+\frac{\partial^2 T_g}{\partial z^2}\right)=\alpha_g I-U_{gamb}\left(T_g-T_{amb}\right)-$$
$$\varepsilon_g\sigma\left({T_g}^4-{T_{sky}}^4\right)-U_{gc}\left(T_g-T_c\right) \tag{3.1}$$

where, k is defined as the thermal conductivity, ρ as the density, c_p as the specific heat, T_g as the glass temperature, α_g as the absorptivity of glass, I as the solar irradiance, U_{gamb} as the heat transfer coefficient between the glass and environment, T_{amb} as the ambient temperature, ε_g as the emissivity of glass, σ as the Stefan-Boltzmann constant, T_{sky} as the sky temperature, U_{gtd} as the heat transfer coefficient between the glass and tedlar, and T_c as the cell temperature.

For the cell;

The first term on the right side of Eq. 3.2 is the energy absorbed by PV cell, the second term is the electricity produced by PV cell, the third term is the heat transfer between the PV cell and tedlar, and the last term is the heat transfer between PV cell and glass layer.

$$-\left(\frac{k}{\rho c_p}\right)_c\left(\frac{\partial^2 T_c}{\partial x^2}+\frac{\partial^2 T_c}{\partial y^2}+\frac{\partial^2 T_c}{\partial z^2}\right)=\alpha_c\tau_g I-\dot{E}_{el}-U_{ctd}(T_c-T_{td})-U_{gc}\left(T_c-T_g\right) \tag{3.2}$$

where, α_c denotes the absorptivity of cell, τ_g the transmissivity of glass, $\dot{E}_{el}$ the electricity production, T_{td} the tedlar temperature, U_{ctd} the heat transfer coefficient between the PV cell and tedlar.

For the tedlar;

The terms on the right side of Eq. 3.3 represent the heat transfer between the PV cell and the tedlar, and between the tedlar and tube, respectively.

$$-\left(\frac{k}{\rho c_p}\right)_{td}\left(\frac{\partial^2 T_{td}}{\partial x^2}+\frac{\partial^2 T_{td}}{\partial y^2}+\frac{\partial^2 T_{td}}{\partial z^2}\right)=-U_{ctd}(T_{td}-T_c)-U_{tdtu}(T_{td}-T_{tu}) \tag{3.3}$$

where, U_{tdtu} expresses the heat transfer coefficient between the tedlar and tube, T_{tu} the tube temperature.

For the tube;

The first term on the right side of Eq. 3.4 is the heat transfer between the tedlar and tube, and the second term is the heat transfer between the tube and fluid.

$$-\left(\frac{k}{\rho c_p}\right)_{tu}\left(\frac{\partial^2 T_{tu}}{\partial x^2}+\frac{\partial^2 T_{tu}}{\partial y^2}+\frac{\partial^2 T_{tu}}{\partial z^2}\right)=-U_{tdtu}(T_{tu}-T_{td})-U_{tuf}\left(T_{tu}-T_f\right) \tag{3.4}$$

where, U_{tdtu} is the heat transfer coefficient between the tedlar and tube, U_{tuf} the heat transfer coefficient between the tube and fluid, T_f the fluid temperature.

For the fluid domain, continuity (Eq. 3.5), momentum (Eqs. 3.6–3.8), and energy (Eq. 3.9) equations governing the laminar, steady and incompressible flow are expressed as:

$$\rho\left(\frac{\partial u}{\partial x}+\frac{\partial v}{\partial y}+\frac{\partial w}{\partial z}\right)=0 \tag{3.5}$$

$$\rho\left(u\frac{\partial u}{\partial x}+v\frac{\partial u}{\partial y}+w\frac{\partial u}{\partial z}\right)=-\frac{\partial p}{\partial x}+\mu\left(\frac{\partial^2 u}{\partial x^2}+\frac{\partial^2 u}{\partial y^2}+\frac{\partial^2 u}{\partial z^2}\right) \tag{3.6}$$

$$\rho\left(u\frac{\partial v}{\partial x}+v\frac{\partial v}{\partial y}+w\frac{\partial v}{\partial z}\right)=-\frac{\partial p}{\partial y}+\mu\left(\frac{\partial^2 v}{\partial x^2}+\frac{\partial^2 v}{\partial y^2}+\frac{\partial^2 v}{\partial z^2}\right) \tag{3.7}$$

$$\rho\left(u\frac{\partial w}{\partial x}+v\frac{\partial w}{\partial y}+w\frac{\partial w}{\partial z}\right)=-\frac{\partial p}{\partial z}+\mu\left(\frac{\partial^2 w}{\partial x^2}+\frac{\partial^2 w}{\partial y^2}+\frac{\partial^2 w}{\partial z^2}\right) \tag{3.8}$$

$$(\rho c_p)\left(u\frac{\partial T}{\partial x}+v\frac{\partial T}{\partial y}+w\frac{\partial T}{\partial z}\right)=k\left(\frac{\partial^2 T}{\partial x^2}+\frac{\partial^2 T}{\partial y^2}+\frac{\partial^2 T}{\partial z^2}\right) \tag{3.9}$$

where, u, v, w are the components of velocity vector, P the pressure, μ the dynamic viscosity of fluid. The finite element method (FEM) is used to solve the energy, momentum and continuity equations in COMSOL Multiphysics under steady-state, laminar and incompressible flow assumptions. A segregated solution approach was employed, in which the fluid flow and heat transfer equations were solved sequentially. Besides, the resulting nonlinear algebraic system was treated within a Newton-based solution framework. For each segregated step, the linearized systems were solved using a GMRES iterative solver combined with an algebraic multigrid (AMG) preconditioner.

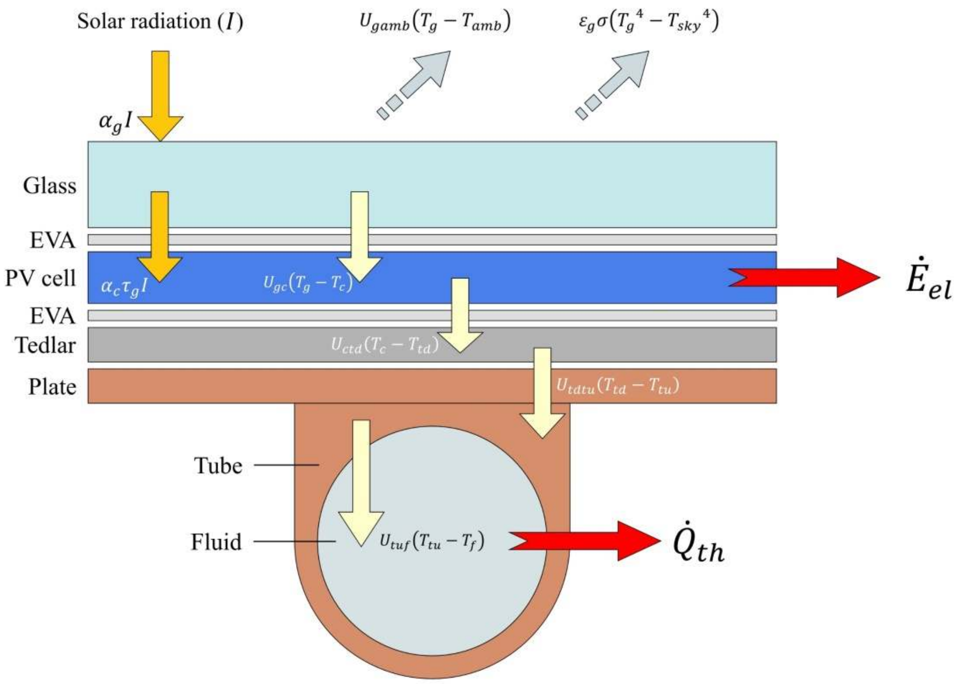

Figure 3.5. Section view and heat transfer processes in the layers of a PVT collector

3.3. Boundary Conditions

The boundary conditions of numerical model were expressed as follows:

- All external walls are insulated except for the top surface of the PVT collector:

$$-n \cdot (-k \cdot \nabla T) = 0 \tag{3.10}$$

where, n denotes the surface normal, k the thermal conductivity, ∇ the vector differential operator, T the temperature.

- At the tube inlet, uniform flow rate and fluid inlet temperature boundary conditions were applied. Some configurations feature a single inlet, while others have multiple inlets. For the cases with multiple inlets, the total mass flow rate is distributed equally among all inlets:

$$\dot{m} = \dot{m}_{in} \tag{3.11}$$

$$T = T_{in} \tag{3.12}$$

- Constant pressure outlet boundary condition was used at the tube outlet.

$$P_{out} = 0 \tag{3.13}$$

- There is a no-slip condition at all solid boundaries of the tube:

$$u = 0\,, v = 0, w = 0 \tag{3.14}$$

- Heat transfer between solid surfaces and fluid:

$$k_{solid}\left(\frac{\partial T}{\partial n}\right)_{solid} = k_{fluid}\left(\frac{\partial T}{\partial n}\right)_{fluid} \tag{3.15}$$

Inward heat flux occurs on the top surface of the glass. Heat losses are considered to occur from the upper surface of the glass to the environment through both convection and radiation.

- Convective heat loss was calculated on the top surface of PVT as follows:

$$-n \cdot q = h_{gamb} \cdot \left(T_{amb} - T_g\right) \tag{3.16}$$

where, q is heat flux vector.

- Radiation heat loss was calculated on the top surface of PVT using Eq. 3.17.

$$-n \cdot q = \varepsilon \cdot \sigma \cdot \left({T_{sky}}^4 - {T_g}^4\right) \tag{3.17}$$

3.4. Energy Analysis

Energy analysis was performed on the PVT collector to determine the total energy gain based on the first law of thermodynamics. In this study, the PVT collector was analyzed as a control volume under steady-state conditions. The incident solar radiation encompasses losses due to convection between the PVT collector surface and the surrounding environment, and the radiation losses on the PVT collector surface, as well as the production of electrical and thermal energy. The energy balance equation for the PVT collector was expressed as follows:

$$\sum \dot{E}_{in} = \sum \dot{E}_{prod} + \sum \dot{Q}_{loss} \tag{3.18}$$

$$\dot{E}_{abs} + \dot{E}_{mass,in} = \dot{E}_{el} + \dot{E}_{mass,out} + \dot{Q}_{loss} \tag{3.19}$$

Solar radiation absorbed by the PVT collector depends on several factors: the incident solar irradiance (*I*), the transmissivity of the glass ($\tau_g = 0.96$), the absorptivity of the PV cell ($\alpha_c = 0.9$), the packing factor ($p_c = 0.9$), and the area of the PVT collector (A_{PVT}). The energy absorbed by PV cell was calculated using Eq. 3.20 (Aghakhani et al., 2022):

$$\dot{E}_{abs} = I \cdot \tau_g \cdot \alpha_c \cdot p_c \cdot A_{PVT} \tag{3.20}$$

Heat losses occur from the upper surface of the PVT collector to the environment by convection and radiation:

$$\dot{Q}_{loss} = \dot{Q}_{con} + \dot{Q}_{rad} \tag{3.21}$$

Convective heat loss varies depending on the heat transfer coefficient (*h*), and the heat transfer coefficient varies depending on the wind velocity (V_{wind}). Convective heat loss and heat transfer coefficient were calculated according to Eqs. 3.22 and 3.23 (McAdams, 1954).

$$\dot{Q}_{con} = h \cdot (T_g - T_{amb}) \cdot A_{PVT} \tag{3.22}$$

$$h = 5.67 + 3.86 \cdot V_{wind} \tag{3.23}$$

where, *h* is the heat transfer coefficient, valid for wind velocity ranging from 0 to 10 m/s.

Heat losses due to radiation were calculated according to Eq. 3.24. The emissivity of the glass (ε) was taken as 0.9 in this study, σ is the Stefan-Boltzmann constant (5.67×10^{-8} W/m^2K^4). Sky temperature was calculated as in Eq. 3.25 depending on the ambient temperature (Swinbank, 1963).

$$\dot{Q}_{rad} = \varepsilon_g \cdot \sigma \cdot ({T_g}^4 - {T_{sky}}^4) \cdot A_{PVT} \tag{3.24}$$

$$T_{sky} = 0.0552 \cdot {T_{amb}}^{1.5} \tag{3.25}$$

Electrical energy produced by the PVT collector was calculated based on the electrical efficiency of the PV cell (η_{el}), as described in Eq. 3.26.

$$\dot{E}_{el} = \dot{E}_{abs} \cdot \eta_{el} \tag{3.26}$$

Electrical efficiency of the PVT collector varies depending on the PV cell surface temperature and was calculated according to Eq. 3.27 (Dehghan et al., 2024). In the equation, η_{ref}, T_{ref} and β_{ref} represent the reference efficiency of the PV cell under standard test conditions (I=1000 W/m^2 and T_{ref}=25 °C), the reference temperature, and the temperature coefficient, respectively. The temperature coefficient varies depending on the cell material. In the numerical analysis, the PV cell temperature was obtained from the numerical simulations, and the electrical efficiency of the PV cell was then calculated through post-processing.

$$\eta_{el} = \eta_{ref} \cdot \left[1 - \beta_{ref} \cdot \left(T_c - T_{ref}\right)\right] \tag{3.27}$$

Thermal energy produced by the PVT collector depends on the water flow rate ($\dot{m}_w$), specific heat ($c_{p,w}$) and the water inlet and outlet temperatures, and was calculated according to Eq. 3.28.

$$\dot{E}_{mass,out} - \dot{E}_{mass,in} = \dot{Q}_{th} = \dot{m}_w \cdot c_{p,w} \cdot \left(T_{w,out} - T_{w,in}\right) \tag{3.28}$$

3.5. Performance Parameters

The performance of a PVT collector is commonly assessed by researchers through calculations of thermal and electrical efficiencies. In this study, water outlet and PV cell temperature and pressure drop were obtained from numerical analysis results, and performance parameters were calculated through post-processing. The thermal efficiency (η_{th}) was defined as the ratio of thermal energy production to the energy absorbed by PV cell, while electrical efficiency (η_{el}) was defined as the ratio of electrical power output to the energy absorbed by PV cell. These efficiencies were calculated using Eqs. 3.29 and 3.30, respectively. The pumping energy demand was considered negligible in relation to the energy production due to its low consumption.

$$\eta_{th} = \frac{\dot{Q}_{th}}{\dot{E}_{abs}} \tag{3.29}$$

$$\eta_{el} = \frac{\dot{E}_{el}}{\dot{E}_{abs}} \tag{3.30}$$

Researchers often define the overall efficiency of a PVT collector by combining thermal and electrical efficiencies. The overall efficiency (η_{ov}) of the PVT collector was determined as the sum of its thermal and electrical efficiencies:

$$\eta_{ov} = \eta_{th} + \eta_{el} \tag{3.31}$$

However, it is important to recognize that the electrical energy generated by the PVT collector is a higher-grade form of energy compared to the thermal energy produced. To appropriately compare these two forms of energy, the efficiency of a PVT collector is often assessed using the concept of primary energy saving efficiency (PES). This approach allows for a more accurate comparison based on the first law of thermodynamics. The electrical energy can be converted into its thermal equivalent using a coefficient of 0.38, which represents the electrical energy production efficiency (η_f) of a conventional power plant. The primary energy saving efficiency of the PVT collector can thus be calculated as follows (Menon et al., 2022):

$$\eta_{PES} = \eta_{th} + \frac{\eta_{el}}{\eta_f} \tag{3.32}$$

3.6. Exergy Analysis

The basic performance parameters of the PVT collector, namely thermal, electrical and primary energy saving efficiencies, are based on the first law of thermodynamics, which focuses on the quantity of energy. In this study, an exergy analysis combining the first and second laws of thermodynamics, which measure the quality as well as the quantity of energy, was also performed. The exergy analysis of the PVT collector includes the exergy of solar radiation, thermal ($\dot{X}_{th}$), electrical ($\dot{X}_{el}$) and output exergies ($\dot{X}_{out}$), and exergy losses ($\dot{X}_{loss}$). The exergy balance for PVT collectors can be expressed as follows (Sreekumar et al., 2022):

$$\sum \dot{X}_{in} = \sum \dot{X}_{out} + \sum \dot{X}_{loss} \tag{3.33}$$

$$\dot{X}_{sun} = \left(\dot{X}_{mass,out} - \dot{X}_{mass,in}\right) + \dot{X}_{el} + \dot{X}_{loss} \tag{3.34}$$

Here, $\dot{X}_{sun}$, the input exergy represents the exergy of solar radiation incident on the PVT collector.

Various models are available for calculating the solar exergy input to such systems. One of the commonly used models for assessing the exergy of radiation is the model of Petela-Landsberg-Press (PLP) (Landsberg and Mallinson, 1976; Petela, 1964; Press, 1976). Radiation exergy is influenced by the type of emitting body and radiation in the environment, which depends on the type of absorber. PLP formula provides accurate prediction of radiation exergy for incident fully concentrated blackbody radiation and blackbody absorbers. However, for scenarios involving non-blackbody absorber such as selective absorber and photovoltaic cell, the radiation in the environment depends on the type of absorber (Badescu, 2008; Badescu, 2015). In this study, given the unconcentrated radiation and non-blackbody conditions such as PVT collectors, the formula proposed by Badescu (2008) was employed to calculate the inlet exergy, as defined by Eq. 3.35. The i_3 and j_2 functions given in the Eq. 3.35 can be calculated using the Eqs. 3.36-3.40. The input exergy depends on the solar irradiance and the PVT collector area as well as the ambient temperature and the sun temperature (T_{sun}=5777 K).

$$\dot{X}_{sun} = I \cdot A_{PVT} \cdot \left[1 - \frac{4}{3} \cdot \left(\frac{T_{amb}}{T_{sun}}\right) - \left(\frac{i_3(x_{\mu0}, x_{g0}, \infty) + j_2(x_{\mu0}, x_{g0}, \infty)}{6.4939}\right) \cdot \left(\frac{T_{amb}}{T_{sun}}\right)^4\right] \quad (3.35)$$

$$i_3(x_{\mu0}, x_{g0}, \infty) = \int_{x_{g0}}^{\infty} \frac{x^3 dx}{\exp(x - x_{\mu0}) - 1} \quad (3.36)$$

$$j_2(x_{\mu0}, x_{g0}, \infty) = \int_{x_{g0}}^{\infty} \{\tilde{n}(x) ln[\tilde{n}(x)] - [1 + \tilde{n}(x)] ln[1 + \tilde{n}(x)]\} x^2 dx \quad (3.37)$$

$$\tilde{n}(x) = [exp(x - x_{\mu0}) - 1]^{-1} \quad (3.38)$$

$$x_{g0} = \frac{e_g}{kT_c} \quad (3.39)$$

$$x_{\mu0} = \frac{qV^0}{kT_c} \quad (3.40)$$

where, e_g and V^0 express the band-gap energy and voltage across the cell, respectively.

Total output exergy ($\dot{X}_{out}$) from the PVT collector was calculated by combining the thermal ($\dot{X}_{th}$) and electrical exergy ($\dot{X}_{el}$) (Arslan et al., 2020).

$$\dot{X}_{out} = \dot{X}_{th} + \dot{X}_{el} \quad (3.41)$$

Thermal exergy of the PVT collector represents the useful thermal energy carried by the liquid from the absorber and is related to the inlet and outlet temperatures of the water and the ambient temperature. Thermal exergy is typically expressed as follows:

$$\dot{X}_{mass,out} - \dot{X}_{mass,in} = \dot{X}_{th} \quad (3.42)$$

where, $\dot{X}_{mass,in}$ and $\dot{X}_{mass,out}$ are exergy inlet and outlet of the working fluid, the $\dot{m}_w$ is the flow rate of the water.

Then, thermal exergy can be calculated as (Abdalla and Shahsavar, 2023; Prakash et al., 2024; Song et al., 2023):

$$\dot{X}_{th} = \dot{m}_w \cdot c_{p,w} \cdot (T_{w,out} - T_{w,in}) \cdot \left(1 - \frac{T_{amb}}{T_{w,out}}\right) \quad (3.43)$$

Since electrical energy is completely convertible, the electrical exergy output is equivalent to the electrical energy itself (Eq. 3.44) (Büyükalaca et al., 2023; Zou et al., 2024).

$$\dot{X}_{el} = \dot{E}_{el} \tag{3.44}$$

Exergy efficiency was defined as the ratio of the total exergy output of the PVT collector to the exergy input from the sun. It provides a measure of how effectively the PVT collector converts the available solar exergy into useful work. The exergy efficiency (η_{ex}) can be calculated using the following equation (Khan et al., 2024):

$$\eta_{ex} = \frac{\dot{X}_{out}}{\dot{X}_{sun}} = 1 - \frac{\dot{X}_{loss}}{\dot{X}_{sun}} \tag{3.45}$$

Sankey diagram of a typical PVT collector configuration is illustrated in Figure 3.6 for energy and exergy balance.

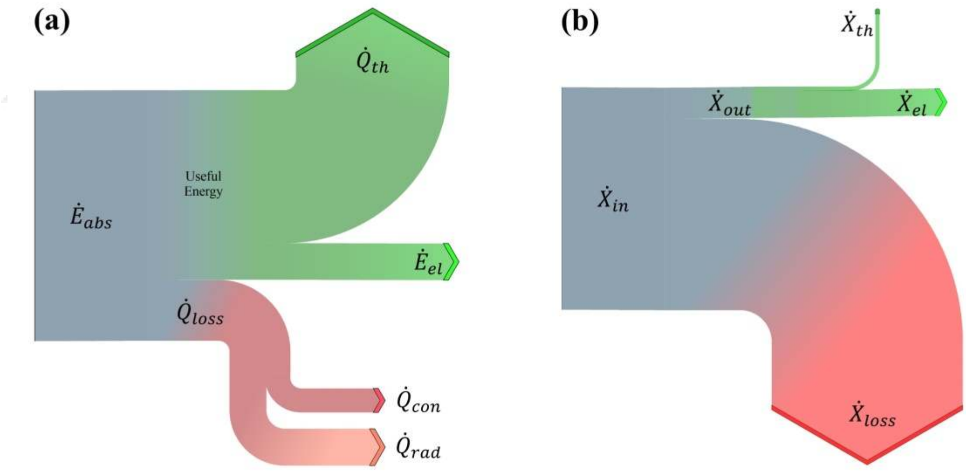

Figure 3.6. Sankey diagram of PVT collector for energy (a) and exergy (b) balance under typical operational conditions

3.7. Mesh Independency Test

In this study, mesh independence tests were conducted to the configurations studied to increase the accuracy of the analyses and time saving of the numerical analysis using COMSOL Multiphysics. Free tetrahedral mesh structure was applied at the boundaries of the copper tubes and fluid domains within the PVT collector, and free triangular mesh was used for the remaining layers for all PVT collector configurations. In addition, a boundary layer mesh was also applied close to the tube walls within the fluid domain. During the mesh independence tests for all PVT collector configurations, solar irradiance was taken as 1000 W/m^2, ambient air temperature as 25 °C, water inlet temperature as 20 °C, wind velocity as 1 m/s and water flow rate as 20 L/h on the base-case conditions (Table 3.3).

Table 3.3. Input parameters used in numerical analysis

Inlet Parameter	Unit	Base-case	Variable
$\dot{V}$	L/h	20	5-50
I	W/m^2	1000	200-1200
T_{amb}	°C	25	15-40
$T_{w,in}$	°C	20	10-40
V_{wind}	m/s	1	1-5

Mesh independence test was evaluated by examining the average PV cell temperature, water outlet temperature and pressure drop for all PVT designs, with examples provided for two configurations each from the parallel, serpentine and spiral designs. The mesh independence test was implemented with 6 different grid elements ranging from 4,605,193 to 13,124,036, and the results are shown in Table 3.4 for vertically arranged parallel tube configuration A. It was observed that there was no significant change in the values of these three parameters when the mesh size was changed. As can be seen in the Table 3.4, the relative error decreased below 0.01% for the cell temperature, water outlet temperature and pressure drop at a mesh number 10,652,225. Thus, numerical analysis was carried out at a mesh number of 10,652,225 (Figure 3.7).

Table 3.4. Grid independency test and relative errors for Config A

Number of Elements	T_{cell} (°C)	RE %	$T_{w,out}$ (°C)	RE %	ΔP (Pa)	RE %
4,605,193	41.246	-	47.765	-	26.0480	-
6,991,838	41.173	0.18	47.859	0.20	24.7012	5.17
8,486,432	41.140	0.08	47.901	0.09	23.9419	3.07
10,652,225	41.141	0.00	47.900	0.00	23.9403	0.01
11,461,997	41.141	0.00	47.900	0.00	23.9423	0.01
13,124,036	41.141	0.00	47.899	0.00	23.9423	0.00

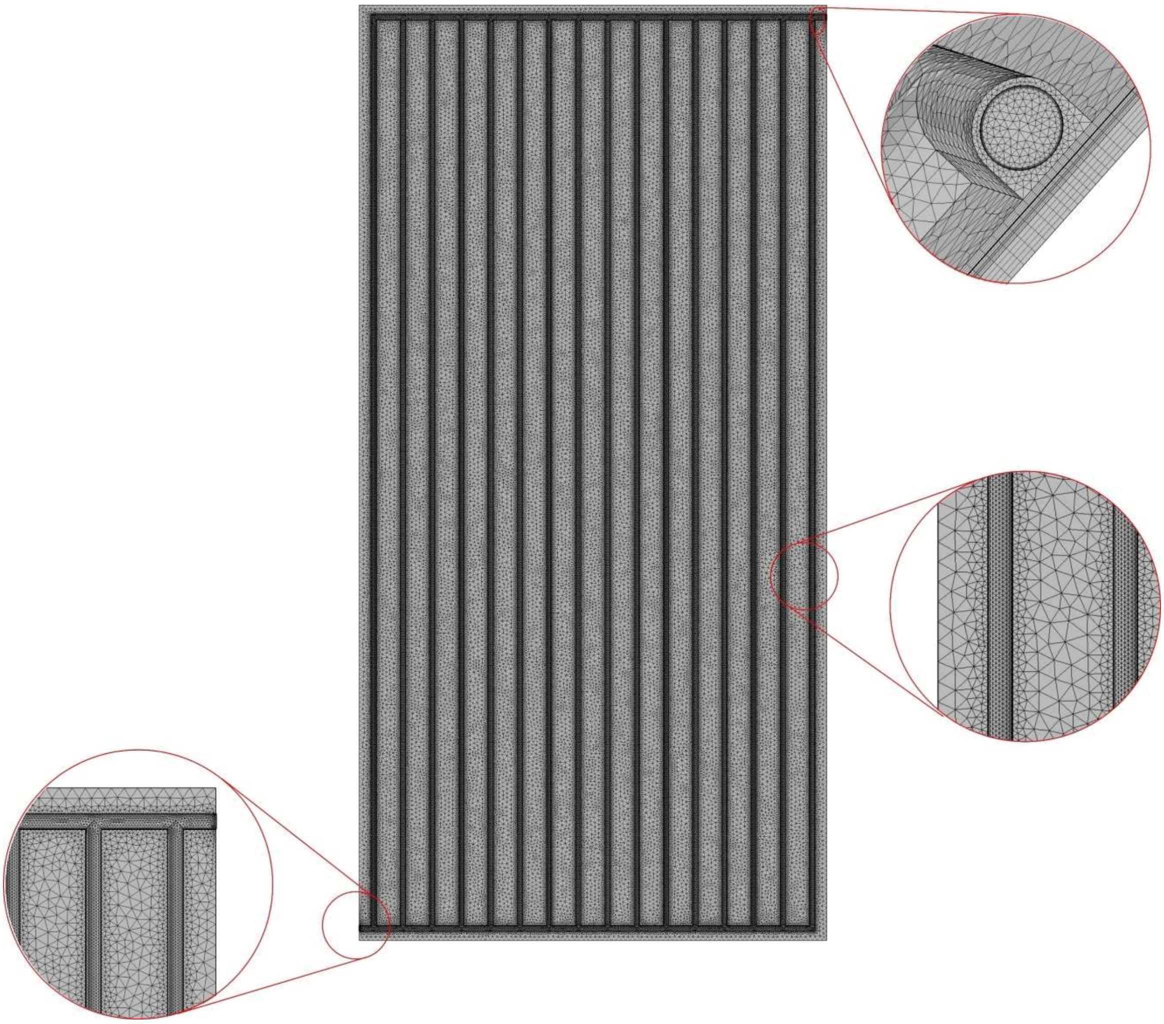

Figure 3.7. Finite element mesh for Config A

For horizontally arranged parallel tube Config B, the test was performed using six different mesh sizes, ranging from 6,179,353 to 12,314,617 elements, with the results presented in Table 3.5. The results showed that beyond a certain mesh size, further refinement had a negligible effect on the key parameters. As seen in the table, the relative error for cell temperature, water outlet temperature, and pressure drop dropped below 0.02% when the mesh size reached 10,329,848 elements. Therefore, to ensure both computational efficiency and accuracy, a mesh size of 10,329,848 elements was chosen for the numerical simulations of Config B (Figure 3.8).

Table 3.5. Grid independency test and relative errors for Config B

Number of Elements	T_{cell} (°C)	RE %	$T_{w,out}$ (°C)	RE %	ΔP (Pa)	RE %
6,179,353	44.010	-	44.642	-	42.443	-
7,909,913	44.228	0.50	43.720	2.07	39.934	5.91
9,189,548	44.498	0.61	43.522	0.45	39.011	2.31
10,329,848	44.498	0.00	43.523	0.00	39.002	0.02
11,324,328	44.499	0.00	43.523	0.00	39.010	0.02
12,314,617	44.500	0.00	43.524	0.00	39.049	0.10

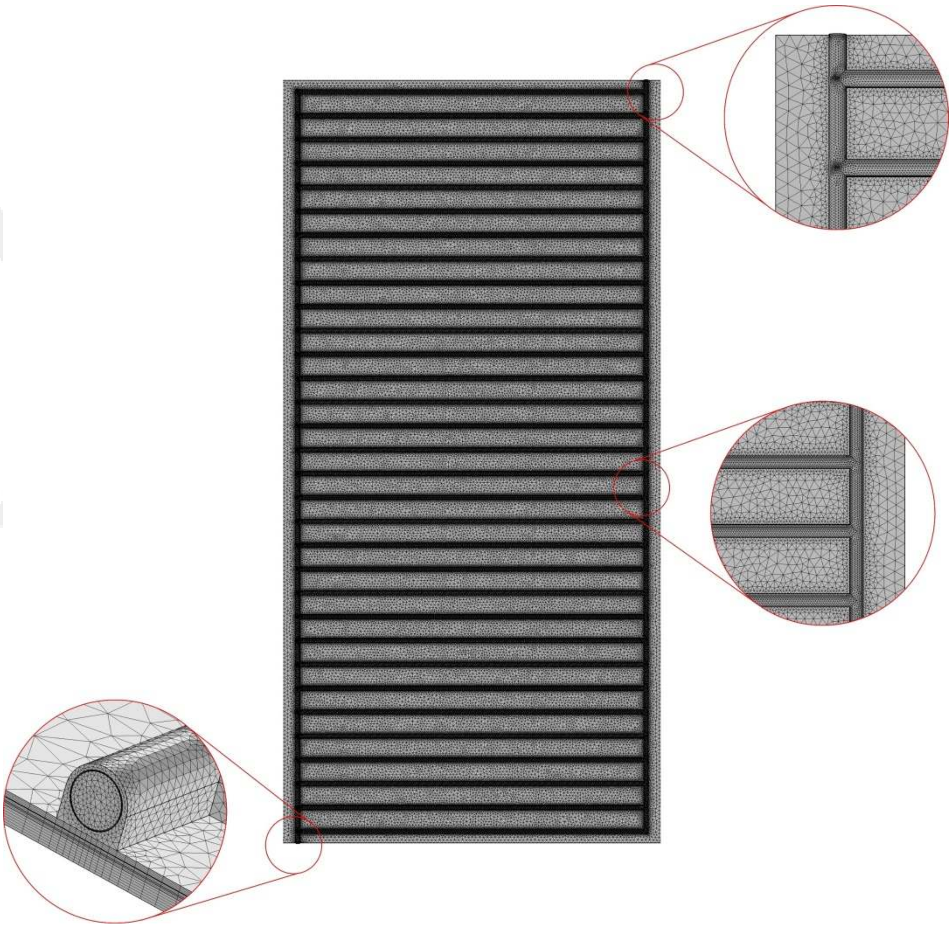

Figure 3.8. Finite element mesh for Config B

For configuration G, which is the vertically arranged serpentine tube configuration, mesh independence test was evaluated by examining the average PV cell temperature, water outlet temperature, and pressure drop across six different mesh sizes ranging from 5,784,355 to 14,395,233 elements. It was observed that varying the mesh size did not lead to significant changes in these three parameters. Specifically, as shown in Table 3.6, the differences between the mesh sizes of 9,421,183 and 14,395,233 were minimal. Based on these findings, the mesh with 10,435,630 elements was selected for further numerical analysis, as the relative errors for the average PV cell temperature, water outlet temperature, and pressure drop were reduced to 0.02%, 0.03%, and 0.01%, respectively (Figure 3.9).

Table 3.6. Grid independency test and relative errors for Config G

Number of Elements	T_{cell} (°C)	RE (%)	$T_{w,out}$ (°C)	RE (%)	ΔP (Pa)	RE (%)
5,784,355	41.364	-	47.739	-	754.852	-
6,867,029	41.181	0.44	47.940	0.42	784.539	3.93
9,421,183	40.981	0.49	48.185	0.51	789.561	0.64
10,435,630	40.974	0.02	48.199	0.03	789.640	0.01
12,952,974	40.976	0.00	48.201	0.00	790.892	0.16
14,395,233	40.974	0.00	48.202	0.00	789.892	0.13

For configuration H, which is the horizontally arranged serpentine tube configuration, the analysis was performed using six different mesh sizes, ranging from 5,825,002 to 14,438,004 elements, and the results are summarized in Table 3.7. The results demonstrated that further increasing the mesh size beyond a certain point had an insignificant effect on the computed values. As observed in the table, the relative error for cell temperature, water outlet temperature, and pressure drop dropped below 0.02% when the mesh size reached 10,579,789 elements. Consequently, a mesh size of 10,579,789 elements was selected for numerical simulations to achieve an optimal balance between accuracy and computational efficiency (Figure 3.10).

Table 3.7. Grid independency test and relative errors for Config H

Number of Elements	T_{cell} (°C)	RE (%)	$T_{w,out}$ (°C)	RE (%)	ΔP (Pa)	RE (%)
5,825,002	40.343	-	49.035	-	805.532	-
6,913,885	40.272	0.18	49.097	0.13	833.660	3.49
9,547,882	40.215	0.14	49.176	0.16	835.862	0.26
10,579,789	40.218	0.01	49.167	0.02	835.761	0.01
13,058,405	40.212	0.01	49.176	0.02	835.712	0.01
14,438,004	40.208	0.01	49.185	0.02	835.092	0.07

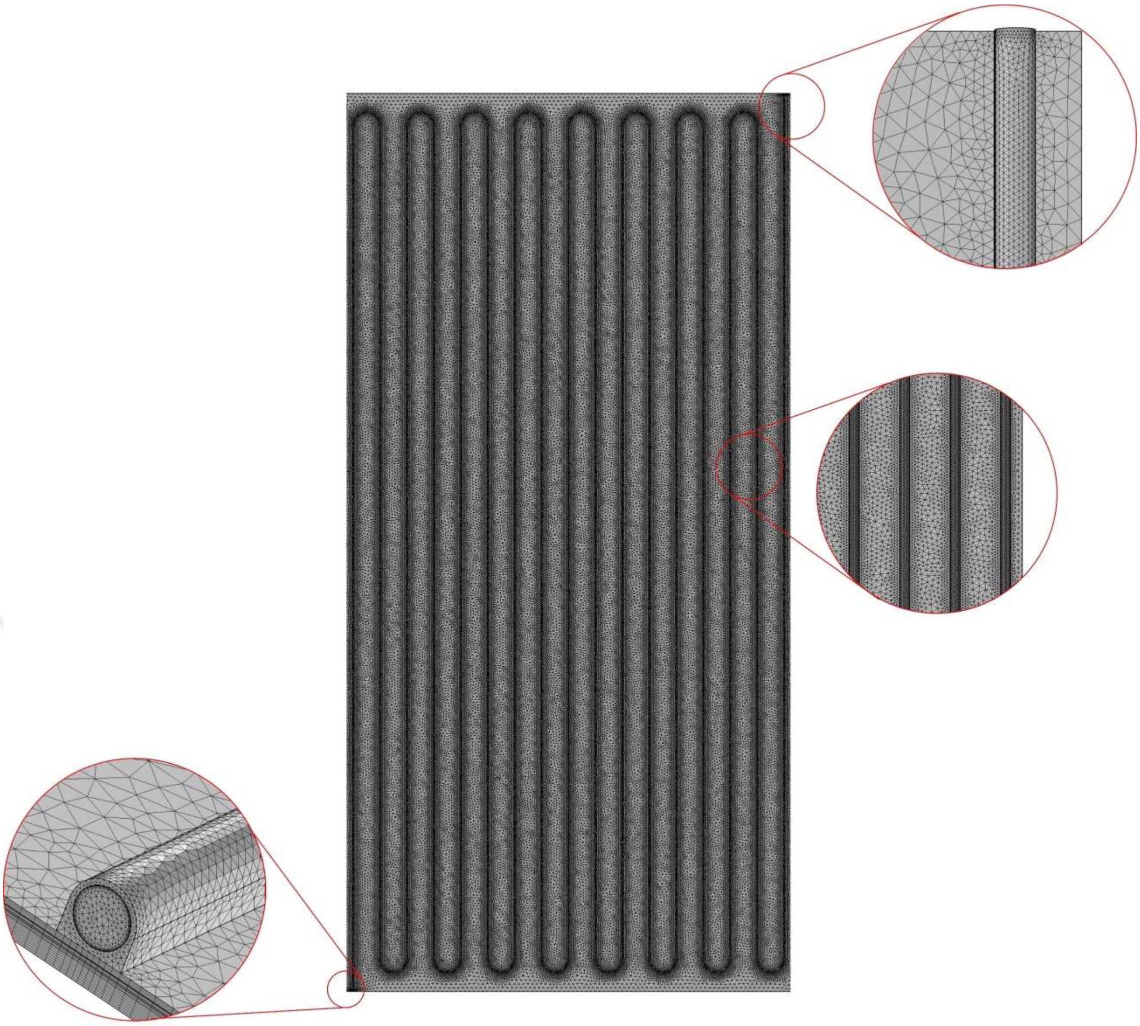

Figure 3.9. Finite element mesh of a Config G

The mesh independence test for configuration T, which is a spiral tube, single-inlet design, was conducted to investigate the influence of different mesh sizes on the average PV cell temperature, water outlet temperature and pressure drop. In this context, six different mesh sizes ranging from 5,685,775 to 18,045,740 elements were employed, and the results were presented in Table 3.8.

The analysis results indicated that beyond a certain mesh size, further refinement had an insignificant impact on the evaluated parameters. In particular, from the mesh size of 14,596,027 elements onwards (Figure 3.11), the relative error values for all parameters dropped below 0.01%. Therefore, to ensure an optimal balance between computational accuracy and processing time, the numerical simulations for configuration T were performed using this mesh size.

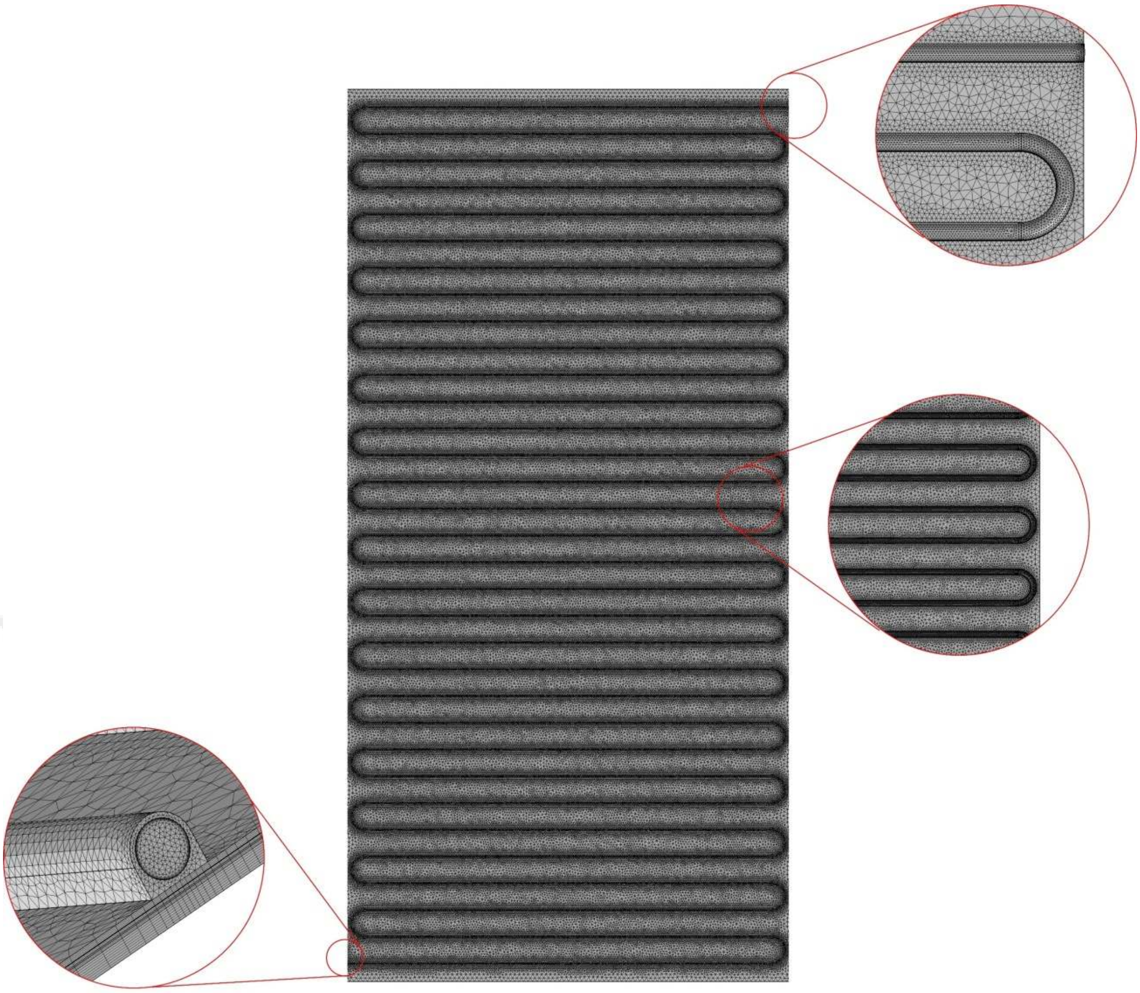

Figure 3.10. Finite element mesh of Config H

Table 3.8. Grid independency test and relative errors for Config T

Number of Elements	**T_{cell} (°C)**	**RE (%)**	**$T_{w,out}$ (°C)**	**RE (%)**	**ΔP (Pa)**	**RE (%)**
5,685,775	44.689	-	43.393	-	715.8596	-
8,696,356	44.915	0.51	43.006	0.89	778.2694	8.72
11,508,743	45.042	0.28	42.800	0.48	838.5699	7.75
14,596,027	45.054	0.03	42.785	0.04	838.6699	0.01
16,320,894	45.051	0.01	42.790	0.01	838.7298	0.01
18,045,740	45.045	0.01	42.793	0.01	838.7600	0.00

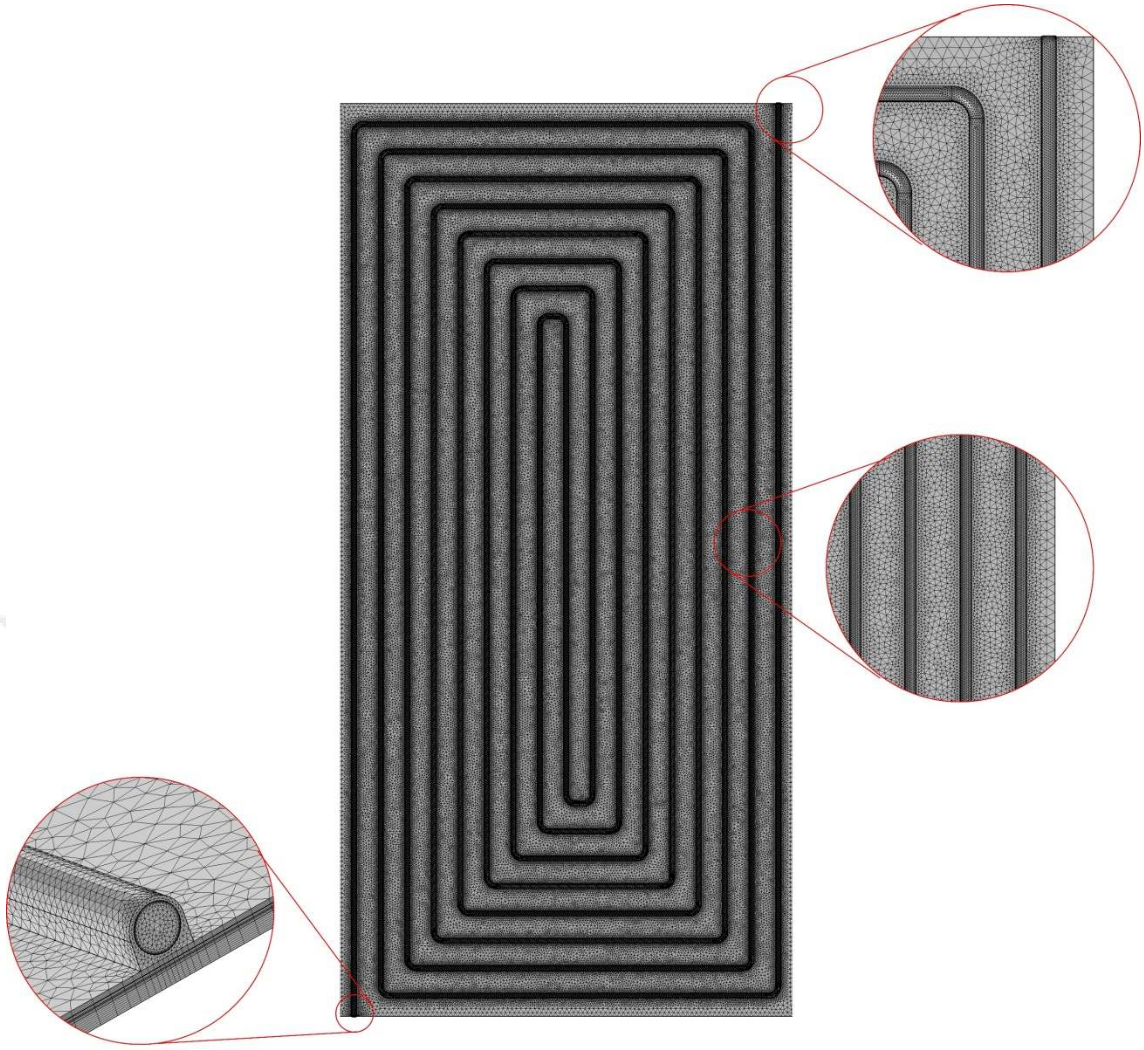

Figure 3.11. Finite element mesh of Config T

The mesh independence study was also conducted for configuration X1, a spiral tube and double-inlet design. Six mesh sizes were tested, ranging from 5,698,346 to 18,046,286 elements, as detailed in Table 3.9. The results revealed that although noticeable variations occur in the initial stages of mesh refinement, the changes in simulation outputs become negligible with finer meshes. From a mesh size of approximately 14.6 million elements onward, the relative errors in all monitored parameters dropped to or below 0.01%, indicating numerical convergence. Based on this observation, a mesh size of 14,596,027 elements was selected for subsequent simulations (Figure 3.12), providing a reliable balance between computational efficiency and accuracy.

Table 3.9. Grid independency test and relative errors for Config X1

Number of Elements	T_{cell} (°C)	RE (%)	$T_{w,out}$ (°C)	RE (%)	ΔP (Pa)	RE (%)
5,698,346	43.195	-	45.453	-	340.8052	-
8,692,348	42.722	1.10	46.045	1.30	370.4045	8.69
11,509,752	42.470	0.59	46.335	0.63	385.1250	3.97
14,596,027	42.465	0.01	46.333	0.00	385.1649	0.01
16,321,562	42.464	0.00	46.329	0.01	385.1729	0.00
18,046,286	42.462	0.00	46.326	0.01	385.1950	0.01

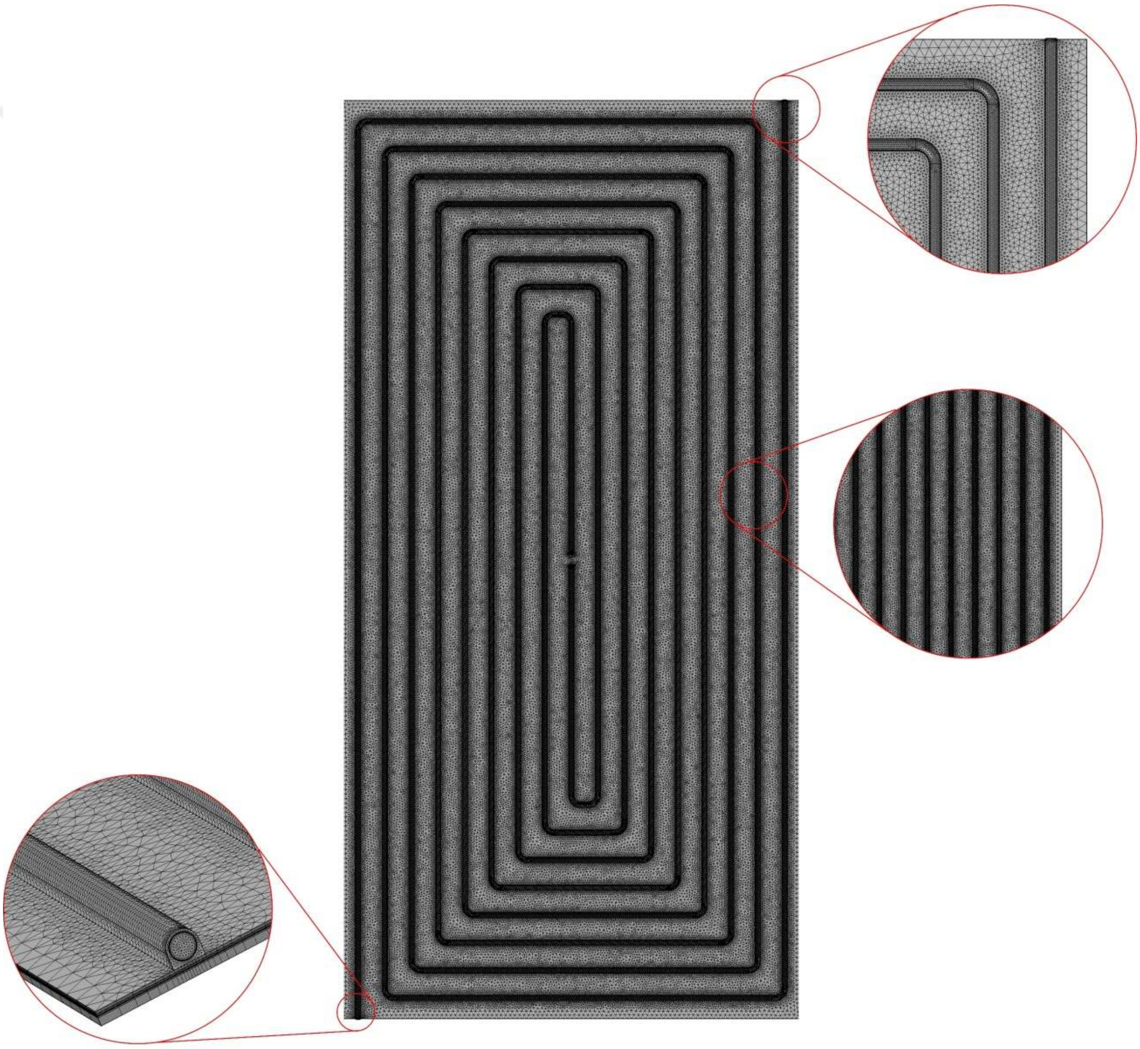

Figure 3.12. Finite element mesh of Config X1

3.8. Validation of Model

To verify the accuracy of the developed numerical model, validation was performed using four different experimental and numerical studies available in the literature. In order to ensure a robust comparison, the selected studies include serpentine, spiral tube and channel-based PVT collector designs. Among these, the geometries used in the validation correspond to configuration H and configuration V in the present study.

To validate the numerical model developed in this study, a simulation was conducted using a PVT collector with identical geometrical features and input parameters to those used in the experimental setup presented by Alous et al. (2019). In their study, the dimensions of the PVT collector were 380 × 675 × 20 mm, serpentine design with copper tubes having inner and outer diameters of 8 mm and 10 mm, respectively. The selected configuration corresponds to Config H, which adopts a serpentine tube design. The researchers presented various operating parameters such as solar radiation (450-920 W/m^2), water inlet temperature (25.4-36.7 °C), and ambient temperature (22.1-34.9 °C), as well as some measurement results on water outlet temperature and PVT surface temperature. The simulation results obtained using the present mathematical model were then compared with the experimental data reported in Alous's study. To assess the accuracy of the numerical model, the PVT surface temperature and water outlet temperature were selected as key parameters for validation (Figure 3.13). In the experimental study, the water flow rate was taken as 0.5 L/min, while solar irradiance, ambient temperature and water inlet temperature varied with time.

Upon examining the performance parameters, the maximum relative error for the PVT surface temperature was determined to be 7.15%, with an average relative error of 3.04% (Figure 3.13a). On the other hand, for the water outlet temperature, the maximum and average relative errors were 7.54% and 4.92%, respectively (Figure 3.13b). This comparison indicated that the results of the numerical model were in good agreement with the experimental data, validating the accuracy of model.

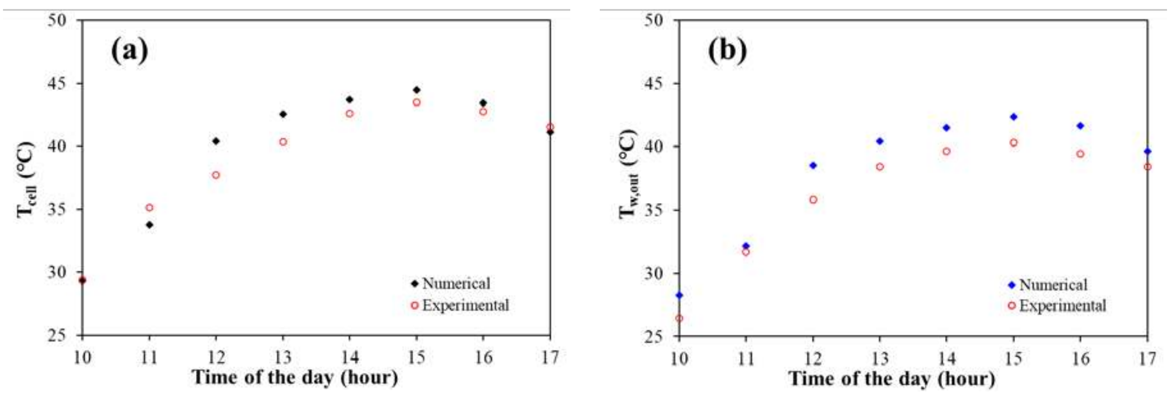

Figure 3.13. Validation of the numerical results with Alous et al. (2019)

The model was also validated using both experimental and numerical data obtained from the study conducted by Fayaz et al. (2019). In the research, a spiral tube design was employed, featuring tubes with a diameter of 10 mm and length of 35000 mm, constructed from aluminum and the PVT collector dimensions were 1984 × 997 mm. The design adopted in the study by Fayaz et al. (2019) is structurally similar to configuration V in the present work. A multi-walled carbon nanotube (MWCNT)-water nanofluid was utilized as the working fluid. Numerical analysis was carried out using COMSOL Multiphysics software. The study considered MWCNT-water nanofluid with a 0.75% weight fraction as the coolant, while the solar irradiance was set at 1000 W/m^2. The refrigerant flow rate was varied at 30, 60, 90 and 120 L/h, with the cell temperature and fluid outlet temperature serving as validation parameters.

The average relative error in the PVT cell temperature obtained from the mathematical model developed in this study was found to be 4% and 7%, respectively, according to the data obtained from experiments and numerical studies by the researchers (Figure 3.14a). The corresponding errors in the fluid outlet temperature were determined as 6.8% and 6%, respectively (Figure 3.14b).

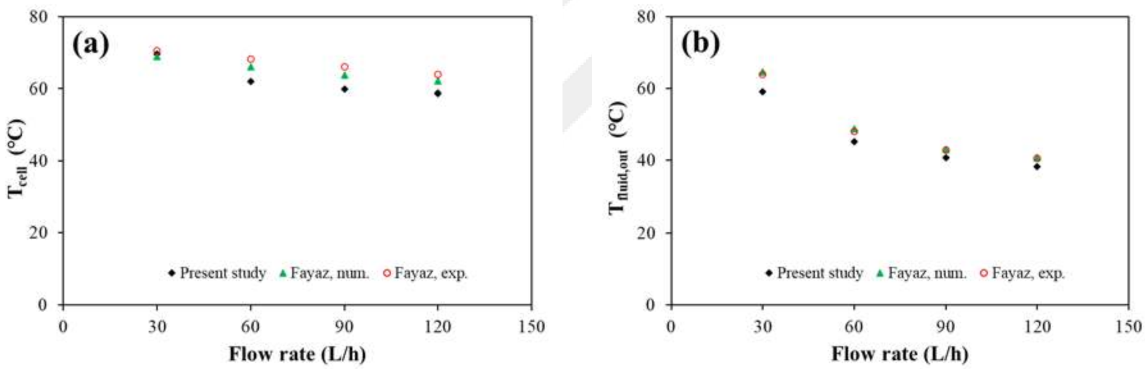

Figure 3.14. Validation of the numerical results with Fayaz et al. (2019)

Another study on spiral tube designs, conducted by Nasrin et al. (2018b), incorporates both experimental and numerical analyses. The spiral tube design investigated by Nasrin et al. (2018b) corresponds closely to Config V in the present analysis. The study was performed under indoor conditions, with both fluid and ambient temperatures set at 32 °C and solar irradiance maintained at 1000 W/m^2. MWCNT-water nanofluid was employed as the coolant, with a flow rate of 0.5 L/min, while the nanoparticle weight fraction varied between 0% and 1%. The validation parameters considered were PVT cell temperature and electrical efficiency. For the PVT cell temperature, the maximum and average relative errors between the mathematical model in this study and the experimental data from Nasrin et al. (2018b) were 3.8% and 2.25%, respectively, while the corresponding errors with respect to the numerical results from Nasrin et al. (2018b) were 2.4% and 1.2% (Figure 3.15a). In terms of electrical efficiency, the maximum and average relative errors were determined to be 1.57% and 0.92% when compared to experimental data, and 0.90% and 0.47% when compared to numerical results (Figure 3.15b).

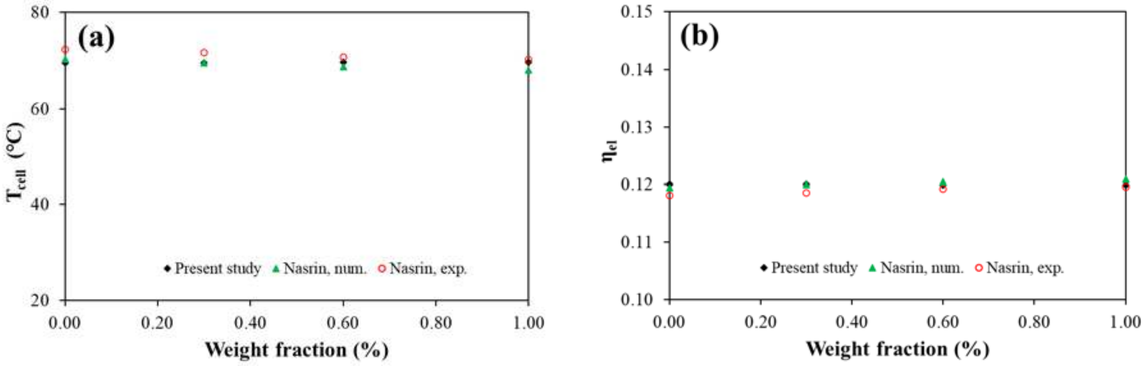

Figure 3.15. Validation of the numerical results with Nasrin et al. (2018b)

The numerical and experimental study conducted by Nahar et al. (2017), utilizing a channel-based design, was also used for validation. In the study, the dimension of the PVT collector is 1570x940 mm, while the dimension of the cooling channel is 1350x920 mm. Water was used as the coolant, with both the water inlet temperature and ambient temperature set at 34 °C. Solar irradiance was maintained at 1000 W/m^2, and the fluid inlet velocity varied between 0.0003 and 0.0007 m/s. Numerical simulations were carried out using COMSOL Multiphysics software. The validation parameters considered were PVT cell temperature and electrical efficiency. When the mathematical model developed in this study is compared with the experimental data, the maximum and average relative errors in PVT cell temperature were found to be 2.87% and 2.0%, respectively. In comparison with numerical results, these errors decreased to 2.1% and 0.7% (Figure 3.16a). Regarding electrical efficiency, the model showed maximum and average relative errors of 0.95% and 0.70% when compared to experimental data, while the corresponding errors with respect to numerical results were 0.75% and 0.24%, respectively (Figure 3.16b).

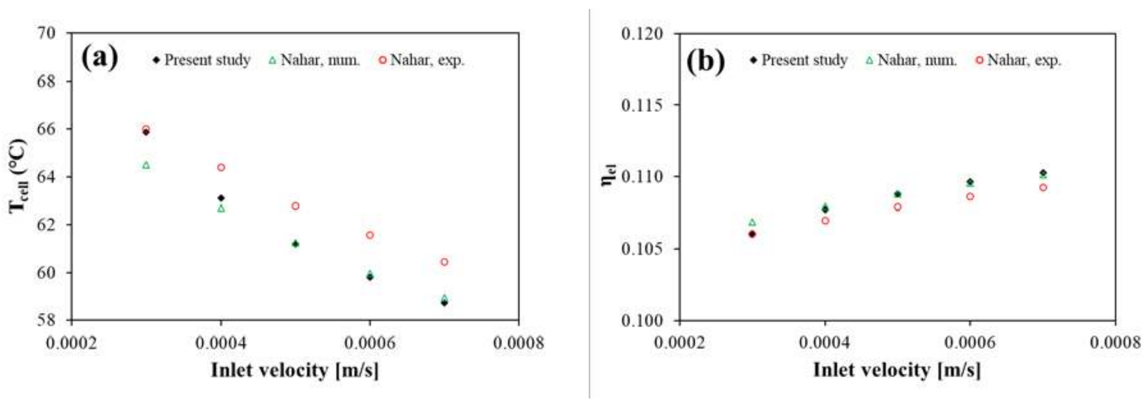

Figure 3.16. Validation of the numerical results with Nahar et al. (2017)

To assess the accuracy of the developed models, three studies containing both numerical and experimental results, along with one experimental study, were considered. The comparison results are presented in Figures 3.13 through 3.16. As shown in these figures, the predictions of the mathematical model exhibit strong agreement with both the experimental data and numerical results. These findings confirm that the developed numerical models are sufficiently accurate and reliable for simulating the thermal and electrical behavior of PVT collectors under various operating conditions.

4. RESULTS AND DISCUSSION

This study presents a numerical comparison of parallel, serpentine and spiral tube PVT collector configurations using COMSOL Multiphysics software. In order to evaluate their comparative performance, 47 different flow configurations including 26 different collector designs and a conventional PV panel were investigated.

This section analyzes different PVT collector configurations categorized into parallel, serpentine and spiral absorber designs. Their performance is assessed under the base-case and variable conditions specified in Table 3.3, considering key parameters such as fluid inlet temperature, fluid flow rate, solar irradiance, ambient temperature and wind velocity. The comparison of different PVT collector designs considers factors such as temperature distribution, cell and water outlet temperatures, thermal and electrical energy production, as well as thermal, electrical, overall and primary energy saving efficiencies. Furthermore, exergy analysis is performed, encompassing thermal, electrical and output exergy, exergy destruction and exergy efficiency.

4.1. Parallel Tube PVT Collector Configurations

This section presents comprehensive comparison of single-inlet vertical and horizontal, two-inlet vertical and horizontal, and multiple-inlet vertical and horizontal arranged configurations, with the same tube length by numerical methods with COMSOL Multiphysics software. These parallel tube PVT collectors were also compared with a conventional PV panel in terms of electrical performance. The research examines the effects of various parameters, including flow rate, solar irradiance, fluid inlet temperature, ambient temperature and wind velocity on the thermal, electrical, overall and primary energy saving efficiency, as well as on the exergetic performance of PVT collectors. Additionally, the surface temperature distribution of the PVT collector and the pressure drop across the configurations were analyzed. Under this section, various parallel tube PVT collector designs are systematically compared in terms of key performance parameters.

4.1.1. Comparison of Parallel Tube PVT Collector Configurations Under Base-case Conditions

Different parallel tube PVT collector configurations were compared based on various performance parameters under the base-case conditions in Table 3.3. To ensure a fair comparison, the tube length, absorber area and PVT collector area were kept the same in all configurations. Temperature distribution is as crucial as other performance parameters when selecting the appropriate design for PVT systems. Non-uniform temperature distribution is undesirable as it adversely affects the performance of PV cells, leading to reductions in the thermal, electrical and overall efficiencies of the PVT collector, as well as a decrease in power production. Moreover, non-uniform temperature distribution accelerates the degradation of PV cells.

The contours of the surface temperature distributions for different parallel tube PVT configurations are illustrated in Figure 4.1. As depicted, the temperature at the collector inlet is initially low as cold water enters the collector, but it gradually increases towards the collector outlet. Notably, Config E and F exhibit a more uniform temperature distribution compared to the other configurations. This uniformity is attributed to the even distribution of flow across the tubes in these configurations. Config A, another design with a single entrance, ranks as the third most uniform configuration in terms of temperature distribution, following configurations E and F. Conversely, Config B demonstrates the most non-uniform temperature distribution. Despite having the same tube length as the other configurations, the flow rate in Config B decreases towards the center of the PVT collector due to a high number of tubes, resulting in a maximum temperature in the middle of the collector.

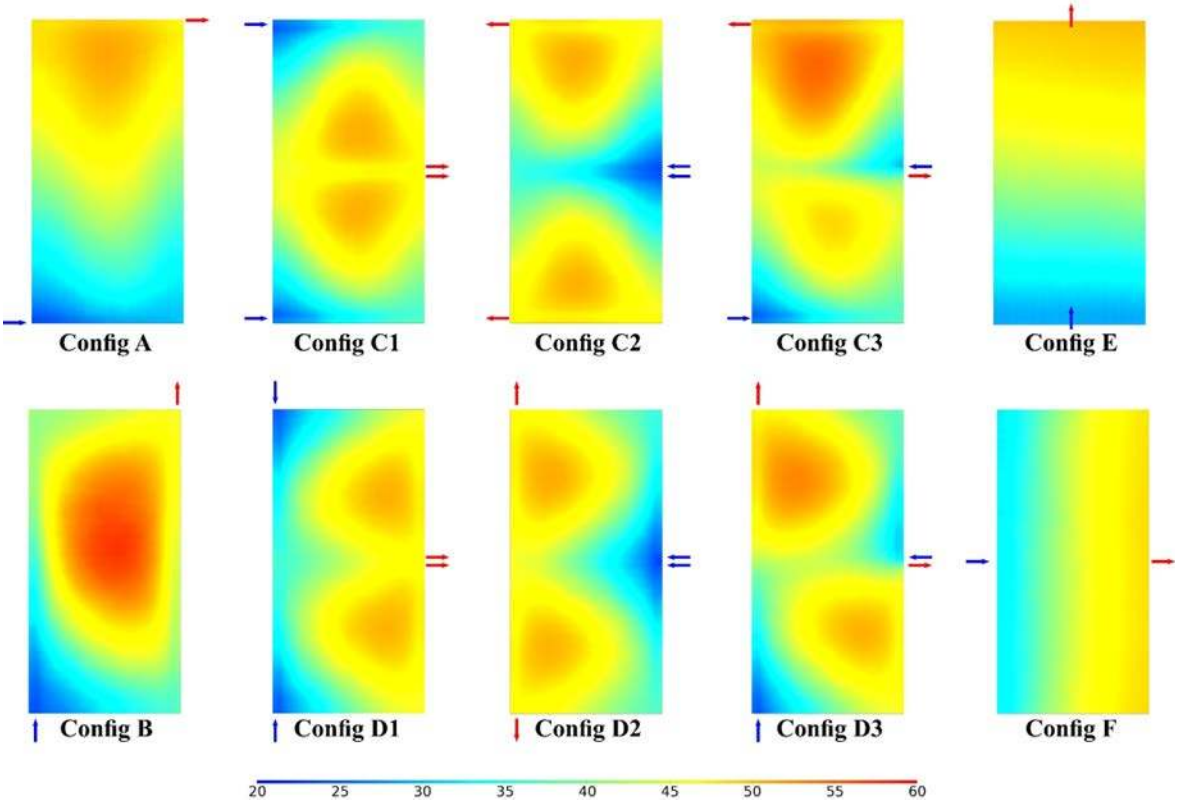

Figure 4.1. Surface temperature contour of different parallel tube PVT configurations under base-case conditions

Furthermore, Config E exhibits the lowest average cell temperature as seen in Figure 4.2a, whereas Config B demonstrates the highest cell temperature, similar to the temperature distribution pattern. Water outlet temperature is inversely related to the surface temperature as shown in Figure 4.2. When comparing Figure 4.2a and Figure 4.2b, it should be noted that Figure 4.2a represents the average surface temperature of the PV cell, while Figure 4.2b depicts the cross-sectionally averaged water outlet temperature at the outlet of the tube. The average surface temperature is lowest in Config E. When two-inlet collector designs (C1-C2-C3-D1-D2-D3) were considered, the cases where the fluid enters from the middle (Config C2 and D2) and from the sides (Config C1 and D1) in the same direction produced very similar results. In addition, these four designs performed better than the other two-inlet configurations, C3 and D3, which have both inlet and outlet at the same position. As observed, locating both an inlet and an outlet at the same position negatively impacts the results. A conventional PV panel was also analyzed, and as illustrated in Figure 4.2a, its cell temperature was higher than that of all parallel tube PVT configurations. The average surface temperature of the PV panel without cooling was measured at 61.8 °C, exceeding the cell temperatures of the PVT collectors by 17 to 21 °C.

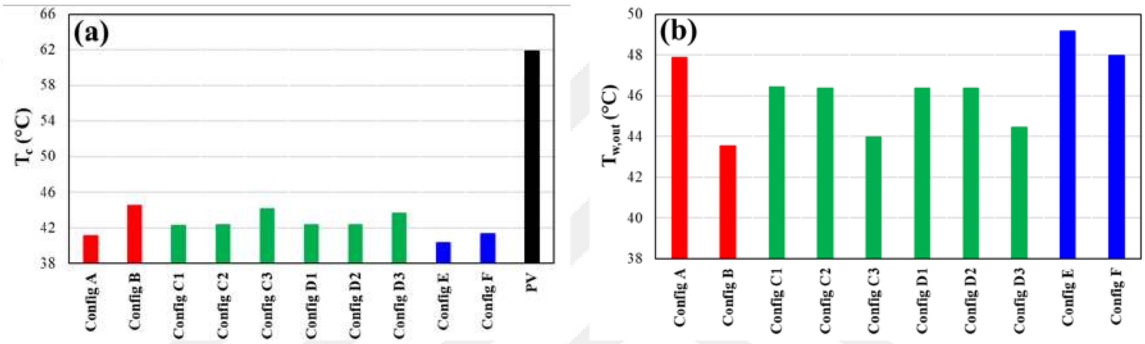

Figure 4.2. Average cell (a) and water outlet (b) temperature of different parallel tube PVT configurations under base-case conditions

Figure 4.3 compares the performance parameters of various parallel tube configurations under base-case conditions. In multi-inlet collectors (Config E and F), heat transfer is enhanced due to the equal distribution of flow rate across the collectors. Consequently, as illustrated in Figure 4.3a, these collectors produce higher thermal energy and exhibit better thermal efficiency compared to other configurations. Figure 4.3b shows the electricity production and electrical efficiency of the configurations. Since electrical efficiency is directly related to cell temperature, it exhibits an opposite trend to cell temperature, as presented in Figure 4.2a. As cell temperature increases, electrical efficiency decreases, which in turn reduces electricity production. Config E exhibits 2% higher electricity production and electrical efficiency compared to Config B, which performs the poorest. The electrical efficiency for all parallel tube PVT configurations ranged from 0.1368 to 0.1397, whereas for the conventional PV panel, this value was 0.1251, approximately 9% to 11% lower than that of the parallel tube PVT configurations.

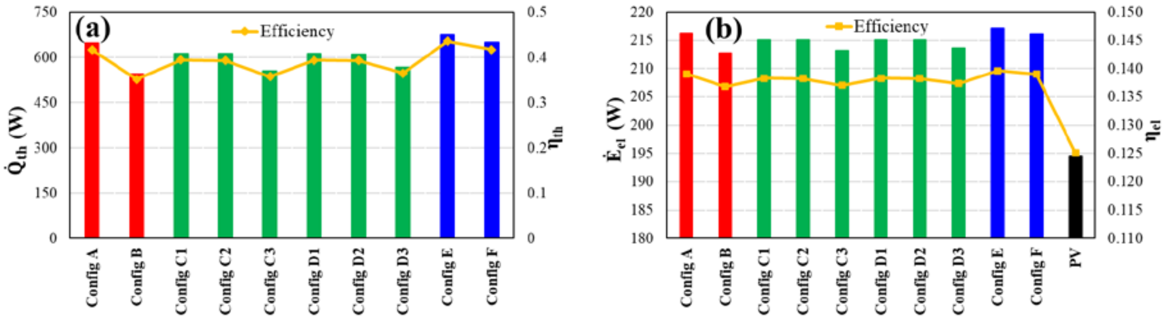

Figure 4.3. Thermal power (a), thermal efficiency (a), electrical power (b), electrical efficiency (b) of different parallel tube PVT configurations under base-case conditions

In the exergy analysis, which examines the quality of energy, the thermal, electrical and output exergy, and exergy destructions for all parallel tube configurations under base-case conditions were compared and presented in Figure 4.4. The electrical exergy of the configurations equals their electrical production. Thermal exergy depends on the water inlet, water outlet, and ambient temperatures. Since the ambient and inlet temperatures are the same across all configurations, the only factor influencing thermal exergy is the water outlet temperature. As the water outlet temperature increases, thermal exergy also increases. Following the same trend as in Figure 4.2b, the highest thermal exergy is observed in Config E, while the lowest thermal exergy is in Config B, where the outlet water temperature is also the lowest. Since output exergy is the sum of thermal and electrical exergies, it follows the same trend as thermal and electrical exergies. Exergy destruction is calculated as the difference between the exergy from the sun and the output exergy (Eq. 3.34). Considering that the exergy inlet is equal for all parallel tube configurations, it shows an inverse trend with the output exergy presented in Figure 4.4c. Consequently, exergy destruction is highest in Config B and lowest in Config E among PVT configurations. For the PV panel, electrical and output exergy are lower than in all parallel tube PVT configurations. This is attributed to the uncooled cells operating at relatively high temperatures, which reduces electrical exergy. Consequently, exergy destruction is higher in the PV panel due to its reduced output exergy.

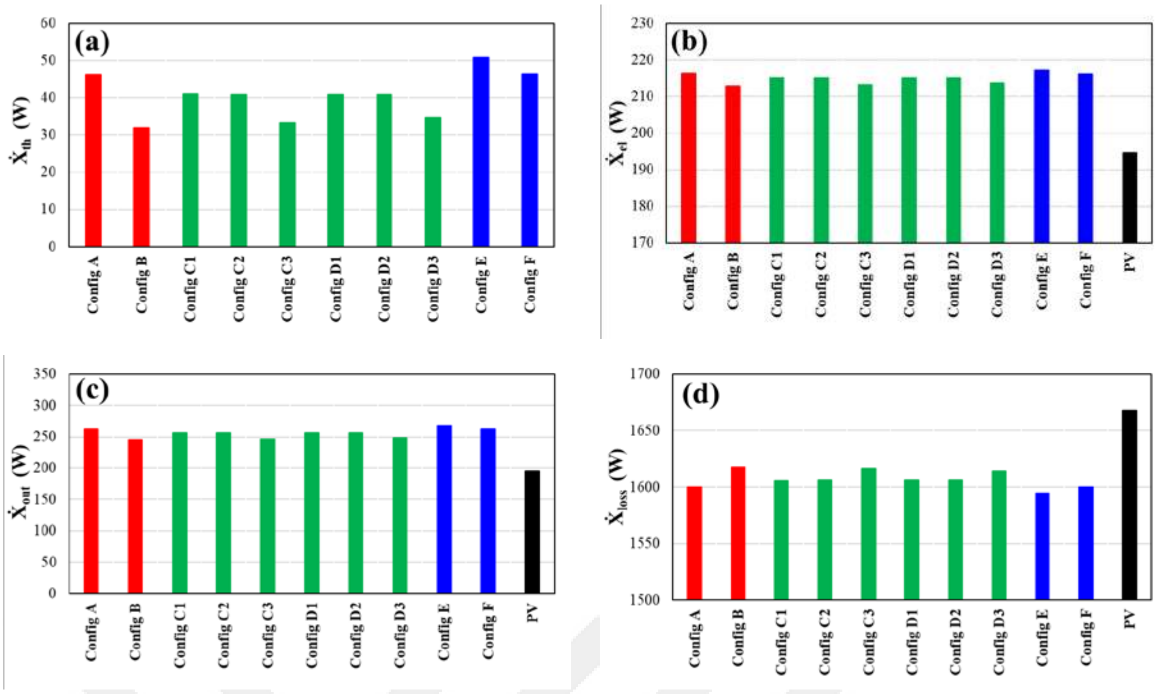

Figure 4.4. Thermal (a), electrical (b) and output (c) exergy, and exergy destruction (d) of different parallel tube PVT configurations under base-case conditions

Overall efficiency is calculated by combining the thermal and electrical efficiency (Eq. 3.31). The overall efficiency of Config E, where thermal and electrical efficiency is highest, is approximately 18% higher than Config B, where both efficiencies are lowest under base-case conditions (Figure 4.5a). On the other hand, with respect to primary energy saving efficiency (Eq. 3.32), configurations A, E, and F outperform the others, delivering approximately 13% higher efficiency than Config B, which ranks lowest in this performance metric (Figure 4.5b). Exergy efficiency is the function of output exergy and input exergy (Eq. 3.45). Since the input exergy is the same in all configurations, the exergy efficiency directly depends on the output exergy. A similar trend is observed in exergy efficiency (Figure 4.5c) as in output exergy, with Config E having the highest and Config B the lowest exergy efficiency. When comparing these efficiencies to those of a conventional PV panel, both the overall and exergy efficiencies of the PV panel are significantly lower than those of the PVT collector configurations. This further underscores the performance advantage of PVT systems over standalone PV systems in harnessing and utilizing energy effectively.

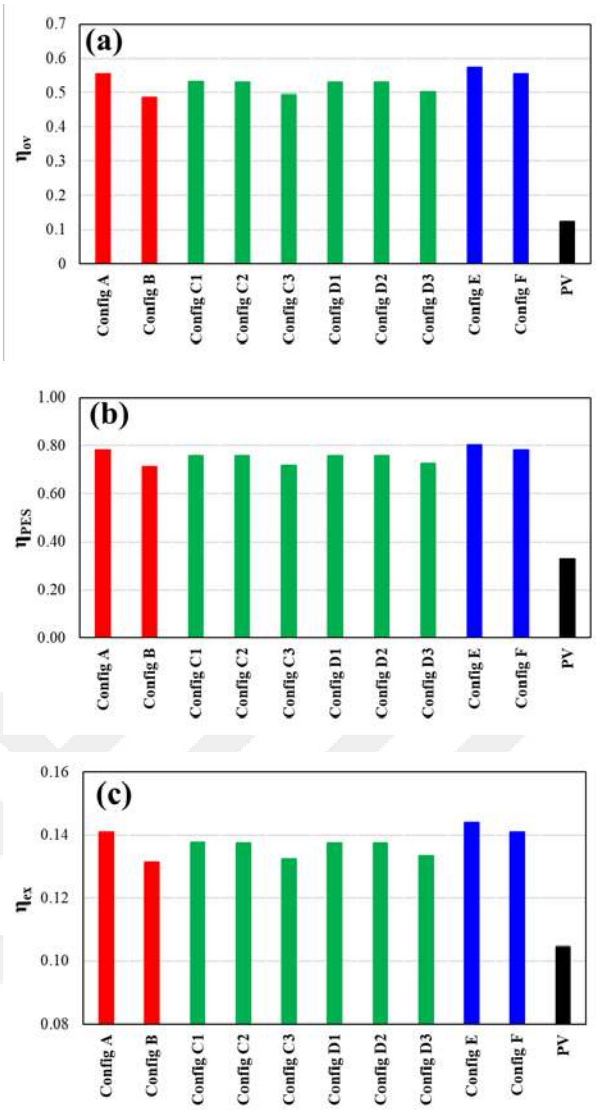

Figure 4.5. Overall (a), primary energy saving (b) and exergy (c) efficiency of different parallel tube PVT configurations under base-case conditions

One of the most important parameters for PVT collectors is the pressure drop. An increase in pressure drop leads to a higher pumping power requirement, making it a critical consideration in collector design. One of the major advantages of vertical and horizontal arranged configurations is their significantly lower pressure drop compared to serpentine and spiral collector designs. Figure 4.6 illustrates both the pressure drop, and the amount of thermal energy produced per pressure drop (TEPD).

The pressure drop in a system is influenced by two main factors: local resistance losses (e.g., at T-junctions) and flow resistance losses along the tubes. While longer tubes are generally expected to exhibit higher pressure losses due to increased flow resistance, this principle is more clearly observed in the comparison between configurations E and F, where pressure losses align with expectations. However, when comparing configurations A and B, despite the longer tubes in Config A, the lengths of the collector tubes in Config B are twice as long. Since the total flow rates through configurations A and B are identical, the flow resistance losses in the collector tubes of Config B are higher. Additionally, the number of T-junctions increases with the number of tubes, contributing to higher local resistance losses. Config B contains twice as many T-junctions as Config A. Considering both the lengths of the collector tubes and the number of T-junctions, the total pressure drop in Config B is greater than in Config A.

A similar analysis of configurations C and D reveals that the lengths of the collector tubes and the number of T-junctions are identical. Since the total tube lengths and flow rates are also equal, the pressure losses in these configurations are nearly the same. The small differences observed are attributed to variations in the physical properties of water due to temperature changes. The highest pressure drop is in Config B, while the lowest pressure drop is in Config F. The results for TEPD show that Config F is the best configuration due to its high thermal energy production and lowest pressure drop. While Config E excels in most performance parameters, it has one of the lowest TEPD due to its higher pressure drop. This result demonstrates that evaluating PVT performance solely based on thermal and electrical output is insufficient. A comprehensive assessment requires considering both energy production and the associated pressure drop within the collector.

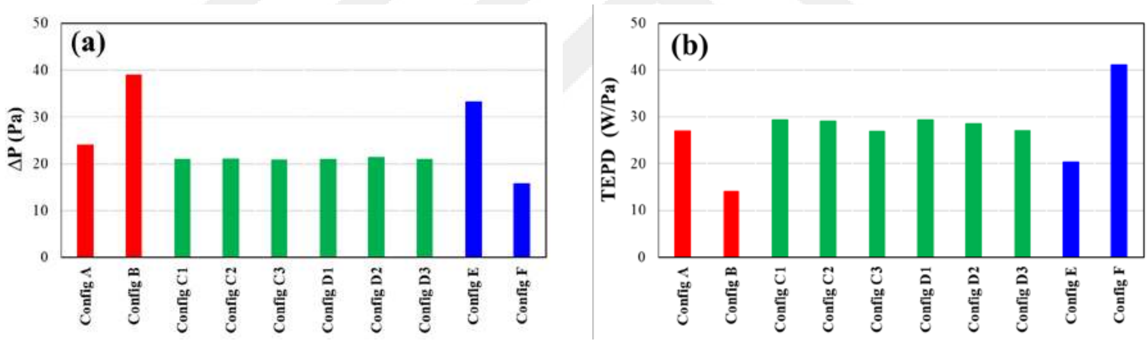

Figure 4.6. Pressure drop (a) and TEPD (b) of different parallel tube PVT configurations under base-case conditions

Figure 4.7 presents a comparative analysis of the configurations based on all performance parameters under base-case operating conditions. In the figure, the green color denotes the best-performing configuration, with performance deteriorating progressively towards red. The figure clearly illustrates that the optimal designs across all performance parameters, except for pressure drop and TEPD, are the multi-inlet configurations E and F, along with the single-inlet vertically arranged Config A. Config F was the most effective in terms of minimizing pressure drop and maximizing TEPD. Conversely, Config B, horizontally arranged single-inlet design, performed the worst across all performance parameters.

Configuration	T_c (°C)	$T_{w,out}$ (°C)	ΔP (Pa)	$\dot{Q}_{th}$ (W)	$\dot{E}_{el}$ (W)	η_{el} (-)	η_{th} (-)	η_{ov} (-)	η_{PES} (-)	TEPD (W/Pa)	$\dot{X}_{th}$ (W)	$\dot{X}_{el}$ (W)	$\dot{X}_{out}$ (W)	$\dot{X}_{loss}$ (W)	η_{ex} (-)
A	41.15	47.90	23.94	646.84	216.33	0.1391	0.4159	0.5550	0.7820	27.02	46.13	216.33	262.46	1599.92	0.1409
B	44.49	43.53	38.98	545.54	212.82	0.1368	0.3508	0.4876	0.7109	14.00	31.92	212.82	244.74	1617.64	0.1314
C1	42.32	46.45	20.90	613.32	215.10	0.1383	0.3944	0.5327	0.7583	29.35	41.16	215.10	256.27	1606.11	0.1376
C2	42.37	46.37	20.99	611.46	215.05	0.1383	0.3932	0.5315	0.7571	29.13	40.90	215.05	255.95	1606.43	0.1374
C3	44.15	43.98	20.75	555.96	213.18	0.1371	0.3575	0.4946	0.7182	26.79	33.27	213.18	246.45	1615.93	0.1323
D1	42.35	46.39	20.85	611.86	215.06	0.1383	0.3934	0.5317	0.7573	29.35	40.95	215.06	256.02	1606.36	0.1375
D2	42.37	46.37	21.45	611.39	215.05	0.1383	0.3931	0.5314	0.7570	28.51	40.89	215.05	255.94	1606.44	0.1374
D3	43.67	44.47	20.93	567.41	213.68	0.1374	0.3648	0.5022	0.7264	27.12	34.78	213.68	248.46	1613.92	0.1334
E	40.33	49.19	33.25	676.90	217.19	0.1397	0.4352	0.5749	0.8028	20.36	50.80	217.19	267.99	1594.39	0.1439
F	41.29	47.97	15.79	648.42	216.18	0.1390	0.4169	0.5559	0.7827	41.08	46.38	216.18	262.56	1599.82	0.1410
PV	61.84	-	-	-	194.60	0.1251	-	0.1251	-	-	-	194.60	194.60	1667.77	0.1045

Figure 4.7. Comparison of performance parameters of all parallel tube PVT configurations under base-case conditions

4.1.2. Effect of Flow Rate on the Parallel Tube PVT Collector Configurations

In this section, the effect of flow rate on performance parameters was examined for all parallel tube configurations. The flow rate range (5-50 L/h) was selected to ensure the flow remained within the laminar regime with an increment of 5 L/h, while solar irradiance, water inlet temperature, ambient temperature and wind velocity were kept at base-case values as specified in Table 3.3.

Figure 4.8 presents the contour of absorber temperature distributions for three parallel tube PVT configurations arranged either vertically or horizontally that demonstrated the highest performance under base-case conditions. Additionally, Figure 4.9 illustrates the variations in both average PV cell temperature and fluid outlet temperature as a function of fluid flow rate for all parallel tube arrangements.

Across all configurations, the fluid temperature is observed to be relatively low at the collector inlet and gradually increases toward the outlet. A higher fluid flow rate results in a more even distribution of temperature across the absorber surface, thereby improving overall thermal homogeneity. Configurations E and F exhibit a noticeably more uniform temperature distribution than Config A, owing to the equal flow rates maintained through the tubes. As shown in Figure 4.9a, cell temperatures among different PVT collectors remain closely aligned at lower flow rates. However, as the flow rate increases, a greater divergence in cell temperatures is observed across configurations. Notably, when the fluid flow rate is increased from 5 L/h to 50 L/h, the PV cell temperatures across all parallel tube PVT collectors decrease significantly, with reductions ranging between 18 °C and 23 °C.

An increase in the fluid flow rate shortens the contact time with the absorber, which in turn reduces the outlet temperature of the fluid (Figure 4.9b). Unlike the PVT cell temperature, the difference between the configurations is significant at lower flow rates, while the gap between them narrows as the fluid flow rate increases. As the fluid flow rate increases from 5 L/h to 50 L/h, the fluid outlet temperature decreases between approximately 17 °C and 24 °C among all PVT collectors. Consistent with the findings reported by Kazem et al. (2020), an increase in the fluid flow rate led to reductions in both the average PVT cell temperature and the outlet fluid temperature. The study reported that when the fluid flow rate increased from 10 kg/h to 40 kg/h, the PVT cell temperature dropped by about 10 °C, while the fluid outlet temperature exhibited a decrease of approximately 13 °C.

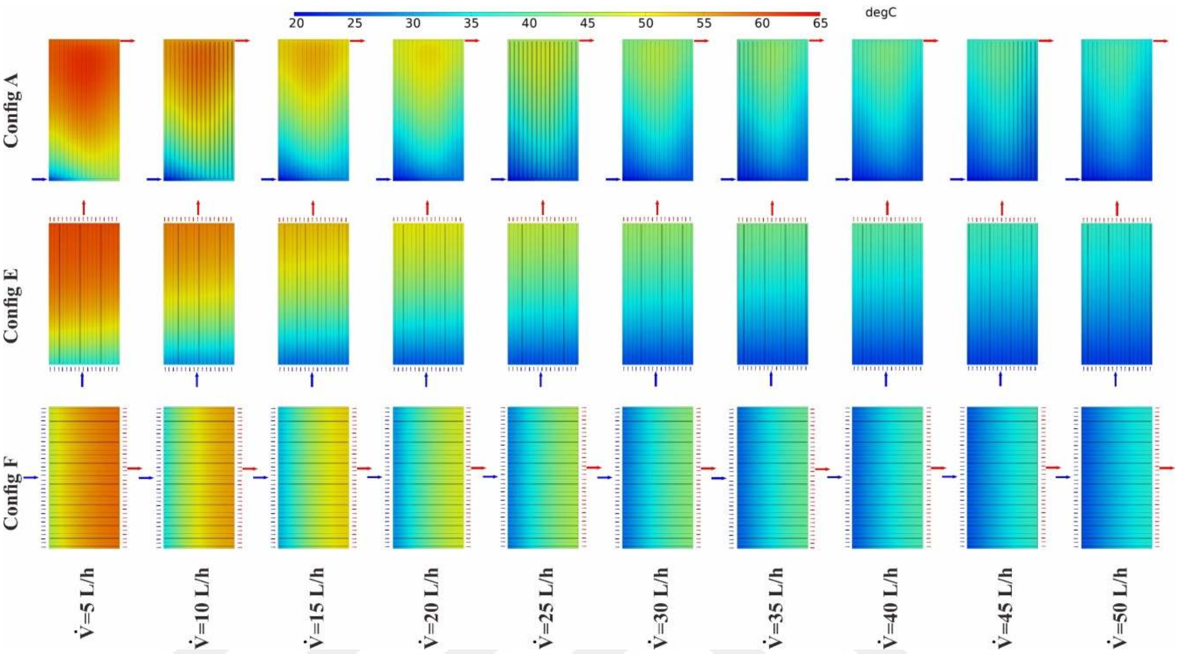

Figure 4.8. PVT absorber temperature distribution of Config A, Config E and Config F for different flow rates

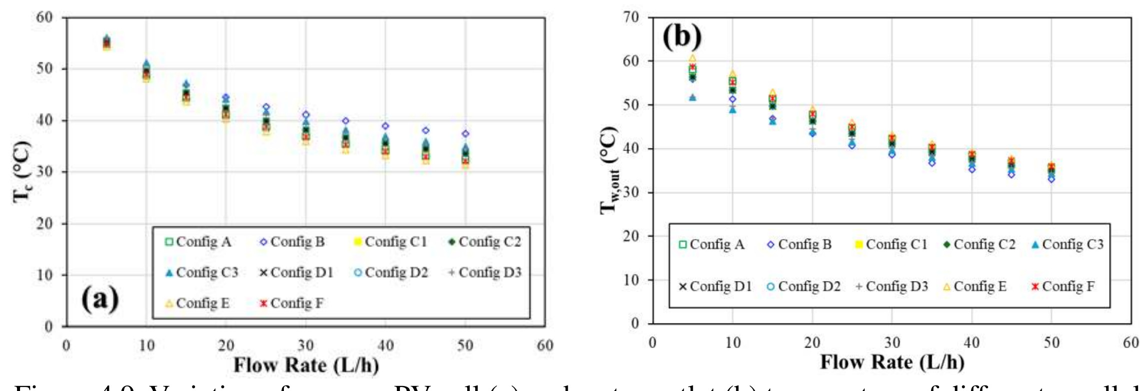

Figure 4.9. Variation of average PV cell (a) and water outlet (b) temperature of different parallel tube PVT configurations under varying flow rate conditions

As the flow rate increases, the outlet temperature of the fluid tends to decrease due to reduced residence time in the tubes (Figure 4.9). However, thermal energy production increases with flow rate, since a larger volume of fluid carries away more heat. Consequently, thermal energy production and thermal efficiency shows an increase for all configurations, as illustrated in Figure 4.10a. This observation is consistent with the findings reported by Abdul-Ganiyu et al. (2021), where an increase in flow rate resulted in a reduced temperature difference between the fluid outlet and inlet temperatures. At the lowest flow rate of 5 L/h, the thermal energy production and thermal efficiency of all configurations are very similar, but as the flow rate increases, the differences in both performance metrics become more pronounced (Figure 4.11). At the lowest flow rate of 5 L/h, Config D3 has the lowest thermal efficiency at 11.86%, while Config E has the highest at 15.23%. When the flow rate increases from 5 L/h to 50 L/h, the thermal efficiency of Config E rises to approximately 61%. Multiple inlet configurations (E and F) exhibit higher thermal efficiency compared to others.

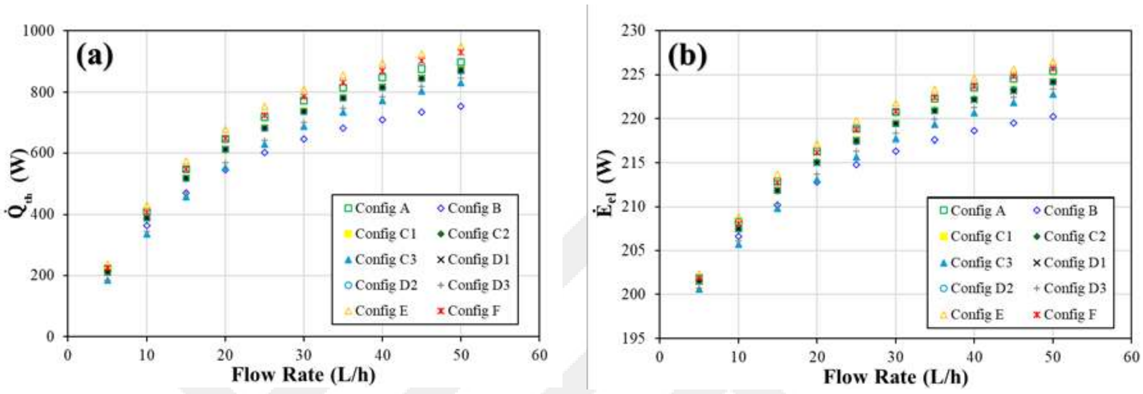

Figure 4.10. Variation of thermal energy production (a) and electrical power (b) of different parallel tube PVT configurations under varying flow rate conditions

The increase in flow rate enhances heat transfer, leading to more heat being extracted from the PV cell, which in turn reduces the PV cell temperature and, improves electrical power (Figure 4.10b) and electrical efficiency (Figure 4.11b). The lowest electrical power and efficiency is observed in Config C3, while the highest is in Config E at 5 L/h. With the increase of flow rate, all configurations show improvements in electrical efficiency ranging from 9% to 11%. When the flow rate increases from 5 L/h to 50 L/h, the least improvement is seen in Config B, which becomes the worst-performing configuration at higher flow rates. Configurations E and F were lightly better from the other configurations with increasing flow rate. As also reported in the work of Abdollahi et al. (2024), an increase in flow rate resulted in significant enhancements in thermal and electrical efficiencies.

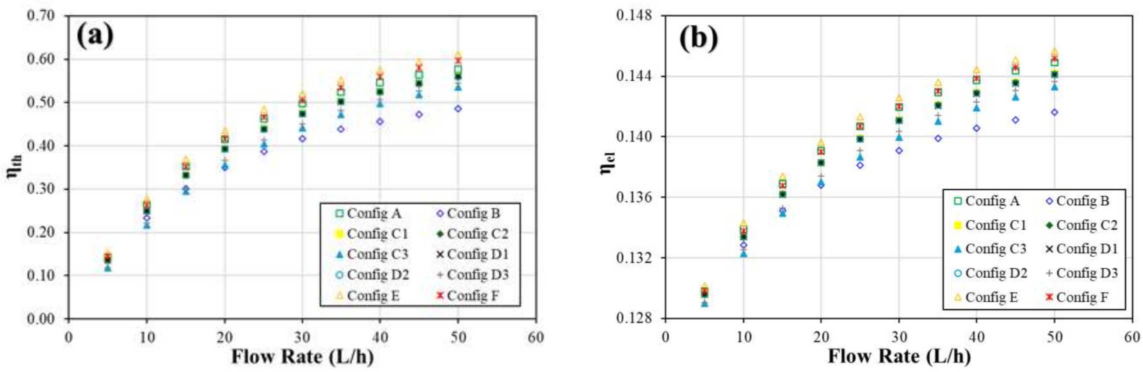

Figure 4.11. Effect of flow rate on the thermal (a) and electrical (b) efficiency of parallel tube PVT collectors

Figure 4.12 compares the exergetic performance parameters across all configurations. According to Equation 3.48, thermal exergy is a function of thermal energy, fluid outlet temperature and ambient temperature. Since the ambient temperature remains constant throughout the analysis, the increase in flow rate enhances thermal energy output but lowers the fluid outlet temperature. These opposing effects lead to an optimal point in thermal exergy. As the flow rate increases from 5 L/h to 20 L/h, thermal exergy also increases. However, increasing the flow rate beyond 20 L/h leads to a decrease in thermal exergy. Config E is defined as the best configuration for thermal exergy at all flow rates, with an optimum flow rate observed at 20 L/h, similar to all other configurations. Since electrical exergy (Figure 4.12b) is directly related to electrical efficiency, it follows the same trend as shown in Figure 4.11b, increasing with the flow rate. Electrical exergy significantly influences both exergy output and exergy destruction more than thermal exergy since electrical energy is completely convertible. Exergy output (Figure 4.12c) increases with the flow rate up to 25 L/h, followed by a slight decrease at higher flow rates. As shown in Figure 4.12d, exergy destruction inversely correlates with exergy output, decreasing as the flow rate rises from 5 L/h to 25 L/h, and then increasing at higher flow rates. The optimal flow rate for maximizing electrical exergy and minimizing exergy destruction is identified as 25 L/h under base-case conditions. Config E demonstrates the best performance among all configurations based on exergetic parameters.

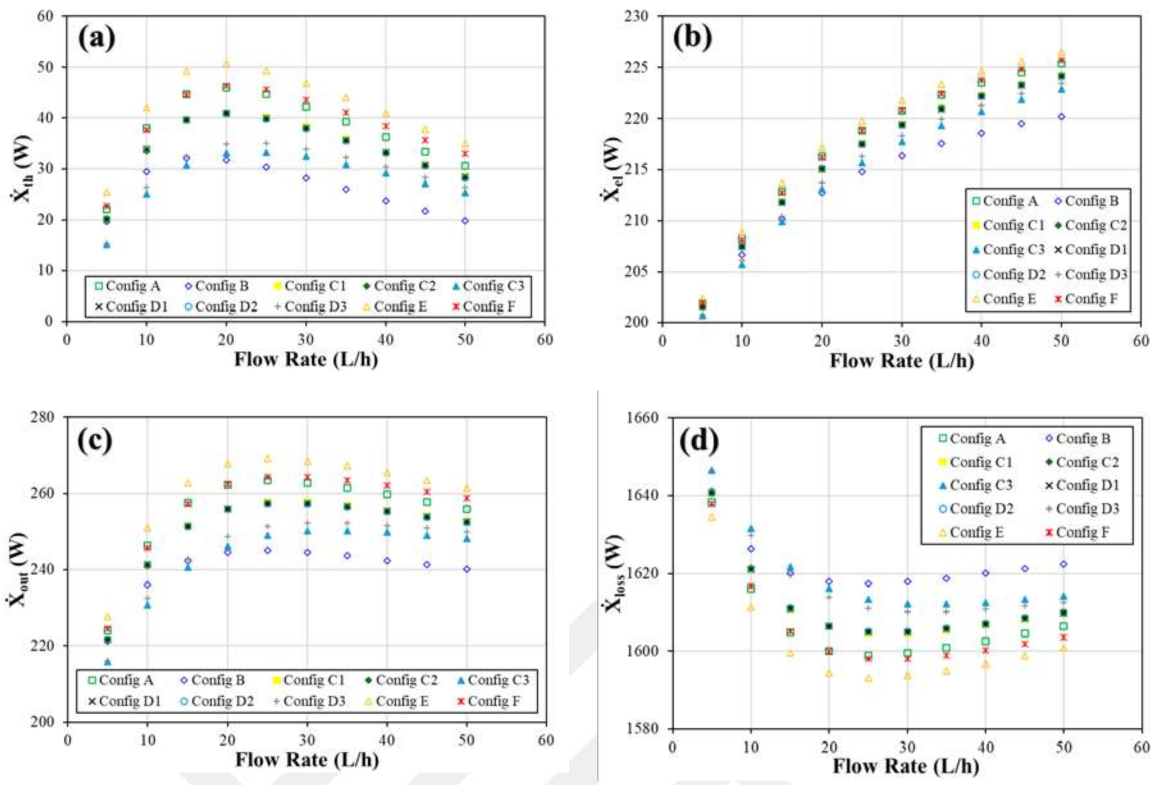

Figure 4.12. Effect of flow rate on the thermal (a), electrical (b) and output (c) exergy, and exergy destruction (d) of parallel tube PVT collectors

The impact of flow rate variation on overall, primary energy saving and exergy efficiency for all configurations is compared in Figure 4.13. As the flow rate increases, it enhances heat transfer, leading to improvements in both thermal and electrical efficiency, which consequently raises the overall and primary energy saving efficiency. Since thermal efficiency is more significantly affected by flow rate, the overall and primary energy saving efficiency trend closely follows it. As also reported in the work of Abdul-Ganiyu et al. (2021), higher flow rates were found to substantially boost overall efficiency. Although the differences between configurations are minimal at low flow rates, the disparities become more pronounced as the flow rate increases. The highest overall and primary energy saving efficiency is observed in Config E at 50 L/h, reaching approximately 75.64% and %99.41 respectively. Exergy efficiency is a function of exergy output and exergy input. Since sun exergy does not change with flow rate, it remains constant across all configurations. Consequently, the trend in exergy efficiency (Figure 4.13c) matches that of exergy output as presented in Figure 4.12c.

Effect of the flow rate on the pressure drop and TEPD is compared in Figure 4.14. An increase in velocity increases the shear stress on the walls of the tubes and therefore increases pressure drop. Additionally, since pressure drop is proportional to the fluid density, higher density further contributes to increased pressure drop. While the pressure drops of all configurations are very close to each other at 5 L/h, they increase sharply with higher flow rates, leading to greater differences between configurations. Config B exhibits the highest pressure drop in response to varying flow rate, whereas Config F demonstrates the lowest pressure drop. Additionally, TEPD is very similar among configurations C1, C2, and F at low flow rates. However, as the flow rate increases, Config F stands out from the other configurations, becoming the best configuration due to its lowest pressure drop.

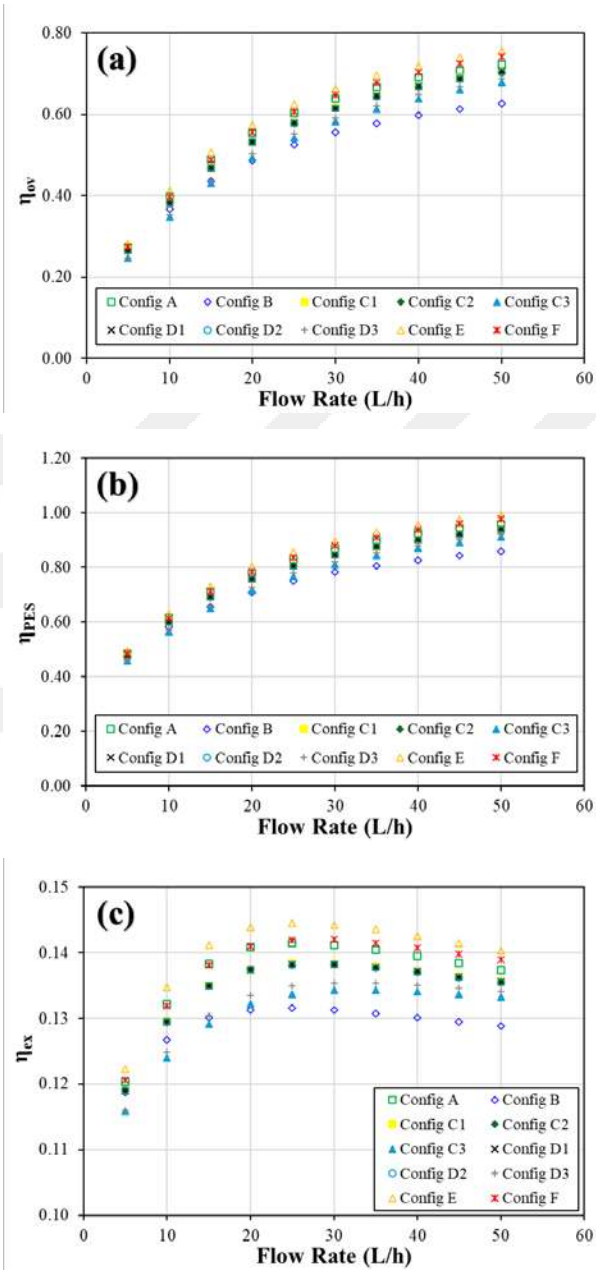

Figure 4.13. Effect of flow rate on the overall (a), primary energy saving (b) and exergy (c) efficiency of parallel tube PVT collectors

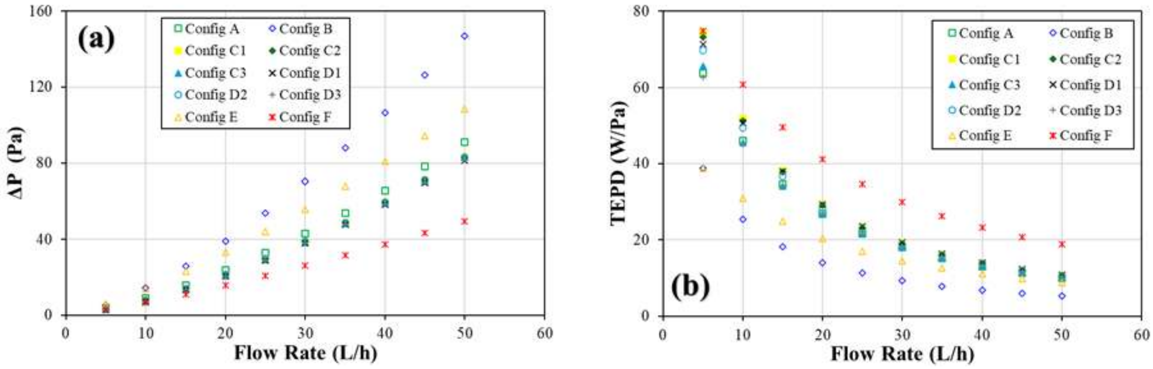

Figure 4.14. Effect of flow rate on the pressure drop (a) and TEPD (b) of parallel tube PVT collectors

4.1.3. Effect of Solar Irradiance on the Parallel Tube PVT Collector Configurations

Solar irradiance is one of the most important parameters affecting PVT collector performance, and its impact was investigated for all configurations. The solar irradiance was varied between 200 and 1200 W/m^2 in 200 W/m^2 increments, while other operating parameters were kept at base-case values.

Figure 4.15 illustrates the variations in absorber temperature distributions with changing solar irradiance for the three best-performing parallel tube configurations. Additionally, Figure 4.16 presents the variations in PV cell temperatures and fluid outlet temperatures across all parallel tube configurations under different solar irradiance levels. As observed from the absorber temperature contours of the top three configurations, lower solar irradiance levels correspond to lower absorber temperatures, while increasing irradiance leads to a rise in absorber temperatures. A similar trend is evident across all PVT configurations, as shown in Figure 4.16.

Figure 4.16a compares the average PV cell temperatures of all PVT collectors with the average surface temperature of a conventional PV panel. At low irradiance values, the PV cell temperatures of the PVT systems are closely aligned, and there is a temperature difference of approximately 3-4 °C between the PVT collectors and the conventional PV panel. However, at maximum irradiance, this temperature difference increases significantly, reaching 20-25 °C. Specifically, under a solar irradiance of 1200 W/m^2, the average surface temperature of the conventional PV panel reaches 69.41 °C, whereas the PV cell temperature in the best-performing configuration, Config E, is significantly lower at 44.27 °C.

Figure 4.16b illustrates the variation in fluid outlet temperature as a function of solar irradiance. Similar to the trend observed for average PV cell temperatures, the fluid outlet temperatures of all investigated PVT collectors are closely aligned at low solar irradiance levels. However, as solar irradiance increases beyond 600 W/m^2 the outlet temperatures begin to diverge among the different configurations. At the lowest irradiance level, the fluid outlet temperature is approximately 25 °C for all PVT collectors. With increasing solar irradiance, the outlet temperatures rise, reaching values between 47.85 °C and 54.84 °C at maximum solar irradiance.

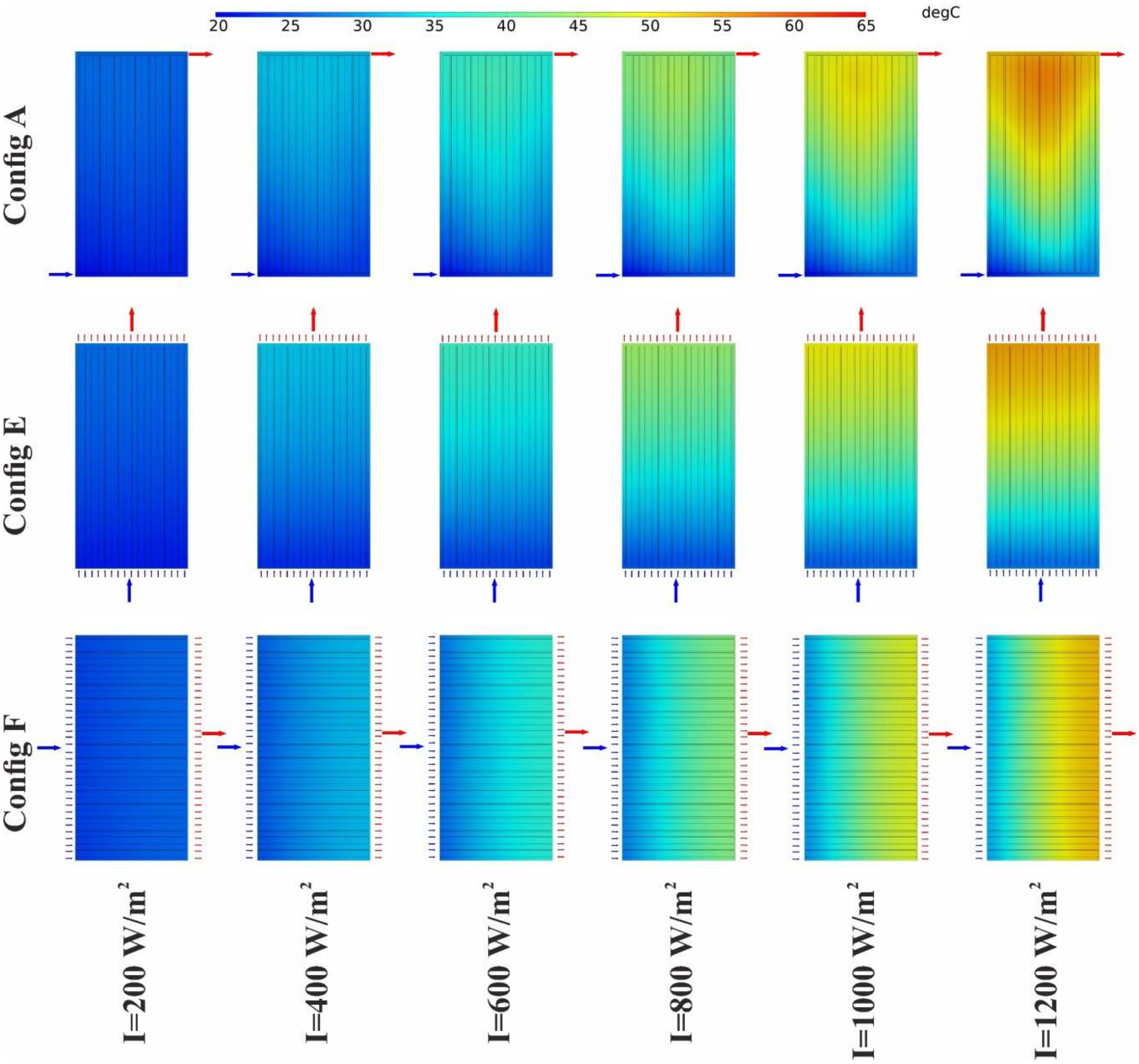

Figure 4.15. PVT absorber temperature distribution of Config A, Config E and Config F for different solar irradiances

The trends observed in PV cell temperatures and fluid outlet temperatures in Figure 4.16 are also reflected in the thermal and electrical energy outputs of the PVT collectors, as well as in the electrical production of conventional PV panels, as shown in Figure 4.17. Figure 4.17a presents the variation of thermal energy production with solar irradiance for all parallel tube PVT collectors.

Since the fluid inlet temperature and flow rate are held constant in this analysis, thermal energy production and fluid outlet temperature exhibit a similar trend. Consequently, a similar pattern to that observed in Figure 4.16b is evident, while the thermal energy outputs of the PVT collectors are closely aligned at low irradiance levels, the differences among the configurations become more pronounced beyond 600 W/m^2 of solar irradiance. Among the configurations, the vertically arranged PVT collector consistently demonstrates the highest thermal performance across all irradiance levels, producing 138 W of thermal energy at the lowest solar irradiance and reaching 808 W at the highest level (Figure 4.17a). On the other hand, regarding electricity production

(Figure 4.17b), the difference between the outputs of the PVT collectors and the conventional PV panel is minimal at low solar irradiance levels. However, beyond an irradiance of 800 W/m^2, the electricity production of the PVT collectors begins to diverge noticeably from that of the PV panel. At maximum solar irradiance, the best-performing configuration, Config E, achieved 13.84% higher electricity production compared to the conventional PV panel.

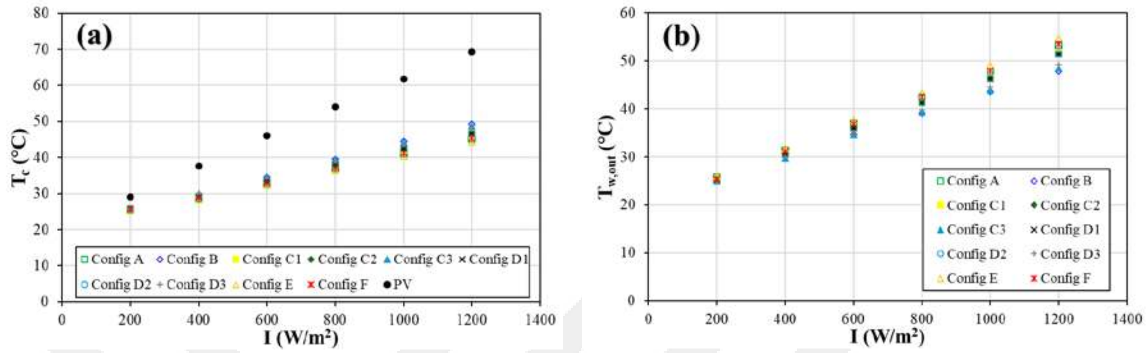

Figure 4.16. Variation of average PV cell (a) and water outlet (b) temperature of different parallel tube PVT configurations under varying solar irradiance conditions

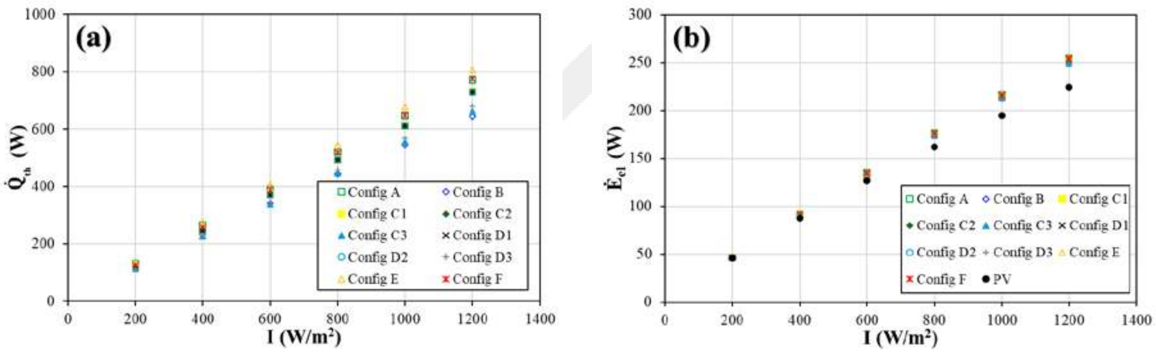

Figure 4.17. Variation of thermal energy production (a) and electrical power (b) of different parallel tube PVT configurations under varying solar irradiance conditions

Figure 4.18 shows the impact of solar irradiance on the thermal and electrical efficiency of all configurations. An increase in solar irradiance directly raises the total amount of energy reaching the absorber surface. As a result, the amount of energy absorbed by the collector also increases, leading to a higher overall thermal energy output from the system. However, the increase in solar irradiance also increases the surface temperature, causing more heat loss to the environment through convection and radiation. Unlike thermal energy production, thermal efficiency tends to decrease with increasing solar irradiance. This is due to the fact that higher irradiance levels lead to elevated surface temperatures, which in turn increase convective heat losses to the environment, thereby reducing thermal efficiency. Among all configurations, the most significant decrease in thermal efficiency is observed in Config B, with a 12% drop as shown in Figure 4.18a. On the other hand, the PV cell temperature also increases with higher solar irradiance, which reduces the electrical efficiency. As solar irradiance increased from 200 W/m^2 to 1200 W/m^2, electrical efficiency was negatively influenced by 8-10% in all configurations. This corresponds to a decrease of approximately 1% for every 100 W/m^2 increase in solar irradiance (Figure 4.18b). On the other hand, when comparing PVT collector configurations with the conventional PV panel, the electrical efficiency of the PV panel was approximately 2% lower under the lowest solar irradiance condition. However, as solar irradiance increases, the efficiency gap widens, reaching approximately 11% to 14% lower at maximum solar irradiance level.

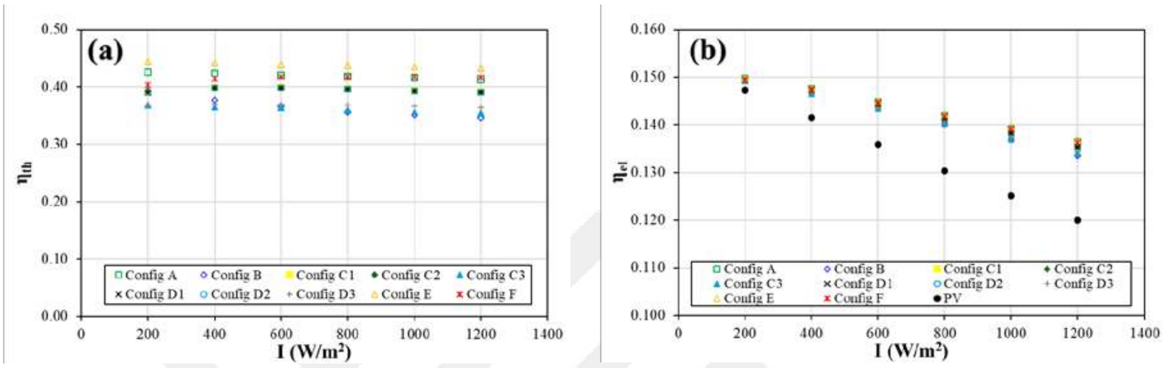

Figure 4.18. Effect of solar irradiance on the thermal (a) and electrical (b) efficiency of parallel tube PVT collectors

The effect of the solar irradiance on the exergetic parameters was compared for all configurations in Figure 4.19. As can be seen from Eq. 3.43, other parameters affecting thermal exergy, except water outlet temperature, were kept constant at the base-case conditions given in Table 3.3. An increase in solar irradiance results in a higher water outlet temperature, thereby enhancing thermal exergy. While the thermal exergy is almost the same for all configurations at low radiation, it increases sharply as solar irradiance increases, leading to greater differentiation between configurations (Figure 4.19a). Electrical exergy depends on electrical efficiency and solar irradiance. Although electrical efficiency decreases with increasing solar irradiance, as illustrated in Figure 4.18b, the effect of solar irradiance on electrical exergy is much greater. Since electrical efficiency is similar across configurations, the change in electrical exergy between configurations is minimal. As both thermal and electrical exergy increase with solar irradiance, the output exergy exhibits a similar trend. Due to the minimal differences in electrical exergy among configurations, significant changes in output exergy are not observed until the solar irradiance value reaches 800 W/m^2. This phenomenon is also reflected in exergy destruction, where notable differences between configurations emerge only beyond a solar irradiance value of 800 W/m^2.

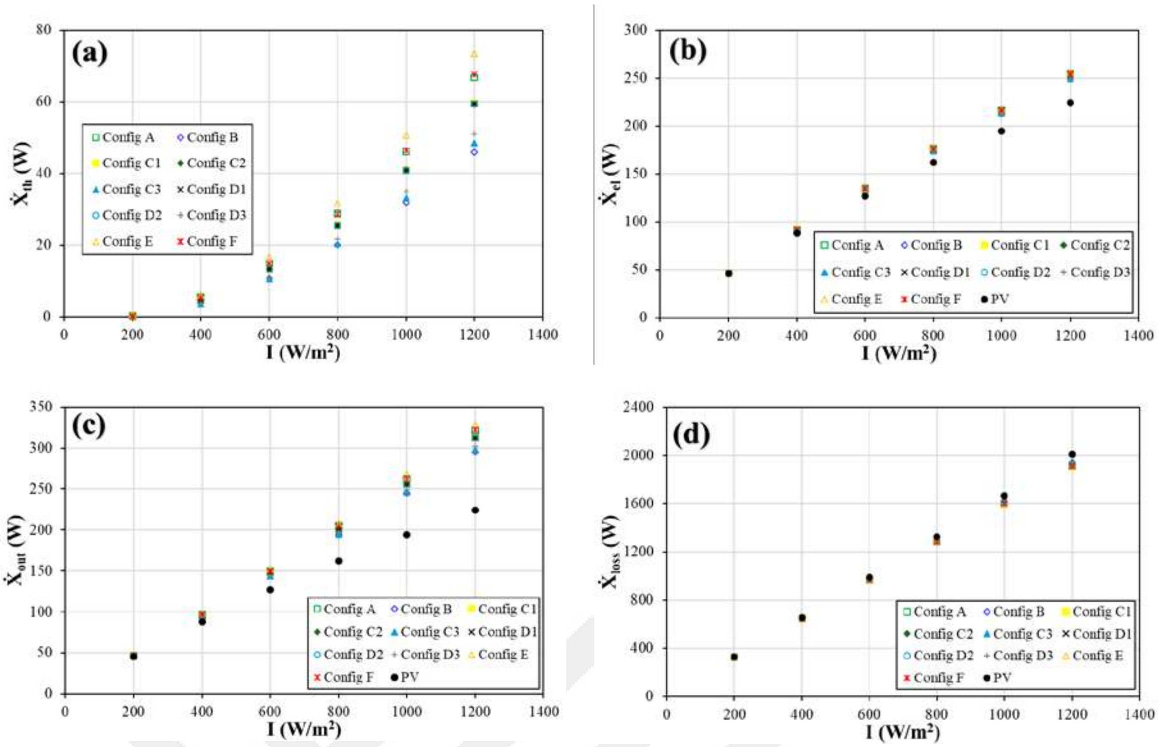

Figure 4.19. Effect of solar irradiance on the thermal (a), electrical (b) and output (c) exergy, and exergy destruction (d) of parallel tube PVT collectors

The overall and primary energy saving efficiency, derived from the electrical and thermal efficiency, exhibits an opposite trend with increasing solar irradiance. As shown in Figure 4.20, as solar irradiance increases from 200 to 1200 W/m^2, the overall efficiency decreases approximately between the range from 0.2% to 11% for PVT configurations. At the same time, primary energy saving efficiency declines with increasing solar irradiance, primarily due to the reduction in both thermal and electrical efficiencies at higher irradiance levels. As solar irradiance rises from its minimum to maximum values, the primary energy saving efficiency decreases by approximately 2.84% to 11.43%.

Conversely, exergy efficiency increases with higher solar irradiance levels as depicted in Figure 4.20c. This is because both thermal and electrical energy outputs increase with increased solar irradiance. For every 100 W/m^2 increase in solar irradiance, exergy efficiency increases by approximately 0.5% to 1.6% across PVT configurations. For the conventional PV panel, the overall efficiency is synonymous with electrical efficiency, which is considerably lower than that of PVT configurations. Although the electrical exergy of the PV panel increases with higher solar irradiance, the exergy efficiency declines. This decrease follows the trend of diminishing electrical efficiency, driven by the rising temperatures of uncooled PV cells.

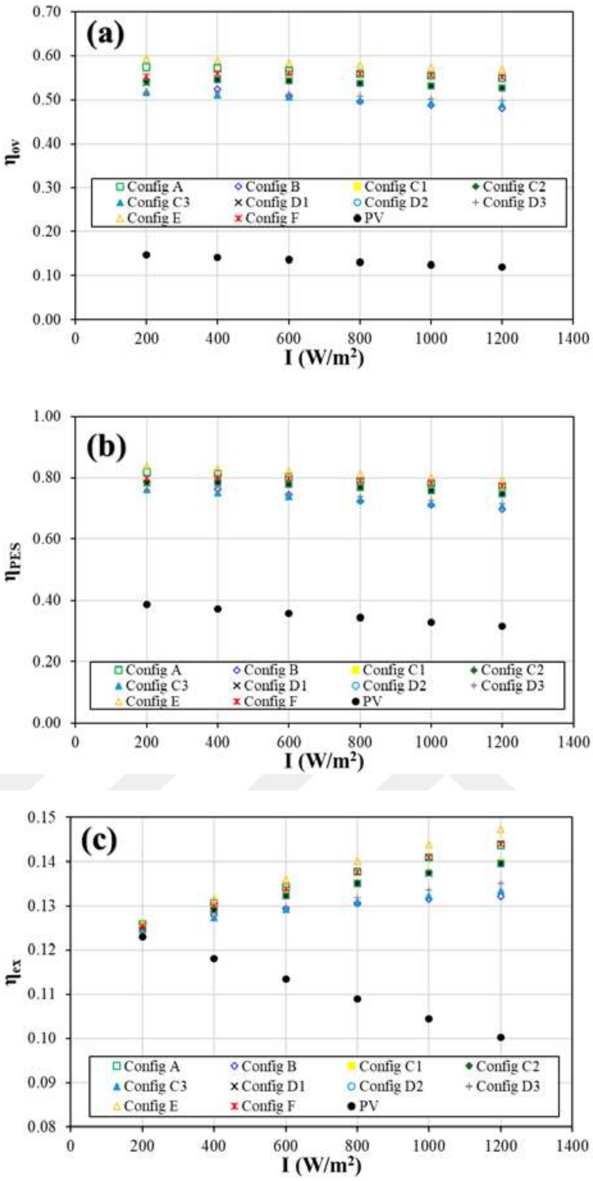

Figure 4.20. Effect of solar irradiance on the overall (a), primary energy saving (b) and exergy (c) efficiency of parallel tube PVT collectors

The impact of solar irradiance on pressure drop and TEPD is shown in Figure 4.21. As water temperature increases in proportion to solar irradiance, the viscosity and density of water decreases, leading to a reduction in pressure drop (Figure 4.21a). Specifically, as solar irradiance rises from 200 to 1200 W/m², the pressure drop decreases by 17% to 30%. Since the amount of energy absorbed by collector also increases with solar irradiance, thermal energy production is enhanced. Consequently, due to both the enhancement in thermal energy production and the reduction in pressure drop, TEPD also increases with increasing solar irradiance (Figure 4.21b).

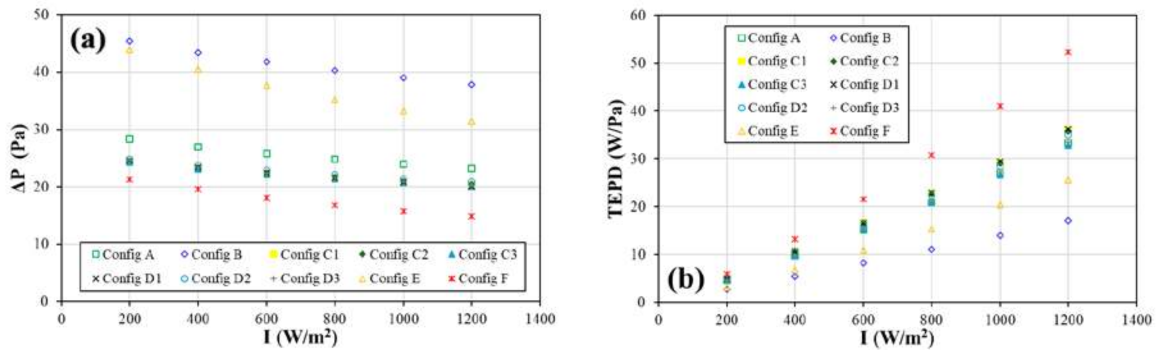

Figure 4.21. Effect of solar irradiance on the pressure drop (a) and TEPD (b) of parallel tube PVT collectors

4.1.4. Effect of Fluid Inlet Temperature on the Parallel Tube PVT Collector Configurations

Another crucial parameter influencing PV cell temperature and overall PVT collector performance is the fluid inlet temperature, with water being utilized as the cooling fluid in this study. The effect of varying water inlet temperature on performance parameters was systematically compared across all configurations. Specifically, the water inlet temperature was adjusted within a range of 10 °C to 40 °C, in 5 °C increments, while other operating conditions were maintained at the base-case values.

Figure 4.22 presents the variation in absorber temperature distributions for the three best-performing parallel tube PVT configurations under different fluid inlet temperatures. Additionally, Figure 4.23 illustrates the changes in PV cell temperatures and fluid outlet temperatures across all parallel tube configurations as a function of fluid inlet temperature.

As observed from the absorber temperature contours of the top three configurations, lower fluid inlet temperatures enhance the cooling of the panel, resulting in lower surface temperatures. Conversely, as the inlet temperature increases, panel temperatures also rise. At low fluid inlet temperatures, the differences between the PVT collectors are more pronounced, whereas these differences diminish as the fluid inlet temperature increases. Specifically, at the lowest inlet temperature of 10 °C, the average PV cell temperature is 39.77 °C for the worst-performing configuration (Config B) and 34.95 °C for the best-performing configuration (Config E). At the maximum fluid inlet temperature, the average PV cell temperatures increase to 53.87 °C for Config B and 50.89 °C for Config E.

Figure 4.23b shows the relationship between fluid outlet temperature and fluid inlet temperature. Similar to the trend observed for average PV cell temperatures, the outlet temperatures of the different PVT collectors diverge more at lower inlet temperatures but converge as the inlet temperature rises. While the outlet temperatures range between 39 °C and 46 °C at the lowest inlet temperature, they narrow to between 51 °C and 55 °C at the highest inlet temperature studied.

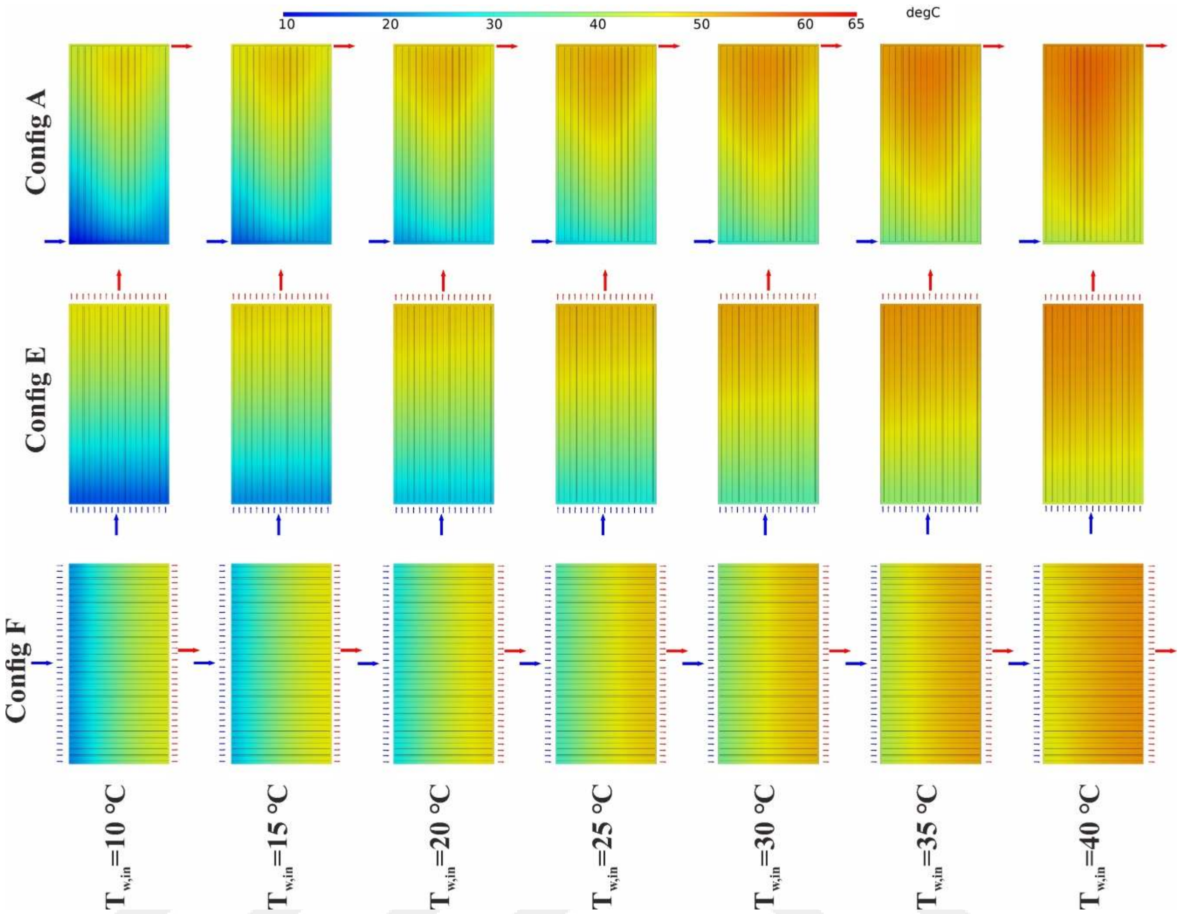

Figure 4.22. PVT absorber temperature distribution of Config A, Config E and Config F for different water inlet temperatures

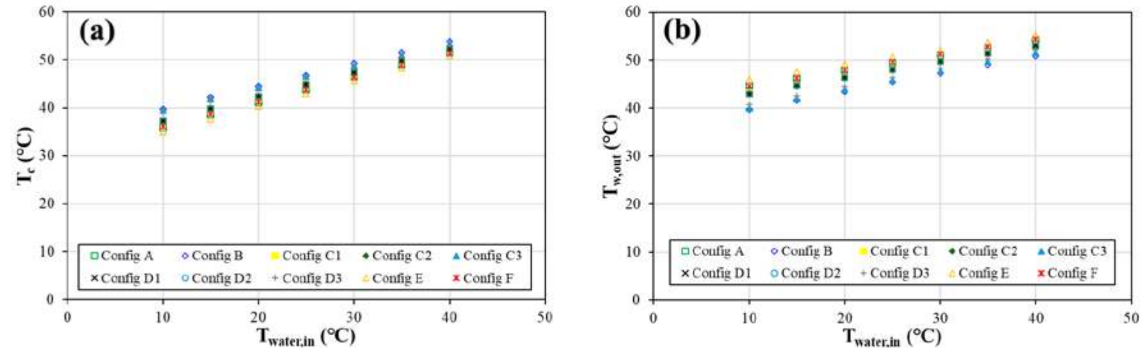

Figure 4.23. Variation of average PV cell (a) and water outlet (b) temperature of different parallel tube PVT configurations under varying water inlet temperature conditions

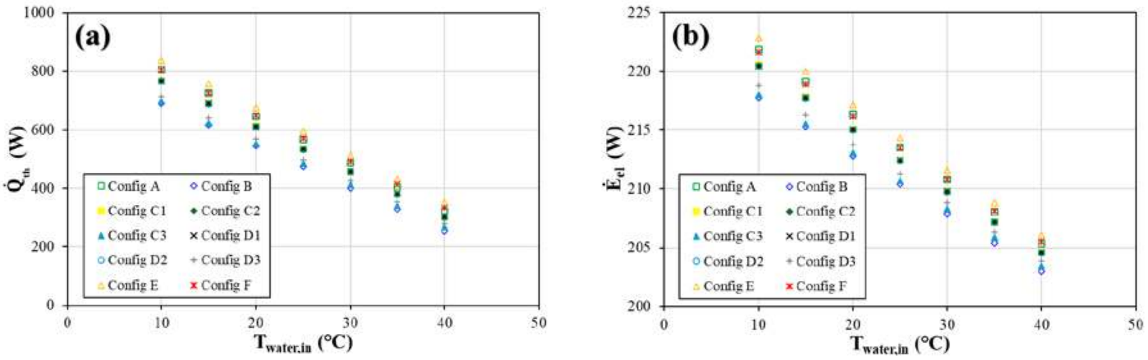

Figure 4.24. Variation of thermal energy production (a) and electrical power (b) of different parallel tube PVT configurations under varying water inlet temperature conditions

Although increasing the inlet temperature raises the fluid outlet temperature, it also elevates the cell temperature, which intensifies heat losses and consequently leads to a significant reduction in thermal energy production (Figure 4.24a). For instance, in the best-performing configuration (Config E), thermal energy production decreases from 838 W at the lowest inlet temperature to 352 W at the highest. Similarly, increasing the fluid inlet temperature also elevates PV cell temperatures, resulting in approximately a 7% reduction in electricity production (Figure 4.24b). The relationship between thermal and electrical efficiency and the water inlet temperature is depicted in Figure 4.25. A lower water inlet temperature creates a significant temperature gradient between the cooling fluid and the PVT collector, which in turn enhances heat transfer, thereby facilitating the extraction of more heat from the PV cell. In contrast, as the water inlet temperature increases, the water outlet temperature also rises, however thermal energy production drops due to the increasing heat losses. This reduction in temperature difference results in a decline in thermal energy production and thermal efficiency, as indicated by Eqs. 3.28 and 3.29.

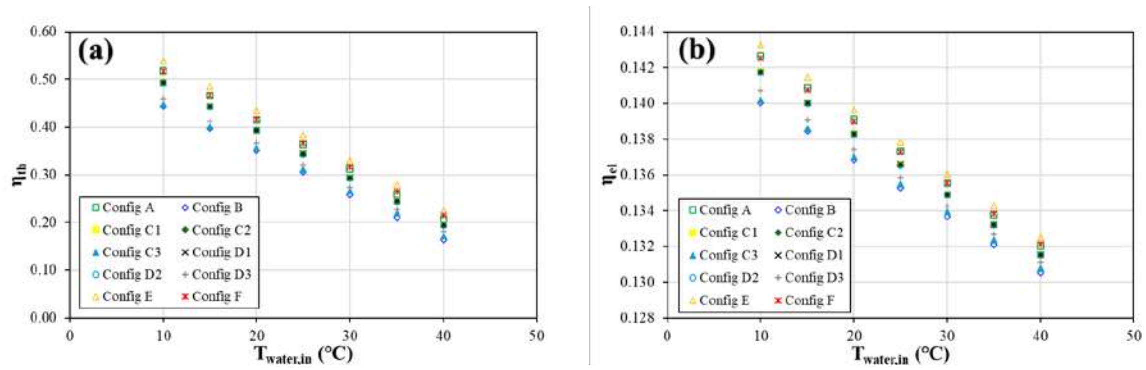

Figure 4.25. Effect of fluid inlet temperature on the thermal (a) and electrical (b) efficiency of parallel tube PVT collectors.

When the water inlet temperature was increased from 10°C to 40°C, the thermal efficiency experienced a substantial decrease of approximately 60% across all configurations. Moreover, an increase in water inlet temperature contributes to a rise in PV cell temperature, which adversely impacts electrical efficiency and, consequently, electricity production. As the water inlet temperature escalates from 10°C to 40°C, the electrical efficiency diminishes by roughly 7%.

The effect of water inlet temperature on exergy performance parameters is illustrated in Figure 4.26. Thermal exergy is contingent on both the water outlet temperature and the temperature differential between the outlet and inlet. Although the outlet temperature rises, the diminishing temperature differential results in a reduction in thermal exergy as the water inlet temperature increases. Consequently, thermal exergy fluctuates between 20% and 55% across different configurations with increasing water inlet temperature. Given that electrical energy directly correlates with electrical efficiency, it mirrors the trend depicted in Figure 4.25b. As the water inlet temperature rises, the variations in electrical exergy among configurations become less pronounced. The total exergy output, influenced by the decline in both thermal and electrical exergies, similarly decreases with higher water inlet temperatures. Conversely, exergy destruction exhibits an inverse trend to that of output exergy. While Config E demonstrates the highest exergy output, Config B is characterized by the highest levels of exergy destruction.

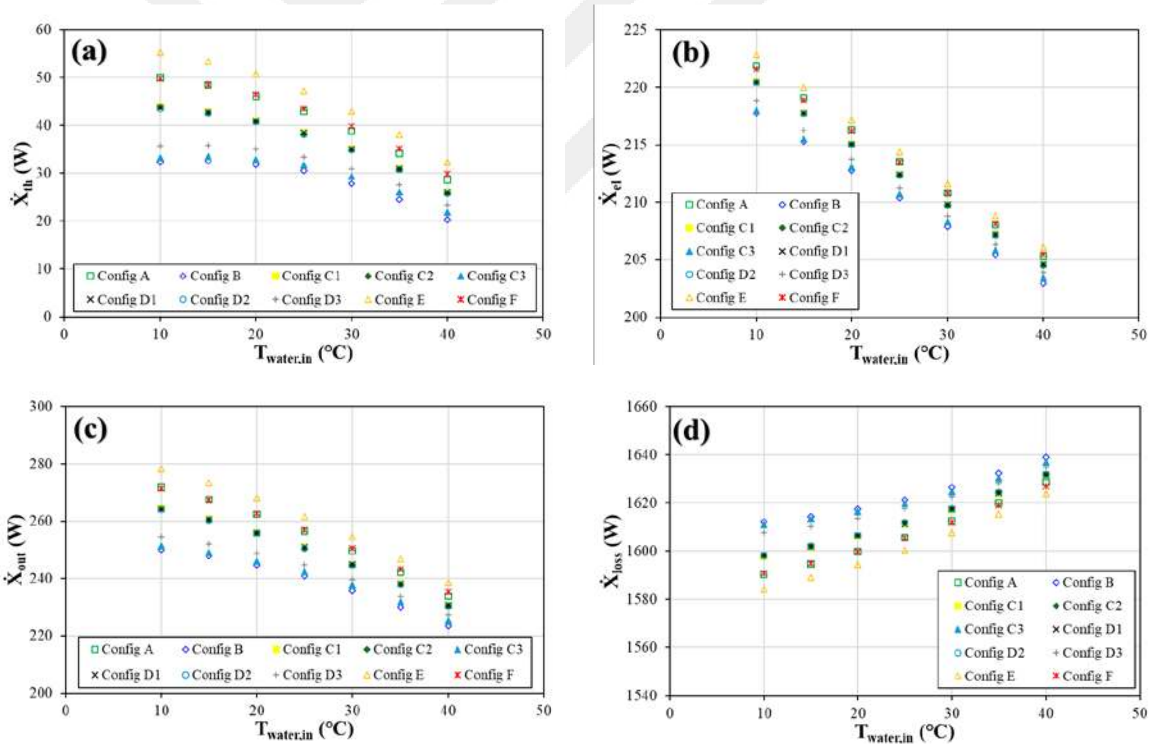

Figure 4.26. Effect of fluid inlet temperature on the thermal (a), electrical (b) and output (c) exergy, and exergy destruction (d) of parallel tube PVT collectors

The overall and primary energy saving efficiency (Figure 4.27) exhibit a declining trend with increasing water inlet temperature, consistent with the trends observed for thermal and electrical efficiency shown in Figure 4.25. Maximum overall and primary energy saving efficiency is achieved at the lowest water inlet temperature, with a significant decrease of approximately 48% and 37% as the temperature varies from 10°C to 40°C. Based on these findings, operating the PVT collector at low fluid inlet temperatures is strongly recommended to achieve optimal thermal, electrical, and overall efficiencies, a conclusion also supported by the results of Evola and Marletta (2014). The study indicated that each 1 °C rise in temperature results in nearly a 1% decrease in overall efficiency.

Given that the exergy input remains constant regardless of the water inlet temperature, exergy efficiency varies in direct proportion to exergy output. As depicted in Figure 4.27c, the exergy efficiency mirrors the trend of output exergy (Figure 4.26c), demonstrating a reduction of between 10% and 14% across various configurations.

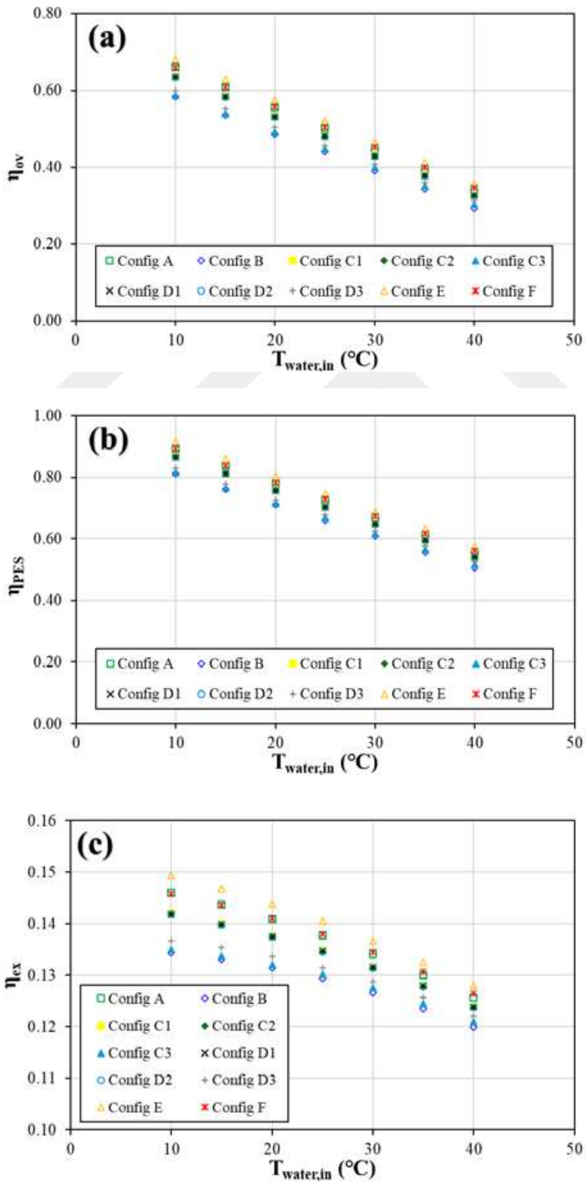

Figure 4.27. Effect of fluid inlet temperature on the overall (a), primary energy saving (b) and exergy (c) efficiency of parallel tube PVT collectors

As illustrated in Figure 4.28a, an increase in the water inlet temperature leads to a decrease in pressure drop, attributed to the corresponding rise in the fluid temperature and the subsequent reduction in water viscosity and density. Despite the reduction in pressure drop, TEPD also diminishes, as the decrease in thermal energy production is more pronounced (Fig 4.28b). Config F demonstrates the best performance, whereas configurations B and E exhibit the poorest performance among the configurations. The other configurations produce very similar results.

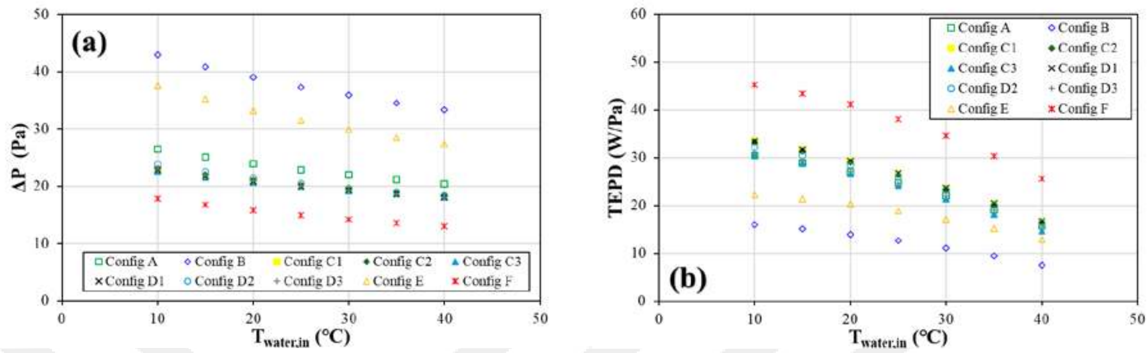

Figure 4.28. Effect of fluid inlet temperature on the pressure drop (a) and TEPD (b) of parallel tube PVT collectors

4.1.5. Effect of Ambient Temperature on the Parallel Tube PVT Collector Configurations

One of the climatic conditions significantly impacting the performance of PVT collectors is the ambient temperature, which influences both the PV cell temperature and heat losses. The effect of ambient temperature on various energetic and exergetic performance parameters was investigated by varying the temperature from 15 °C to 40 °C in increments of 5 °C for different configurations. During these variations, other operating conditions such as solar irradiance, flow rate, water inlet temperature, and wind velocity were maintained constant, as specified in Table 3.3.

Figure 4.29 illustrates the absorber temperature distribution contours for the three best-performing configurations, Config A, E and F, under different ambient temperature conditions, based on the base-case condition. Figure 4.30 presents the corresponding changes in average PV cell temperatures and fluid outlet temperatures across all parallel tube configurations as ambient temperature varies. As evident from both figures, increases in ambient temperature lead to higher absorber and average PV cell temperatures. Additionally, because heat losses decrease at higher ambient temperatures, the fluid outlet temperature also increases (Fig 4.30b). Figure 4.30a further displays the change in the average surface temperature of a conventional PV panel with ambient temperature, which follows a similar upward trend as observed in the PVT collectors. As ambient temperature rises from its minimum to maximum value, the average surface temperature of the PV panel increases from 52.55 °C to 76.34 °C. In comparison, the PV cell temperatures of the parallel tube PVT collectors range from 35.63 °C to 53.77 °C over the same ambient temperature range.

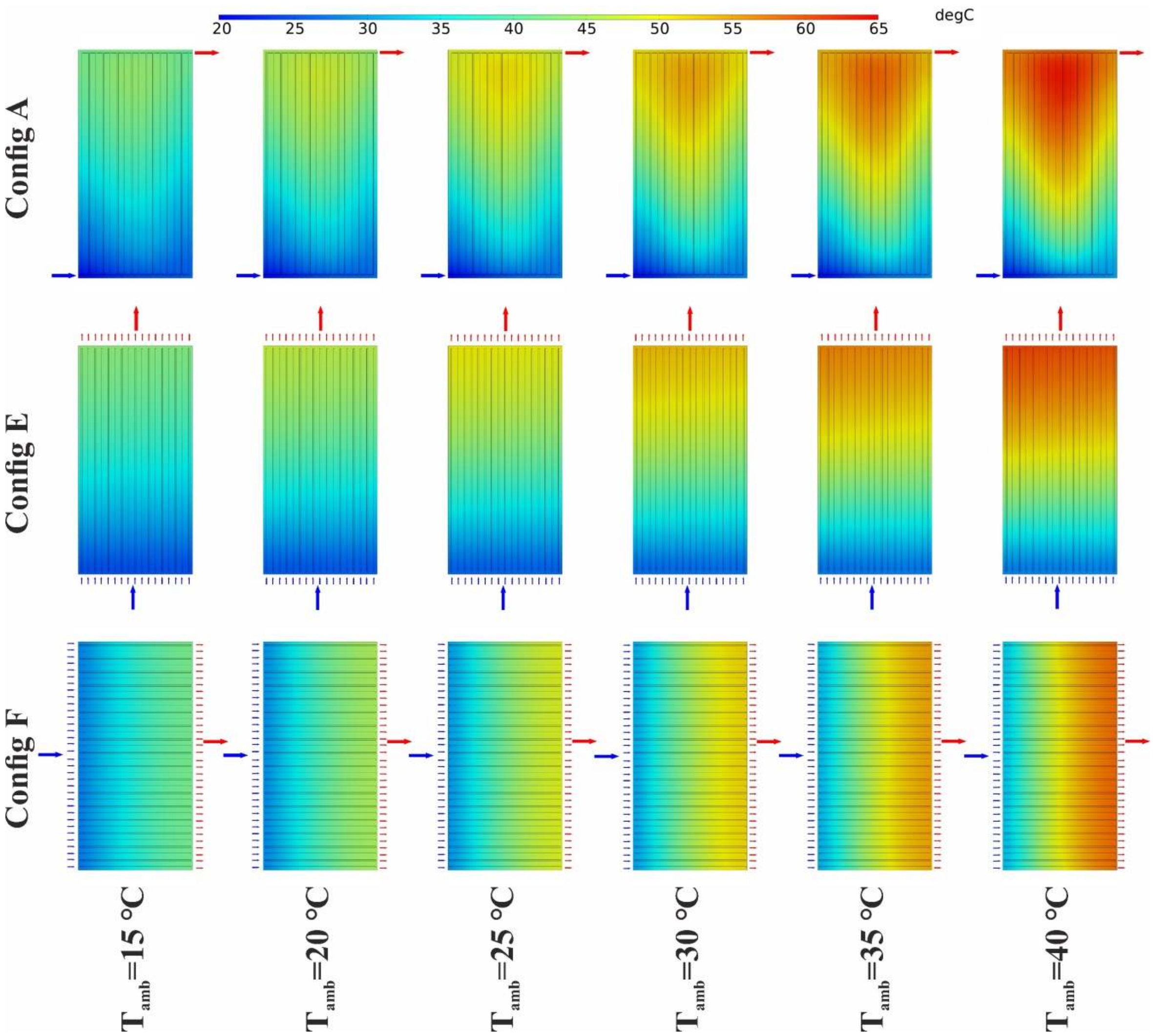

Figure 4.29. PVT absorber temperature distribution of Config A, Config E and Config F for different ambient temperatures

Figure 4.31 illustrates the variation in thermal and electrical energy production of the PVT collectors, along with the electricity generation of a conventional PV panel, as a function of ambient temperature. Rising ambient temperatures reduce heat losses and increase thermal energy output (Fig 4.31a). While differences among the top three configurations, Config A, E and F, and the remaining systems are minimal at low ambient temperatures, the difference between the configurations becomes more pronounced as ambient temperature increases. At the highest ambient temperature, the best-performing configuration, Config E, produced 25.80% more thermal energy than the lowest-performing configuration, Config B.

On the other hand, as the ambient temperature increases, the PV cell temperature rises, leading to a decrease in the electrical energy output of both the PVT collectors and the conventional PV panel (Fig 4.31b). At the lowest ambient temperature, there was little variation in electricity production among the PVT collectors. However, as ambient temperature increases, slight differences between configurations become more noticeable. When comparing the PVT collectors to the conventional PV panel, it was observed that at the lowest ambient temperature, the PVT systems produced 7% to 8.69% more electricity. As the ambient temperature reached its maximum value, this advantage widened, with the PVT collectors generating 13.2% to 17% more electricity than the conventional PV panel.

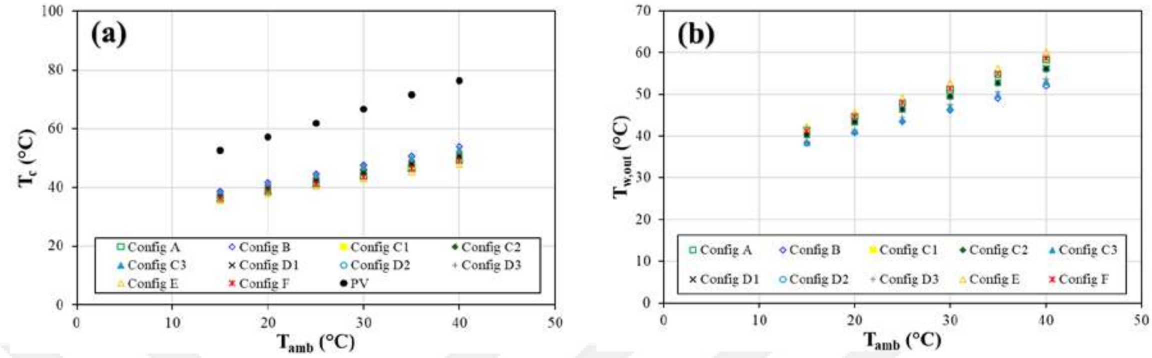

Figure 4.30. Variation of average PV cell (a) and water outlet (b) temperature of different parallel tube PVT configurations under varying ambient temperature conditions

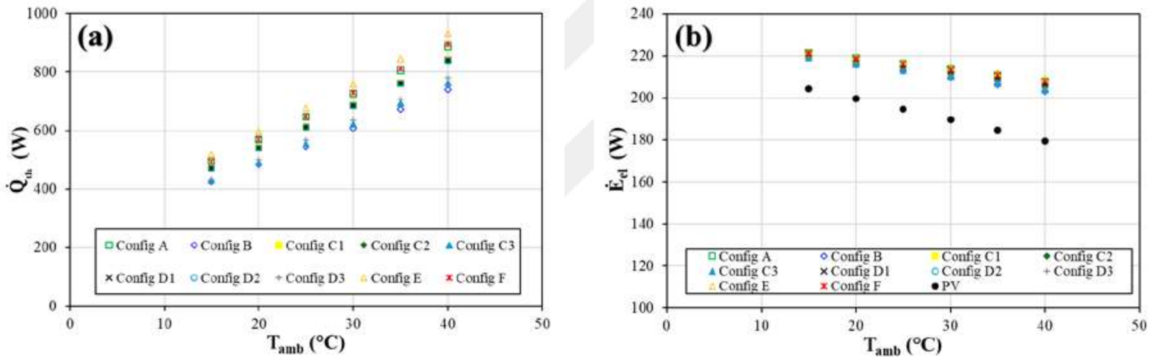

Figure 4.31. Variation of thermal energy production (a) and electrical power (b) of different parallel tube PVT configurations under varying ambient temperature conditions

An upward trend in the water outlet temperature is observed with the rise in ambient temperature. Given that the reduction in heat losses leads to an increase in thermal energy production. Consequently, thermal efficiency also shows an upward trend, ranging from 74% to 80% across different configurations, when ambient temperature increases from 15°C to 40°C as illustrated in Figure 4.32a. The highest thermal efficiency is observed at an ambient temperature of 40°C, with a value of 0.59 for Config E, while the lowest efficiency is recorded at 15°C, with a value of 0.27 for Config B. As the ambient temperature increases, the PV cell temperature also rises, leading to a decrease in electrical efficiency (Figure 4.32b). Unlike thermal efficiency, electrical efficiency exhibits slight decreases, varying between 5.83% and 7.23% for all configurations. Considering the conventional PV panel, electrical efficiencies were 8% to 9% lower than those of PVT collectors at the lowest ambient temperature considered. However, when the ambient temperature reached its peak, this difference increased to 13% to 17%.

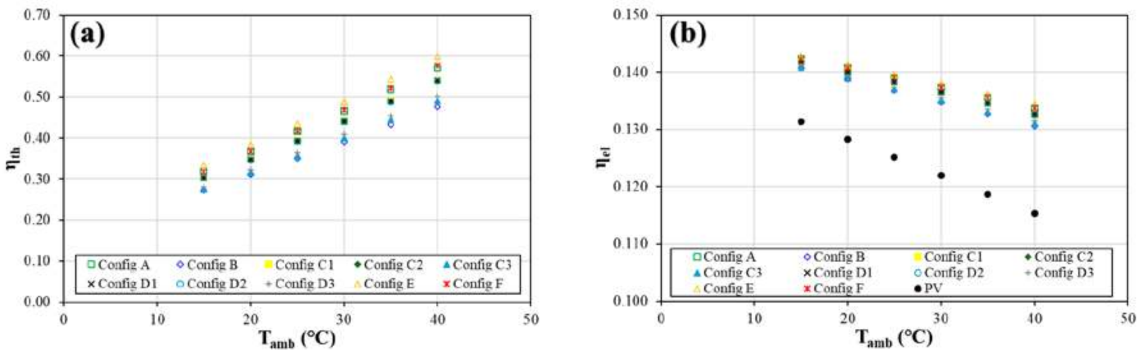

Figure 4.32. Effect of ambient temperature on the thermal (a) and electrical (b) efficiency of parallel tube PVT collectors

Figure 4.33 presents the variation of thermal, electrical and output exergies, along with exergy destruction, as a function of ambient temperature. Among these, the behavior of thermal exergy (Figure 4.33a) with ambient temperature is particularly influenced by both thermal energy production and the Carnot efficiency factor, as discussed below. As shown in Figure 4.31, thermal energy production increases with rising ambient temperature for all cases. According to Equation 3.48, thermal exergy includes a Carnot efficiency term, $\left(1-\frac{T_{amb}}{T_{w,out}}\right)$, which decreases as ambient temperature rises. However, in the best-performing configurations (A, E and F), the increase in thermal energy outweighs this effect, resulting in a net rise in thermal exergy, despite the decreasing Carnot factor. For the other configurations, although thermal energy production increases with ambient temperature, the more pronounced decrease in the Carnot efficiency factor causes thermal exergy to peak and then decline at higher ambient temperatures.

The electrical exergy (Figure 4.33b) follows the same trend as electrical efficiency, as presented in Figure 4.32, decreasing with the rise in ambient temperature. Given that the impact of electrical exergy on the output exergy is greater than that of thermal exergy, the output exergy remains nearly constant for some configurations (Config A, E, F) and decreases for others as the ambient temperature rises (Figure 4.33c). Conversely, exergy destruction exhibits a trend opposite to that of output exergy (Figure 4.33d). While the conventional PV panel exhibits similar exergetic performance trends to PVT configurations, it displays a consistently negative divergence in performance metrics.

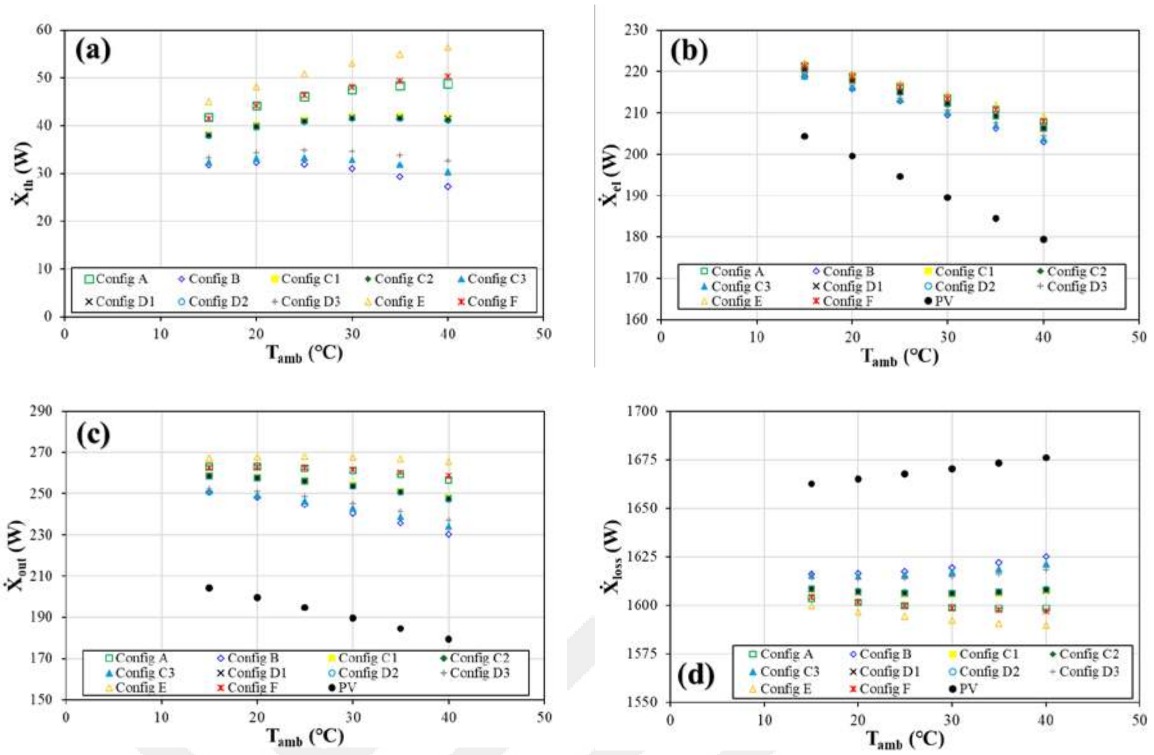

Figure 4.33. Effect of ambient temperature on the thermal (a), electrical (b) and output (c) exergy, and exergy destruction (d) of parallel tube PVT collectors

Since the variation in thermal efficiency with ambient temperature is much greater than that of electrical efficiency, the overall and primary energy saving efficiency follows the same trend as presented in Figure 4.32a. When the ambient temperature increases from 15 °C to 40 °C, the overall efficiency for all PVT configurations increases, ranging from 45.75% to 54.13% (Figure 4.34a). The overall efficiency reaches a maximum value of 0.73 for Config E at an ambient temperature of 40 °C. Similarly, as the ambient temperature increased from its minimum to maximum value, the primary energy saving efficiency across all PVT configurations improved, ranging from 27.47% to 34.31% (Figure 4.34b). At an ambient temperature of 40 °C, the highest primary energy saving efficiency was recorded as 0.95 for the best-performing configuration, Config E, whereas the lowest value was observed as 0.82 in Config B, the configuration with the poorest performance.

Exergy efficiency (Figure 4.34c), which is dependent on both output exergy and exergy input, tends to decrease with rising ambient temperatures for configurations other than A, E, and F, due to the exergy output decreasing more sharply than the input. An optimum value is reached at an ambient temperature of 20 °C, with exergy efficiency ranging from 0.141 to 0.144 for configurations A, E, and F. The conventional PV panel, experiencing declining electrical efficiency due to elevated cell temperatures, also shows decreases in both overall and exergy efficiencies as ambient temperature rises.

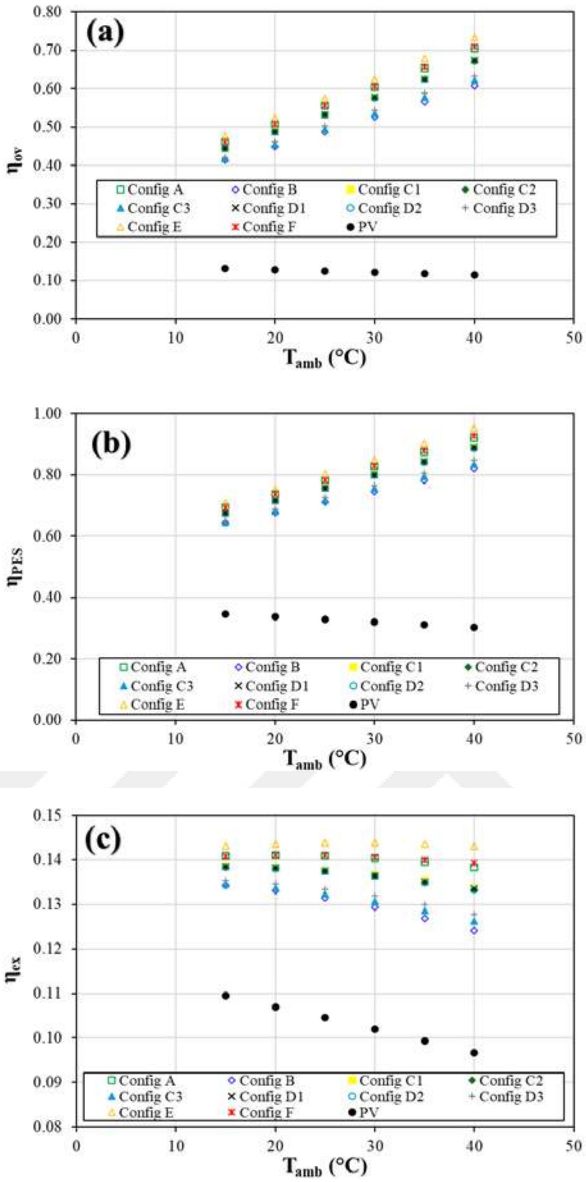

Figure 4.34. Effect of ambient temperature on the overall (a), primary energy saving (b) and exergy (c) efficiency of parallel tube PVT collectors

The effect of ambient temperature on the pressure drop and TEPD is depicted in Figure 4.35. An increase in ambient temperature leads to a higher water temperature, which in turn decreases water viscosity and density, and consequently reduces the pressure drop. As the ambient temperature rises from 15 °C to 40 °C, there is an approximate 9% decrease in pressure drop for Config B, which exhibits the highest pressure drop, and an approximate 17.5% decrease for Config F, which exhibits the lowest pressure drop. Additionally, the increase in ambient temperature enhancing the thermal energy output and substantially affecting TEPD.

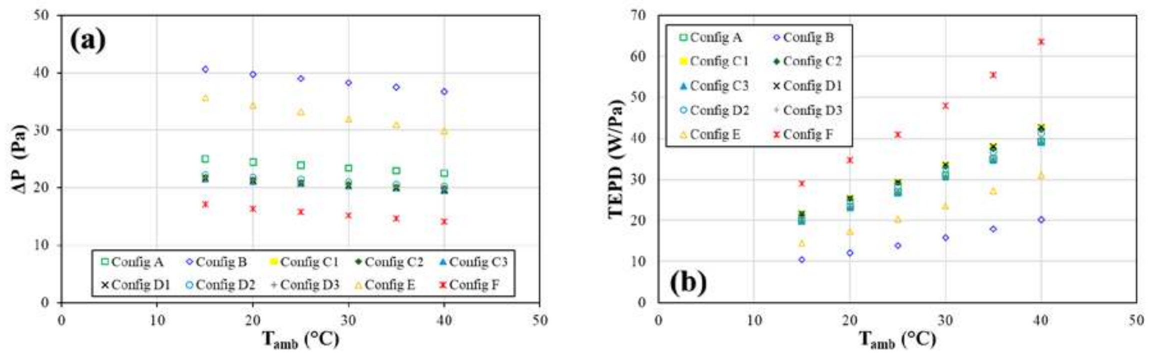

Figure 4.35. Effect of ambient temperature on the pressure drop (a) and TEPD (b) of parallel tube PVT collectors

4.1.6. Effect of Wind Velocity on the Parallel Tube PVT Collector Configurations

Wind velocity is another climatic condition that affects the heat losses due to convection. The effect of wind velocity on various energetic and exergetic performance parameters was studied by varying the wind velocity from 1 m/s to 5 m/s in 1 m/s increments for different PVT collector configurations. While the wind velocity was varied, other operating parameters were held constant.

Figures 4.36 and 4.37 present the absorber temperature distribution contours for the three best-performing parallel tube PVT configurations and the variations in PV cell and fluid outlet temperatures with changing wind velocity for all PVT collectors, respectively. To better visualize the influence of operational parameters discussed in previous sections, the temperature scale in Figure 4.36 was standardized across the different parameters.

As illustrated in the figure, increasing wind velocity leads to a reduction in absorber temperatures. A similar trend is observed in Figure 4.37a, where the average PV cell temperature decreases as wind velocity increases. The variation in the average surface temperature of a conventional PV panel with wind velocity is also presented, showing the same declining pattern. Although notable differences exist between the PVT collectors and the conventional PV panel at lower wind velocities, these differences diminish as wind velocity increases. Specifically, when wind velocity increased from 1 m/s to 5 m/s, the average surface temperature of the conventional PV panel dropped by approximately 17.75 °C. In the same conditions, average PV cell temperatures of the PVT collectors decreased by between 4.59 °C and 7.09 °C. Under maximum wind velocity, the PV cell temperature of the best-performing configuration, Config E, was approximately 19% lower than that of the conventional PV panel. Due to the enhanced convective heat transfer associated with higher wind velocities, heat losses increased, resulting in a reduction in fluid outlet temperatures. For example, in Config E, the fluid outlet temperature decreased from 49.17 °C to 40.59 °C as wind velocity rose from its minimum to maximum value, whereas in Config B, it decreased from 43.50 °C to 36.97 °C under the same conditions. The reduction in both the PV cell temperature and the fluid outlet temperature with increasing wind velocity is also clearly demonstrated in the study conducted by Ahmadinejad and Moosavi (2023). According to the study, increasing the wind velocity from 1 m/s to 4 m/s led to a 3.94% reduction in PVT cell temperature and a 5.11% decrease in the fluid outlet temperature.

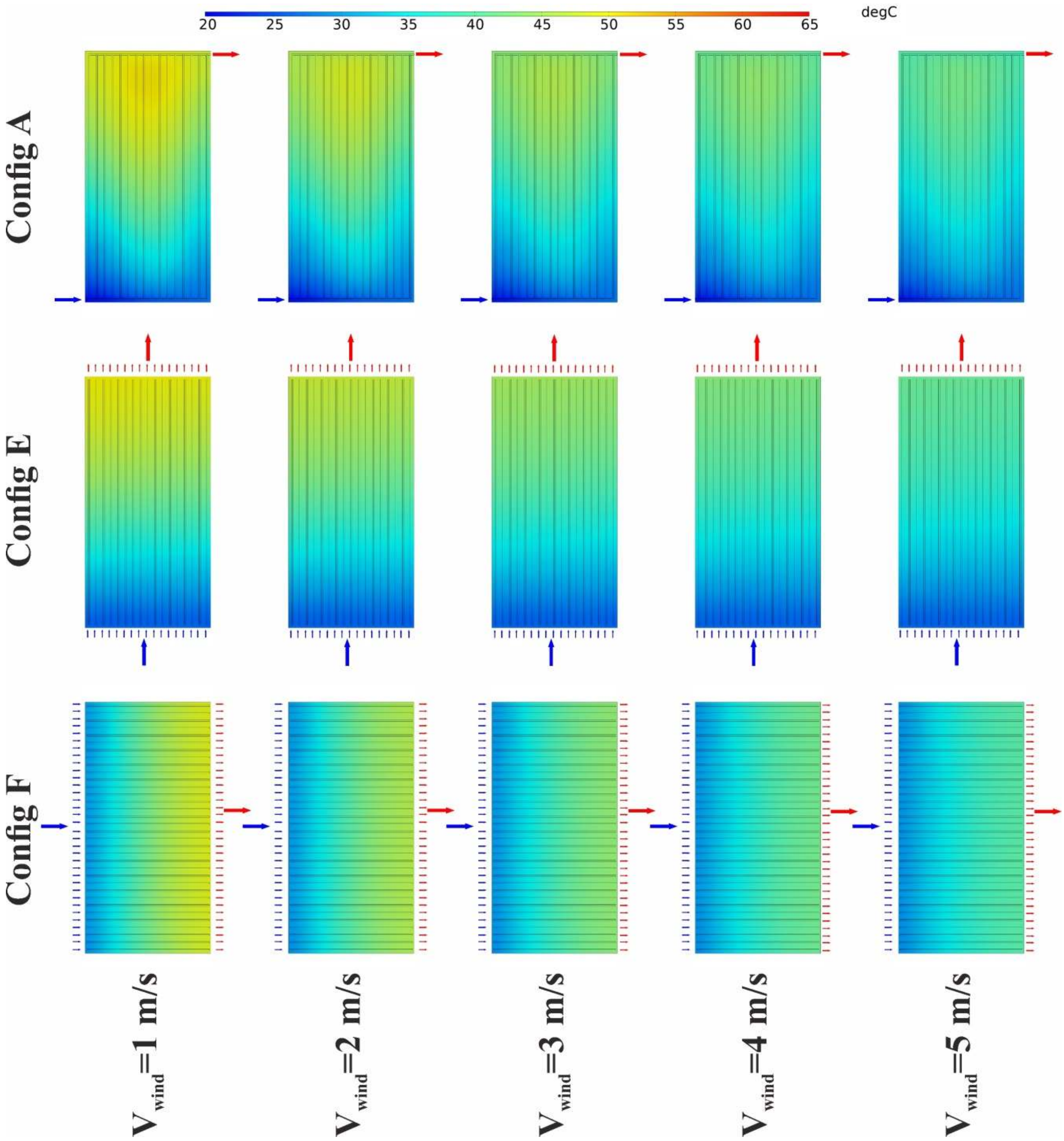

Figure 4.36. PVT absorber temperature distribution of Config A, Config E and Config F for different wind velocities

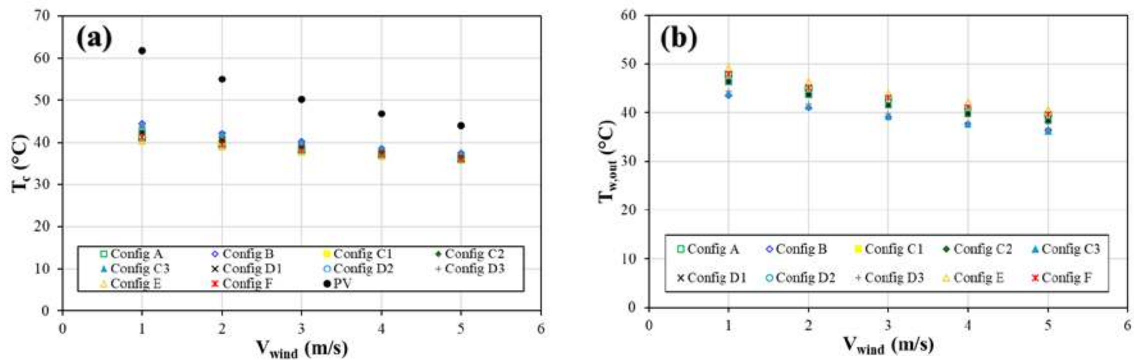

Figure 4.37. Variation of average PV cell (a) and water outlet (b) temperature of different parallel tube PVT configurations under varying wind velocity conditions

Figure 4.38 illustrates the changes in thermal and electrical energy production of the PVT collectors, as well as the electricity generation of conventional PV panels, as a function of wind velocity. Since both the fluid inlet temperature and flow rate are held constant, the trend between thermal energy production and fluid outlet temperature is similar. As shown in Figure 4.37b, the fluid outlet temperature decreases with increasing wind velocity due to the increasing convective heat losses, which in turn also leads to a reduction in thermal energy production. Specifically, the thermal energy output of the PVT collectors decreases by approximately 29% to 32% as wind velocity increases from 1 m/s to 5 m/s.

On the other hand, as the PV cell temperatures of the PVT collectors decrease with increasing wind velocity, their electrical energy production improves (Figure 4.38b). A similar trend is observed for the conventional PV panels.

Although there are visually observable differences among PVT collectors themselves and significant disparities between PVT collectors and conventional PV panels at low wind velocities, increasing wind speed leads to a convergence in the electrical output of PVT collectors and a reduction in the performance gap between them and PV panels.

At a wind velocity of 1 m/s, the PVT collectors produce 9.35% to 11.6% more electricity than the conventional PV panel. However, at 5 m/s, the gap narrows, with PVT collectors generating 3.29% to 4.10% more electricity compared to the conventional PV panel.

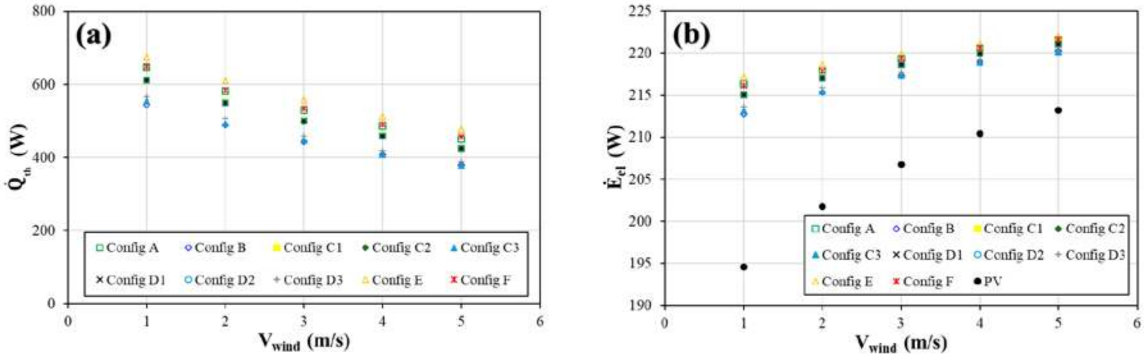

Figure 4.38. Variation of thermal energy production (a) and electrical power (b) of different parallel tube PVT configurations under varying wind velocity conditions

Increasing wind velocity increases heat loss due to convection through the PVT collector as it alters the heat transfer coefficient (Eq. 3.23). These losses reduce both the PV cell temperature and the water outlet temperature. Figure 4.39 illustrates the impact of varying wind velocity on the thermal and electrical efficiency. As wind velocity increases, thermal energy production and water outlet temperature decrease due to the convective heat losses, consequently, a decline in thermal efficiency. Specifically, an increase in wind velocity from 1 to 5 m/s results in an approximate 30% reduction in thermal efficiency across all configurations. The highest thermal efficiency, observed at 0.43, occurs in Config E at a wind velocity of 1 m/s. Conversely, the reduction in PV cell temperature due to higher wind velocities enhances electrical efficiency and electrical output. As wind velocity increases from 1 to 5 m/s, electrical efficiency shows a modest increase, ranging from 2.4% to 3.5% across all configurations. This indicates that wind velocity has a relatively minor effect on electrical efficiency. The highest electrical efficiency, recorded at 0.1427, is also observed in Config E at a wind velocity of 5 m/s. For the conventional PV panel, the electrical efficiency is approximately 9% to 11% lower than that of PVT collectors at the lowest wind velocity studied. However, as wind velocity increases, the electrical efficiency of the PV panel improves due to increased convective heat loss, narrowing the performance gap with PVT collectors to about 4%.

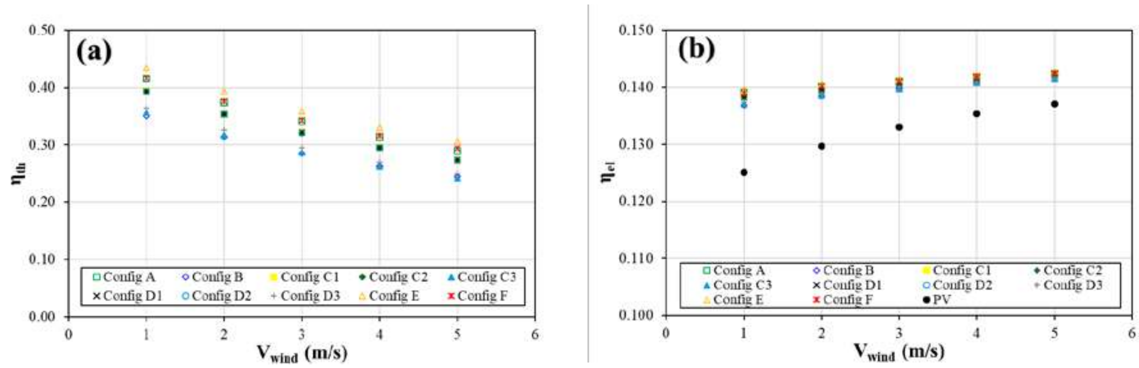

Figure 4.39. Effect of wind velocity on the thermal (a) and electrical (b) efficiency of parallel tube PVT collectors

The impact of wind velocity variations on exergetic parameters is comprehensively analyzed in Figure 4.40. An increase in wind velocity results in a decrease in the water outlet temperature, which in turn significantly reduces the thermal exergy. Moreover, the decrease in PV cell temperature due to the increased wind velocity enhances electrical efficiency, leading to a slight increase in electrical exergy for PVT configurations. Despite this minor increase in electrical exergy, the substantial reduction in thermal exergy results in an overall decrease in exergy output. Conversely, exergy destruction exhibits an increasing trend with higher wind velocities, as depicted in Figure 4.40d. For the conventional PV panel, which lacks the thermal component of exergy, the analysis highlights a different behavior. As wind velocity increases, the electrical exergy of the PV panel rises due to the cooling effect reducing cell temperatures. This improvement narrows the gap between the electrical exergy of the PV panel and PVT collectors. Additionally, since the output exergy of the PV panel is solely based on electrical exergy, it mirrors the trend observed in electrical exergy, showing a consistent improvement with higher wind velocities.

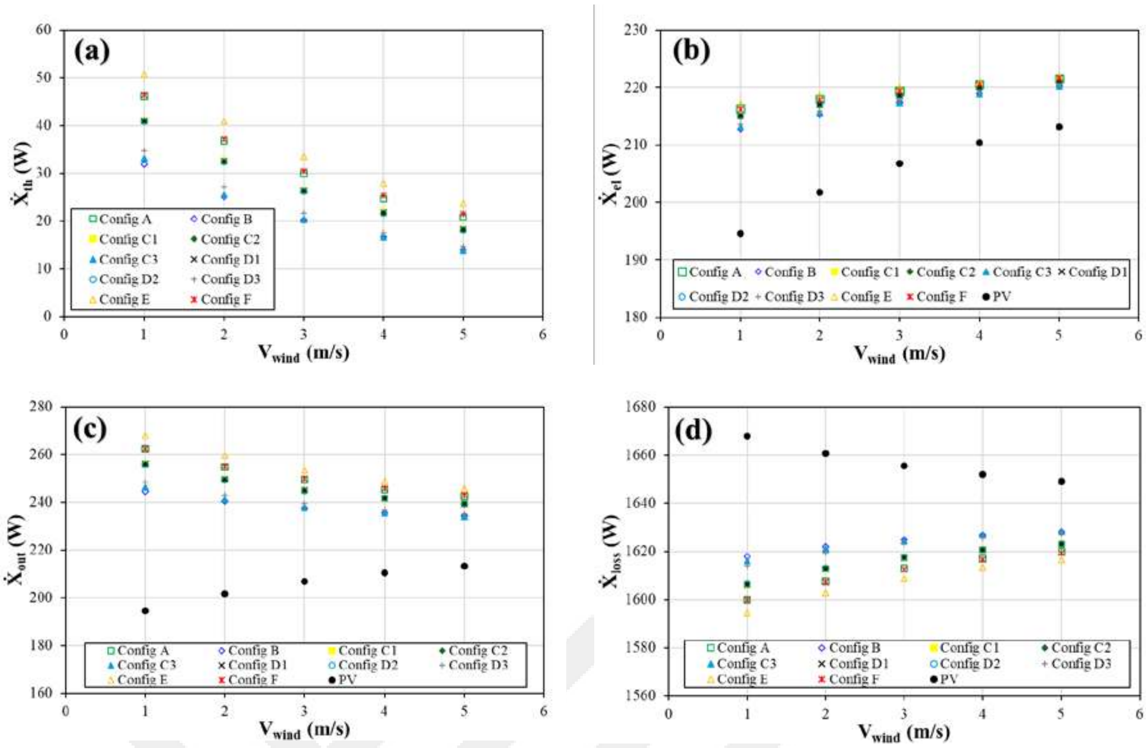

Figure 4.40. Effect of wind velocity on the thermal (a), electrical (b) and output (c) exergy, and exergy destruction (d) of parallel tube PVT collectors

Overall and primary energy saving efficiency decreases with increasing wind velocity as shown in Figure 4.41. This decline is primarily attributed to a significant reduction in thermal efficiency by approximately 30% while electrical efficiency exhibits only a slight increase. Consequently, the overall efficiency is more profoundly influenced by changes in thermal efficiency. Across all PVT configurations, the overall efficiency decreases by approximately 22%, with the highest overall efficiency observed in Config E, reaching 0.57 at a wind velocity of 1 m/s. The primary energy saving efficiency decreases by approximately 13% to 14% as the wind velocity increases from its minimum to maximum value for all PVT collectors. The highest primary energy saving efficiency is recorded for Config E, reaching 0.80 at a wind velocity of 1 m/s, while the lowest value is observed as 0.62 at 5 m/s.

Since the exergy input remains constant and independent of wind velocity across all configurations, the exergy efficiency (Figure 4.41c) is directly linked to the output exergy, shown in Figure 4.40c. As wind velocity increases, the output exergy decreases, leading to a corresponding decline in exergy efficiency for PVT configurations. The maximum exergy efficiency is achieved in Config E with 0.144 at a wind velocity of 1 m/s. For the conventional PV panel, the absence of thermal exergy production leads to efficiency metrics exhibiting a trend opposite to that of PVT configurations. Similar to the present study, Ahmadinejad and Moosavi (2023) also reported that while thermal efficiency decreased by 13.11% and electrical efficiency improved by 0.55% with increasing wind velocity from 1m/s to 4 m/s, the overall efficiency exhibited a downward trend. Moreover, their results demonstrated a reduction in exergy efficiency under higher wind velocity conditions.

Increasing wind velocity results in a reduction of the water temperature, which in turn leads to an increase in water viscosity and density. Although the pressure drop rises with the increased water properties, the overall effect of wind velocity on the pressure drop remains negligible, as illustrated in Figure 4.42a. Conversely, the reduction in thermal energy production due to increased heat loss, combined with the minimal change in pressure drop, results in a significant reduction of approximately 34% in TEPD (Figure 4.42b).

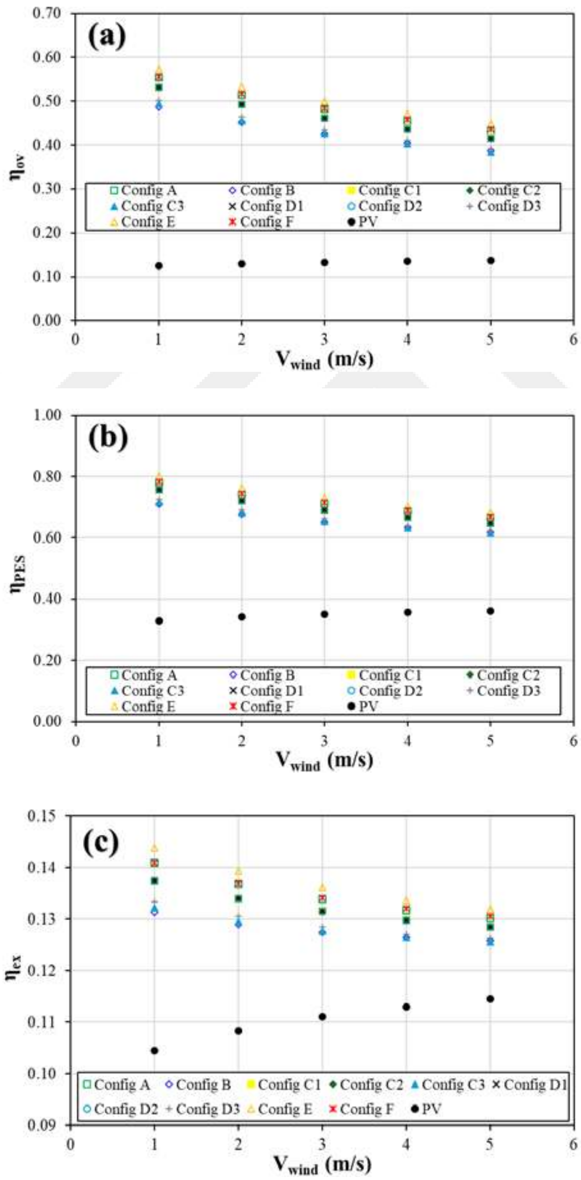

Figure 4.41. Effect of wind velocity on the overall (a), primary energy saving (b) and exergy (c) efficiency of parallel tube PVT collectors

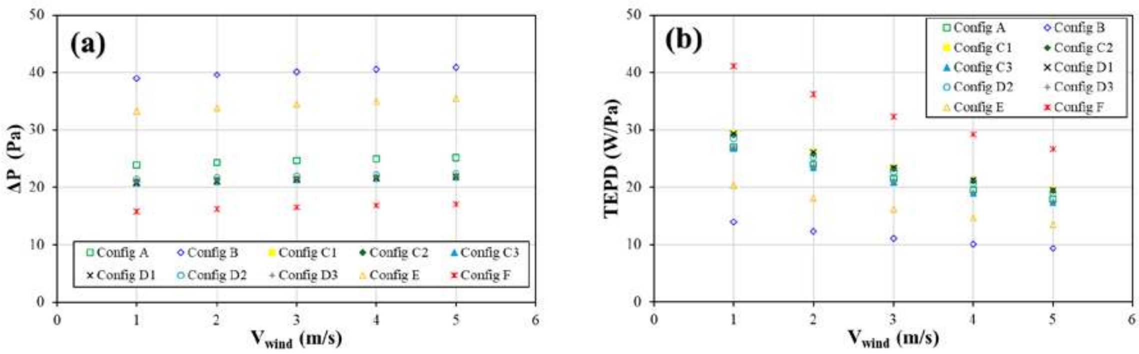

Figure 4.42. Effect of wind velocity on the pressure drop (a) and TEPD (b) of parallel tube PVT collectors

4.2. Serpentine Tube PVT Collector Configurations

In this section, a comprehensive comparison was conducted across twenty-five different serpentine tube PVT configurations featuring single, double and triple inlets, with tube arranged either vertically or horizontally (Figure 3.3). The finite element method was used to analyze key performance metrics, including average PV cell temperature, water outlet temperature, pressure drop, thermal and electrical energy production, thermal, electrical, overall and primary energy saving efficiency and exergy performance under base-case conditions and variable operation conditions such as flow rate, solar irradiance, fluid inlet temperature, ambient temperature and wind velocity. These serpentine tube PVT collectors were also compared with a conventional PV panel in terms of electrical performance. Moreover, the surface temperature distribution of the twenty-five different serpentine tube PVT collectors was compared under base-case conditions, and the absorber temperature distributions of the top three configurations were further analyzed under varying flow rate, solar irradiance, fluid inlet temperature, ambient temperature and wind velocity to provide insights into how different design configurations impact PVT collector performance under varying operating conditions.

4.2.1. Comparison of Serpentine Tube PVT Collector Configurations Under Base-case Conditions

The serpentine tube configurations were categorized based on the number of inlets, the position and direct of the fluid inlet. Different configurations of serpentine tube PVT collectors are compared with respect to various performance parameters under the base-case conditions. In order to eliminate the influence of geometric and hydraulic variables, the total tube length, absorber area and fluid flow rate were maintained constant for all configurations.

In the design of PVT collectors, temperature distribution is as critical as thermal and electrical performance metrics. Non-uniform temperature distribution is undesirable, as it negatively impacts PV cell performance, leading to reductions in thermal, electrical, primary energy saving and overall efficiency. Furthermore, prolonged exposure to uneven temperature fields can accelerate the physical degradation of PV cells, thereby shortening the operational lifespan of the system.

Figure 4.43 displays the surface temperature distribution contours of 25 serpentine tube PVT configurations under base-case operating conditions. Configurations G and H are designed with a single inlet, while configurations I, J, K, L, M, N, O and P feature double inlets with horizontally arranged tubes. Configurations S and Q, by contrast, are triple-inlet PVT collectors. Additionally, configurations G, I, J, M, O, P and S are vertically arranged, whereas configurations H, K, L, N, R and Q are horizontally oriented.

As illustrated in the figure, temperature is lowest near the fluid inlet zones and gradually increases toward the collector outlet, indicating the expected thermal gradient. Among the evaluated designs, configurations G, H, N1, P1, R1 and Q exhibit more uniform temperature distributions compared to the others. In contrast, Config N2 demonstrates the most pronounced non-uniformity, primarily due to the opposing flow directions in adjacent tubes. Furthermore, in Config S, elevated temperatures are observed in areas where the working fluid does not make direct contact with the absorber surface, suggesting localized thermal energy accumulation.

One of the most crucial parameters affecting PVT collector performance is the PV cell temperature. An increase in PV cell temperature reduces electrical efficiency and can lead to cell deterioration over time. In the figures below (Figures 4.44 to 4.48), which are color-coded by inlet number, green is used to represent single-input configurations, blue for double-input configurations, red for triple-input configurations and black for conventional PV panel.

Average PV cell and water outlet temperatures of different serpentine tube PVT configurations are presented in Figure 4.44. Four configurations stand out for their low PV cell temperatures: the single-inlet configuration H, the double-inlet configurations N1 and R1, and the triple-inlet configuration Q (Figure 4.44a). When the inlets were positioned at the center of the collector or spaced farther apart, the performance of the PVT collectors deteriorated. Additionally, the same figure includes a comparison between the investigated serpentine tube PVT collectors and a conventional PV panel. Even the least efficient configuration in terms of PV cell temperature, Config N2, maintains a cell temperature that is 13.44 °C lower than that of the conventional PV panel. On the other hand, configurations H, N1, R1 and Q exhibit the highest water outlet temperatures (Figure 4.44b). These configurations, which exhibit lower PVT cell temperature and higher water outlet temperature, highlighted the importance of inlet placement and alignment in optimizing PVT collector performance.

The thermal and electrical energy productions, along with their corresponding efficiencies, are presented for all serpentine tube configurations (Figure 4.45). The configurations with horizontal tube alignment generally exhibited better energetic performance compared to other arrangements. Electrical energy production and related efficiency were directly influenced by the PV cell temperature. As PV cell temperature increased, electrical efficiency decreased, leading to reduced electricity output. Configurations with lower PV cell temperatures and higher water outlet temperatures, as highlighted in Figure 4.44, demonstrated better performance. Considering all the energetic performance parameters depicted in Figure 4.45, the configurations that yield the best overall results were H, N1, R1 and Q. These configurations consistently exhibited lower PV cell temperatures and higher water outlet temperatures, which are key to achieving optimal thermal and electrical performance in PVT collectors.

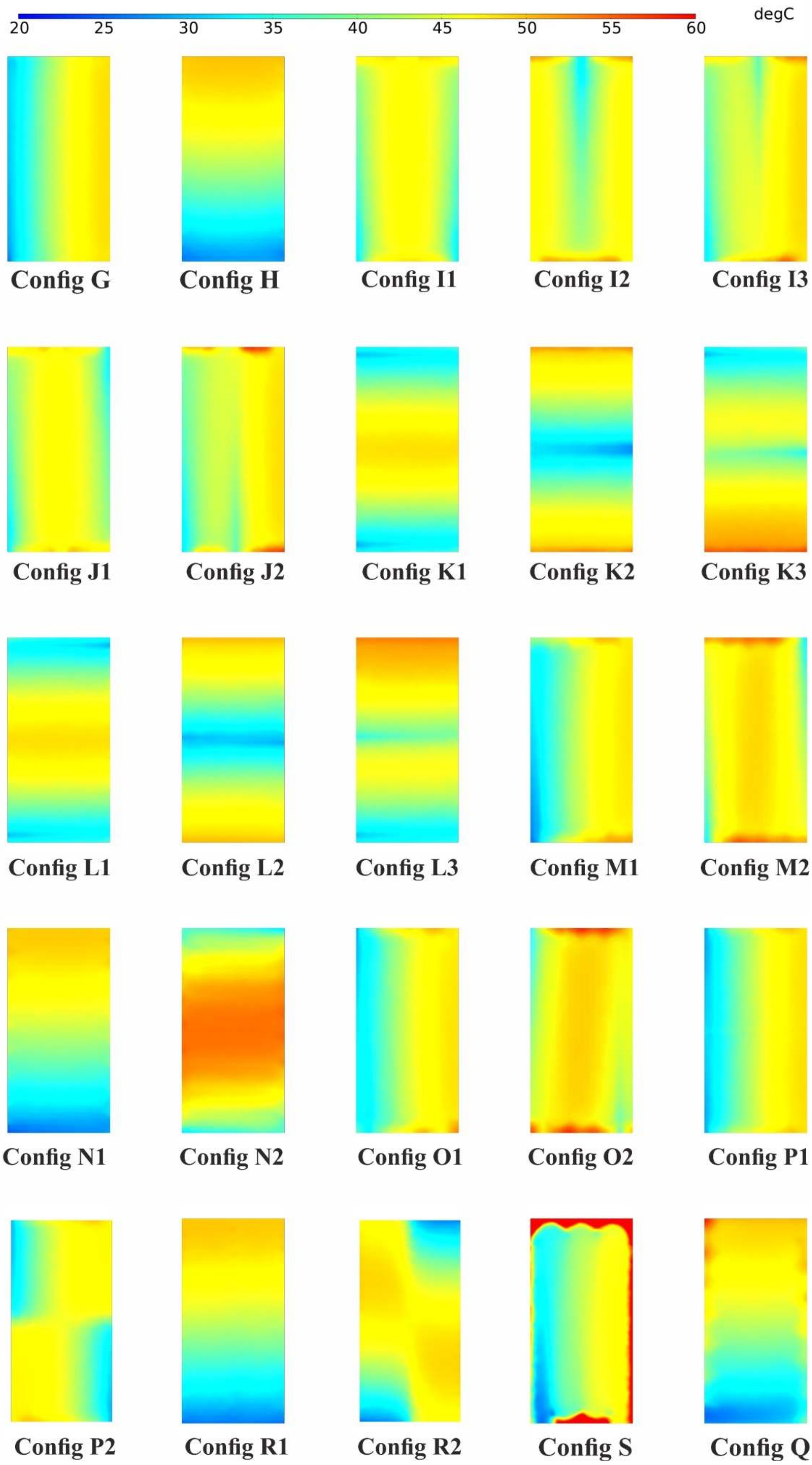

Figure 4.43. Temperature contour of different serpentine tube PVT configurations under base-case conditions

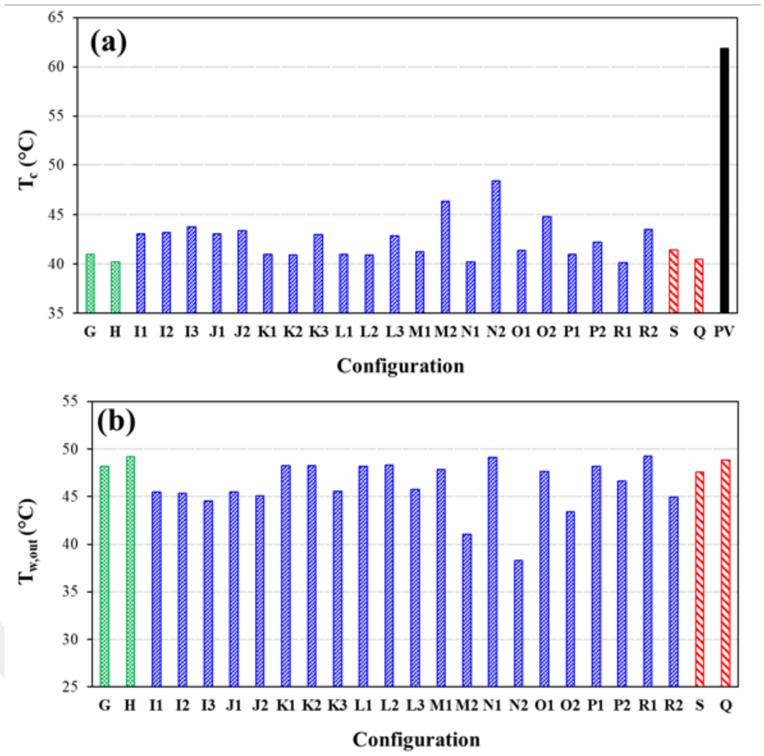

Figure 4.44. Average cell (a) and water outlet (b) temperature of different serpentine tube PVT configurations under base-case conditions

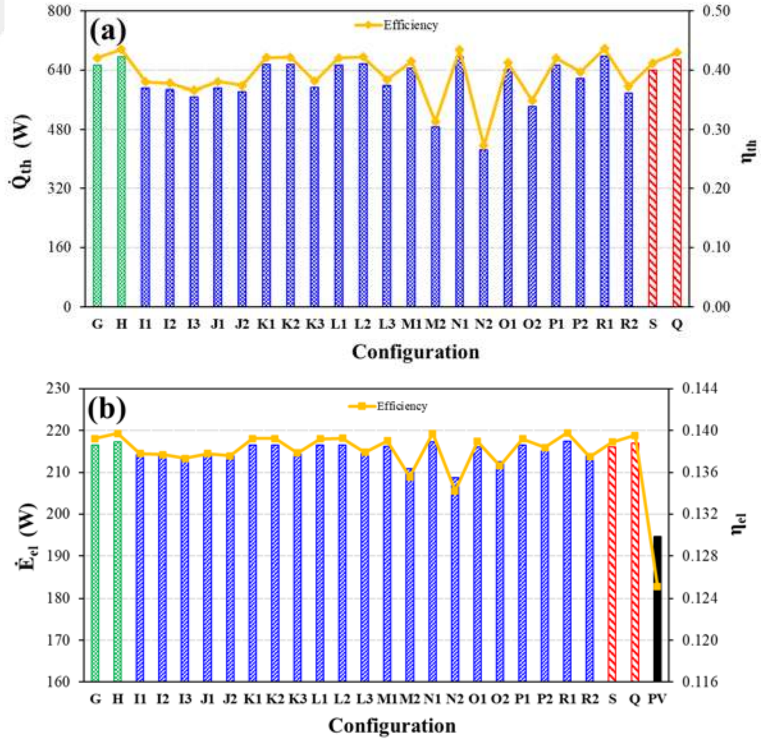

Figure 4.45. Thermal power and thermal efficiency (a), electrical power and electrical efficiency (b) of different serpentine tube PVT configurations under base-case conditions

Although serpentine tube PVT collectors generally suffer from high pressure drop, the extent varied across designs. The pressure drop and the amount of thermal energy produced per pressure drop (TEPD) of all serpentine tube configurations are presented in Figure 4.46. Since the flow rate through a collector was higher in single-inlet configurations, the highest pressure drop among all configurations occurs in configurations G and H (Figure 4.46a). Similarly, double-inlet configurations generally experience higher pressure drops than triple-inlet configurations, leading to the lowest pressure drops occurring in configurations S and Q. When all serpentine tube configurations were compared, the pressure drops were lower in vertically arranged configurations due to the lower local losses. Examining TEPD revealed an inverse relationship with pressure drop: configurations with more inlets, such as S and Q, which have lower pressure drops, achieved the highest TEPD values (Figure 4.46b). Conversely, configurations G and H, which have the highest pressure drops, exhibited the lowest TEPD values. These results highlight the importance of optimizing inlet configuration and alignment to balance thermal energy production with manageable pressure drops in serpentine tube PVT collectors.

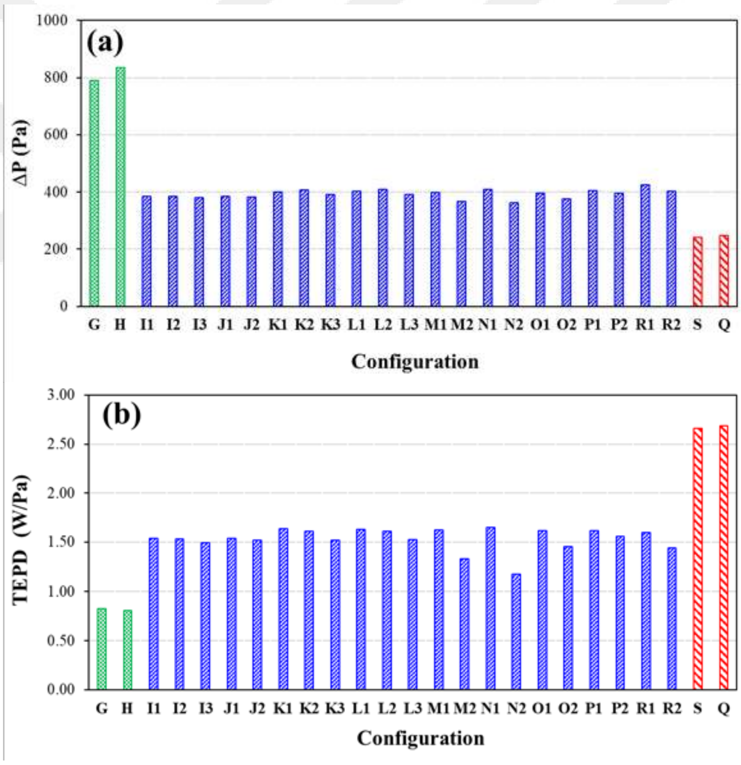

Figure 4.46. Pressure drop (a) and TEPD (b) of different serpentine tube PVT configurations under base-case conditions

The exergetic performance parameters, which assess both the quality and quantity of energy, are compared in Figure 4.47. Since the other operating conditions were identical across configurations, the thermal exergy production was primarily dependent on the water outlet temperature. As a result, thermal exergy (Figure 4.47a) followed the same trend as the water outlet temperature presented in Figure 4.44b, with the highest values in configurations R1, H, N1 and Q, while configuration N2 exhibited the lowest thermal exergy. Electrical exergy (Figure 4.47b) was relatively consistent across all serpentine tube configurations and align closely with the electrical efficiency (Figure 4.45b). Given that output exergy (Figure 4.47c) was a combination of both thermal and electrical exergies, it followed the same trend as these exergies. However, due to the higher quality of electrical power, output exergy was significantly influenced by the electrical power production. Exergy destruction, depicted in Figure 4.47d, shows an inverse relationship to output exergy. Since exergy destruction represented the difference between the exergy input from the sun and the output exergy, and the solar exergy input was identical across all configurations, the configurations with higher output exergy exhibited lower exergy destruction. Conversely, configurations with lower output exergy, such as N2, had higher exergy destruction. This analysis underscored the critical role of both thermal and electrical exergies in determining the overall exergetic performance of PVT collectors, emphasizing that optimizing both was essential for minimizing exergy destruction and maximizing the quality of energy produced.

The efficiencies of serpentine tube PVT collectors, which are the final results of the general energy and exergy performance parameters, were compared in Figure 4.48. Since overall and primary energy saving efficiencies are a function of both thermal and electrical efficiencies, the highest values were reached in the configurations R1, H, N1 and Q where both of these efficiencies were high, while the lowest value was observed in configuration N2. The configurations with the highest efficiency outperformed configuration N2 by approximately 39.87% and 27.31% for overall (Figure 4.48a) and primary energy saving efficiency (Figure 4.48b), demonstrating the significant impact of optimizing both thermal and electrical outputs. On the other hand, regarding exergy efficiency, since the input exergy was constant across all configurations, exergy efficiency was directly related to the output exergy. The highest exergy efficiencies were also achieved in configurations R1, H, N1 and Q, with values reaching approximately 0.1440 (Figure 4.48c).

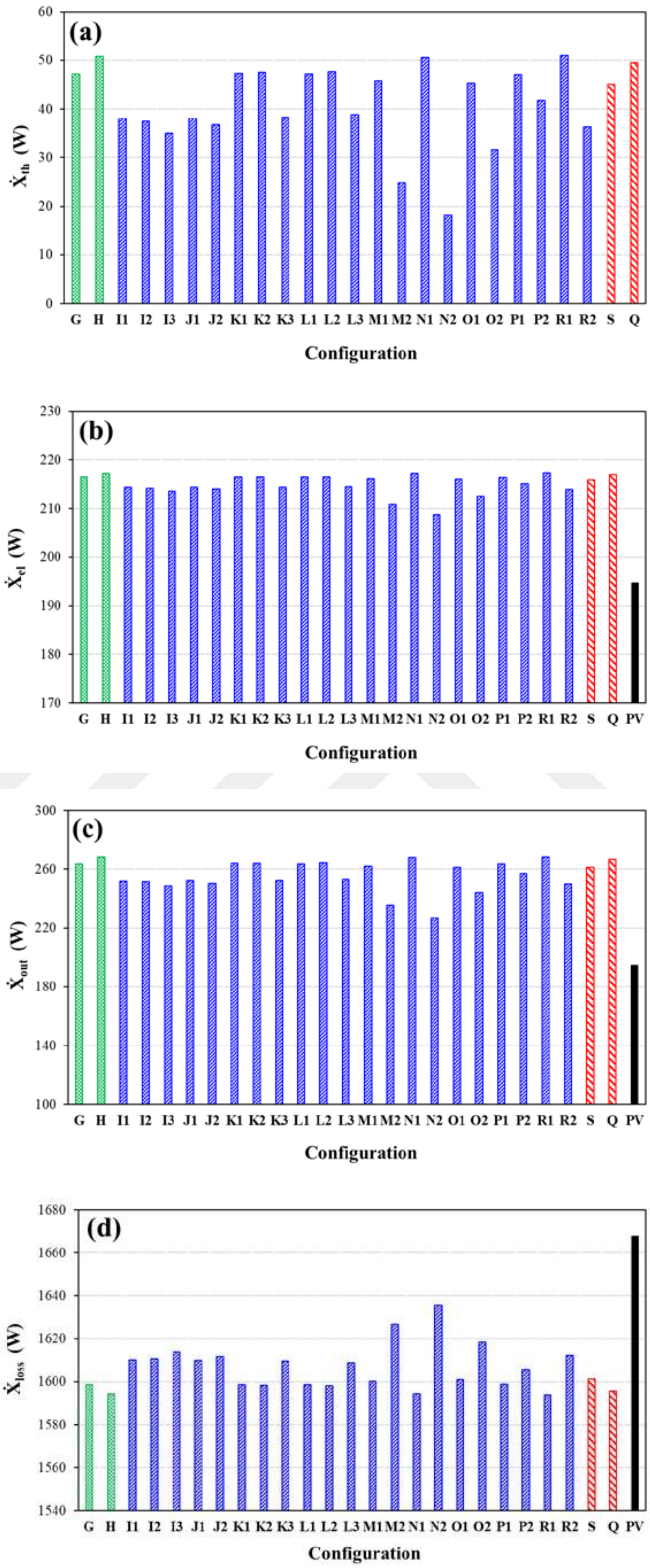

Figure 4.47. Thermal (a), electrical (b) and output (c) exergy and exergy destruction (d) of serpentine tube PVT configurations under base-case conditions

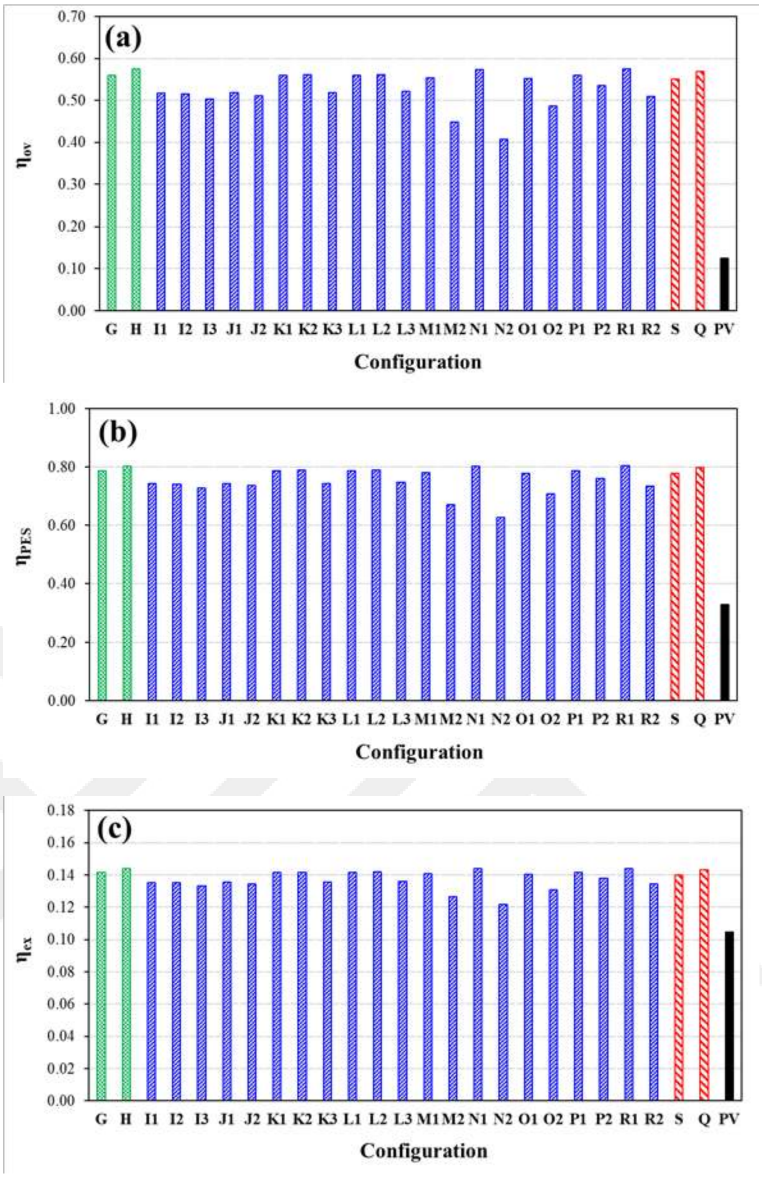

Figure 4.48. Overall (a), primary energy saving (b) and exergy (c) efficiency of different serpentine tube PVT configurations under base-case conditions

Figure 4.49 presents a comprehensive comparison of all performance parameters for the serpentine tube PVT collectors and the conventional PV panel under base-case operating conditions. In the figure, green indicates the configuration with the highest performance, while red denotes the configuration with the lowest. When the temperature distribution results from Figure 4.43 are considered alongside the performance metrics, the horizontally arranged serpentine tube configurations, specifically H, R1 and Q, stand out as the most effective designs.

Configuration	T_c (°C)	$T_{w,out}$ (°C)	ΔP (Pa)	$\dot{Q}_{th}$ (W)	$\dot{E}_{el}$ (W)	η_{el} (-)	η_{th} (-)	η_{ov} (-)	η_{PES} (-)	TEPD (W/Pa)	$\dot{X}_{th}$ (W)	$\dot{X}_{el}$ (W)	$\dot{X}_{out}$ (W)	$\dot{X}_{loss}$ (W)	η_{ex} (-)
G	40.97	48.19	789.78	653.75	216.51	0.1392	0.4204	0.5596	0.7867	0.83	47.19	216.51	263.70	1598.67	0.1416
H	40.23	49.18	835.29	676.56	217.29	0.1397	0.4350	0.5747	0.8027	0.81	50.75	217.29	268.04	1594.34	0.1439
I1	43.10	45.49	384.36	590.98	214.28	0.1378	0.3800	0.5178	0.7426	1.54	38.00	214.28	252.28	1610.10	0.1355
I2	43.22	45.33	383.74	587.34	214.16	0.1377	0.3777	0.5154	0.7400	1.53	37.49	214.16	251.65	1610.72	0.1351
I3	43.77	44.53	380.60	568.85	213.58	0.1373	0.3658	0.5031	0.7272	1.49	34.98	213.58	248.55	1613.82	0.1335
J1	43.08	45.52	384.76	591.72	214.30	0.1378	0.3805	0.5183	0.7431	1.54	38.10	214.30	252.40	1609.98	0.1355
J2	43.42	45.10	383.33	581.96	213.94	0.1376	0.3742	0.5118	0.7362	1.52	36.75	213.94	250.70	1611.68	0.1346
K1	40.98	48.23	400.55	654.66	216.51	0.1392	0.4209	0.5602	0.7873	1.63	47.33	216.51	263.83	1598.54	0.1417
K2	40.94	48.29	406.94	655.98	216.54	0.1392	0.4218	0.5610	0.7882	1.61	47.53	216.54	264.07	1598.30	0.1418
K3	43.00	45.56	390.42	592.76	214.38	0.1379	0.3811	0.5190	0.7439	1.52	38.24	214.38	252.63	1609.75	0.1356
L1	41.00	48.21	401.73	654.10	216.49	0.1392	0.4206	0.5598	0.7869	1.63	47.24	216.49	263.73	1598.64	0.1416
L2	40.92	48.32	408.09	656.58	216.57	0.1393	0.4222	0.5614	0.7886	1.61	47.62	216.57	264.19	1598.19	0.1419
L3	42.90	45.76	391.93	597.28	214.49	0.1379	0.3841	0.5220	0.7470	1.52	38.88	214.49	253.36	1609.01	0.1360
M1	41.27	47.82	397.40	645.13	216.20	0.1390	0.4148	0.5538	0.7807	1.62	45.87	216.20	262.07	1600.31	0.1407
M2	46.41	41.03	366.32	487.54	210.81	0.1356	0.3135	0.4490	0.6702	1.33	24.87	210.81	235.68	1626.69	0.1265
N1	40.24	49.13	409.73	675.42	217.28	0.1397	0.4343	0.5740	0.8020	1.65	50.57	217.28	267.85	1594.53	0.1438
N2	48.40	38.31	361.84	424.47	208.71	0.1342	0.2729	0.4071	0.6261	1.17	18.13	208.71	226.85	1635.53	0.1218
O1	41.38	47.67	396.23	641.63	216.09	0.1389	0.4126	0.5515	0.7782	1.62	45.34	216.09	261.43	1600.94	0.1404
O2	44.80	43.43	374.50	543.27	212.49	0.1366	0.3493	0.4860	0.7089	1.45	31.63	212.49	244.12	1618.25	0.1311
P1	41.02	48.17	404.71	653.18	216.46	0.1392	0.4200	0.5592	0.7863	1.61	47.10	216.46	263.56	1598.81	0.1415
P2	42.25	46.63	396.01	617.47	215.17	0.1384	0.3970	0.5354	0.7611	1.56	41.77	215.17	256.94	1605.44	0.1380
R1	40.15	49.25	424.87	678.20	217.38	0.1398	0.4361	0.5759	0.8039	1.60	51.01	217.38	268.38	1593.99	0.1441
R2	43.53	44.96	402.24	578.78	213.83	0.1375	0.3722	0.5096	0.7340	1.44	36.32	213.83	250.15	1612.23	0.1343
S	41.46	47.62	240.59	640.35	216.00	0.1389	0.4118	0.5506	0.7772	2.66	45.15	216.00	261.15	1601.23	0.1402
Q	40.51	48.84	248.94	668.61	217.00	0.1395	0.4299	0.5695	0.7971	2.69	49.49	217.00	266.50	1595.88	0.1431
PV	61.84	-	-	-	194.60	0.1251	-	0.1251	-	-	-	194.60	194.60	1667.77	0.1045

Figure 4.49. Comparison of performance parameters of all serpentine tube PVT configurations under base-case conditions

4.2.2. Effect of Flow Rate on the Serpentine Tube PVT collector configurations

In this section, the impact of varying fluid flow rates on the performance parameters of all serpentine tube PVT collectors is investigated. While the fluid flow rate is varied between 5 L/h and 50 L/h in 5 L/h increments, all other operating parameters including solar irradiance, fluid inlet temperature, ambient temperature, and wind velocity are kept constant according to the base-case conditions.

Figure 4.50 presents the contours of absorber temperature distributions as a function of fluid flow rate for the three best-performing serpentine tube PVT collectors under base-case conditions: configurations H, R1 and Q. At 5 L/h, the fluid inlet regions remained cooler, with temperatures remarkably increasing toward the outlet compared with the higher flow rates. The PVT surface temperature exceeded 60 °C in some regions across configurations H, R1 and Q at this low flow rate. However, the maximum surface temperature dropped below 60 °C once the flow rate exceeded 15 L/h. Config Q exhibited a maximum surface temperature approximately 6 °C higher than configurations H and R1 at lower flow rates due to less distance between panel edges and bends of the tubes. As the flow rate increased, the temperature difference diminished, reducing to about 3 °C at a flow rate of 50 L/h. Notably, the most significant reduction in surface temperature with increasing flow rate was observed in configuration Q, which features a horizontally arranged triple-inlet design.

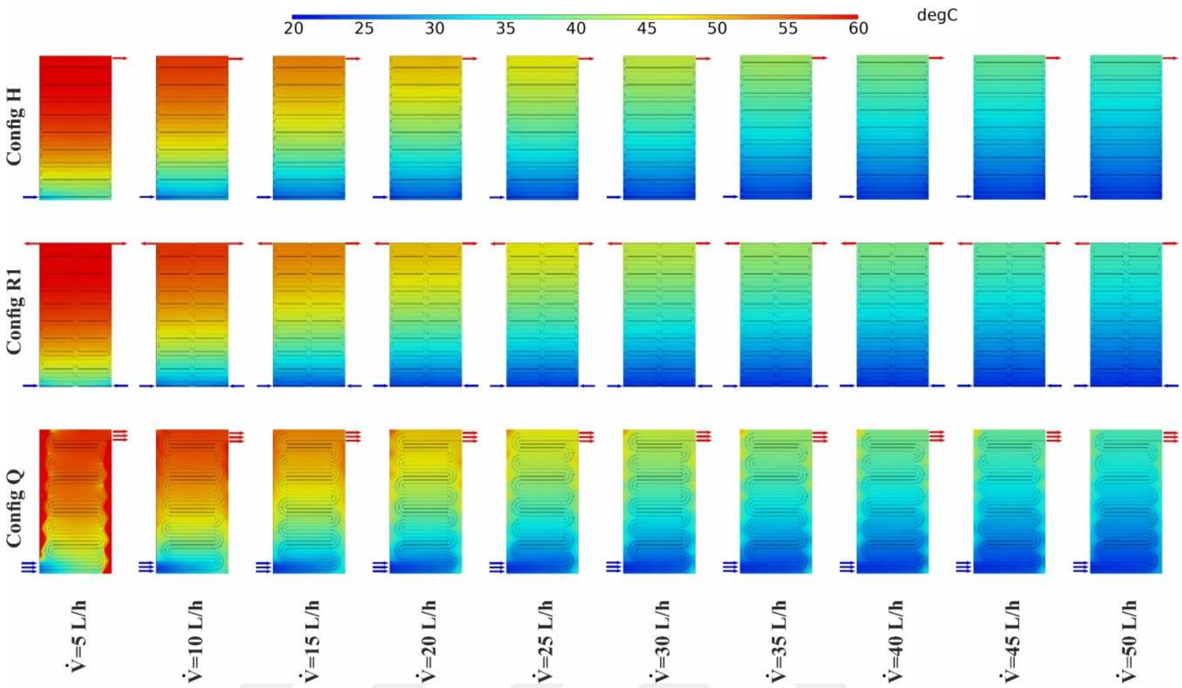

Figure 4.50. PVT absorber temperature distribution of Config H (a), Config R1 (b) and Config Q (c) for different flow rates

Figure 4.51 illustrates the average PV cell surface temperatures and the corresponding variations in fluid outlet temperatures with respect to fluid flow rate for all serpentine tube PVT collectors. At low flow rates, the PV cell temperatures across different configurations are relatively similar (Figure 4.51a). However, as the flow rate increases, the temperature values begin to diverge. Due to the enhanced heat removal from the PV cells at higher flow rates, cell temperatures decrease significantly, with reductions ranging from 32% to 42% across all configurations.

Similarly, Figure 4.51b shows that fluid outlet temperatures decrease with increasing flow rate. Unlike the trend observed for PV cell temperatures, the temperature rise of the working fluid is greater at lower flow rates, leading to greater variation among the PVT collectors. Under these conditions, configurations H, R1 and Q stand out with superior thermal performance. As the flow rate increases, the outlet temperatures of all serpentine tube configurations converge. At a flow rate of 5 L/h, fluid outlet temperatures range from 60.59 ℃ to 47.17 ℃, whereas at the highest flow rate, the values narrow to between 36.06 ℃ and 32.55 ℃.

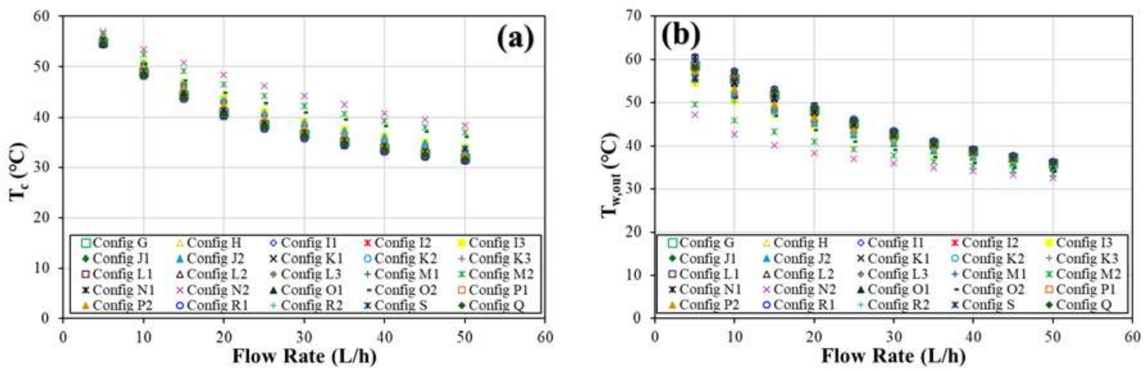

Figure 4.51. Variation of average PV cell (a) and water outlet (b) temperature of different serpentine tube PVT configurations under varying flow rate conditions

The behavior of PVT collector electricity production, which is directly affected by PV cell temperature (Eq. 3.27), and thermal energy production, which affects the fluid outlet temperature (Eq. 3.28), with fluid flow rate is shown in Figure 4.52. Although the fluid outlet temperature decreases with increasing flow rate, thermal energy production rises significantly due to the fluid's enhanced capacity to extract and carry heat from the PV cell.

Among the evaluated configurations, H, R1 and Q yield the highest thermal energy outputs (Figure 4.52a), whereas Config N2 demonstrates the lowest performance, producing approximately 30% less thermal energy compared to Config R1. As previously shown in Figure 4.51, increasing the fluid flow rate results in a notable decrease in PV cell temperature, which in turn enhances electricity production (Figure 4.52b). As the flow rate increases from its minimum to its maximum value, electricity output improves by approximately 10% to 12%.

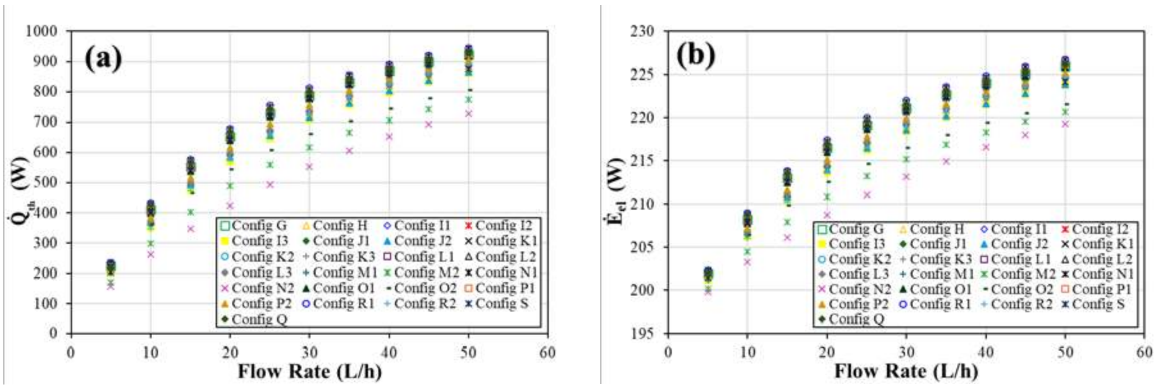

Figure 4.52. Variation of thermal energy production (a) and electrical power (b) of different serpentine tube PVT configurations under varying flow rate conditions

Figure 4.53 presents the variation in thermal and electrical efficiencies of all serpentine tube PVT collectors as a function of fluid flow rate. Both efficiencies exhibit a non-linear increase with rising flow rate. Notably, thermal efficiency improved by approximately 300% as the flow rate increased from its minimum to maximum value (Figure 4.53a). At the same time, the decrease in PV cell temperature contributed to an enhancement in electrical efficiency, which rose by about

12%, as shown in Figure 4.53b. Similarly, Alsharifi et al. (2024) reported that both thermal and electrical efficiencies improved with increasing fluid flow rate. In their study, when the flow rate increased from 0.1 L/min to 1.4 L/min, electrical efficiency rose by 11.65%, while thermal efficiency exhibited a substantial increase of approximately 165%.

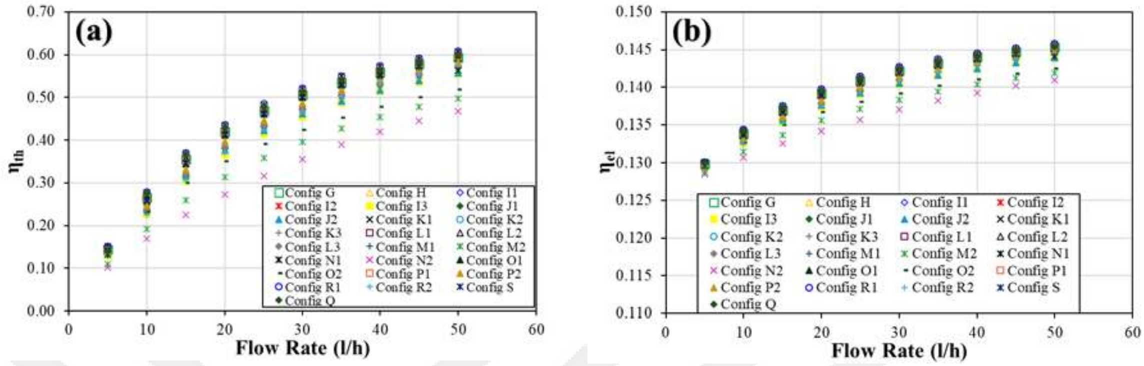

Figure 4.53. Effect of flow rate on the thermal (a) and electrical (b) efficiency of serpentine tube PVT collectors

Figure 4.54 shows the variation of exergy-related performance parameters of serpentine tube PVT collectors including thermal exergy, electrical exergy, output exergy and exergy destruction with respect to fluid flow rate. As the flow rate increases from 5 L/h to 20 L/h, thermal exergy rises correspondingly (Figure 4.54a). However, beyond 20 L/h, a decline in thermal exergy is observed. The findings of Alsharifi et al. (2024) also indicated that thermal exergy increased as the fluid flow rate increased from 0.1 L/min to 0.4 L/min, but began to decline beyond this point. Figure 4.54b presents the electrical exergy, which represents the maximum useful work potential of the electrical output from the PV cell. Since electricity is a directly usable form of energy, the observed increase in this parameter reflects improvements in PV performance. Similar to the trend seen in Figure 4.53b, electrical exergy increases with rising flow rate.

Compared to thermal exergy, electrical exergy has a more significant impact on the total output exergy due to its higher variation. As the flow exergy increases up to 30 L/h, the output exergy also increases (Figure 4.53c). However, beyond this point, the reduction in thermal exergy outweighs the gains in electrical exergy, resulting in a downward trend in total exergy output showing a decrease of approximately 3%.

Figure 4.54d shows the exergy destruction values, which represent the system's irreversibilities. Unlike output exergy, exergy destruction exhibits a decreasing trend with increasing flow rate up to 25 L/h, after which it starts to rise again. Since the input exergy remains constant, exergy destruction follows an inverse trend with output exergy, reaching its minimum between 25 L/h and 30 L/h.

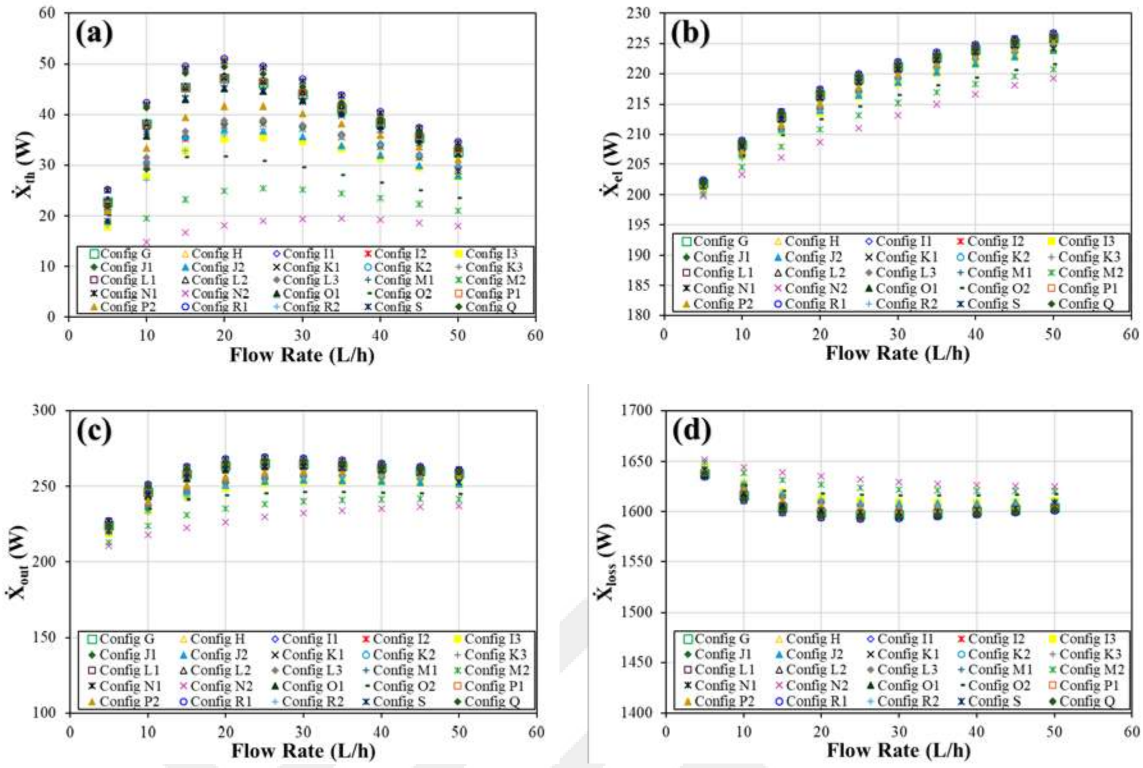

Figure 4.54. Effect of flow rate on the thermal (a), electrical (b) and output (c) exergy, and exergy destruction (d) of serpentine tube PVT collectors

The variation of overall, primary energy saving and exergy efficiencies of all serpentine tube PVT collectors with fluid flow rate is compared in Figure 4.55. Given that the thermal efficiency value has a much stronger effect on overall and primary energy saving efficiencies than electrical efficiency, both of these efficiencies metrics follow a similar trend and increase with increasing fluid flow rate (Eq. 3.31). The highest overall (Figure 4.55a) and primary energy saving (Figure 4.55b) efficiencies reach about 75.36% and 99.15%, respectively, at 50 L/h flow rate in Config R1, followed by Config H and Q. Exergy efficiency is a function of exergy output and exergy input. Since sun exergy does not vary with flow rate, exergy efficiency (Eq. 3.45) directly depends on output exergy presented in Figure 4.54 and follows the same trend. Exergy efficiency reaches its peak at 25 L/h level and then shows a slight decrease (Figure 4.55c). Exergy efficiency increased by approximately 18% as the fluid flow rate increased from 5 L/h to 25 L/h, while it decreased by 3% as the flow rate increased from 25 L/h to 50 L/h.

Figure 4.56a presents the pressure drop behavior with increasing fluid flow rate for different serpentine tube PVT configurations. In general, a significant increase in pressure drop is observed in all configurations with increasing flow rate. This increase is due to the fluid experiencing more friction with the tube walls at higher flow rates and the increase in hydraulic resistance due to the increase in flow rate. While the single-inlet configurations G and H in particular exhibit the highest pressure drop, the PVT collectors with double inlets and especially the triple-inlet designs Config S and Q have much lower pressure drops since the flow rate through a single tube is lower, even though the total flow rates are the same. Figure 4.56b shows the variation of the parameter of thermal energy produced per unit pressure drop (TEPD) with fluid flow rate. As the flow rate increases, a decreasing trend is observed in the TEPD values. This decrease is related to the fact that although the amount of thermal energy increases with increasing flow rate, the pressure drop increases much more. Among serpentine tube PVT collectors, the highest TEPD value is obtained with 5.55 W/Pa at 5 L/h flow rate in configuration Q, while this value drops to 1.06 W/Pa for configuration Q at 50 L/h flow rate.

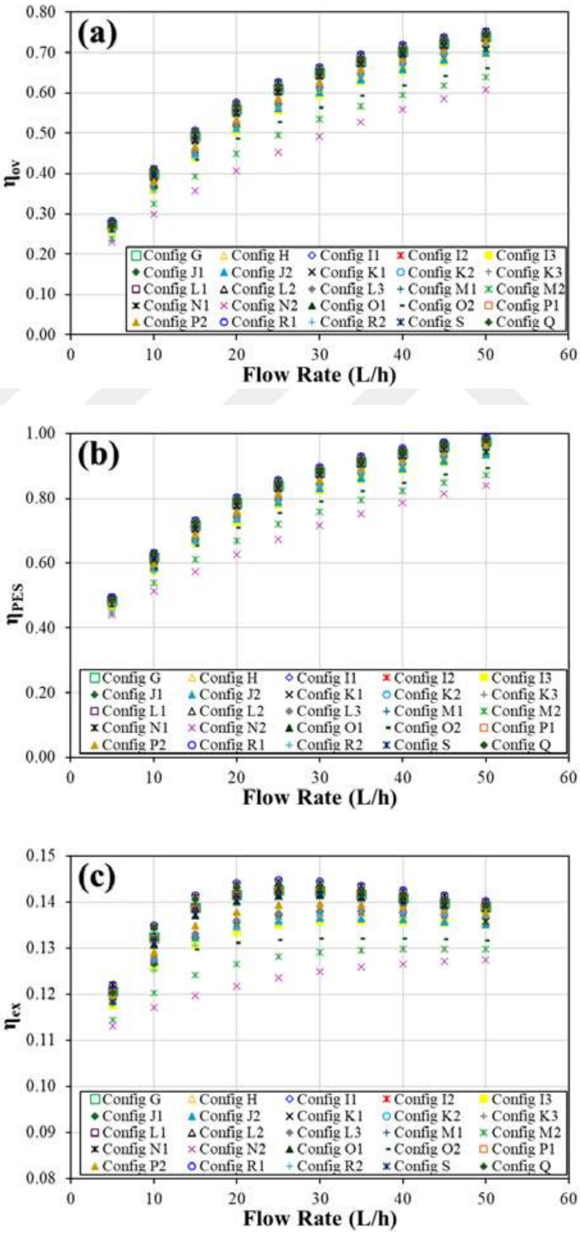

Figure 4.55. Effect of flow rate on the overall (a), primary energy saving (b) and exergy (c) efficiency of serpentine tube PVT collectors

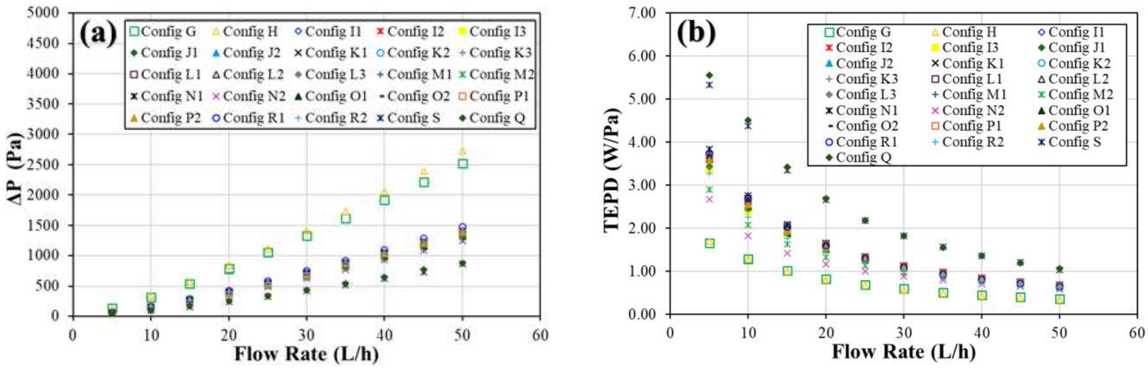

Figure 4.56. Effect of flow rate on the pressure drop (a) and TEPD (b) of serpentine tube PVT collectors

Overall, the results demonstrate that increasing the flow rate positively impacts both temperature distribution and efficiency metrics in serpentine tube PVT collectors. Higher flow rates enhance heat extraction from the PV cell, resulting in lower cell temperatures, improved electrical efficiency and increased electricity production. Additionally, thermal efficiency and thermal energy production also increases across all configurations.

4.2.3. Effect of Solar Irradiance on the Serpentine Tube PVT Collector Configurations

Solar irradiance is a critical factor influencing the performance of PVT collectors, particularly in terms of the PV cell temperature and its subsequent impact on electrical efficiency. In this study, solar irradiance was varied from 200 W/m^2 to 1200 W/m^2 in increments of 200 W/m^2, while other operating parameters were kept constant (Table 3.3).

The effect of solar irradiance on the absorber temperature distributions of the best three serpentine tube configurations (H, R1 and Q) are presented in Figure 4.57. Due to the reduced thermal input at low solar irradiance levels, the absorber temperatures remain low, while elevated irradiance causes a noticeable increase in absorber temperature. As solar irradiance increased, the maximum surface temperatures of the PVT collectors rose significantly. The maximum surface temperatures increased almost 30 °C for Config H and R1, and 38 °C for Config Q, with increasing the solar irradiance from minimum to maximum value. Config Q consistently exhibited the highest maximum surface temperature, particularly in the area between the panel edges and bends of the tubes. This was attributed to its design, where the tubes are positioned farther from the panel edges, leading to reduced heat transfer between the coolant and the collector.

Figure 4.58a compares the average PV cell temperatures of all serpentine tube PVT collectors with the surface temperature of a conventional PV panel across varying levels of solar irradiance. At the lowest irradiance level of 200 W/m^2, the temperature differences among the serpentine tube PVT collectors are minimal, with less than 1 °C variation. However, as solar irradiance increases, cell temperatures also rise, and the performance gap between the serpentine tube configurations becomes more pronounced. For instance, at 1200 W/m^2, the temperature difference between the best-performing configurations H, R1 and Q and the poorest-performing configuration N2 reaches approximately 9 °C. A similar trend is observed in the comparison between the serpentine tube PVT collectors and the conventional PV panel. While the temperature difference at low irradiance is around 4 °C, this gap widens significantly with increasing irradiance. At the highest solar irradiance level, the PVT collectors exhibit surface temperatures approximately 16 °C to 25 °C lower than those of the conventional PV panel.

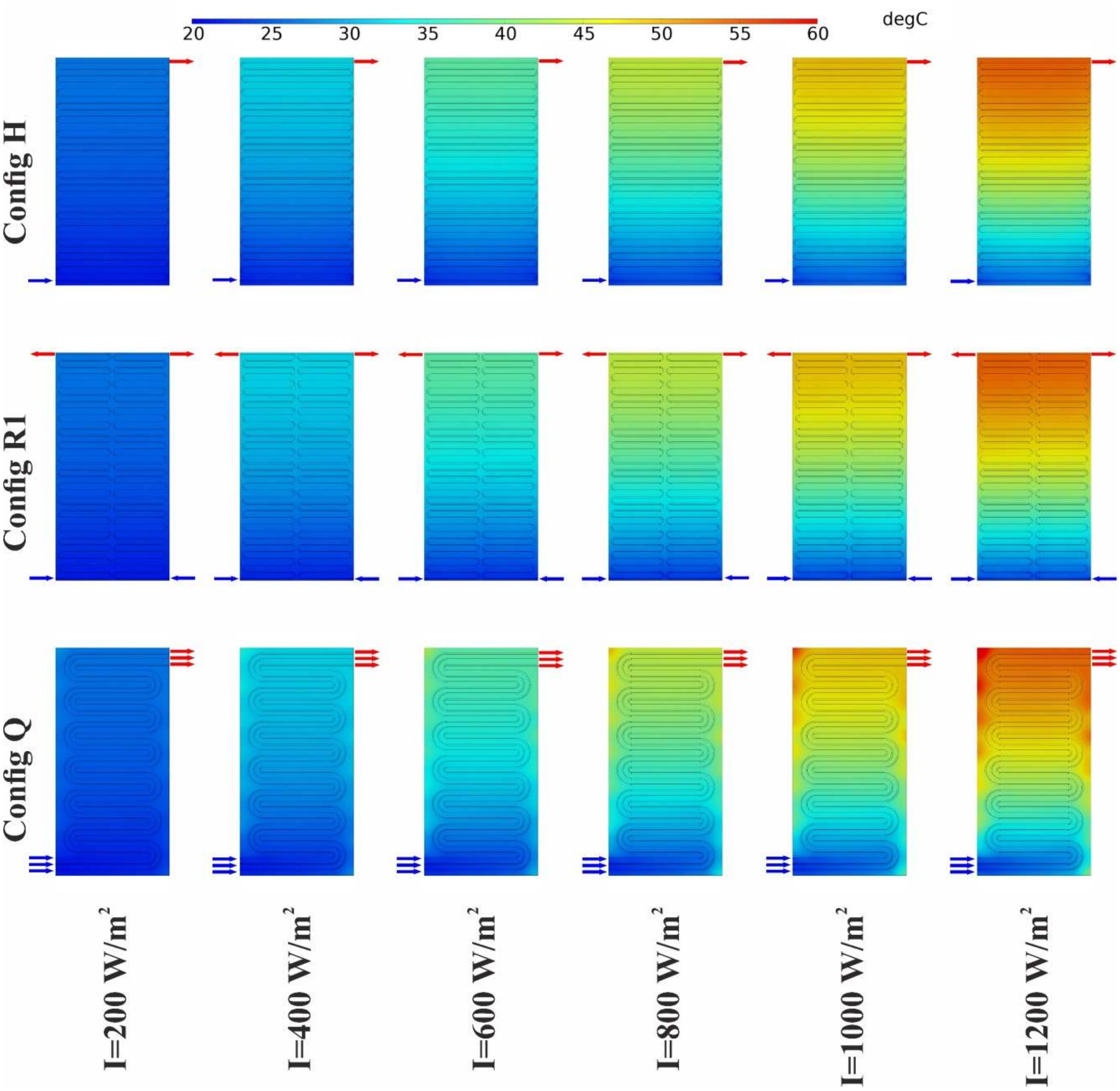

Figure 4.57. PVT absorber temperature distribution of Config H (a), Config R1 (b) and Config Q (c) for different solar irradiances

On the other hand, average fluid outlet temperature increased significantly with rising solar irradiance, as shown in Figure 4.58b. As solar irradiance rose from its minimum to maximum level, the outlet temperature increased by approximately 17 °C to 29 °C across the various serpentine tube PVT configurations. The configurations demonstrating the highest increases were H, N1 and Q. In contrast, configuration N2 exhibited the lowest temperature rise, with an outlet temperature approximately 23% lower than that of the best-performing configurations under maximum solar irradiance.

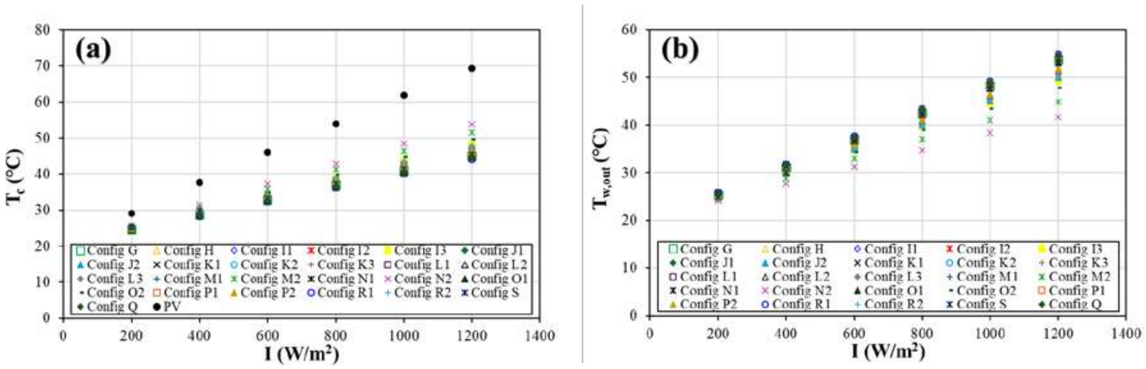

Figure 4.58. Variation of average PV cell (a) and water outlet (b) temperature of different serpentine tube configurations under varying solar irradiance conditions

The variation of thermal and electrical energy production of PVT collectors with solar irradiance is given in Figure 4.59. Both parameters increased significantly with solar irradiance for all PVT collectors. As the inlet water temperature and flow rate are kept constant, higher levels of solar irradiance lead to increased thermal energy production due to the greater amount of solar energy absorbed by the collector surface. While the produced thermal energy varied between 100 and 135 W at 200 W/m^2 solar irradiance, it varied between 505 W and 810 W at 1200 W/m^2 (Figure 4.59a). Although increasing solar irradiance leads to higher PV cell temperatures and a consequent reduction in electrical efficiency, the overall electrical energy output increases significantly across all serpentine tube PVT collectors due to the greater availability of solar energy (Figure 4.59b). While the difference in electrical energy production between serpentine tube PVT collectors and conventional PV panels is minimal at low irradiance levels, the disparity becomes more pronounced beyond 800 W/m^2. Under maximum solar irradiance, serpentine tube PVT collectors generate approximately 9% to 14% more electrical energy compared to conventional PV panels.

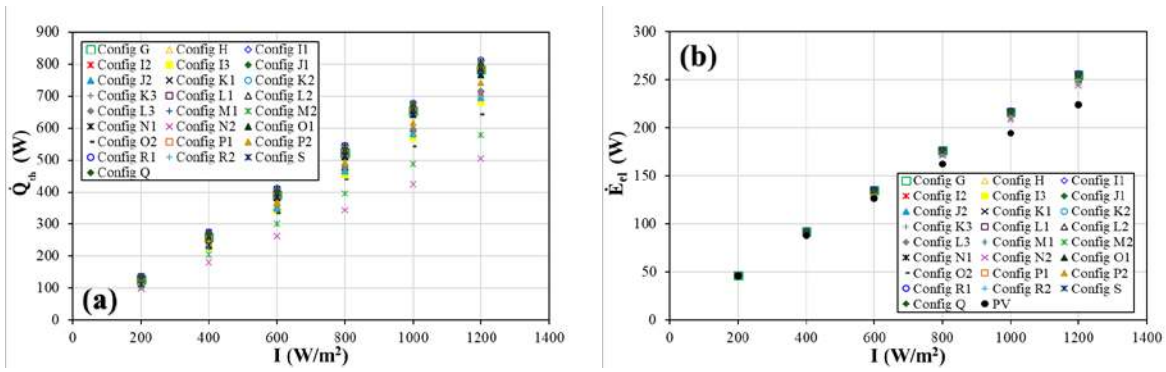

Figure 4.59. Variation of thermal energy production (a) and electrical power (b) of different serpentine tube configurations under varying solar irradiance conditions

Figure 4.60 illustrates the variation in thermal and electrical efficiencies of serpentine tube PVT collectors as a function of increasing solar irradiance. Thermal energy production increases with irradiance, since higher radiation results in more energy input to the system. Although a slight increase in thermal efficiency is observed for most serpentine tube PVT configurations, some designs exhibit a decline (Figure 4.60a). This variation is attributed to elevated surface temperatures at higher solar irradiance levels, which enhance convective and radiative heat losses to the environment.

In contrast, electrical efficiency, which is strongly influenced by PV cell temperature (Eq. 3.27), tends to decrease as solar irradiance increases (Figure 4.60b). Specifically, as solar irradiance rises from its minimum to maximum value, the electrical efficiency of serpentine tube PVT collectors drops by approximately 8% to 12%. The findings presented by Alsharifi et al. (2024) support this result. As solar irradiance increased from 200 W/m^2 to 1000 W/m^2, the PVT cell temperature rose, leading to a decline in electrical efficiency by approximately 8.36%. Similarly, in the study by Yan et al. (2022), it was found that for every 200 W/m^2 increase in solar irradiance, the average temperature increased by 3.86 °C, while the electrical efficiency decreased by 2.09%. For the conventional PV panel, which lacks an active cooling mechanism, the reduction in electrical efficiency is about 19% greater compared to that of the PVT collectors at 1200 W/m^2 solar irradiance.

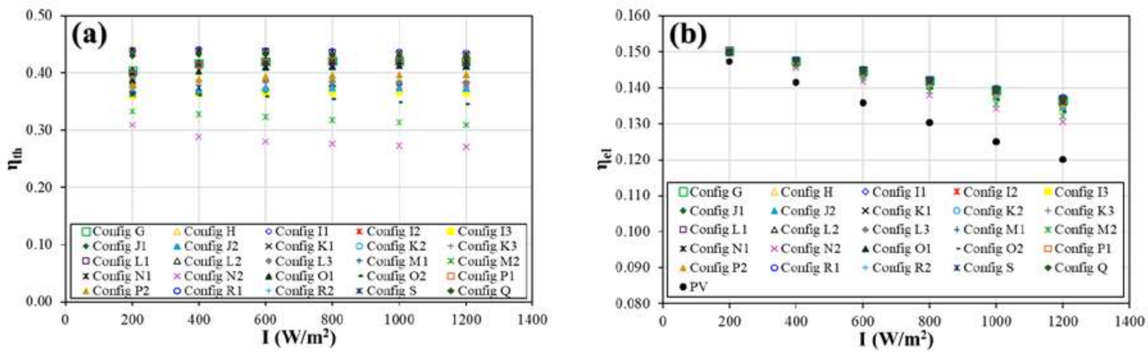

Figure 4.60. Effect of solar irradiance on the thermal (a) and electrical (b) efficiency of serpentine tube PVT collectors

The effect of solar irradiance on the exergetic performance metrics is investigated in Figure 4.61 for all serpentine tube PVT collectors. Figure 4.61a presents the thermal exergy produced by the PVT collectors, which is influenced by parameters such as ambient temperature, fluid flow rate, and fluid inlet and outlet temperatures (Eq. 3.43). As all parameters except the outlet temperature are held constant, and the outlet temperature increases with rising solar irradiance, the thermal exergy follows a trend similar to that of thermal energy production (Figure 4.59). Although thermal exergy values are low and closely aligned at low irradiance levels, they increase significantly as solar irradiance intensifies. At maximum solar irradiance, the highest thermal exergy is recorded for Config R1 at 74 W, while the lowest is observed for Config N2 at 27 W.

Since electrical exergy is equivalent to the electrical energy produced, and there are minimal differences in electrical output among configurations, no significant variation is observed in electrical exergy (Figure 4.61b). Figure 4.61c illustrates the variation of output exergy defined as the sum of thermal and electrical exergies with increasing solar irradiance. Although electrical exergy contributes more to output exergy, the relatively uniform electrical performance among serpentine tube PVT configurations means that differences in output exergy primarily stem from variations in thermal exergy.

Configurations H, R1 and Q exhibited the highest output exergy, generating approximately 20% more than the lowest-performing configuration, N2. Although output exergy increases with solar irradiance due to higher absorbed energy, exergy losses also tend to rise because the temperature difference between the absorber surface and surroundings becomes larger, leading to increased irreversibilities in the system (Figure 4.61c).

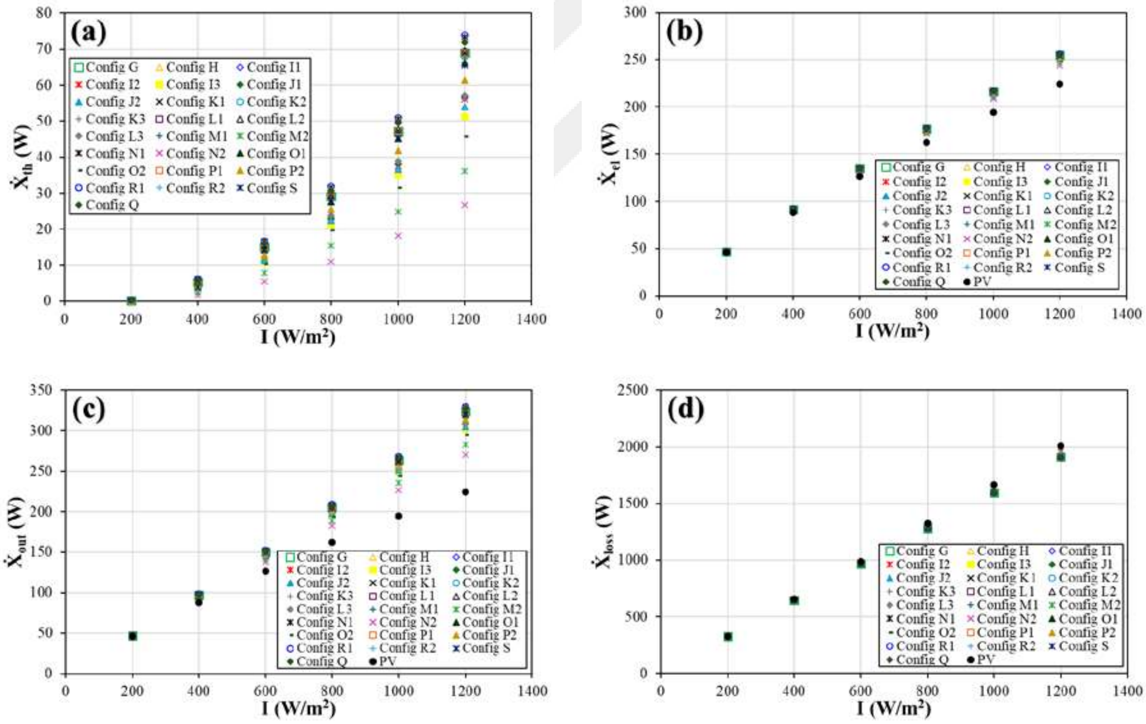

Figure 4.61. Effect of solar irradiance on the thermal (a), electrical (b) and output (c) exergy, and exergy destruction (d) of serpentine tube PVT collectors

As shown in Figure 4.62, both overall and primary energy saving efficiency which represent the combined effect of thermal and electrical efficiencies exhibit a decreasing trend with increasing solar irradiance. This behavior is primarily attributed to the relatively stable thermal efficiency and the noticeable decline in electrical efficiency at higher irradiance levels. As solar irradiance increases from its minimum to maximum value, the overall efficiency decreases by approximately 4% to 13% (Figure 4.62a), while the primary energy saving efficiency decreases by around 6% to 12% (Figure 4.62b) across all serpentine tube configurations. Notably, exergy efficiency (Figure 4.62c) reached its peak value of 0.1476 for Config R1 at a solar irradiance level of 1200 W/m^2.

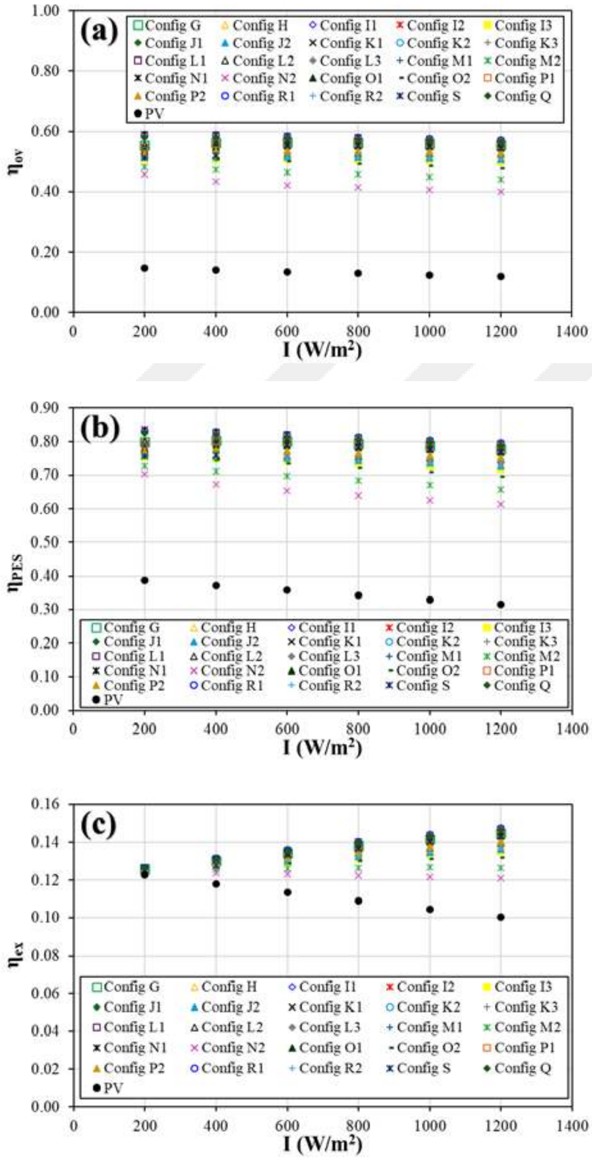

Figure 4.62. Effect of solar irradiance on the overall (a), primary energy saving (b) and exergy (c) efficiency of serpentine tube PVT collectors

The effect of solar irradiance on pressure drop and thermal energy production per unit pressure drop (TEPD) is illustrated in Figure 4.63. As solar irradiance increases, the water temperature rises proportionally, resulting in a decrease in water viscosity and density, consequently, a reduction in pressure drop. Specifically, as solar irradiance increases from 200 to 1200 W/m^2, the pressure drop decreases by approximately 24% to 27%. Simultaneously, the rise in energy absorbed by the collector enhances thermal energy production. As a result, due to the combined effect of increased thermal output and reduced pressure drop, TEPD also increases with higher levels of solar irradiance. Among all irradiance levels, Config S and Q yields the best TEPD performance, attributed to their high thermal exergy output and low pressure drop.

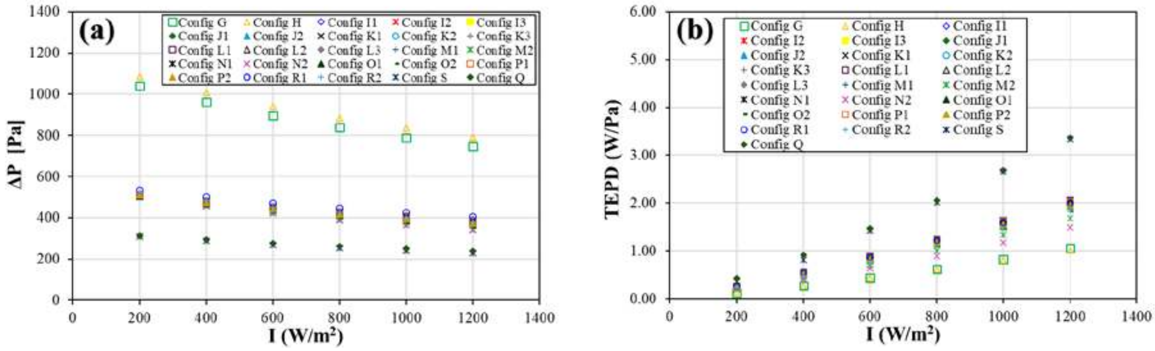

Figure 4.63. Effect of solar irradiance on the pressure drop (a) and TEPD (b) of serpentine tube PVT collectors

While higher solar irradiance levels enhance energy production due to increased thermal and electrical outputs, they also necessitate careful management of PV cell temperatures to mitigate adverse effects on electrical efficiency.

4.2.4. Effect of Fluid Inlet Temperature on the Serpentine Tube PVT Collector Configurations

One of the most critical parameters influencing the performance of PVT collectors is the fluid inlet temperature. In this study, water was used as the working fluid, and its inlet temperature was varied from 10 °C to 40 °C in increments of 5 °C to evaluate its effect on the performance of the serpentine tube PVT collectors. All other operating parameters, including solar irradiance, fluid flow rate, ambient temperature and wind velocity were held constant according to the base-case conditions (Table 3.3).

Figure 4.64 illustrates the variation in absorber temperature distributions for the three best-performing serpentine tube configurations under base-case conditions, Config H, R1 and Q as a function of fluid inlet temperature. Moreover, Figure 4.65 provides a comparison of the average PV cell surface temperatures and fluid outlet temperatures for all PVT collectors under the same inlet temperature variations. The temperature distribution results show that lower inlet temperatures enable more effective cooling of the PV panel. As the inlet temperature increases, the panel temperature also rises. At lower regions near the inlet, the absorber remains relatively cool, while local temperature hotspots exceeding 60 °C are observed near the outlet, particularly in Config Q. At low inlet temperatures, the difference in PV cell temperatures among serpentine tube configurations is more pronounced; however, this disparity gradually diminishes as the inlet temperature increases (Figure 4.65a). For instance, at a 10 °C inlet temperature, the PV cell temperature in Config R1 was measured at 34.69 °C, compared to 45.11 °C in Config N2. At 40 °C inlet temperature, Config Q reached 50.86 °C, while Config N2 reached 54.83 °C.

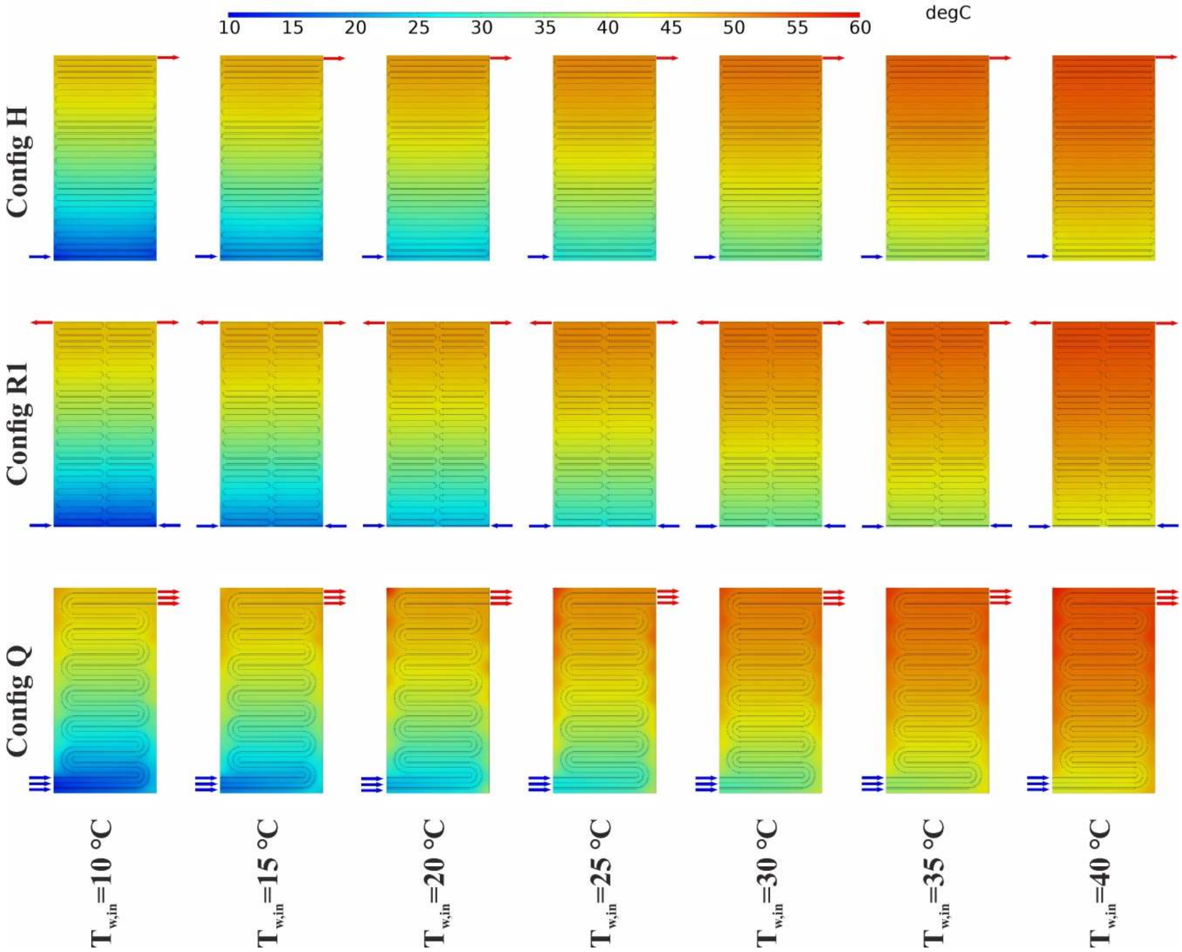

Figure 4.64. PVT absorber temperature distribution of Config B (a), Config K1 (b), and Config M (c) for different water inlet temperatures

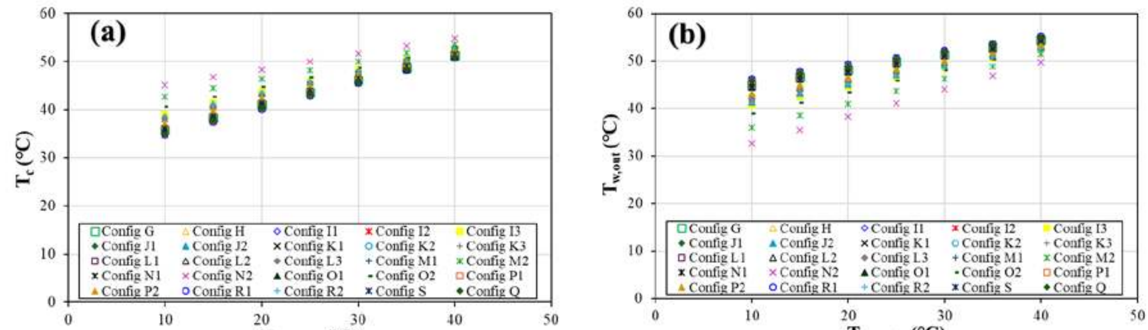

Figure 4.65. Variation of average PV cell (a) and water outlet (b) temperature of different serpentine tube configurations under varying water inlet temperature conditions

The fluid outlet temperature (Figure 4.65b) also increases with inlet temperature. However, unlike PV cell temperature, the difference in outlet temperatures among configurations is more significant at lower inlet temperatures. At 10 °C, the outlet temperature difference between the best-performing configuration R1 and the worst-performing one N2 was 13.62 °C, which decreased to 5.49 °C at a 40 °C inlet temperature.

Since all other parameters were kept constant, the thermal energy output of the PVT collectors is directly dependent on the temperature difference between the fluid outlet and inlet (Eq. 3.28). Although the outlet temperature increases with higher inlet temperatures, thermal energy production tends to decrease due to the heat losses (Figure 4.66a). At the lowest inlet temperature, thermal energy output ranged from 525 W (Config N2) to 841 W (Config R1). At the highest inlet temperature, it declined to 224 W and 351 W, respectively. A similar decreasing trend is observed in electrical energy production (Figure 4.66b) due to reduced electrical efficiency caused by elevated cell temperatures (Eq. 3.27). However, the impact of fluid inlet temperature on electrical output is less pronounced than on thermal performance. At the lowest inlet temperature, electrical energy production ranged from 212 W to 223 W, while at the highest inlet temperature, it ranged from 202 W to 206 W. In both thermal and electrical performance metrics, Config R1 consistently demonstrated the best results, whereas Config N2 exhibited the lowest performance.

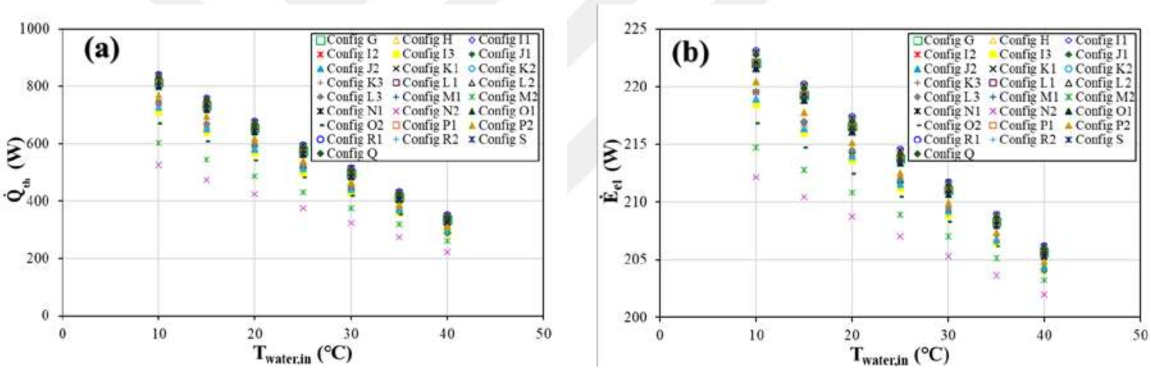

Figure 4.66. Variation of thermal energy production (a) and electrical power (b) of different serpentine tube configurations under varying water inlet temperature conditions

The results indicated that, across all serpentine tube configurations, both thermal and electrical efficiency metrics exhibited closely aligned values and followed a near-linear decline with increasing fluid inlet temperature (Figure 4.67). The rise in inlet temperature led to a reduction in thermal efficiency (Figure 4.67a), primarily due to elevated PVT surface temperatures and the resulting increase in heat losses through convection and radiation. An increase in inlet temperature from 10 °C to 40 °C caused an approximate 58% reduction in thermal efficiency across all serpentine tube configurations. For the best-performing configuration, R1, the highest thermal efficiency of 0.5409 was recorded at 10 °C, while the lowest, 0.2215, was observed at 40 °C. In contrast, for the worst-performing serpentine tube configuration, N2, thermal efficiency declined from 0.3377 to 0.1437 over the same temperature range.

Higher inlet temperatures also reduce the temperature difference between the working fluid and the PV cell, thereby limiting heat transfer. As a result, less heat is extracted from the PV cell, which increases its temperature and reduces electrical efficiency (Figure 4.67b). As the fluid inlet temperature increased from its minimum to maximum value, the electrical efficiency of all serpentine tube PVT collectors decreased by approximately 4.8% to 7.5%. The highest electrical efficiency, 0.1434, was recorded for Config R1 at an inlet temperature of 10 °C. A similar trend was observed in the study by Yan et al. (2022), where increasing the fluid inlet temperature from 19 °C to 34 °C resulted in an approximate decrease of 30% in thermal efficiency and 4.5% in electrical efficiency. Hosseinzadeh et al. (2018)'s research also revealed that elevating the fluid inlet temperature from 20 °C to 40 °C caused a significant 16.21% drop in thermal efficiency, accompanied by a slight 0.71% decline in electrical efficiency.

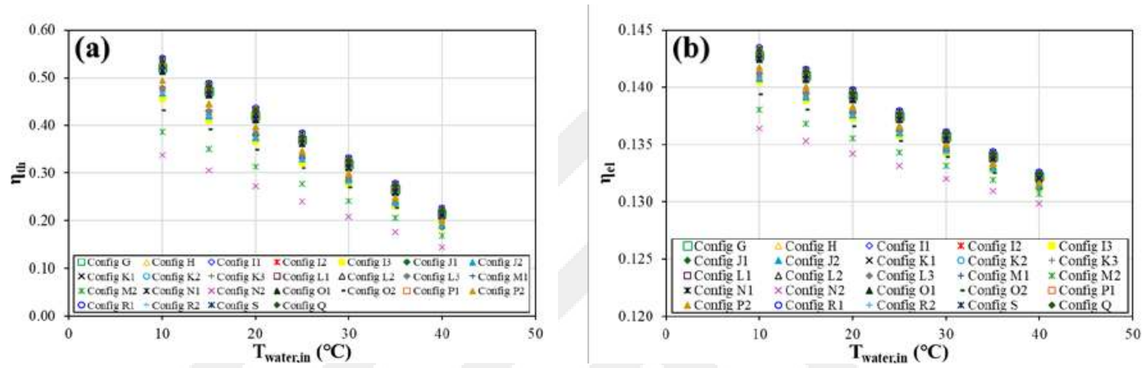

Figure 4.67. Effect of water inlet temperature on the thermal (a) and electrical (b) efficiency of serpentine tube PVT collectors

The impact of water inlet temperature on exergy performance parameters is presented in Figure 4.68. Thermal exergy (Figure 4.68a) depends on both the outlet temperature and the temperature difference between the inlet and outlet (Eq. 3.43). Although the outlet temperature increases with higher inlet temperatures, the narrowing temperature differential leads to a reduction in thermal exergy for all serpentine tube PVT collectors except Config O2, M2 and N2 since the rise in Carnot efficiency factor in Eq. 3.43. As a result, thermal exergy varies between 31% and 42% across configurations as the water inlet temperature increases. Since electrical exergy (Figure 4.68b) is directly proportional to electrical efficiency, it follows a similar trend to that shown in Figure 4.67b. With increasing inlet temperature, differences in electrical exergy among the serpentine tube configurations become less distinct. Consequently, total exergy output (Figure 4.68c) decreases due to the combined reduction in both thermal and electrical exergy. In contrast, exergy destruction (Figure 4.68d) demonstrates an inverse relationship with output exergy. Config R1 delivers the highest total exergy output, whereas Config N2 exhibits the greatest exergy destruction.

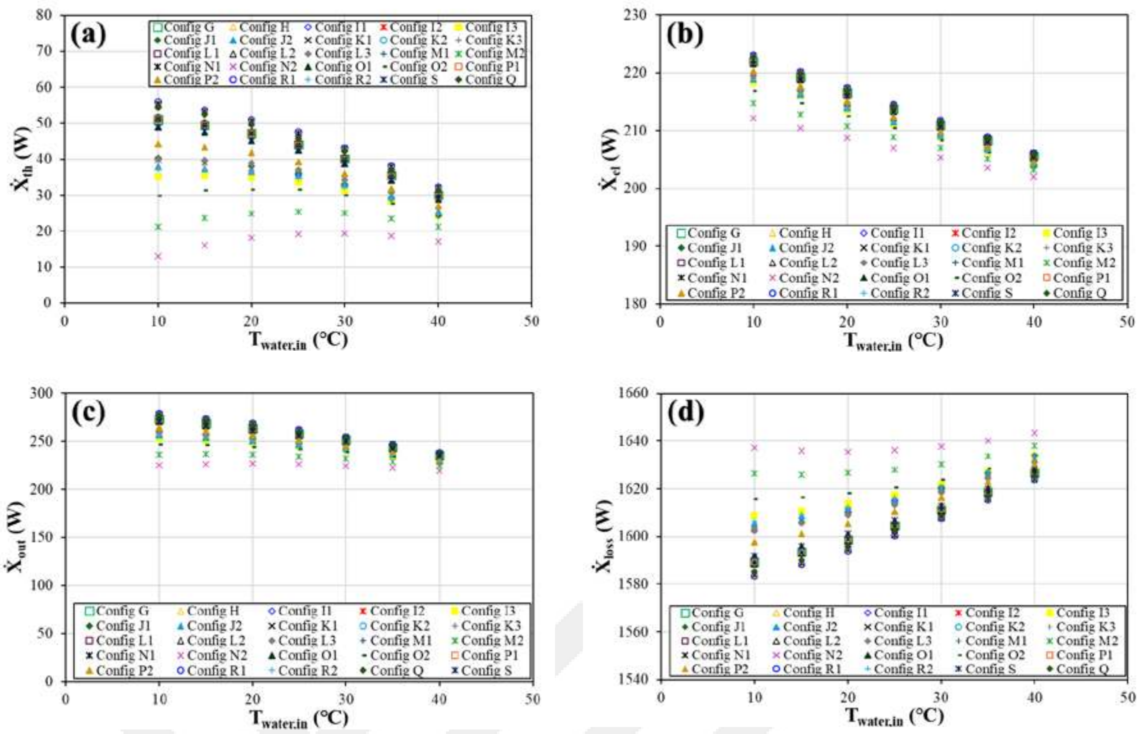

Figure 4.68. Effect of water inlet temperature on the thermal (a), electrical (b) and output (c) exergy, and exergy destruction (d) of serpentine tube PVT collectors

Overall and primary energy saving efficiencies exhibit a decreasing trend with increasing fluid inlet temperature, primarily due to the decline in both thermal and electrical efficiencies (Figure 4.69). The highest overall (Figure 4.69a) and primary energy saving (Figure 4.69b) efficiencies were recorded in Config R1 at an inlet temperature of 10 °C, with values of 0.6843 and 0.9183, respectively. For this configuration, an increase in inlet temperature to 40 °C results in a 47% reduction in overall efficiency and a 37% reduction in primary energy saving efficiency. Given that the exergy input remains constant across different water inlet temperatures, exergy efficiency (Figure 4.69c) varies directly with exergy output (Eq. 3.45). As illustrated in Figure 4.69c, the exergy efficiency closely follows the trend of output exergy shown in Figure 4.68c. The highest exergy efficiency is observed in Config R1 at a fluid inlet temperature of 10 °C, with a recorded value of 0.1498.

As shown in Figure 4.70a, pressure drop decreases with increasing fluid inlet temperature. This behavior is primarily attributed to the reduction in water viscosity and density at higher temperatures, which lowers internal friction and local losses. Across all serpentine tube PVT collectors, increasing the inlet temperature from its minimum to maximum value results in a pressure drop reduction of approximately 23% to 26%. However, when thermal energy produced per unit pressure drop (TEPD) is examined as a function of fluid inlet temperature, a decreasing trend is again pressure drop decreases with increasing inlet temperature, the reduction in thermal energy output is proportionally greater. As a result, TEPD declines. The highest TEPD value is observed in Config R1 at an inlet temperature of 10 °C, reaching 3.02 W/Pa.

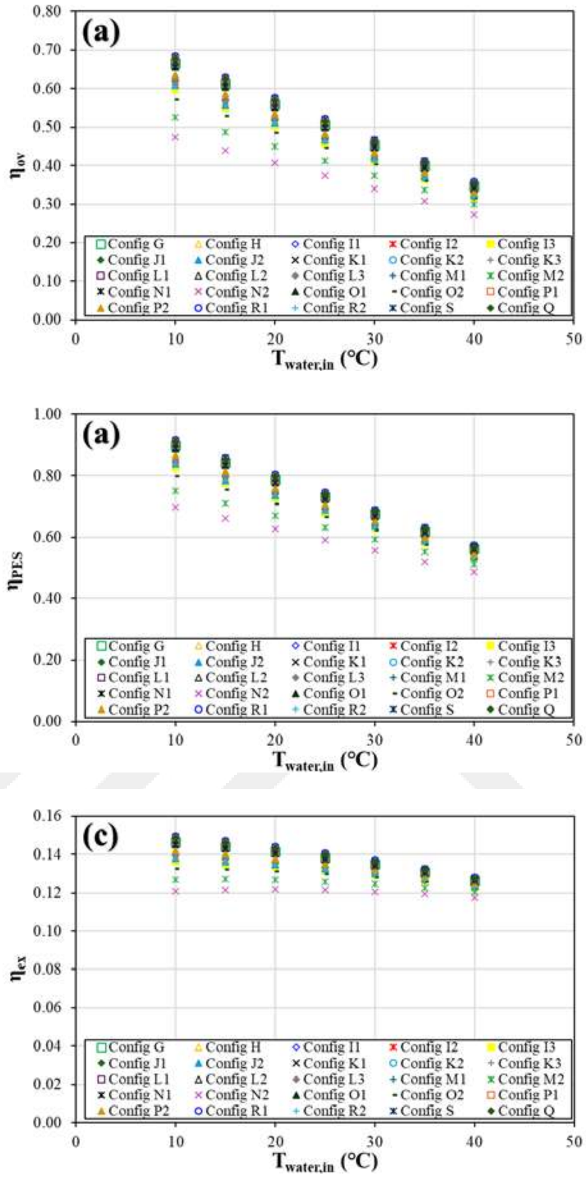

Figure 4.69. Effect of water inlet temperature on the overall (a), primary energy saving (b) and exergy (c) efficiency of serpentine tube PVT collectors

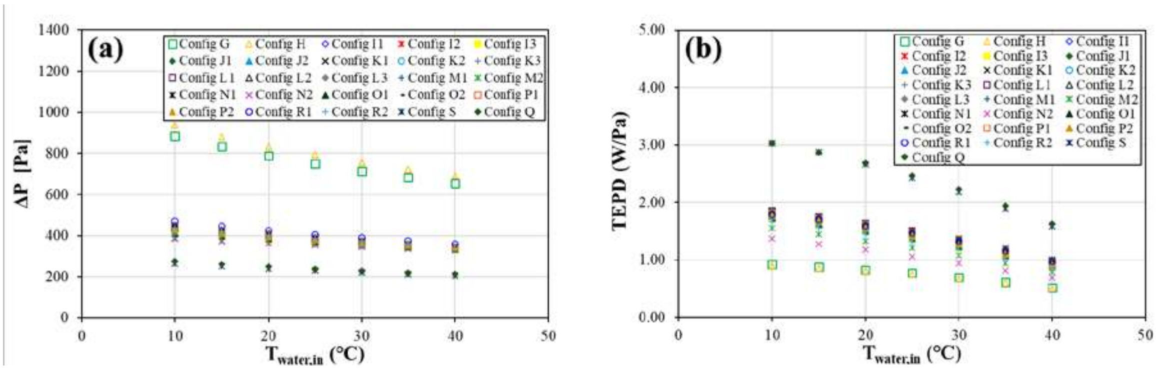

Figure 4.70. Effect of water inlet temperature on the pressure drop (a) and TEPD (b) of serpentine tube PVT collectors

4.2.5. Effect of Ambient Temperature on the Serpentine Tube PVT Collector Configurations

Ambient temperature is another critical parameter that significantly influences the performance of PVT collectors. In this section, its effect on energy and exergy performance metrics is examined. The ambient temperature was varied from 15 °C to 40 °C in increments of 5 °C, while solar irradiance, fluid flow rate, fluid inlet temperature and wind velocity were held constant according to the base-case conditions (Table 3.3).

Figure 4.71 presents the variation in absorber temperature distributions for the three best-performing serpentine tube configurations (H, R1 and Q), which yielded closely aligned results across the tested ambient temperature range. Figure 4.72, on the other hand, shows the changes in average PV cell surface temperatures and fluid outlet temperatures for all serpentine tube PVT configurations as a function of ambient temperature.

The results clearly indicate that lower ambient temperatures contribute positively to absorber cooling. At ambient temperatures of 15 °C, 20 °C, and 25 °C, the fluid effectively cools the collector surface nearly to the center of the panel. However, as ambient temperature increases, absorber temperatures also rise. Once ambient temperature exceeds 30 °C, localized thermal hotspots become apparent particularly along the panel edges in Config Q. At 40 °C ambient temperature, these local surface temperatures exceed 60 °C.

Figure 4.72a compares the variation in average PV cell temperatures of the PVT collectors and the average surface temperature of a conventional PV panel with ambient temperature. When the ambient temperature is 15 °C, PVT cell temperatures range from 35.79 °C to 41.84 °C, while the surface temperature of the conventional PV panel is 52.55 °C. As ambient temperature increases, both types of systems exhibit rising surface temperatures. However, the uncooled PV panel experiences a much steeper increase reaching 24 °C above its initial value compared to a 12-17 °C increase in serpentine tube PVT collectors.

The effect of the ambient temperature is also clearly seen in the fluid outlet temperatures (Figure 4.72b) of serpentine tube PVT collectors. As ambient temperature rises, convective heat losses decrease, allowing more heat to be transferred from the PV cells to the working fluid and this leads to higher outlet temperatures. At the lowest ambient temperature, outlet fluid temperatures range between 34.16 °C and 44.97 °C. When the ambient temperature reaches 40 °C, the fluid outlet temperature increases by approximately 32% to 42%, depending on the configuration. The highest outlet temperature is observed in Config R1 at 60.28 °C, while the lowest, 44.97 °C, is recorded for the least efficient configuration, Config N2.

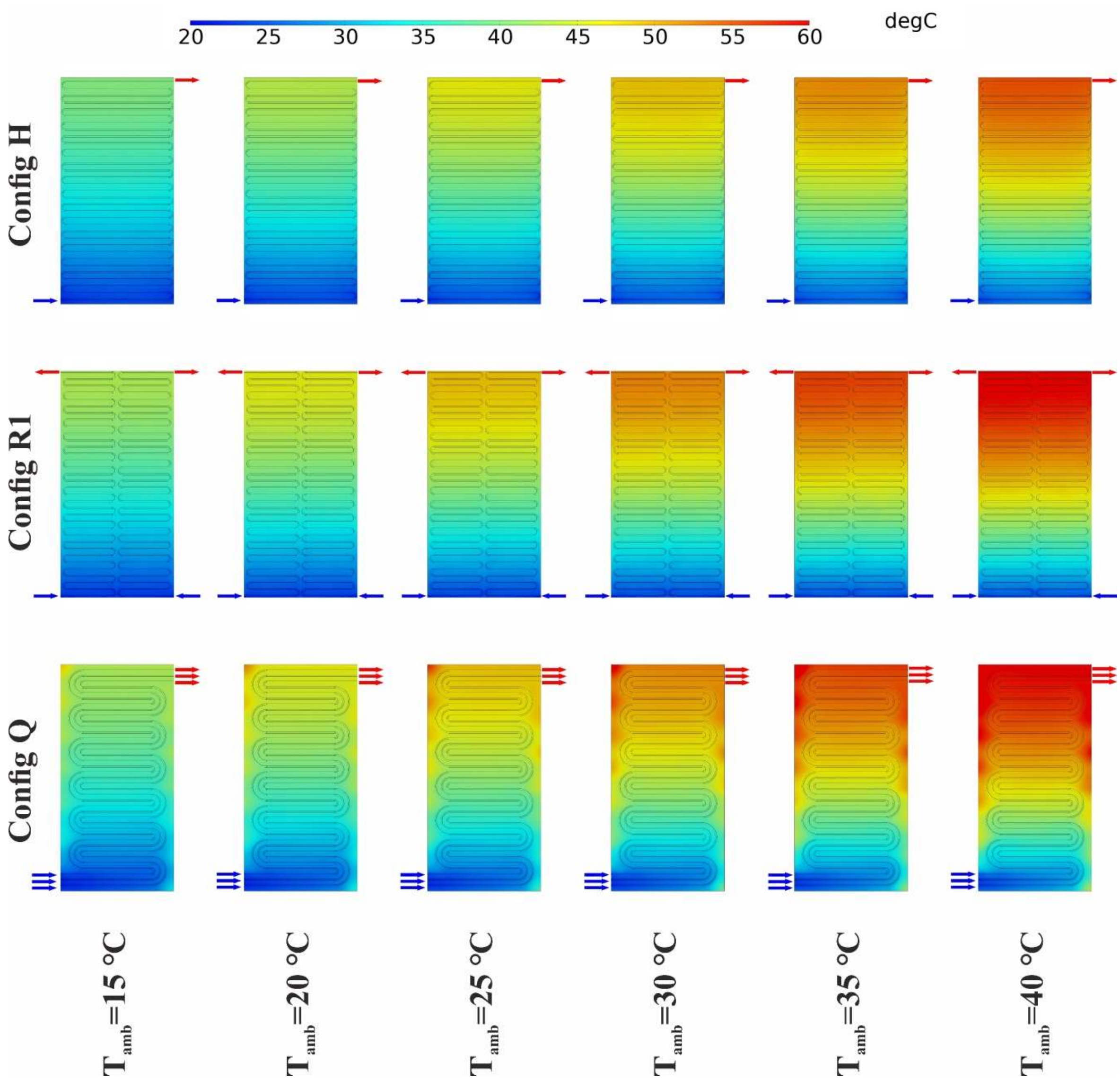

Figure 4.71. PVT absorber temperature distribution of Config H (a), Config R1 (b) and Config Q (c) for different ambient temperatures

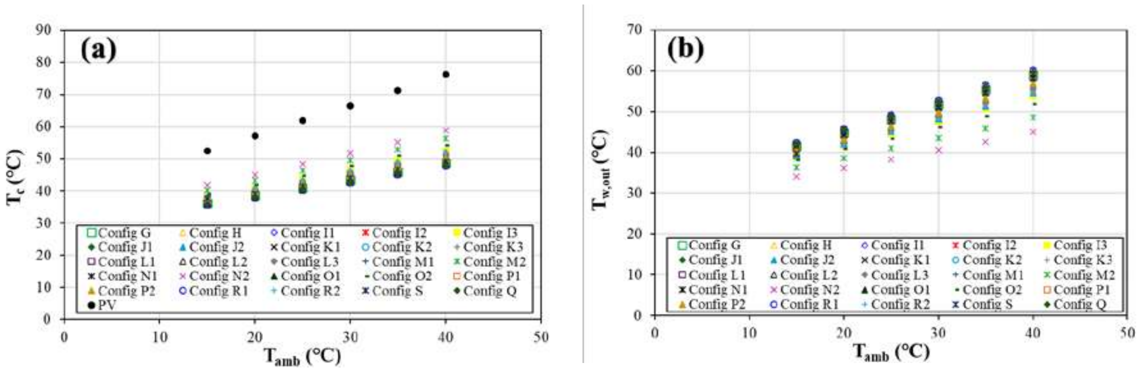

Figure 4.72. Variation of average PV cell (a) and water outlet (b) temperature of different serpentine tube configurations under varying ambient temperature conditions

Figure 4.73 shows the changes in thermal and electrical energy production of serpentine tube PVT collectors with ambient temperature. The decrease in heat losses with the increase in ambient temperature causes the thermal energy produced by PVT collectors to increase (Figure 4.73a). As the ambient temperature increases from minimum to maximum, the thermal energy produced by PVT collectors increases by 76% to 79%. The highest thermal energy production was observed at Config R1 with 934 W at maximum ambient temperature. In contrast, electricity generation (Figure 4.73b) is negatively affected by increasing ambient temperature due to the corresponding rise in PV cell temperature. As ambient temperature increases, the electrical output of PVT collectors decreases by approximately 5.9% to 7.9%, whereas conventional PV panels exhibit a larger decline of about 12%. Despite this reduction, configuration R1 consistently demonstrates the highest electrical performance among all serpentine tube PVT designs, producing 8% to 16% more electricity than the conventional PV panel across the evaluated ambient temperature range.

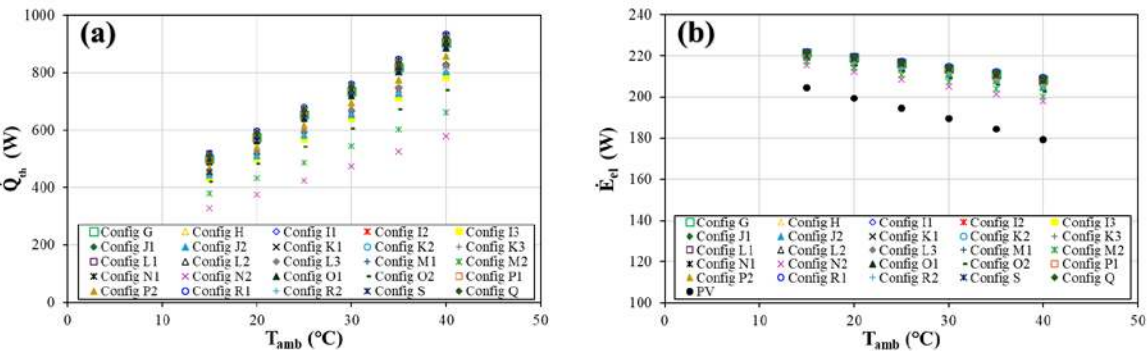

Figure 4.73. Variation of thermal energy production (a) and electrical power (b) of different serpentine tube configurations under varying ambient temperature conditions

Figure 4.74 presents the thermal and electrical efficiencies of serpentine tube PVT collectors as a function of ambient temperature. Thermal efficiency (Figure 4.74a) shows a significantly stronger response to ambient temperature changes compared to electrical efficiency, closely following the trend observed in thermal energy production. At an ambient temperature of

15 °C, the highest thermal efficiency was recorded in Config R1 at 0.3342, while the lowest value was observed in Config N2 at 0.2111. As ambient temperature increased, the performance gap between the configurations widened. At the maximum ambient temperature, Config R1 reached a thermal efficiency of 0.6008, which is 61.42% higher than that of Config N2.

In contrast, electrical efficiency (Figure 4.74b) exhibited only modest declines with rising ambient temperature, ranging from approximately 5.88% to 8.22% across all serpentine tube configurations. As PV cell temperature increases with ambient temperature, electrical efficiency (Eq. 3.27) correspondingly decreases. When compared to a conventional PV panel, electrical efficiency values at the lowest ambient temperature were 5.5% to 8.6% lower than those of serpentine tube PVT collectors. However, as the ambient temperature reached its maximum, this difference increased to between 10% and 16%. The maximum electrical efficiency was recorded in Config R1, reaching 0.1429 at an ambient temperature of 15 °C. According to Yan et al. (2022), the increase in ambient temperature from 15 °C to 35 °C resulted in enhanced thermal efficiency, showing a 36% improvement, while electrical efficiency slightly declined by about 2%.

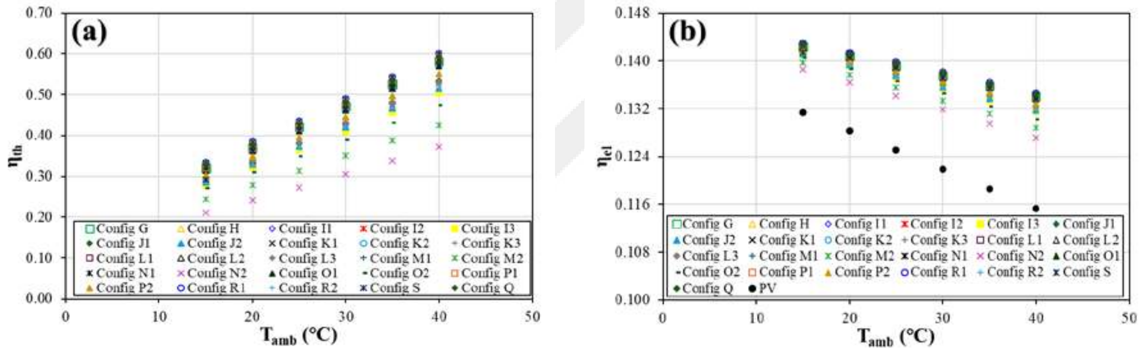

Figure 4.74. Effect of ambient temperature on the thermal (a) and electrical (b) efficiency of serpentine tube PVT collectors

Variations in ambient temperature significantly affect the exergetic performance parameters of PVT collectors. As illustrated in Figure 4.75a, increasing ambient temperature leads to higher thermal exergy production (Eq. 3.43) in some serpentine tube configurations, while it causes a decline in others, depending on the behavior of the Carnot efficiency factor. Electrical exergy (Figure 4.75b) follows the same pattern as electrical efficiency (Figure 4.74b), showing a consistent decrease with rising ambient temperature. Given that electrical exergy has a greater influence on total exergy output than thermal exergy, the exergy output remains nearly constant in some configurations, while it declines in others as ambient temperature increases (Figure 4.74c).

In contrast, exergy destruction (Figure 4.75d) exhibits an inverse relationship with output exergy. Config R1 demonstrates the highest total exergy output across the temperature range, whereas Config N2 consistently shows the highest level of exergy destruction.

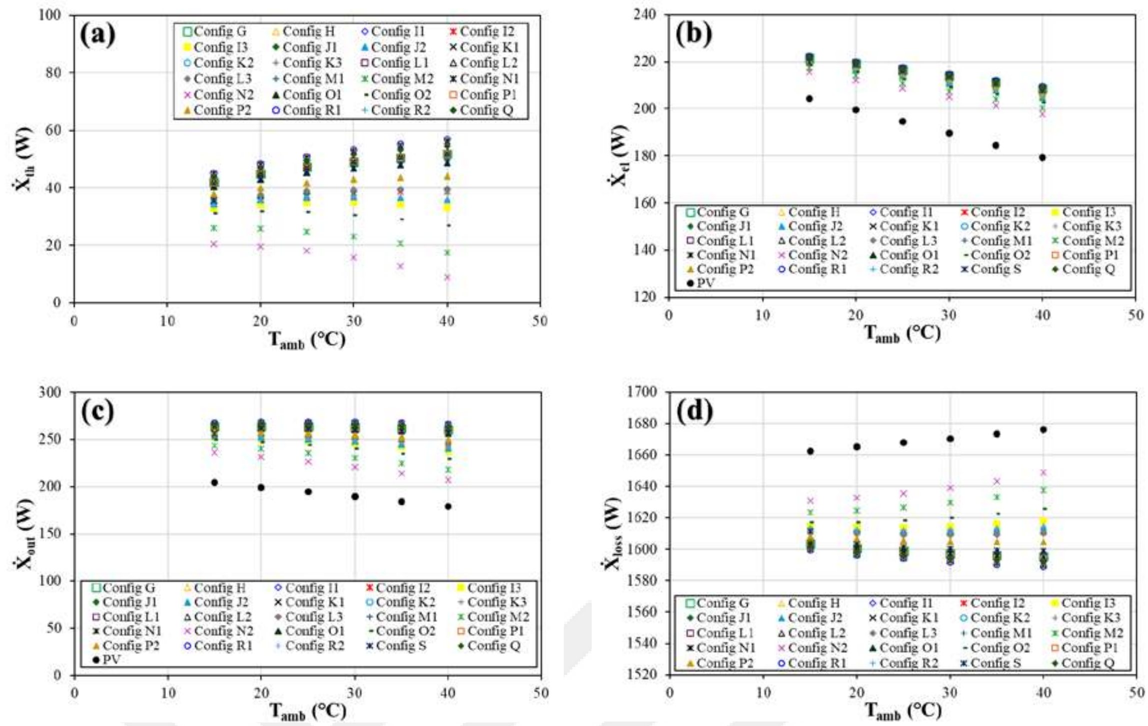

Figure 4.75. Effect of ambient temperature on the thermal (a), electrical (b) and output (c) exergy, and exergy destruction (d) of serpentine tube PVT collectors

Overall and primary energy saving efficiencies (Figure 4.76) increase with rising ambient temperature, despite the decline in electrical efficiency (Figure 4.74b). This is primarily because the variation in thermal efficiency (Figure 4.74a) with ambient temperature is much more pronounced than that of electrical efficiency. As the ambient temperature increases from 15 °C to 40 °C, the overall efficiency of all serpentine tube PVT configurations enhances, ranging from 43% to 54% (Figure 4.76a). The highest overall efficiency is recorded for Config R1 at 0.7356 when the ambient temperature reaches 40 °C. At the same temperature, the lowest overall efficiency is observed in Config N2 at 0.4994, a value nearly equal to that of Config R1 at 15 °C.

In a similar manner, as the ambient temperature increases from its minimum to maximum, primary energy saving efficiency (Figure 4.76b) also improves across all serpentine tube configurations, ranging from 22.7% to 34.5%. At 40 °C, the highest primary energy saving efficiency is observed in Config R1 at 0.9553, while the lowest value is recorded for Config N2 at 0.7102.

Exergy efficiency, illustrated in Figure 4.76c, is influenced by both exergy output and input (Eq. 3.45). As ambient temperature increases, the exergy input slightly decreases. However, as shown in Figure 4.75c, variations in exergy output remain relatively small across serpentine tube configurations. Consequently, exergy efficiency exhibits only minor changes for most configurations. The maximum exergy efficiency is achieved at an ambient temperature of 25 °C, reaching 0.1441 for Config R1. At the same temperature, Config N2 yields a lower exergy efficiency of 0.1218.

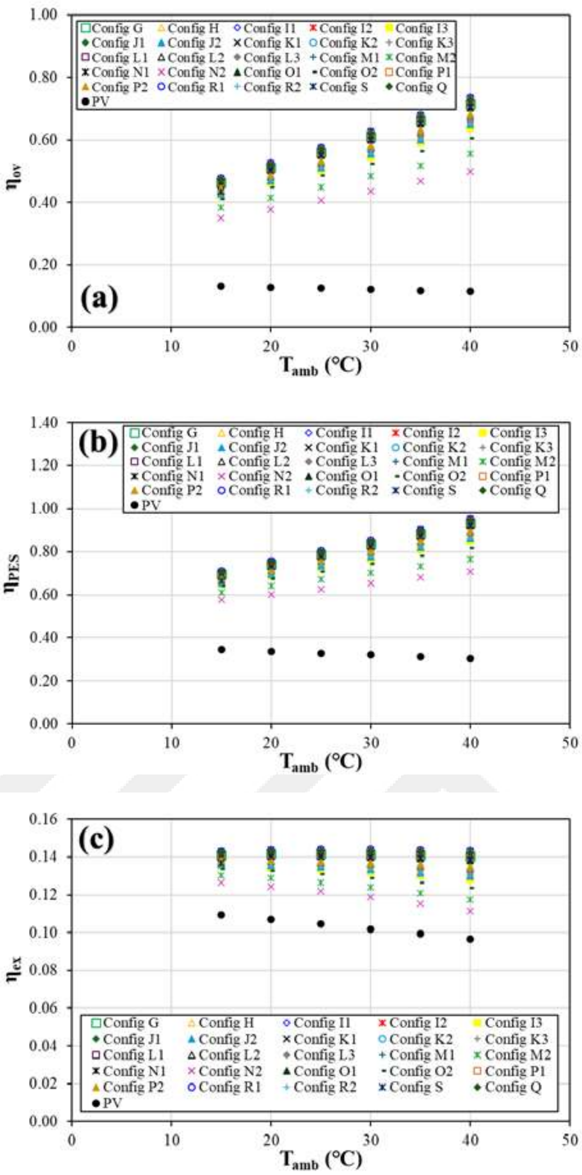

Figure 4.76. Effect of ambient temperature on the overall (a), primary energy saving (b) and exergy (c) efficiency of serpentine tube PVT collectors

The effect of ambient temperature on pressure drop and thermal energy produced per unit pressure drop (TEPD) is illustrated in Figure 4.77. As ambient temperature increases, the water outlet temperature also rises, resulting in decreased water viscosity and density. The reduction in these fluid properties lowers internal fluid friction and local losses, thereby reducing the overall pressure drop (Figure 4.77a). As the ambient temperature increases from 15 °C to 40 °C, the pressure drop decreases by approximately 14.1% to 18.5% across different serpentine tube PVT configurations. The highest pressure drop at 40 °C ambient temperature is recorded as 220 Pa in Config Q. In addition, the significant increase in water outlet temperature with rising ambient temperature enhances thermal energy output. Combined with the reduction in pressure drop, this results in a substantial increase in TEPD (Figure 4.77b). The highest TEPD value is achieved in Config R1 at 40 °C ambient temperature, reaching 4.04 W/Pa.

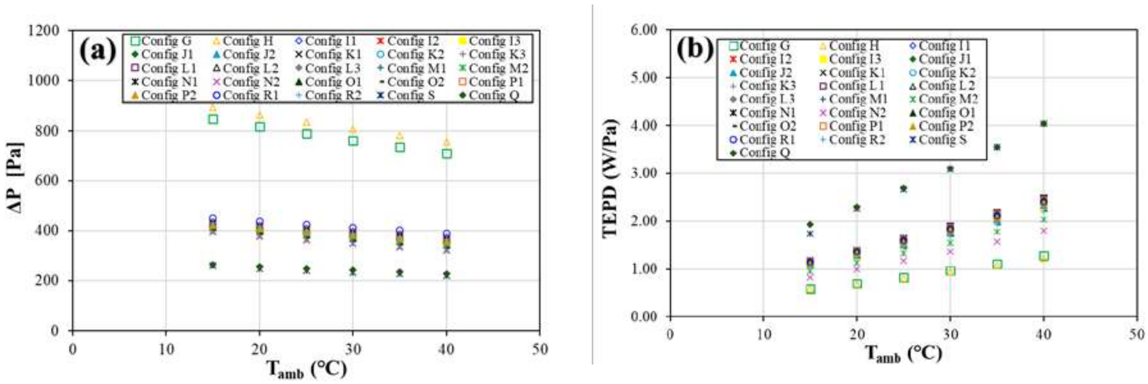

Figure 4.77. Effect of ambient temperature on the pressure drop (a) and TEPD (b) of serpentine tube PVT collectors

4.2.6. Effect of Wind Velocity on the Serpentine Tube PVT Collector Configurations

The final operational parameter evaluated in this study is wind velocity, which considerably influences the energetic and exergetic performance of PVT collectors. In this section, the effects of varying wind velocity on several performance indicators are investigated. Wind velocity is altered in 1 m/s increments, ranging from 1 m/s to 5 m/s, while solar irradiance, fluid flow rate, fluid inlet temperature, and ambient temperature are held constant according to the base-case conditions.

Figure 4.78 compares the absorber temperature distribution contours of the three best-performing serpentine tube configurations under base-case conditions, configurations H, R1 and Q across the wind velocity range. To ensure consistency with previously analyzed operational parameters, a standardized temperature scale is applied to these contour plots. Figure 4.79 presents variations in average PV cell surface temperatures and fluid outlet temperatures of all serpentine tube PVT collectors with respect to wind velocity. As wind velocity increases, convective heat losses rise, leading to a decrease in absorber surface temperature. Furthermore, the temperature distribution within the PVT collectors becomes more uniform with increasing wind velocity, indicating enhanced thermal homogeneity. At all examined wind velocities, local absorber temperatures remain below 60 °C.

The trend in PV cell temperatures (Figure 4.79a) of serpentine tube PVT collectors and the surface temperature of a conventional PV panel is also analyzed. With increasing wind velocity, the cooling effect reduces surface thermal energy accumulation, resulting in lower cell temperatures. While significant temperature differences exist between PVT collectors and the conventional PV panel at low wind velocities (13 °C to 21 °C at 1 m/s), this gap narrows at higher wind velocities, with differences ranging between 5 °C and 8 °C at 5 m/s. Additionally, the PVT configurations exhibit closer temperature values among themselves as wind velocity increases.

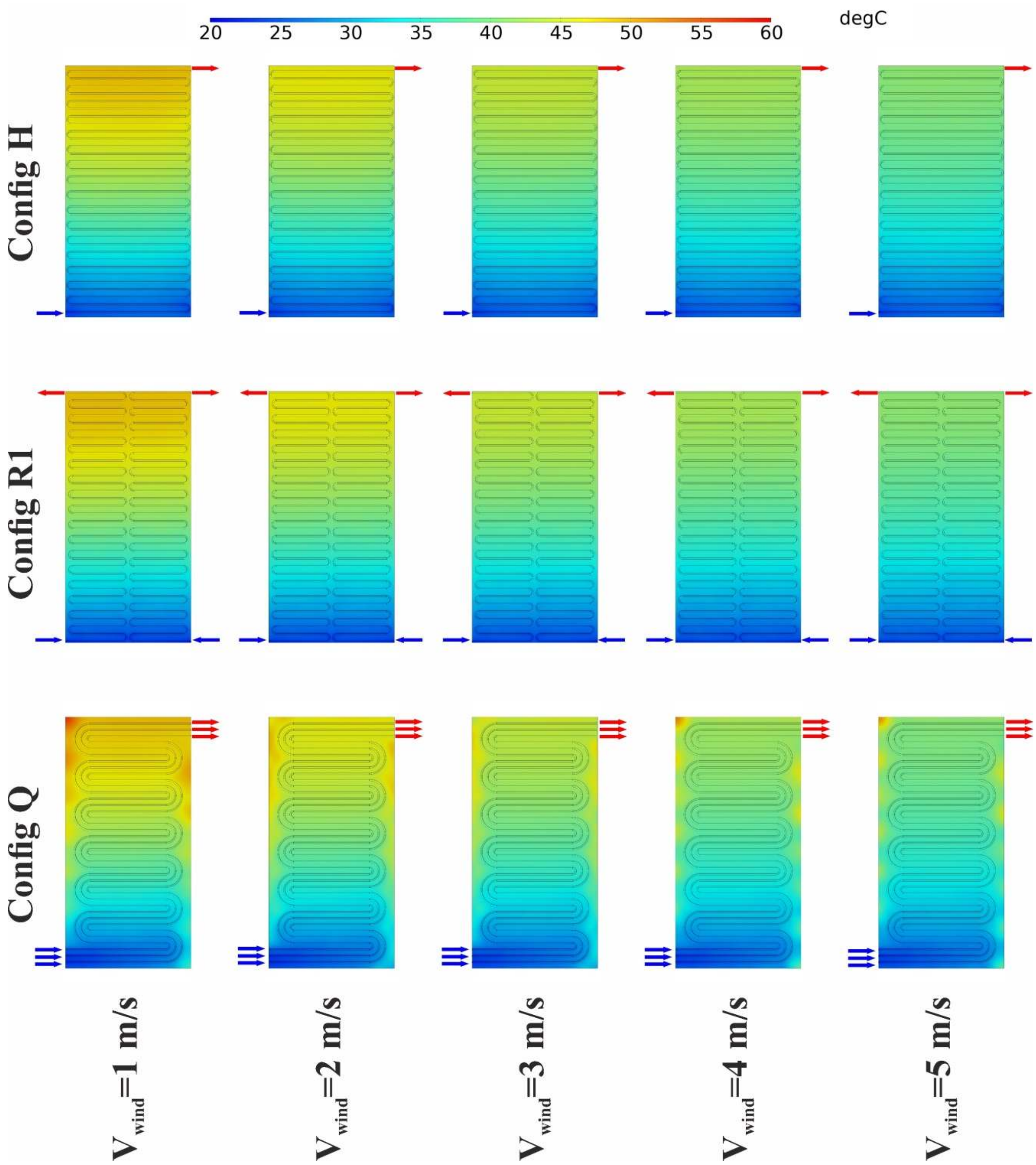

Figure 4.78. PVT absorber temperature distribution of Config H (a), Config R1 (b) and Config Q (c) for different wind velocities

Regarding fluid outlet temperatures (Figure 4.79b), a general decline is observed with higher wind velocities due to increased convective losses. For instance, at 1 m/s, Config R1 and Config N2 record outlet temperatures of 49.25 °C and 38.29 °C, respectively. At the maximum wind velocity of 5 m/s, these values decrease to 40.57 °C and 32.88 °C, showing both an overall temperature drop and a convergence among configurations.

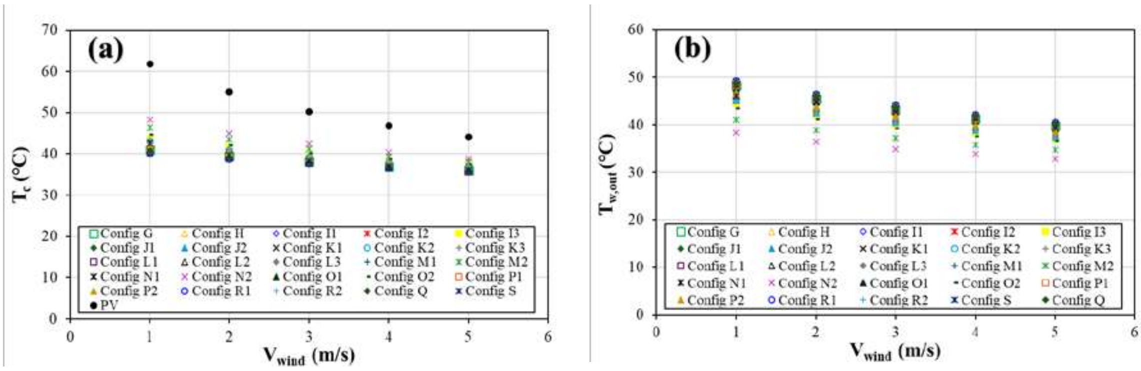

Figure 4.79. Variation of average PV cell (a) and water outlet (b) temperature of different serpentine tube configurations under varying wind velocities

Figure 4.80 presents the variation in thermal and electrical energy production of the serpentine tube PVT collectors, as well as the electrical output of conventional PV panels, as a function of wind velocity. Thermal energy production (Figure 4.80a) in serpentine tube PVT collectors is primarily influenced by convective heat losses. The increase in wind velocity intensifies these losses, thereby reducing thermal energy output. Specifically, thermal energy production decreases by approximately 29% as wind velocity increases from 1 m/s to 5 m/s.

In contrast, the reduction in PV cell temperatures due to increased convective losses at higher wind velocities leads to improved electrical performance in both serpentine tube PVT collectors and conventional PV panels (Figure 4.80b). At low wind velocities, notable differences exist among PVT configurations and between PVT collectors and the conventional PV panel. However, as wind velocity increases, these differences diminish, and the electrical outputs of the PVT collectors converge, narrowing the performance gap with the conventional PV panel. At a wind velocity of 1 m/s, PVT collectors generate 7.2% to 10.6% more electricity compared to the conventional PV panel. When the wind velocity reaches 5 m/s, this difference decreases to between 2.7% and 3.6%, indicating the homogenizing effect of increased wind velocity on electrical performance.

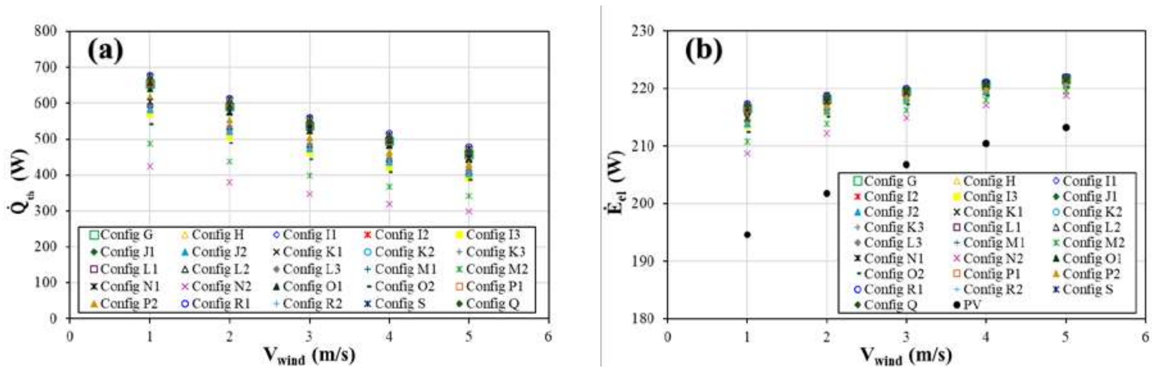

Figure 4.80. Variation of thermal energy production (a) and electrical power (b) of different serpentine tube configurations under varying wind velocities

An increase in wind velocity enhances convective heat loss from the collector surface, resulting in reduced thermal energy generation and a corresponding drop in thermal efficiency (Figure 4.81a). Specifically, an increase in wind velocity from 1 m/s to 5 m/s leads to an average reduction of 29.6% in thermal efficiency across all serpentine tube configurations. The highest thermal efficiency, recorded at 0.4361, is observed in Config R1 at a wind velocity of 1 m/s. Even at 5 m/s, Config R1 maintains a thermal efficiency of 0.3067, which is still 12.5% higher than the efficiency of the lowest-performing configuration, N2, at 1 m/s wind velocity.

Conversely, the reduction in PV cell temperature at higher wind velocities leads to improved electrical efficiency (Figure 4.81b) and output (Eq. 3.28). As wind velocity increases from 1 m/s to 5 m/s, electrical efficiency demonstrates an increase ranging from 2.15% to 4.77% across all serpentine tube configurations, indicating that wind velocity exerts a relatively minor effect on electrical performance. The highest electrical efficiency, 0.1427, is again observed in Config R1 at 5 m/s wind velocity. For the conventional PV panel, electrical efficiency is approximately 7.27% to 11.67% lower than that of the PVT collectors at the lowest wind velocity. However, as wind velocity increases, the electrical efficiency of the PV panel improves, narrowing the performance gap to between 2.55% and 4% compared to the PVT systems.

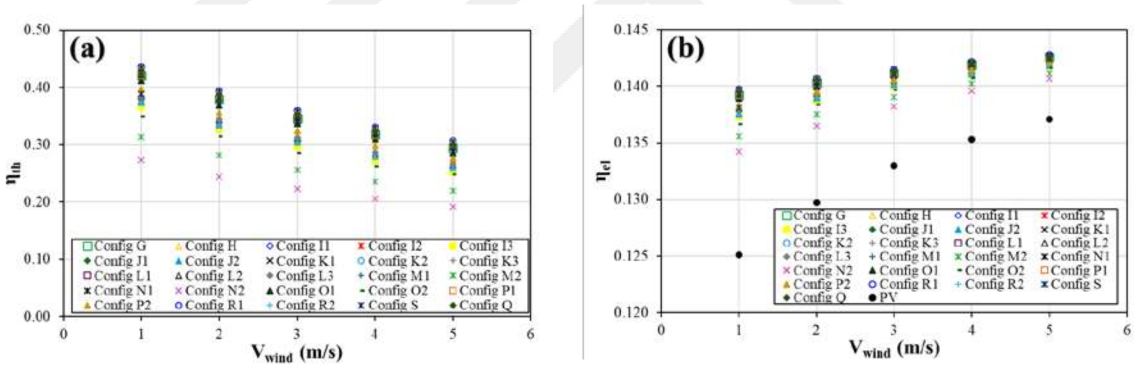

Figure 4.81. Effect of wind velocity on the thermal (a) and electrical (b) efficiency of serpentine tube PVT collectors

The effects of wind velocity on thermal exergy, electrical exergy, total exergy output and exergy destruction are presented in Figure 4.82. Given that the fluid inlet temperature is kept constant, and the fluid outlet temperature decreases with increasing wind velocity, thermal exergy (Figure 4.82a) exhibits a decreasing trend (Eq. 3.43). Among all serpentine tube configurations, Config R1 consistently delivers the highest thermal exergy production at all wind velocities, followed by Config H and Q. While significant differences are observed between configurations at low wind velocity, these differences diminish as wind velocity increases, leading to convergence in thermal exergy performance.

Moreover, the reduction in PV cell temperature caused by higher wind velocity slightly improves electrical efficiency (Figure 4.82b), resulting in a modest increase in electrical exergy across PVT configurations. At a wind velocity of 1 m/s, electrical exergy values range between 208 W and 217 W, when wind velocity reaches 5 m/s, they increase slightly to a range of 218 W to 222 W. Although total exergy output is predominantly influenced by electrical exergy, the limited variation in electrical exergy and the more significant drop in thermal exergy cause the total exergy output to follow a declining trend, mirroring that of thermal exergy. Conversely, exergy destruction increases with higher wind velocities. While the highest exergy output is achieved by Config R1, the greatest exergy destruction is observed in Config N2.

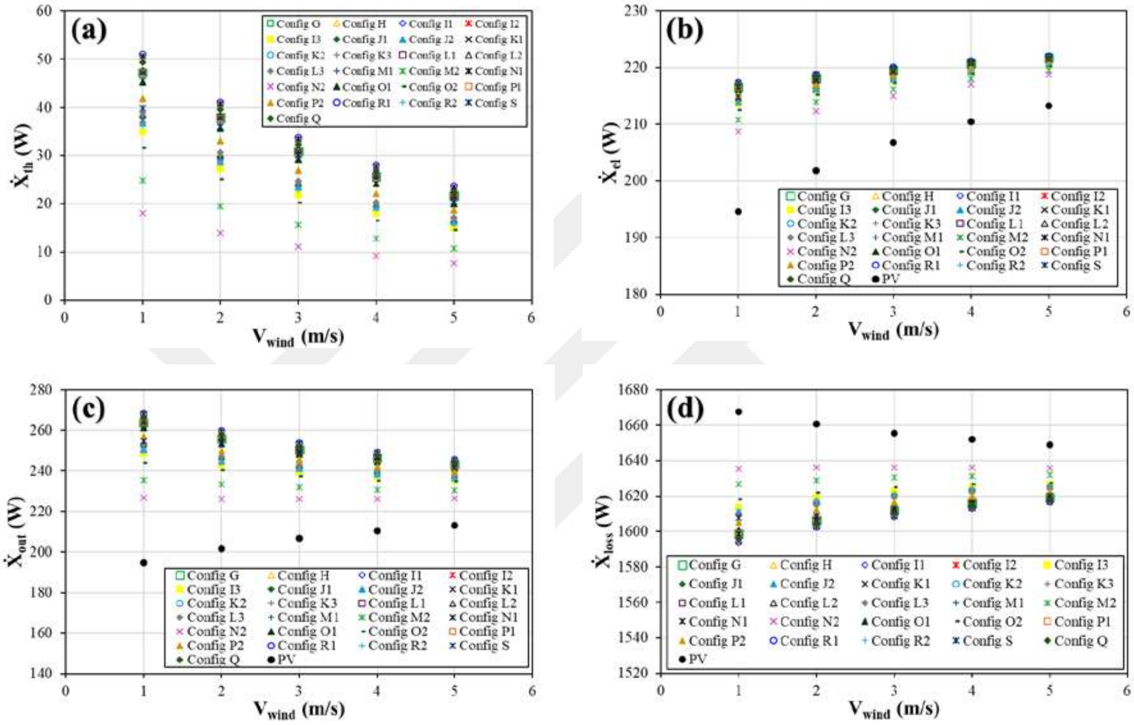

Figure 4.82. Effect of wind velocity on the thermal (a), electrical (b) and output (c) exergy, and exergy destruction (d) of serpentine tube PVT collectors

As thermal efficiency shows a more significant change with wind velocity than electrical efficiency, overall and primary energy saving efficiencies reflect a similar pattern, as shown in Figure 4.83. Due to the decline in thermal efficiency at higher wind velocities, both performance metrics also show a decreasing trend.

Among all serpentine tube PVT configurations, the highest overall (Figure 4.83a) and primary energy saving (Figure 4.83b) efficiencies are observed in Config R1 at a wind velocity of 1 m/s, with values of 0.5758 and 0.8039, respectively. As wind velocity increases from its minimum to maximum value, the overall efficiency decreases by approximately 18% to 22%, while the primary energy saving efficiency declines by about 10% to 15%, depending on the configuration. A similar outcome was reported in the study by Hosseinzadeh et al. (2018), where increasing the wind speed from 1 m/s to 9 m/s led to a 3.5% reduction in thermal efficiency, while the improvement in electrical efficiency remained marginal.

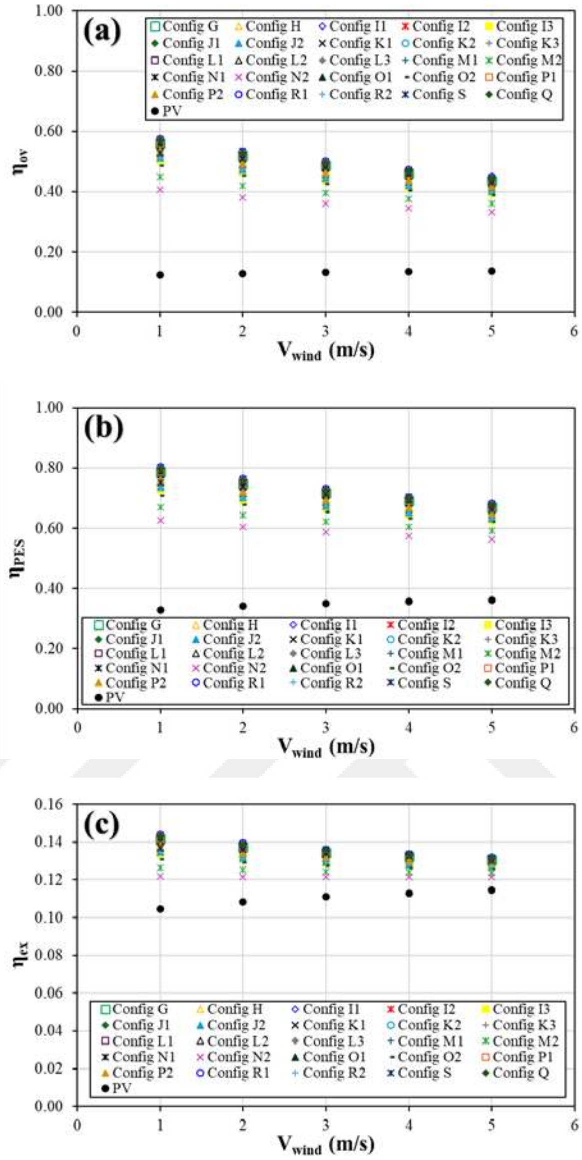

Figure 4.83. Effect of wind velocity on the overall (a), primary energy saving (b) and exergy (c) efficiency of serpentine tube PVT collectors

On the other hand, when examining exergy efficiency, it is evident that since the sun exergy remains constant and is independent of wind velocity across all configurations exergy efficiency (Figure 4.83c) is directly governed by the output exergy (Eq. 3.45), as presented in Figure 4.82c. As wind velocity increases, output exergy decreases, resulting in a corresponding decline in exergy efficiency for the PVT collectors. The highest exergy efficiency is achieved by Config R1, with a value of 0.1441 at a wind velocity of 1 m/s.

Increasing wind velocity leads to a reduction in water outlet temperature, which subsequently increases the water viscosity and density. Although the higher fluid properties contribute to an increase in pressure drop, the overall effect remains limited, with an approximate

3% rise in pressure drop observed, as shown in Figure 4.84a. The lowest pressure drop is recorded in configurations S and Q at a wind velocity of 1 m/s, with values around 245 Pa.

Conversely, the decline in thermal energy production due to heat losses, combined with the relatively small change in pressure drop, results in a substantial decrease in thermal energy produced per unit pressure drop (TEPD), reaching approximately 34%. The highest TEPD is observed in Config Q at a wind velocity of 1 m/s, with a value of 2.68 W/Pa (Figure 4.84b).

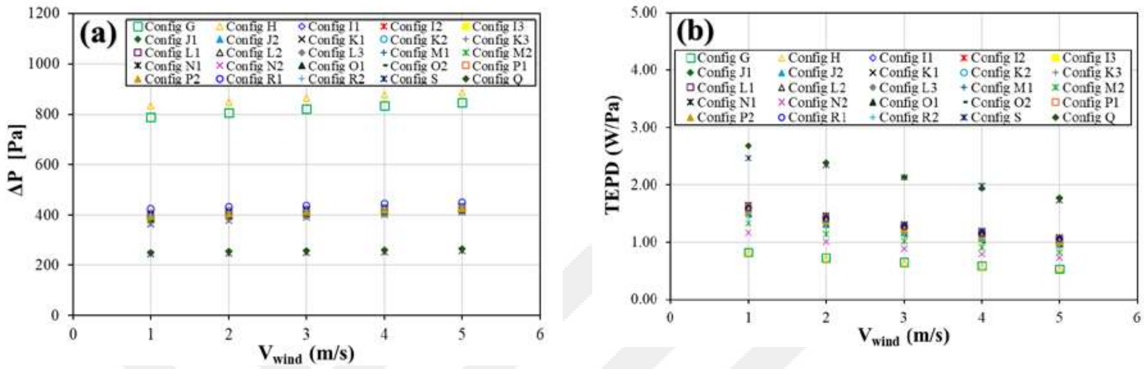

Figure 4.84. Effect of wind velocity on the pressure drop (a) and TEPD (b) of serpentine tube PVT collectors

4.3. Spiral Tube PVT Collector Configurations

In addition to parallel and serpentine configurations, spiral designs are also widely utilized in the literature due to their compact geometry and favorable flow distribution characteristics. In this section, a total of twelve spiral-type configurations comprising both single and double inlet designs were comprehensively examined based on fluid inlet direction and positioning. To ensure a consistent and fair comparison, the tube length and absorber area were kept constant across all configurations. Numerical simulations were carried out using finite element method in COMSOL Multiphysics software.

The study investigated the influence of several operational parameters including solar irradiance, fluid inlet temperature, flow rate, ambient temperature and wind velocity on various energetic and exergetic performance indicators. Furthermore, the thermal and electrical behavior of the proposed spiral tube PVT collectors was compared with that of a conventional PV panel, with particular focus on cell temperature and electrical output parameters.

4.3.1. Comparison of Spiral Tube PVT Collector Configurations Under Base-case Conditions

In this section, twelve spiral tube PVT collector configurations are evaluated under the base-case conditions defined in Table 3.3. The comparison includes a wide range of performance metrics such as PV cell temperature, fluid outlet temperature, thermal and electrical energy production, thermal, electrical, overall, and primary energy saving efficiencies, pressure drop, thermal energy produced per unit pressure drop (TEPD), various exergetic performance indicators and exergy efficiency.

In addition to these performance parameters, surface temperature distribution is a critical factor in PVT collector design. A homogeneous temperature profile on the collector surface is essential for maintaining PV cell durability and ensuring long-term performance. Localized thermal energy accumulation and elevated temperatures can accelerate cell degradation and shorten the operational lifespan of the system. The surface temperature distribution contours of the twelve spiral tube PVT configurations are presented in Figure 4.85. To ensure consistency in comparative analysis, the temperature scale used here is the same as that employed for the parallel and serpentine tube PVT collectors.

Configurations T, U, V and W feature single inlets, while configurations X, Y and Z are equipped with double inlets. These configurations differ based on fluid inlet location and the number of internal helical. In general, the fluid provides effective cooling near the inlet region, but temperature tends to rise toward the center and outlet sections of the collector, depending on helical arrangement.

Among the single-inlet designs, Config W demonstrates the most homogeneous surface temperature distribution. For double-inlet designs, configurations X1 and Z1 exhibit both thermal uniformity and low surface temperature. In contrast, Config T shows significant non-uniformity, with elevated temperatures concentrated at the center of the panel due to the coolant flow path. Notably, Config X1, a two-inlet adaptation of Config T, improves temperature distribution by introducing the working fluid at the center of collector.

An analysis of the remaining spiral tube PVT configurations reveals varying levels of thermal uniformity based on inlet arrangement and helical structure. In Config U, which features a single inlet and double helical structure, effective cooling is observed over approximately half of the panel surface. However, the remaining areas exhibit noticeable thermal energy accumulation due to insufficient fluid coverage. Config V, which employs a single inlet with four helical segments, exhibits a distinct temperature gradient. The initial helical section remains cool, while a gradual temperature rise is observed beyond the second helical segment as the coolant absorbs more heat along its path. Config Y represents the double-inlet counterpart of Config U. While the double entry in Config Y help to redistribute the fluid more evenly and reduce localized thermal energy accumulation seen in Config U, cooling remains limited to specific regions, and a fully homogeneous temperature distribution is not achieved.

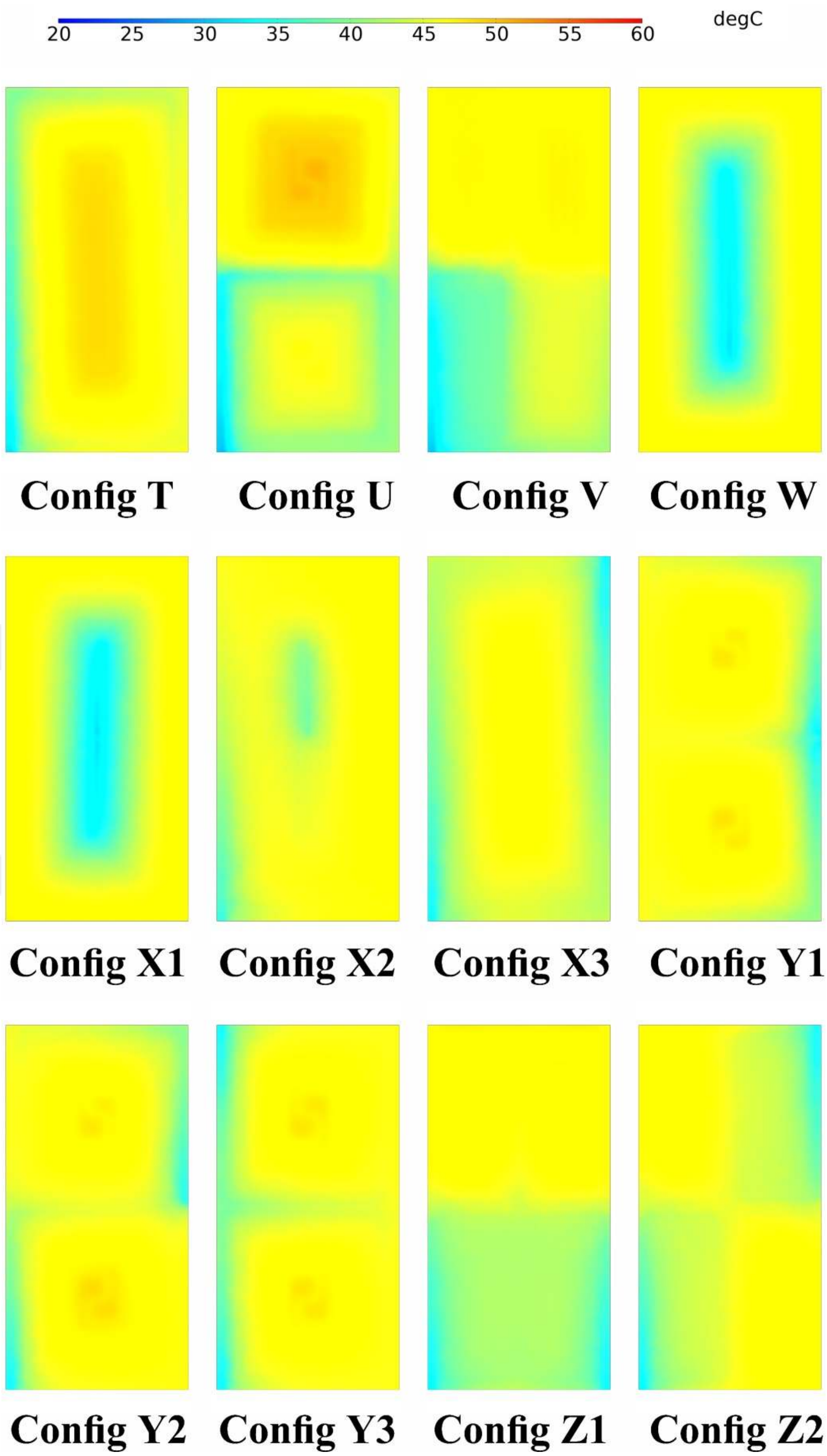

Figure 4.85. Temperature contour of different spiral tube configurations under base-case conditions

Similarly, Config Z is derived from Config V by incorporating a double-inlet design into the four-helical structure. This modification enhances thermal performance, especially in Config Z1, where the improved flow distribution allows more uniform surface cooling. However, in

Config Z2, where the fluid enters diagonally from opposite corners, cooling is concentrated around the helical paths, leaving the outer panel edges relatively undercooled.

Figure 4.86 presents a comparative analysis of average PV cell temperature and fluid outlet temperature, two key parameters that directly influence the thermal and electrical performance of PVT collectors, for spiral tube PVT collectors and a conventional PV panel. In this figure, and throughout this section, red indicates single-inlet PVT collectors, blue indicates double-inlet PVT collectors, and black represents the conventional PV panel.

Among the spiral tube configurations evaluated, single-inlet Config W, double-inlet Config X1, and the double-inlet, four-helical structure Config Z1 exhibit the lowest PV cell temperatures (Figure 4.86a). Under base-case conditions, the average PV cell temperatures of PVT collectors are observed to be 16.79 °C to 19.38 °C lower than that of the conventional PV panel, highlighting the effective cooling capacity of these configurations.

Regarding fluid outlet temperature (Figure 4.86b), values range from 42.78 °C to 46.36 °C across the spiral tube PVT collectors. A strong correlation is observed between low PV cell temperature and high outlet fluid temperature; specifically, Config W, X1 and Z1, which demonstrate the most efficient cell cooling, also achieve the highest fluid outlet temperatures.

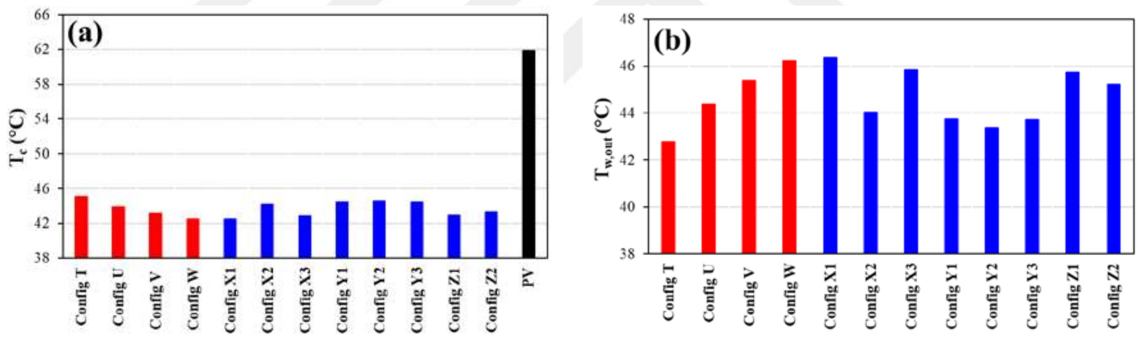

Figure 4.86. Average cell (a) and water outlet (b) temperature of different spiral tube configurations under base-case conditions

Figure 4.87 compares the thermal and electrical energy outputs, along with their respective efficiencies, for various spiral tube PVT collector configurations. Among the evaluated configurations, Config W, X1 and Z1 demonstrate superior thermal performance. Config X1 exhibits the highest thermal energy output and efficiency (Figure 4.87a), with values of 611 W and 0.3929, respectively, representing a 15.6% improvement over Config T, which shows the lowest thermal performance.

Similarly, due to the inverse relationship between PV cell temperature and electrical efficiency, configurations W, X1, and Z1, identified in Figure 4.86a as having the lowest cell temperatures, also achieve the highest electrical energy output and efficiency. Among these, configuration X1 again stands out, delivering the highest electrical efficiency (Figure 4.87b). When compared to a conventional PV panel, X1 provides a 10.5% increase in electrical efficiency, underscoring its overall effectiveness in thermal management and energy conversion.

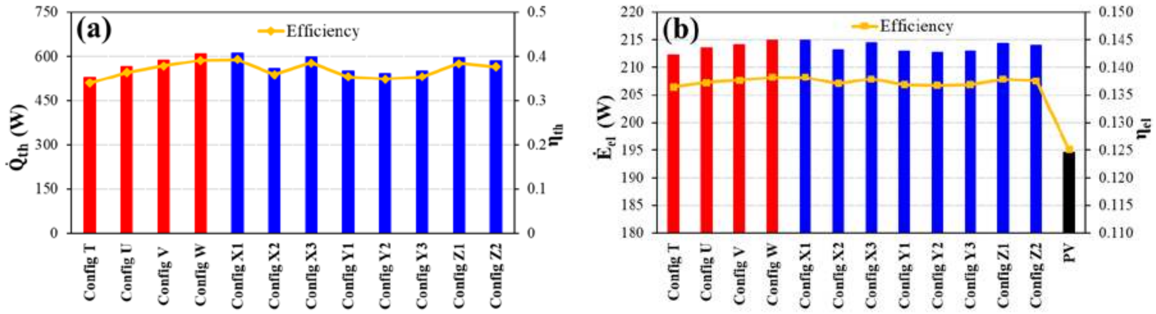

Figure 4.87. Thermal power and thermal efficiency (a), electrical power and electrical efficiency (b) of different spiral tube configurations

Although spiral tube PVT collectors are generally disadvantaged in terms of pressure drop, this drawback can be mitigated through appropriate design modifications. Figure 4.88 presents the pressure drop and the thermal energy produced per unit pressure drop (TEPD) for all configurations. As illustrated, single-inlet configurations (indicated in red) exhibit significantly higher pressure drops compared to their double-inlet counterparts.

Configurations T, U, V and W are designed with single-inlet and different helical channels, forcing the fluid to follow long and tortuous paths with numerous bends. This extended flow path increases both frictional and local losses, leading to a significant rise in pressure drop. The highest pressure drop is observed in Config V, which incorporates a four-helical design (Figure 4.88a). This is primarily due to increased local losses associated with its complex internal geometry. In contrast, the pressure drops across the double-inlet configurations are nearly identical, as these designs share identical total tube lengths and flow rates. The minor differences observed among them are attributed to variations in fluid properties particularly water viscosity and density resulting from temperature fluctuations. When evaluating TEPD (Figure 4.88b), single-inlet configurations perform poorly due to their inherently high pressure drop. In double-inlet designs, where pressure drops are comparable, thermal energy production becomes the key differentiating factor. Config X1 stands out by delivering the highest thermal energy output among all tested designs, which is reflected in its TEPD value of 1.58 W/Pa, the best performance recorded in this analysis.

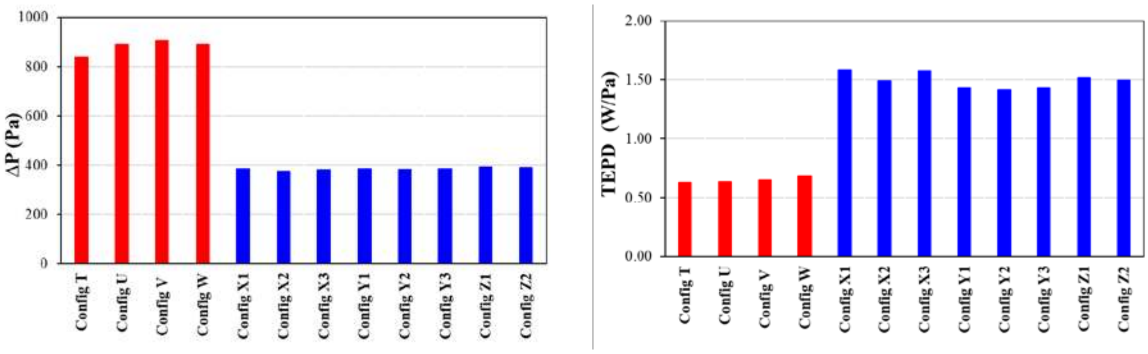

Figure 4.88. Pressure drop (a) and TEPD (b) of different spiral tube configurations

Figure 4.89 presents a comparative analysis of exergetic performance metrics namely thermal exergy, electrical exergy, output exergy and exergy destruction for spiral tube PVT collector configurations. Thermal exergy is influenced by fluid inlet temperature, outlet temperature and ambient temperature (Eq. 3.43). As all parameters except the outlet temperature remain constant under base-case conditions, thermal exergy trends (Figure 4.89a) follow those of the fluid outlet temperature. In this context, Config X1 achieves the highest thermal exergy, followed by Config W and Z1. Electrical exergy (Figure 4.89b) is equivalent to the electrical energy produced by each configuration. Since electrical exergy dominates the total output exergy, and the variations in electrical output across configurations are relatively small, the differences in output exergy are moderate (Figure 4.89c). Nonetheless, Config X1, which performs best overall, produces approximately 14 W more output exergy than the lowest-performing Config T.

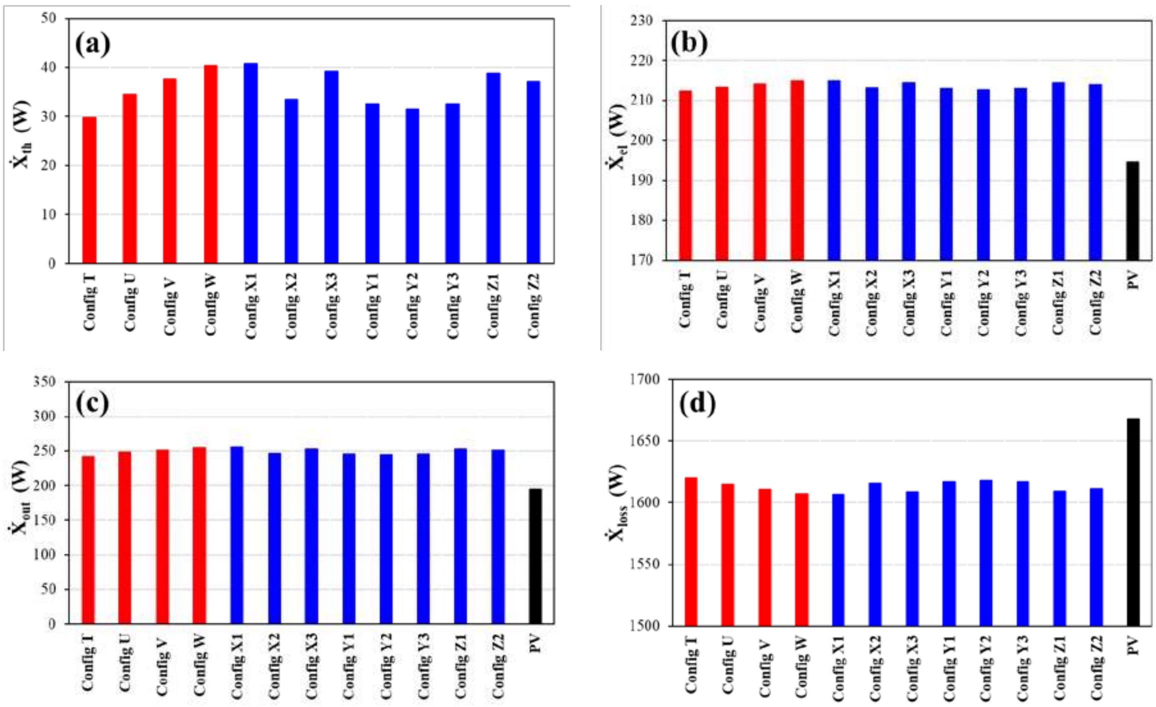

Figure 4.89. Thermal (a), electrical (b) and output (c) exergy, and exergy destruction (d) of different spiral tube configurations under base-case conditions

Given that the solar exergy input is identical for all configurations, exergy destruction (Figure 4.89d) follows an inverse trend relative to output exergy. Accordingly, Config T exhibits the highest exergy destruction, while Config X1 demonstrates the lowest, confirming its superior thermodynamic performance among the spiral tube PVT collectors.

The comparison of overall, primary energy saving and exergy efficiency metrics of all spiral tube PVT collectors under base-case conditions is presented in Figure 4.90. Although overall and primary energy saving efficiencies incorporate both thermal and electrical outputs, their trends are largely dictated by thermal efficiency due to its more pronounced variation. Config X1 demonstrates the best performance in both metrics, achieving an overall efficiency (Figure 4.90a) of 0.5312 and a primary energy saving efficiency (Figure 4.90b) of 0.7566. These values represent improvements of 11.6% and 8.3%, respectively, over Config T, which exhibits the lowest performance. Consistent with trends observed in other performance metrics, configurations W and Z1 follow X1 in ranking for both overall and primary energy saving efficiencies.

Exergy efficiency, which reflects the second-law performance of the PVT collectors, is also compared in Figure 4.90c. Although it depends on both exergy input and output, the input exergy is constant across all spiral tube configurations. Therefore, exergy efficiency follows the same trend as output exergy. Configurations X1, W and Z1 once again show superior performance, with exergy efficiencies of 0.1373, 0.1371 and 0.1359, respectively. Configuration T records the lowest exergy efficiency at 0.1299.

Figure 4.91 presents a comprehensive comparison of all spiral tube PVT collectors and a conventional PV panel under base-case conditions, based on all evaluated performance parameters. In the figure, green represents the best-performing configuration for a given parameter, while performance degrades progressively toward red.

Across all performance indicators, Config X1 emerges as the top-performing design in nearly every category, with the exception of pressure drop. Even in this parameter, X1 ranks among the most efficient configurations, with only marginal differences compared to the best performer. Config W and Z1 also exhibit strong overall performance and closely follow X1 in most metrics. However, Config W shows a slight disadvantage in pressure drop. Conversely, Config T demonstrates the weakest performance overall, consistently ranking lowest across multiple performance criteria.

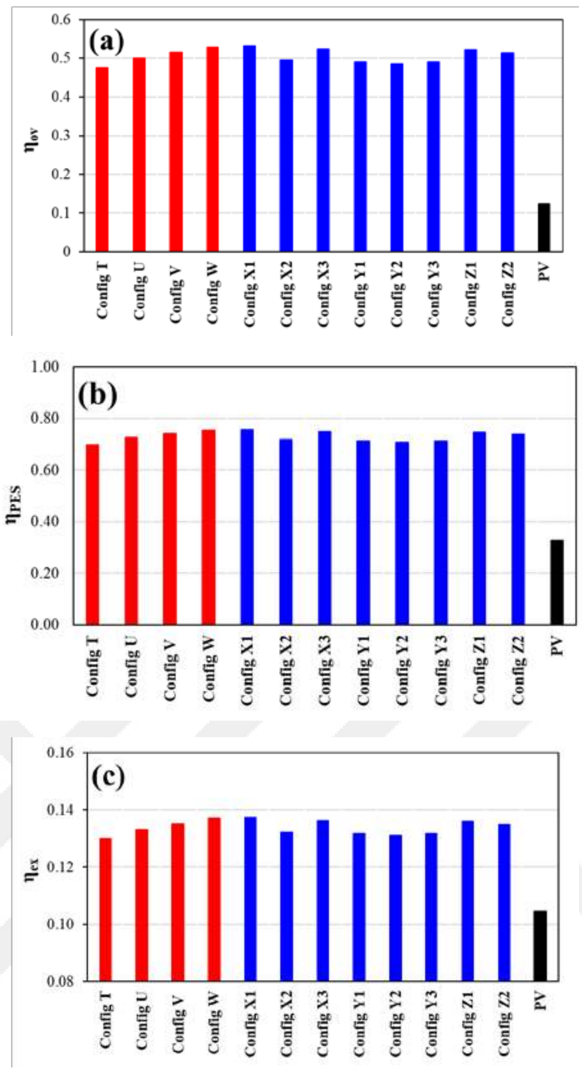

Figure 4.90. Overall (a), primary energy saving (b) and exergy (c) efficiency of different spiral tube configurations under base-case condition

Configuration	T_c (°C)	$T_{w,out}$ (°C)	ΔP (Pa)	$\dot{Q}_{th}$ (W)	$\dot{E}_{el}$ (W)	η_{el} (-)	η_{th} (-)	η_{ov} (-)	η_{PES} (-)	TEPD (W/Pa)	$\dot{X}_{th}$ (W)	$\dot{X}_{el}$ (W)	$\dot{X}_{out}$ (W)	$\dot{X}_{loss}$ (W)	η_{ex} (-)
T	45.06	42.79	838.66	528.30	212.23	0.1365	0.3397	0.4762	0.6988	0.63	29.74	212.23	241.97	1620.41	0.1299
U	43.90	44.37	890.22	565.08	213.44	0.1372	0.3633	0.5006	0.7245	0.63	34.47	213.44	247.91	1614.47	0.1331
V	43.21	45.38	903.69	588.56	214.16	0.1377	0.3784	0.5162	0.7408	0.65	37.66	214.16	251.83	1610.55	0.1352
W	42.50	46.23	889.83	608.23	214.91	0.1382	0.3911	0.5293	0.7547	0.68	40.43	214.91	255.35	1607.03	0.1371
X1	42.47	46.36	384.96	611.12	214.94	0.1382	0.3930	0.5312	0.7567	1.59	40.85	214.94	255.79	1606.59	0.1373
X2	44.16	44.05	373.54	557.57	213.16	0.1371	0.3585	0.4956	0.7192	1.49	33.48	213.16	246.65	1615.73	0.1324
X3	42.87	45.84	380.04	599.18	214.52	0.1379	0.3853	0.5232	0.7483	1.58	39.15	214.52	253.67	1608.71	0.1362
Y1	44.43	43.74	384.56	550.45	212.88	0.1369	0.3539	0.4908	0.7142	1.43	32.55	212.88	245.44	1616.94	0.1318
Y2	44.62	43.40	383.16	542.48	212.68	0.1368	0.3488	0.4856	0.7087	1.42	31.53	212.68	244.21	1618.17	0.1311
Y3	44.42	43.73	384.42	550.08	212.89	0.1369	0.3537	0.4906	0.7139	1.43	32.51	212.89	245.40	1616.98	0.1318
Z1	42.98	45.74	393.65	596.86	214.41	0.1379	0.3838	0.5216	0.7466	1.52	38.82	214.41	253.23	1609.15	0.1360
Z2	43.36	45.22	391.02	584.85	214.01	0.1376	0.3761	0.5137	0.7382	1.50	37.15	214.01	251.16	1611.22	0.1349
PV	61.84	-	-	-	194.60	0.1251	-	0.1251	-	-	-	194.60	194.60	1667.77	0.1045

Figure 4.91. Comparison of performance parameters of all spiral tube configurations under base-case conditions

4.3.2. Effect of Flow Rate on the Spiral Tube PVT Collectors

In this section, the influence of flow rate on the performance parameters of all spiral tube configurations was systematically investigated. The flow rate was varied from 5 to 50 L/h in increments of 5 L/h, ensuring that the flow remained within the laminar regime throughout the analysis. During this investigation, all other operational parameters including solar irradiance, water inlet temperature, ambient temperature, and wind velocity were maintained at their base-case values, as detailed in Table 3.3.

Figure 4.92 shows the change in the absorber temperature distribution contours of the three configurations, W, X1 and Z1, which were compared under base-case conditions in section 4.3.1 and produced the best results according to different performance parameters, with fluid flow rate.

As clearly observed from the temperature contour plots, an increase in fluid flow rate leads to a reduction in the absorber surface temperature of PVT collectors. The inlet edges remain relatively cool, while temperatures gradually rise toward the outlet side. At the lowest flow rate, the maximum absorber temperatures are recorded as 57 °C for Config W, 58 °C for Config X1 and 60 °C for Config Z1. With increasing flow rate, temperature distributions become more uniform, as evidenced by the contours. Under the maximum flow rate condition, the maximum absorber temperatures drop significantly and are recorded as 38.04 °C, 38.50 °C and 38.61 °C for Config W, X1 and Z1, respectively.

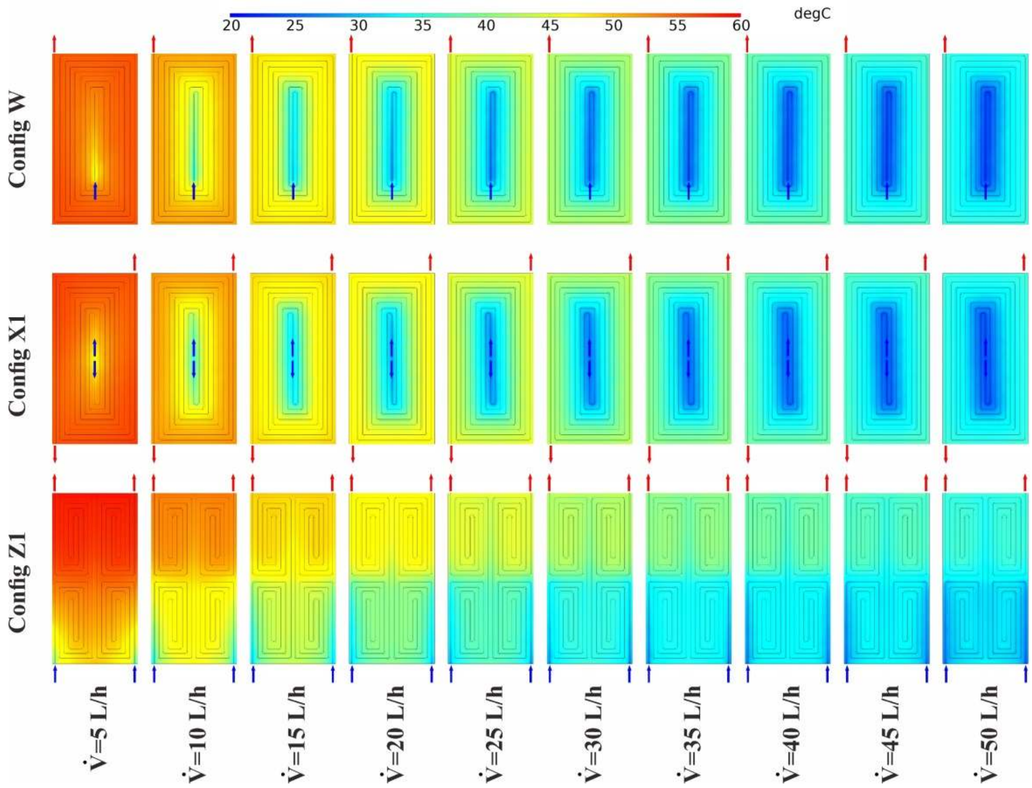

Figure 4.92. PVT absorber temperature distribution of Config W, Config X1 and Config Z1 for different flow rates

Figure 4.93 compares the average PV cell temperatures and fluid outlet temperatures of twelve spiral tube PVT collectors as a function of fluid flow rate. Since PV cell temperature directly influences electrical efficiency and energy output, its variation with flow rate is of critical importance. At low flow rates, all spiral tube configurations exhibit similar cell temperatures (Figure 4.93a). However, as the flow rate increases, performance differences among the collectors become more pronounced. Specifically, increasing the flow rate from its minimum to maximum value results in a reduction of cell temperature ranging from 22 °C to 25 °C, depending on the configuration. Under base-case conditions, Config X1 demonstrates the lowest cell temperature. However, at the maximum flow rate, Config W slightly outperforms X1 in terms of cell cooling. Regarding fluid outlet temperature (Figure 4.93b), a decreasing trend is also observed with increasing flow rate. Despite the reduction in cell temperature, the shorter contact time of the fluid within the absorber leads to lower outlet temperatures. At the lowest flow rate, outlet temperatures range between 55.6 °C and 58.4 °C, whereas at the highest flow rate, they decline to values between 33.9 °C and 35.5 °C.

The reduction in both cell and fluid outlet temperatures of PVT collectors with increasing flow rate was also observed in the study conducted by Kazem et al. (2020). In this study, as the fluid flow rate increased from 10 kg/h to 40 kg/h, the cell temperature dropped from above 54 °C to 40.9 °C. Similarly, the outlet temperature of the fluid decreased from 49.3 °C to 36.9 °C. In the study by Fayaz et al. (2018), it was observed that increasing the flow rate by 10 L/h resulted in a 0.72 °C reduction in PVT cell temperature and a 2.62 °C decrease in fluid outlet temperature.

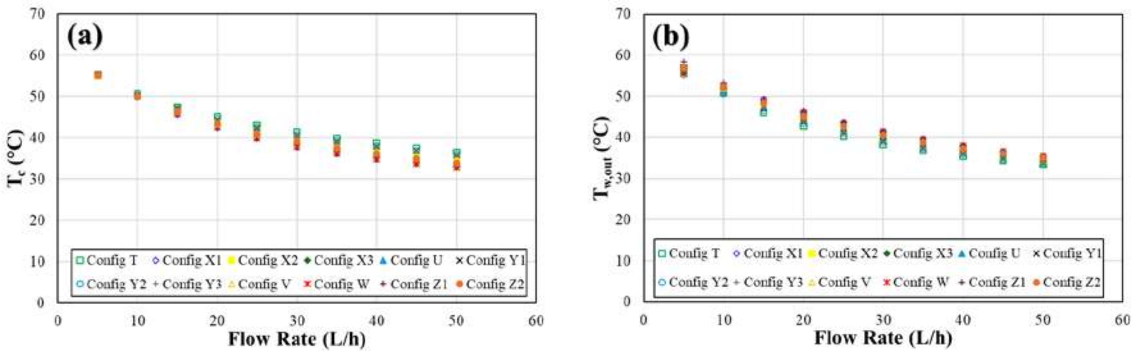

Figure 4.93. Variation of average PV cell (a) and water outlet (b) temperature of different spiral tube configurations under varying flow rate conditions

As the fluid flow rate increases, both the heat extracted from the PVT collector surface and the heat transferred to the working fluid decrease due to reduced contact time. However, the total thermal energy production and thus thermal efficiency increases significantly. At the lowest flow rate, thermal energy production and thermal efficiency is nearly identical across all spiral tube configurations. Yet, as the flow rate increases, performance differences between configurations become more evident (Figure 4.94a). At the maximum flow rate, Config X1 demonstrates the highest thermal performance, producing approximately 15% more thermal energy than Config T, which exhibits the lowest thermal energy output among all spiral tube designs. At a fluid flow rate of 5 L/h, the difference in thermal efficiency between the two configurations is relatively small, at only 2.87%. However, as the flow rate increases, this gap widens progressively, reaching approximately 15% at the maximum flow rate. The highest thermal efficiency is observed in Config X1 at a flow rate of 50 L/h, with a recorded value of 0.5787 (Figure 4.95a).

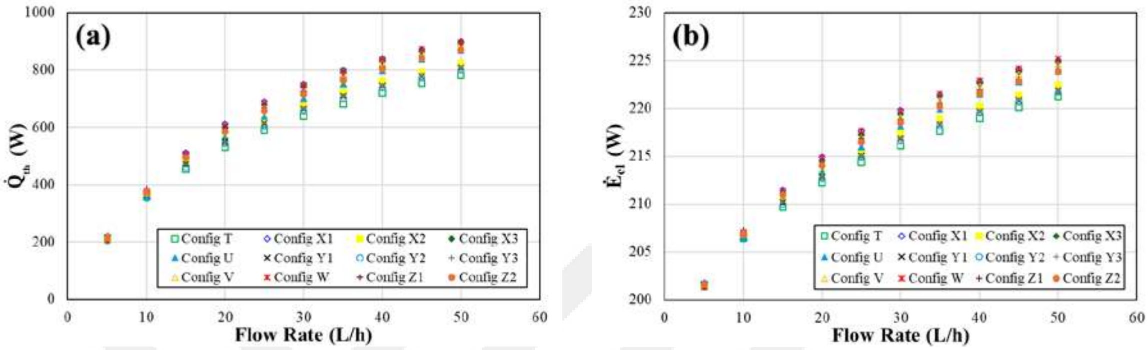

Figure 4.94. Variation of thermal energy production (a) and electrical power (b) of different spiral tube configurations under varying flow rate conditions

On the other hand, as the fluid flow rate increases, more heat is extracted from the PV cells, leading to a reduction in cell temperature. This improved thermal regulation enhances electrical efficiency and subsequently increases electricity production (Eq. 3.27). Similar to thermal performance, all spiral tube PVT configurations exhibit comparable electrical performance at low flow rates. However, as the flow rate increases, performance disparities become more evident, with certain configurations outperforming others.

Electrical efficiency (Figure 4.95b) and electricity generation (Figure 4.94b) were observed to increase by approximately 9% to 12% as the flow rate rose from its minimum to maximum value. The highest electrical efficiency and power output were recorded in Config X1 at a flow rate of 50 L/h, reaching 0.1447 and 225 W, respectively. The increase in electrical efficiency with increasing fluid flow rate was also supported by the findings of Fayaz et al. (2018), who reported a 0.05% rise in electrical efficiency for every 10 L/h increment in flow rate.

The variation of exergetic performance parameters with respect to fluid flow rate is illustrated in Figure 4.96. As the flow rate increases, thermal exergy (Figure 4.96a) increases for all spiral tube configurations up to approximately 25 L/h, after which it begins to decline. This trend reflects the balance between thermal energy and Carnot efficiency factor at higher flow rates (Eq. 3.43). Since electricity is a high-grade form of energy, electrical exergy (Figure 4.96b) is equivalent to the electrical energy produced and continues to increase with fluid flow rate. The total output exergy (Figure 4.96c), which is the sum of thermal and electrical exergy (Eq. 3.41), closely follows the trend of thermal exergy, given that the variations in electrical exergy among the configurations are relatively small. Because the exergy input to the system remains constant regardless of flow rate, exergy destruction (Figure 4.96d) follows an inverse trend to output exergy. Among all spiral tube configurations, Config X1, W and Z1 demonstrate the highest output exergy, while Config T exhibits the greatest exergy destruction.

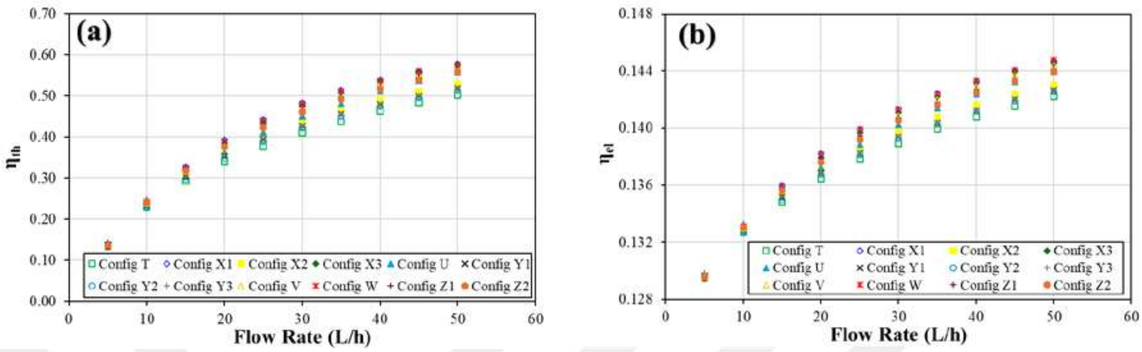

Figure 4.95. Effect of flow rate on the thermal (a) and electrical (b) efficiency of spiral tube PVT collectors

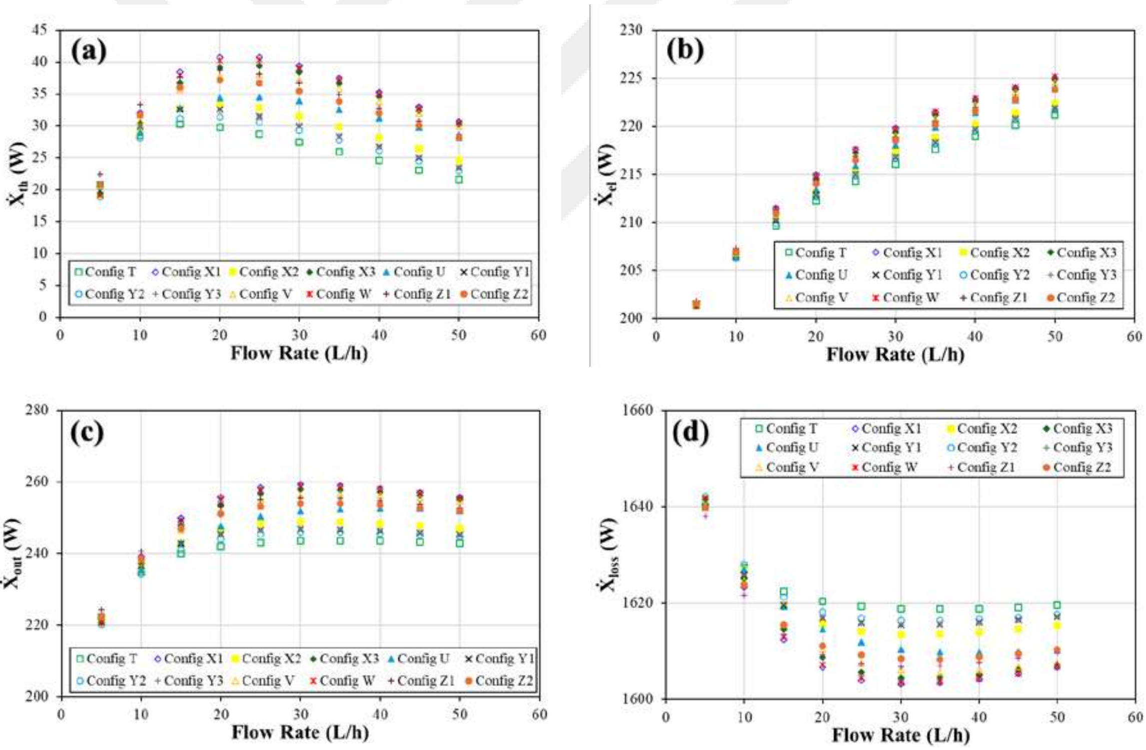

Figure 4.96. Effect of flow rate on the thermal (a), electrical (b) and output (c) exergy, and exergy destruction (d) of spiral tube PVT collectors

Figure 4.97 illustrates the variation of overall efficiency, primary energy saving efficiency and exergy efficiency key indicators derived from the thermal and electrical performance of spiral tube PVT collectors as a function of fluid flow rate. As flow rate increases, both thermal and electrical efficiencies improve, leading to a non-linear increase in overall (Figure 4.97a) and primary energy saving (Figure 4.97b) efficiencies. While the efficiencies of all spiral tube configurations remain relatively close at low flow rates, certain configurations begin to outperform others as the flow rate increases. At a flow rate of 50 L/h, Config X1 achieves the highest overall efficiency and primary energy saving efficiency, with values of 0.7234 and 0.9595, respectively.

In contrast, exergy efficiency defined as the ratio of total output exergy to input exergy (Eq. 3.45) follows the same trend as output exergy, since input exergy remains constant across all spiral tube configurations. The maximum exergy efficiency (Figure 4.97c) is observed in Config X1 at a flow rate of 30 L/h, with a value of 0.1392. Under the same conditions, this value is approximately 6.5% higher than that of Config T, which demonstrates the lowest exergy efficiency.

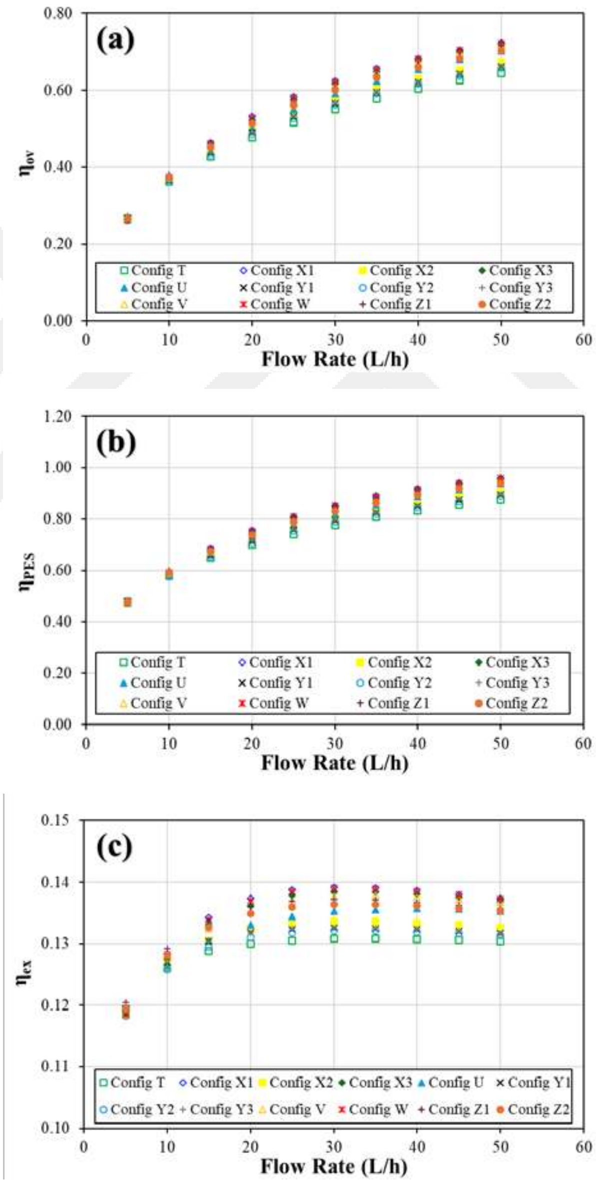

Figure 4.97. Effect of flow rate on the overall (a), primary energy saving (b) and exergy (c) efficiency of spiral tube PVT collectors

Figure 4.98 presents the variation of pressure drop and thermal energy produced per unit pressure drop (TEPD) with fluid flow rate for all spiral tube PVT collector configurations.

Consistent with the base-case conditions, single-inlet configurations exhibit higher pressure drops (Figure 4.98a) than double-inlet designs, and this disparity becomes more pronounced as the fluid flow rate increases. This is attributed to the increased fluid-wall interaction and rising hydraulic resistance at higher flow velocities. Moreover, an increase in fluid density amplifies pressure drop due to local losses. Among all spiral tube configurations, Config X1 and X2 demonstrate the lowest pressure drops across the examined flow rate range. Although thermal energy production increases with fluid flow rate, the rate of pressure drop increases more rapidly, resulting in a decreasing trend in TEPD (Figure 4.98b). The highest TEPD is recorded in Config X1 at 3.65 W/Pa, corresponding to the lowest flow rate of 5 L/h, where the pressure drop is minimal.

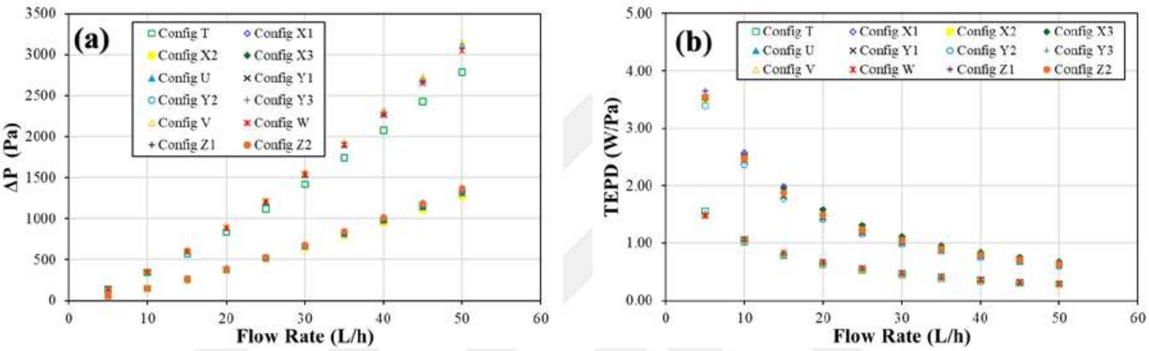

Figure 4.98. Effect of flow rate on the pressure drop (a) and TEPD (b) of spiral tube PVT collectors

4.3.3. Effect of Solar Irradiance on the Spiral Tube PVT Collectors

Solar irradiance, the primary source of photovoltaic electricity generation, is one of the most influential parameters affecting the performance of PVT collectors. In this section, the impact of solar irradiance on system performance is comprehensively investigated. The irradiance level is varied from 200 W/m^2 to 1200 W/m^2 in increments of 200 W/m^2, while other operating parameters are held constant, fluid flow rate at 20 L/h, fluid inlet temperature at 20 °C, ambient temperature at 25 °C, and wind velocity at 1 m/s, as specified under base-case conditions.

Given that solar irradiance directly influences the PV cell temperature and thus the thermal and electrical performance indicators, the absorber temperature distributions of the three best-performing Config W, X1 and Z1 are analyzed in detail (Figure 4.99). Additionally, the variation in PV cell temperatures and fluid outlet temperatures across all spiral tube configurations is examined as a function of solar irradiance. As clearly observed from the absorber temperature contour plots, an increase in solar irradiance leads to a rise in the absorber surface temperature of PVT collectors. While temperature distributions are relatively uniform under low irradiance conditions, noticeable temperature gradients begin to appear across different regions of the absorber surface when irradiance exceeds 800 W/m^2. For all three configurations, each 100 W/m^2 increase in solar irradiance corresponds to an average temperature rise of approximately 2.8 °C. At the lowest irradiance level, the maximum absorber temperatures are recorded as 25.47 °C for Config W, 25.60 °C for Config X1 and 25.89 °C for Config Z1. Under maximum irradiance conditions, these values rise significantly to 53.50 °C, 54.04 °C and 54.07 °C, respectively.

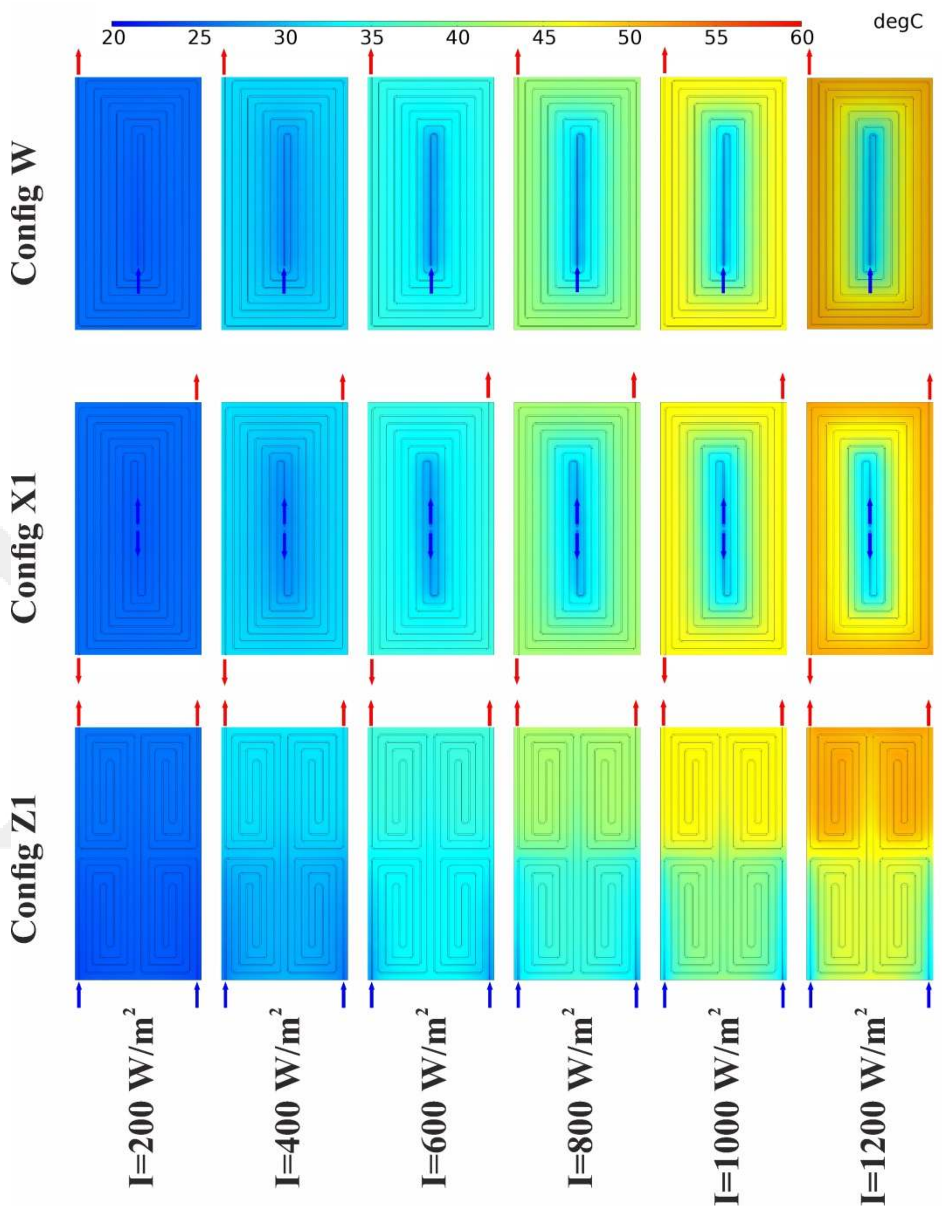

Figure 4.99. PVT absorber temperature distribution of Config W (a), Config X1 (b) and Config Z1 (c) for different solar irradiances

It is evident that both the average PV cell temperatures and fluid outlet temperatures of PVT collectors and conventional PV panels exhibit a pronounced increasing trend with rising solar irradiance (Figure 4.100). At a solar irradiance level of 200 W/m^2, the cell (Figure 4.100a) and outlet (Figure 4.100b) temperatures of all spiral tube PVT collectors are nearly identical, and the temperature difference between PVT collectors and the conventional PV panel is approximately 4 °C. However, as solar irradiance reaches its maximum value of 1200 W/m^2, this temperature difference expands significantly, ranging from 19 °C to 22 °C. Similarly, fluid outlet temperatures increase with solar irradiance. While outlet temperatures are around 25 °C at 200 W/m^2, they rise to between 47 °C and 51.66 °C across different PVT configurations at 1200 W/m^2. The effect of solar radiation on PVT cell temperature in a spiral tube configuration was also studied by Kazem et al. (2020). Consistent with the current study, they found that higher levels of solar radiation led to increased cell temperatures. Specifically, when solar irradiance increased from 200 W/m^2 to 1000 W/m^2, the cell temperature rose from 28.1 °C to 40.9 °C.

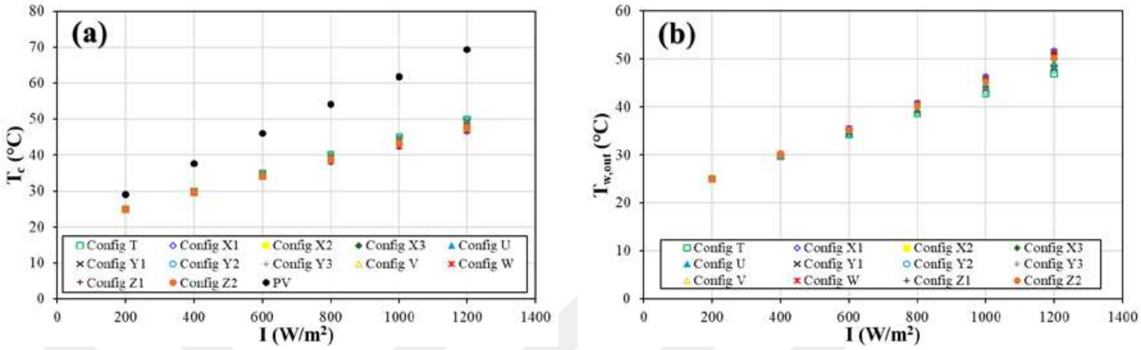

Figure 4.100. Variation of average PV cell (a) and water outlet (b) temperature of different spiral tube configurations under varying solar irradiance conditions

An increase in solar irradiance leads to a higher thermal energy output due to the greater amount of absorbed solar energy. At low irradiance levels, both thermal and electrical energy outputs are similar across all spiral tube PVT configurations (Figure 4.101). However, as solar irradiance intensifies, the performance gap between configurations widens for both parameters. Config X1, which demonstrated the best thermal performance, produced 115 W of thermal energy at 200 W/m^2, increasing to 734 W at 1200 W/m^2 representing a 17.6% advantage over the lowest-performing configuration under the same conditions (Figure 4.101a). Regarding electrical energy generation (Figure 4.101b), although higher solar irradiance leads to increased PV cell temperatures thereby reducing cell efficiency (Eq. 3.27), the overall electricity production increases due to the larger energy input from solar irradiance. At peak solar irradiance, spiral tube PVT collectors generated approximately 13% more electrical energy than the conventional PV panel, despite elevated cell temperatures.

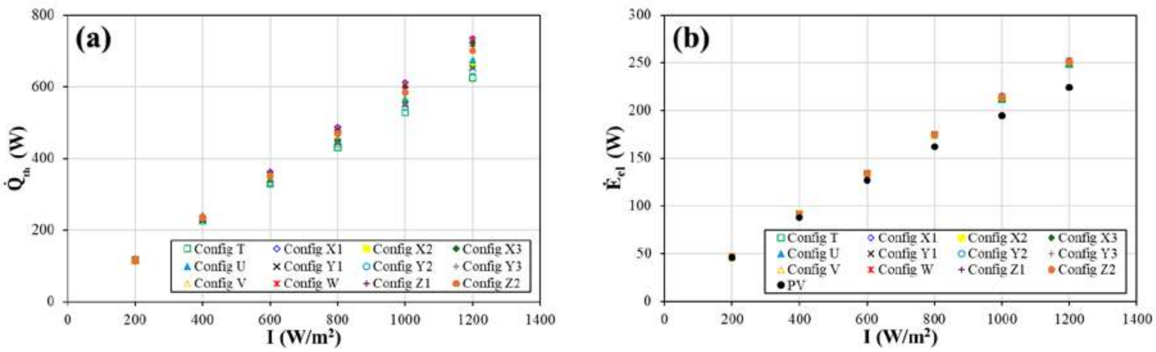

Figure 4.101. Variation of thermal energy production (a) and electrical power (b) of different spiral tube configurations under varying solar irradiance conditions

Although both thermal and electrical energy outputs increase with rising solar irradiance, the higher irradiance also elevates the surface and cell temperatures of the PVT collectors, which in turn leads to increased heat losses. As a result, thermal efficiency (Figure 4.102a) declines by approximately 1% to 9% in configurations with elevated surface temperatures, whereas it increases by 1% to 6% in configurations.

Conversely, electrical efficiency (Figure 4.102b) consistently decreases with increasing solar irradiance due to the rise in PV cell temperature (Eq. 3.27). At 200 W/m^2, all spiral tube PVT collectors exhibit similar electrical efficiency, outperforming the conventional PV panel by approximately 1.9%. As irradiance increases, PVT collectors show a significantly greater advantage, with electrical efficiency improvements ranging from 12.6% to 15% compared to the conventional PV panel.

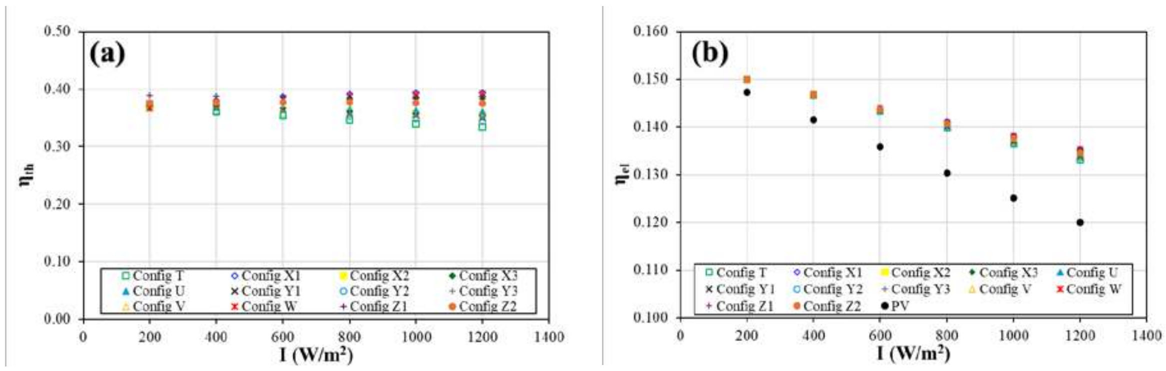

Figure 4.102. Effect of solar irradiance on the thermal (a) and electrical (b) efficiency of spiral tube PVT collectors

Figure 4.103 illustrates the variation in thermal exergy, electrical exergy, total output exergy and exergy destruction of all spiral tube PVT collectors as a function of solar irradiance. Among these parameters, thermal exergy (Figure 4.103a) is directly influenced by fluid outlet temperature and therefore follows the same trend. While thermal exergy values are similar across spiral tube configurations at low irradiance levels, significant divergence is observed beyond

800 W/m^2. At the maximum irradiance of 1200 W/m^2, Config X1 achieves the highest thermal energy, reaching 60.25 W.

Since electrical exergy (Figure 4.103b) is equivalent to the electrical energy output, and electrical performance among configurations remains relatively close, the overall exergy output being the sum of thermal and electrical exergy (Eq. 3.41) exhibits a trend largely dictated by thermal exergy. At peak solar irradiance, the output exergy of the best-performing Config X1 is approximately 5.5% higher than that of the lowest-performing Config T (Figure 4.103c).

Although exergy destruction (Figure 4.103d) generally shows an inverse relationship with output exergy under most operating conditions, in this case it also increases with solar irradiance. This is due to a significant rise in exergy input at higher irradiance levels, which offsets the improvements in exergy output.

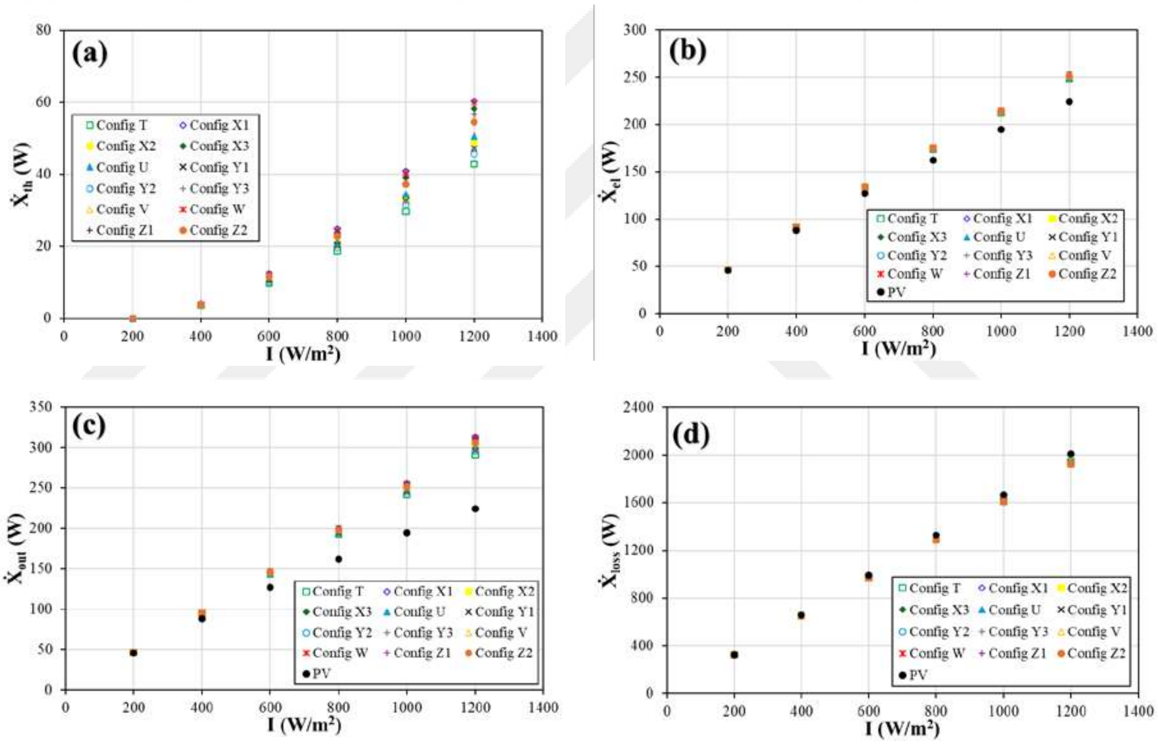

Figure 4.103. Effect of solar irradiance on the thermal (a), electrical (b) and output (c) exergy, and exergy destruction (d) of spiral tube PVT collectors

Figure 4.104 illustrates the variation of overall efficiency, primary energy saving efficiency and exergy efficiency with solar irradiance for spiral tube PVT collectors. As electrical efficiency tends to decline with increasing irradiance, and thermal efficiency exhibits configuration-dependent behavior, the overall efficiency demonstrates configuration-dependent trend. Among all spiral tube designs, Config T shows the highest decline in overall efficiency (Figure 4.104a) as solar irradiance increases. In contrast, Config X1 achieves the highest overall efficiency, reaching 0.5319 at 800 W/m^2.

Primary energy saving efficiency, which places greater weight on electrical performance, is more sensitive to reductions in electrical efficiency. As a result, it declines across all spiral tube configurations with increasing solar irradiance. When irradiance increases from 200 W/m^2 to 1200 W/m^2, primary energy saving efficiency (Figure 4.104b) decreases by approximately 1.7% to 10.5%, depending on the configuration.

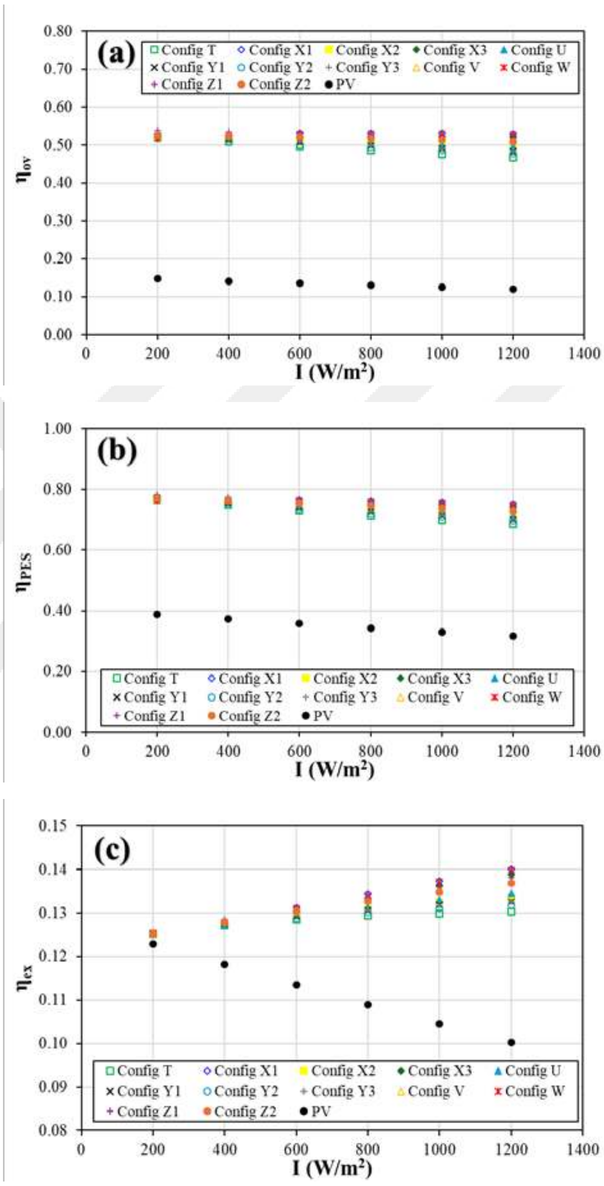

Figure 4.104. Effect of solar irradiance on the overall (a), primary energy saving (b) and exergy (c) efficiency of spiral tube PVT collectors

Exergy efficiency, which reflects the combined effect of thermal and electrical exergy outputs, exhibits an increasing trend with solar irradiance. This is primarily due to the rise in output exergy driven by elevated thermal and electrical exergies. While differences between configurations are minimal at low irradiance levels, they become more pronounced at higher irradiance levels. The highest exergy efficiency (Figure 4.104c) is recorded in Config X1 with a value of 0.1401 at 1200 W/m^2, which is approximately 7.5% higher than that of the lowest-performing configuration under the same conditions.

Figure 4.105 illustrates the variation of pressure drop and thermal energy produced per unit pressure drop (TEPD) with solar irradiance for various spiral tube PVT collector configurations. As solar irradiance increases, the fluid outlet temperature rises, resulting in decreased fluid viscosity and density. Consequently, hydraulic resistance is reduced and pressure drop decreases accordingly. When solar irradiance increases from its minimum to maximum value, the pressure drops of the spiral tube PVT collectors are reduced by approximately 27% to 32% (Figure 4.105a). In parallel, thermal energy production increases due to the higher thermal input, and when combined with the declining pressure drop, TEPD exhibits a rising trend.

At low irradiance levels, both single and double-inlet designs produce similar TEPD values. However, as solar irradiance intensifies, double-inlet configurations begin to outperform their single-inlet counterparts more noticeably. The highest TEPD is observed in configuration X1, reaching 2.01 W/Pa at the maximum irradiance of 1200 W/m^2 (Figure 4.105b).

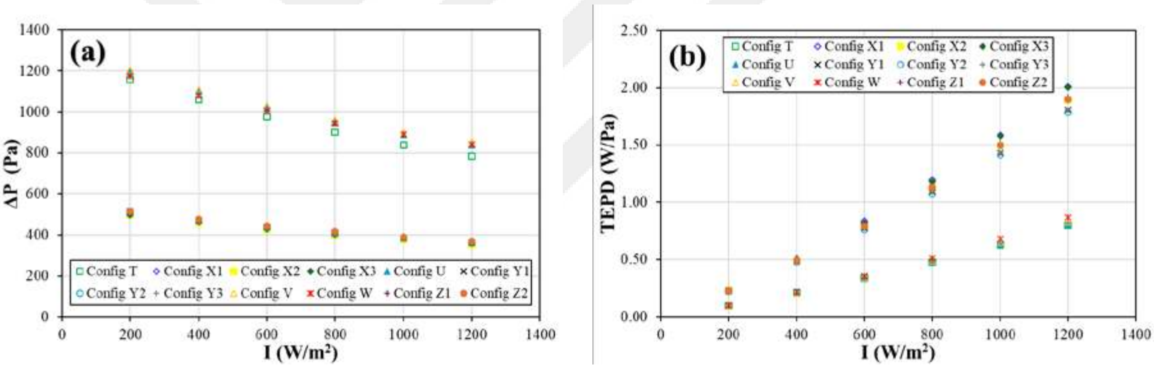

Figure 4.105. Effect of solar irradiance on the pressure drop (a) and TEPD (b) of spiral tube PVT collectors

4.3.4. Effect of Fluid Inlet Temperature on the Spiral Tube PVT Collector Configurations

The inlet temperature of the working fluid is one of the most influential factors affecting the performance of PVT collectors. In this analysis, water was selected as the heat transfer medium, and its inlet temperature was systematically varied between 10 °C and 40 °C in 5 °C intervals to assess its impact on system performance. Throughout the study, all other operating conditions including solar irradiance, flow rate, ambient temperature and wind velocity were maintained constant as defined by the base-case conditions (Table 3.3).

Figure 4.106 depicts how the absorber surface temperature distribution varies with changing fluid inlet temperatures for the top three performing, Config W, X1 and Z1 configurations under base-case conditions. Additionally, Figure 4.107 compares the average PV cell surface temperatures and fluid outlet temperatures across all spiral tube PVT collectors subjected to the same inlet temperature variations. The results indicate that lower fluid inlet temperatures enhance the cooling effectiveness of the PV panel, resulting in lower surface temperatures. Conversely, as the inlet temperature increases, the overall panel temperature also rises. Notably, regions closer to the fluid entry section remain cooler, particularly along the lower sections of the absorber.

As evidenced by the temperature contour plots, an increase in water inlet temperature leads to a corresponding rise in the absorber temperature of PVT collectors. While temperature distributions remain relatively uniform at lower inlet temperatures, noticeable temperature gradients begin to emerge across the absorber surface when the inlet temperature exceeds 30 °C.

At the lowest inlet temperature, the maximum absorber temperatures are recorded as 44.68 °C for Config W, 45.17 °C for Config X1 and 45.10 °C for Config Z1. Under the highest inlet temperature condition (40 °C), these values increase to 54.25 °C, 54.85 °C and 55.66 °C, respectively.

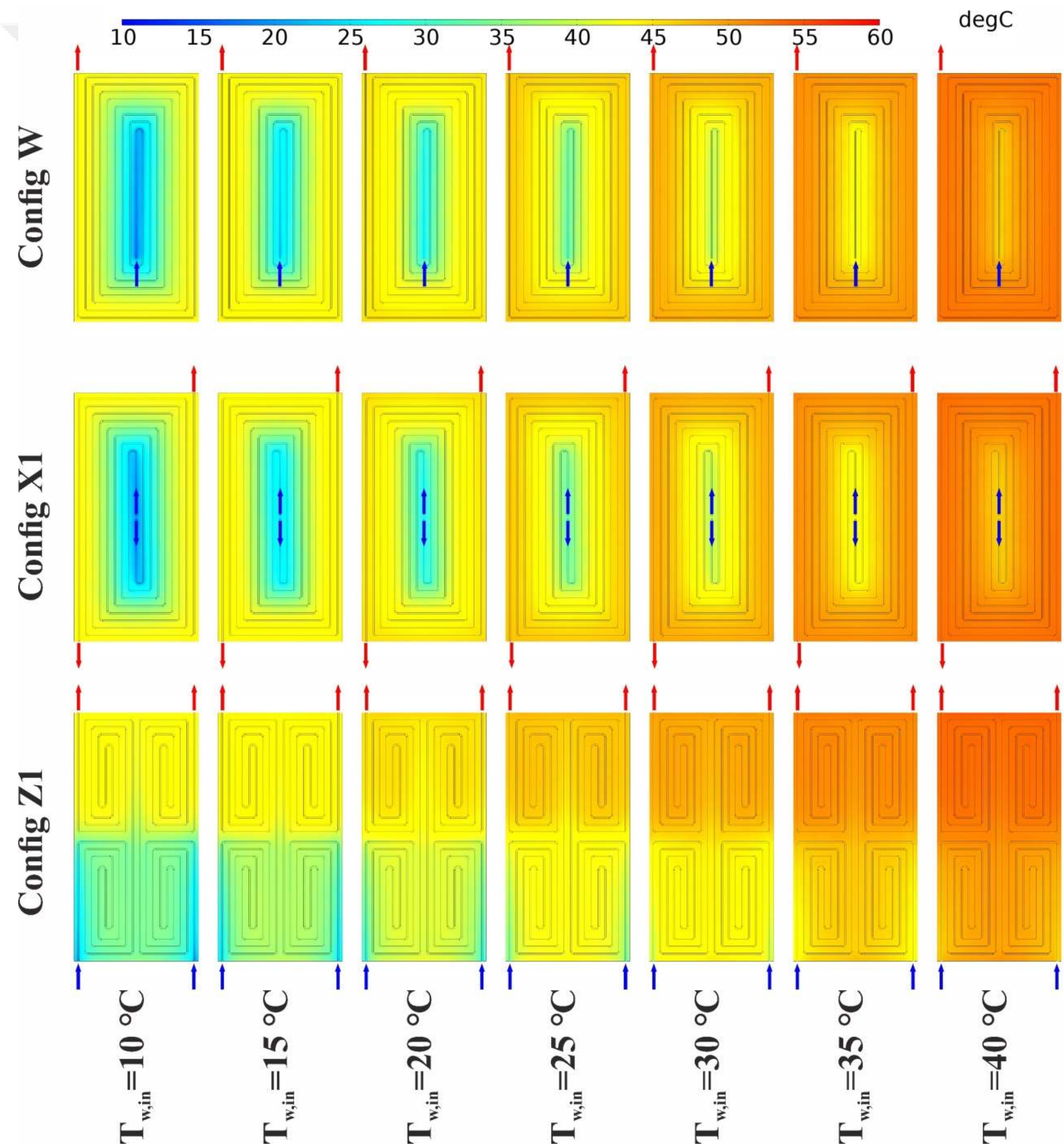

Figure 4.106. PVT absorber temperature distribution of Config W (a), Config X1 (b) and Config Z1 (c) for different water inlet temperatures

At lower fluid inlet temperatures, the performance differences among spiral tube PVT collector designs become more distinct for PVT cell temperature. However, as the inlet temperature rises, the temperature between the PV cell and the coolant decreases, resulting in reduced heat transfer efficiency. Consequently, average PV cell temperatures (Figure 4.107a) increase and the thermal performance of the different configurations converges. For instance, at an inlet temperature of 10 °C, cell temperatures range between 37.45 °C and 41.19 °C across spiral tube configurations. When the inlet temperature reaches its maximum, cell temperatures rise to approximately 52.28 °C to 52.79 °C. The fluid outlet temperature (Figure 4.107b) increases in parallel with the rise in inlet temperature. However, unlike the PV cell temperature, the variation in outlet temperatures among different spiral tube configurations is more pronounced at lower inlet temperatures, gradually diminishing as the inlet temperature increases. At the lowest fluid inlet temperature, the outlet temperatures of the PVT collectors range from 37.83 °C to 42.73 °C, depending on the configuration. When the inlet temperature reaches its maximum, the outlet temperature rises accordingly and converges around 53 °C across all spiral tube configurations.

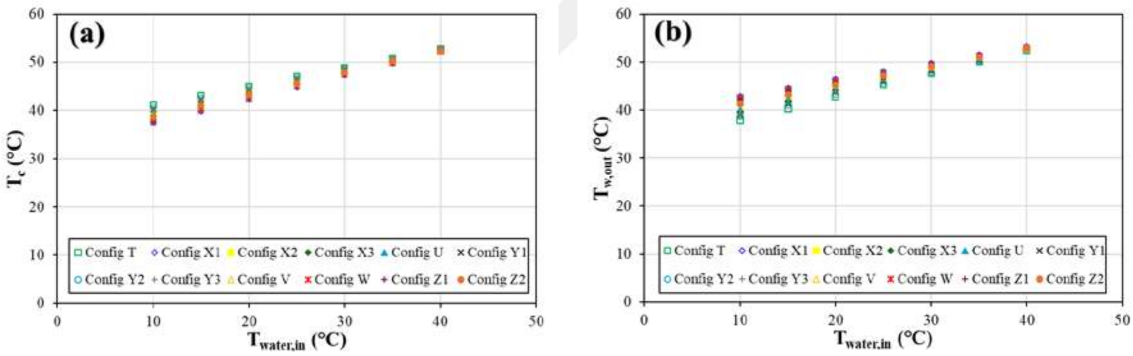

Figure 4.107. Variation of average PV cell (a) and water outlet (b) temperature of different spiral tube configurations under varying water inlet temperature conditions

Although increasing the inlet temperature raises the fluid outlet temperature, it also elevates the absorber and cell temperature, which in turn increases the heat losses to the surroundings. As a result, thermal energy production decreases despite the higher outlet temperature (Figure 4.108a). The highest thermal energy output is observed in Config X1, reaching 762 W at an inlet temperature of 10 °C. A similar trend is observed in electrical energy production; however, the change in electrical output (Figure 4.108b) is notably smaller compared to thermal energy.

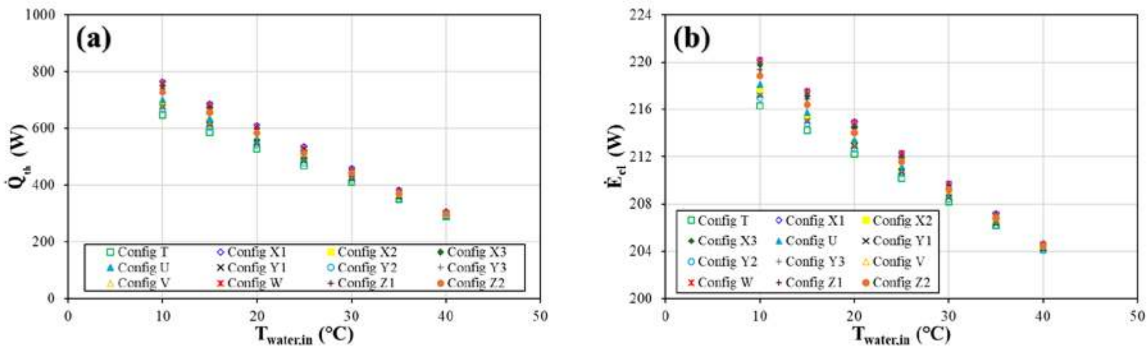

Figure 4.108. Variation of thermal energy production (a) and electrical power (b) of different spiral tube configurations under varying water inlet temperature conditions

Figures 4.109 compares the thermal and electrical performance metrics of spiral tube PVT collectors as a function of fluid inlet temperature. Both performance indicators exhibit similar trends, while the collectors respond differently at lower inlet temperatures, the differences among the spiral tube PVT collectors become less distinguishable as the inlet temperature increases.

In particular, thermal efficiency (Figure 4.109a) decreases with increasing inlet temperature since the increasing heat losses. The highest thermal efficiency was recorded for Config X1, reaching 0.4903 at an inlet temperature of 10 °C, which corresponds to an improvement of approximately 18% compared to the lowest-performing configuration.

A similar trend is observed for electrical performance. As the temperature differences between the PV cell and the working fluid decreases with higher inlet temperatures, the rate of heat transfer diminishes. Consequently, the PV cell temperature rises, resulting in a decline in electrical efficiency (Figure 4.109b). When the inlet temperature increased from its minimum to maximum value, the electrical efficiency of all spiral tube PVT collectors dropped by approximately 5.9% to 7.1%. The highest electrical efficiency, 0.1416, was again achieved by Config X1 at an inlet temperature of 10 °C.

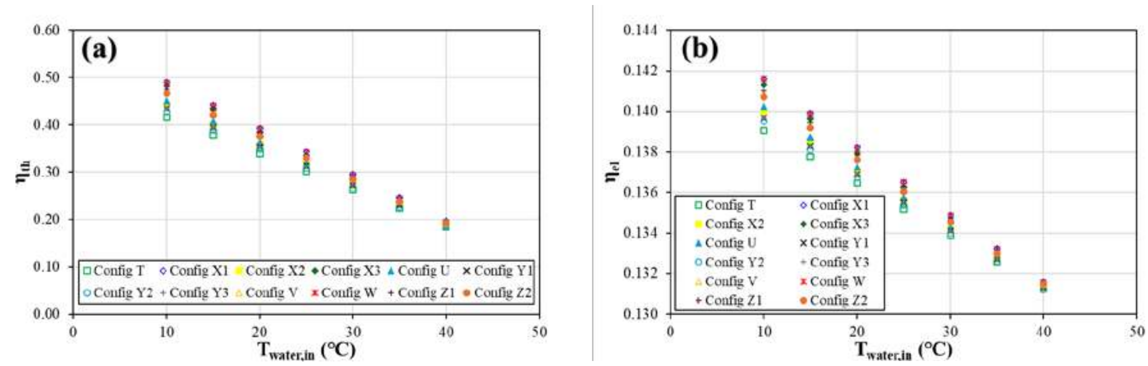

Figure 4.109. Effect of water inlet temperature on the thermal (a) and electrical (b) efficiency of spiral tube PVT collectors

The influence of water inlet temperature on exergy performance parameters is illustrated in Figure 4.110. Thermal exergy depends on both the outlet temperature and the temperature differential between the inlet and outlet (Eq. 3.43). Although the outlet temperature increases with rising inlet temperatures, the narrowing temperature difference leads to a decline in thermal exergy (Figure 4.100a) for all spiral tube configurations except in some cases where the outlet temperature increases sharply.

Electrical exergy, being directly proportional to electrical efficiency, follows the same trend observed in Figure 4.109b. As the inlet temperature rises, variations in electrical exergy among different configurations become less pronounced. As a result, the total exergy output (Figure 4.100c) decreases due to the combined reduction in both thermal and electrical exergy contributions. In contrast, exergy destruction (Figure 4.100d) exhibits an inverse relationship with output exergy. Among all configurations, Config X1 yields the highest total exergy output, while Config T shows the highest level of exergy destruction.

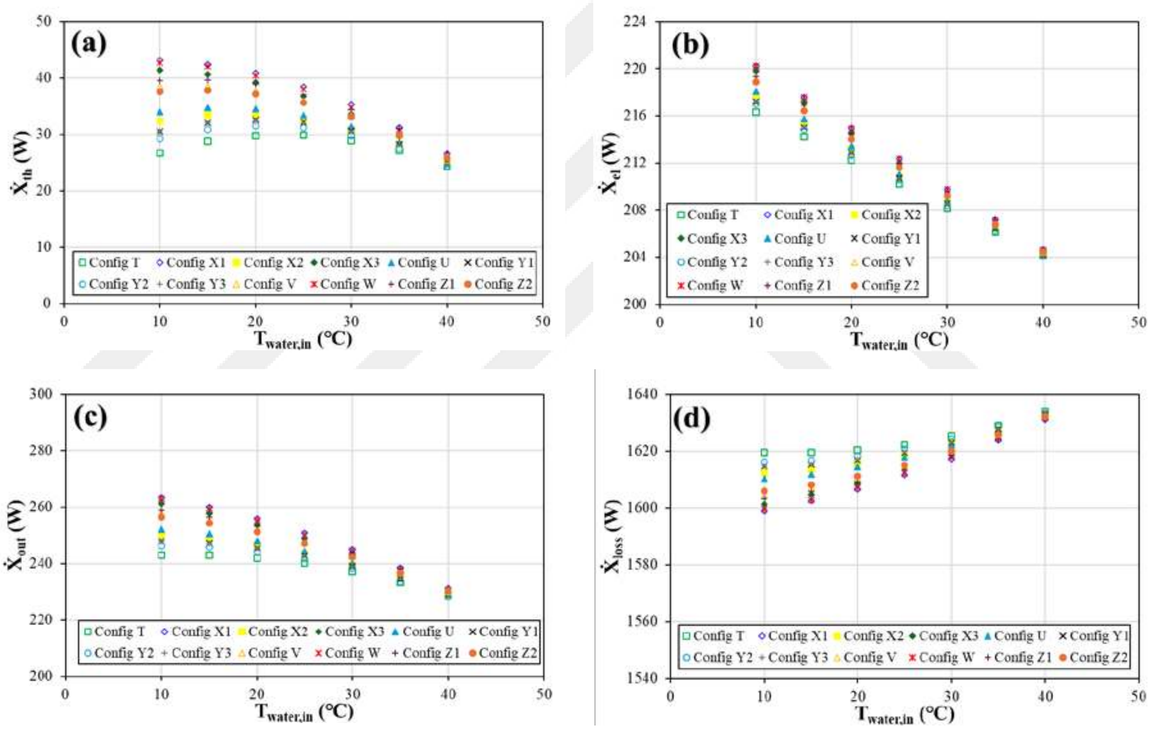

Figure 4.110. Effect of water inlet temperature on the thermal (a), electrical (b) and output (c) exergy, and exergy destruction (d) of spiral tube PVT collectors

Figure 4.111 compares the variation of overall, primary energy saving and exergy efficiencies which are the final performance indicators derived from thermal and electrical metrics with respect to fluid inlet temperature for different spiral tube PVT collector configurations.

Both overall (Figure 4.111a) and primary energy saving (Figure 4.111b) efficiencies exhibit a declining trend as the inlet temperature increases, primarily due to the simultaneous decrease in thermal and electrical efficiencies. The highest values for these metrics were observed in Config X1 at an inlet temperature of 10 °C, with overall and primary energy saving efficiencies recorded as 0.6319 and 0.8629, respectively. For this configuration, increasing the inlet temperature to 40 °C resulted in a 48% reduction in overall efficiency and a 37% reduction in primary energy saving efficiency.

Since exergy input remains constant across all inlet temperature levels, exergy efficiency is directly influenced by the variation in exergy output (Eq. 3.45). As shown in Figure 4.111c, its trend closely follows that of the output exergy depicted in Figure 4.110c. The highest exergy efficiency, 0.1414, was again recorded in Config X1 at a fluid inlet temperature of 10 °C.

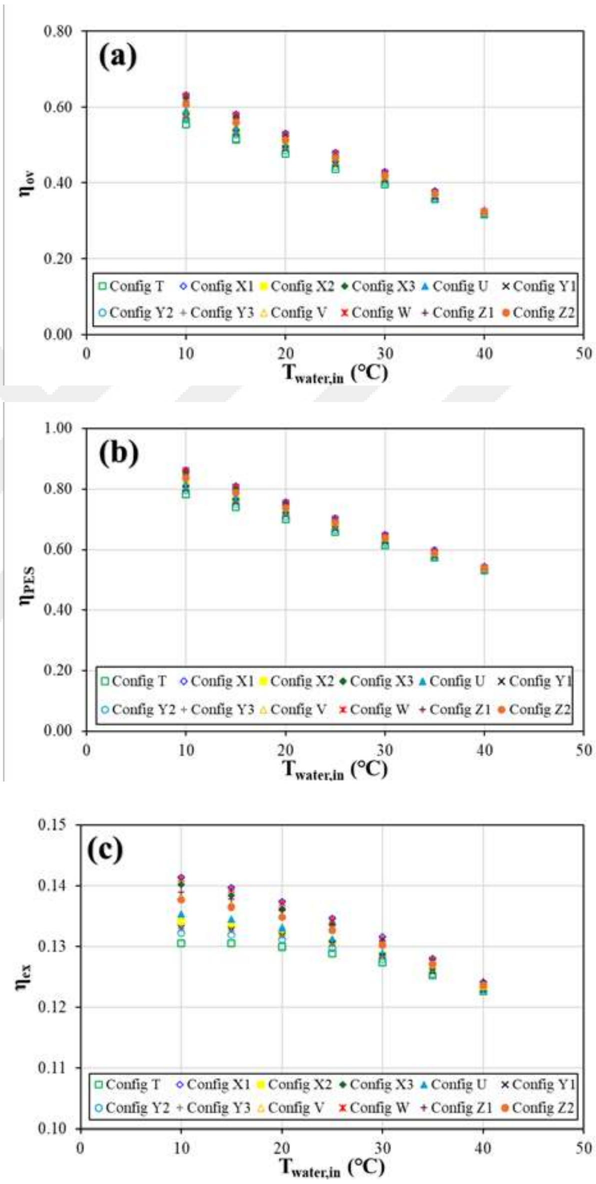

Figure 4.111. Effect of water inlet temperature on the overall (a), primary energy saving (b) and exergy (c) efficiency of spiral tube PVT collectors

As illustrated in Figure 4.112a, the pressure drop decreases with increasing fluid inlet temperature. This trend is primarily attributed to the reduction in water viscosity and density at elevated temperatures, which leads to lower internal frictional losses and local losses. Across all spiral tube PVT collector configurations, increasing the inlet temperature from its minimum to maximum value results in a pressure drop reduction of approximately 16% to 22%.

However, when the thermal energy produced per unit pressure drop (TEPD) is evaluated as a function of fluid inlet temperature, a declining trend is also observed (Figure 4.112b). Although pressure drop decreases with increasing inlet temperature, the corresponding decrease in thermal energy output is proportionally greater. Consequently, TEPD exhibits a net decline with rising inlet temperature. The highest TEPD value is observed in Config X1 at an inlet temperature of 10 °C, reaching 1.81 W/Pa.

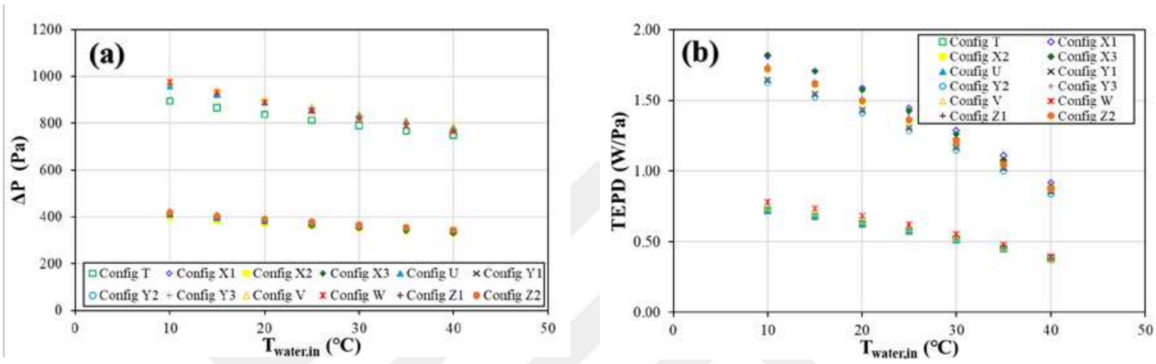

Figure 4.112. Effect of water inlet temperature on the pressure drop (a) and TEPD (b) of spiral tube PVT collectors

4.3.5. Effect of Ambient Temperature on the Spiral Tube PVT Collector Configurations

Ambient temperature is another critical parameter that substantially affects the performance of PVT collectors. In this chapter, its influence on both energy and exergy performance metrics is investigated for spiral tube PVT collectors. The ambient temperature was varied from 15 °C to 40 °C in 5 °C increments, while other operating parameters such as solar irradiance (1000 W/m^2), fluid flow rate (20 L/h), fluid inlet temperature (20 °C), and wind velocity (1 m/s) were kept constant in accordance with the base-case conditions.

Figure 4.113 illustrates the variation in absorber temperature distributions for the three best-performing spiral tube configurations (W, X1 and Z1), all of which exhibited closely aligned results throughout the tested ambient temperature range. In contrast, Figure 4.114 presents the changes in average PV cell surface temperatures and fluid outlet temperatures for all spiral tube PVT configurations as a function of ambient temperature.

The contour plots indicate that a rise in ambient temperature leads to a corresponding increase in the absorber temperature of PVT collectors. At lower ambient conditions, temperature distribution remains relatively uniform, and absorber temperatures are lower. However, once the ambient temperature exceeds 30 °C, distinct temperature gradients begin to develop across the absorber. At the lowest ambient temperature, the maximum absorber temperatures are recorded as 41.21 °C for Config W, 41.61 °C for Config X1, and 41.95 °C for Config Z1. These values increase significantly at the highest ambient temperature, reaching 58.74 °C, 59.32 °C, and 59.18 °C, respectively.

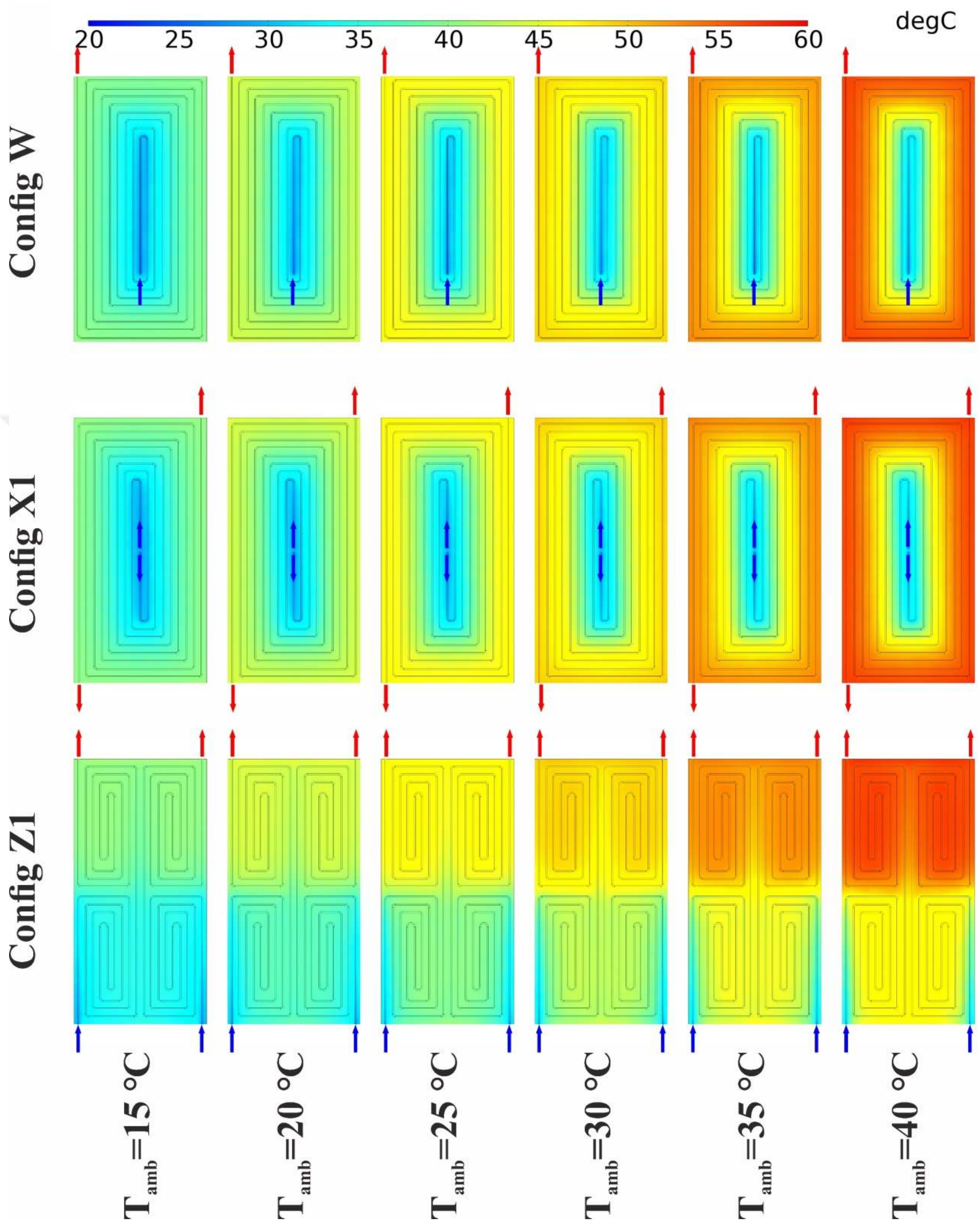

Figure 4.113. PVT absorber temperature distribution of Config W (a), Config X1 (b) and Config Z1 (c) for different ambient temperatures

Figure 4.114a illustrates the variation in average PV cell temperatures of the spiral tube PVT collectors and the average surface temperature of a conventional PV panel as a function of ambient temperature. At an ambient temperature of 15 °C, the PV cell temperatures of the PVT collectors range between 37.46 °C and 39.09 °C, while the surface temperature of the conventional

PV panel is significantly higher, recorded at 52.55 °C. As ambient temperature increases, both systems show a corresponding rise in surface temperature. However, the uncooled PV panel exhibits a much steeper increase, reaching 24 °C above its initial value, whereas the PVT collectors show a more moderate rise of approximately 13 to 15.6 °C, depending on the configuration.

As the ambient temperature increases, convective heat losses to the environment decrease, enabling more thermal energy to be transferred from the PV cells to the working fluid. This results in higher outlet fluid temperatures. At the lowest ambient temperature (15 °C), outlet temperatures (Figure 4.114b) range between 37.33 °C and 39.96 °C. When the ambient temperature reaches 40 °C, outlet fluid temperatures increase by approximately 13.07 to 16.69 °C, depending on the configuration. The highest outlet temperature is observed in Config X1, reaching 56.64 °C, while the lowest, 50.83 °C, is recorded in Config T at the maximum ambient temperature.

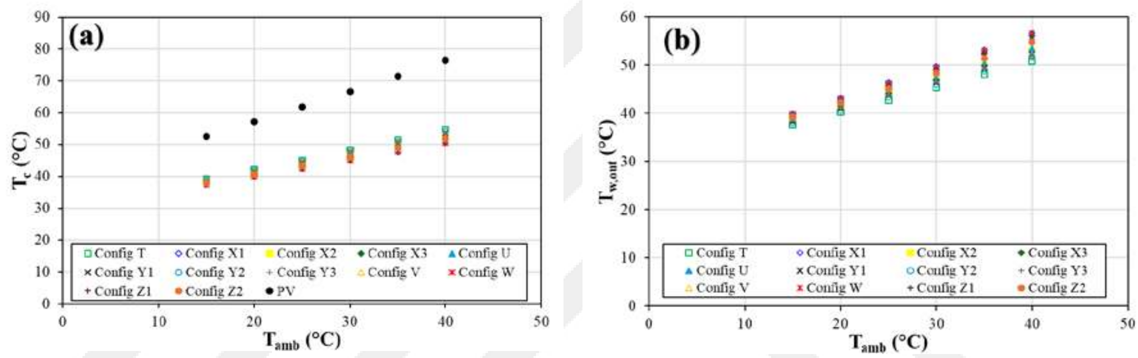

Figure 4.114. Variation of average PV cell (a) and water outlet (b) temperature of different spiral tube configurations under varying ambient temperature conditions

Figure 4.115 compares the variation in thermal and electrical energy production of spiral tube PVT collectors with respect to ambient temperature. As ambient temperature increases, heat losses to the environment are reduced, resulting in higher thermal energy production (Figure 4.115a) across all spiral tube PVT collectors.

In contrast, as ambient temperature rises, PV cell temperatures also increase, leading to a decrease in electrical efficiency and consequently a reduction in electrical energy output (Figure 4.115b). The highest thermal energy production was observed in Config X1, reaching 850 W at the maximum ambient temperature of 40 °C, which represents an improvement of approximately 19% over Config T under the same conditions.

Likewise, Config X1 consistently delivered the best electrical performance across all ambient temperature levels. Compared to a conventional PV panel, it produced approximately 8% more electricity at the lowest ambient temperature, with this margin increasing to around 15% at the highest ambient temperature.

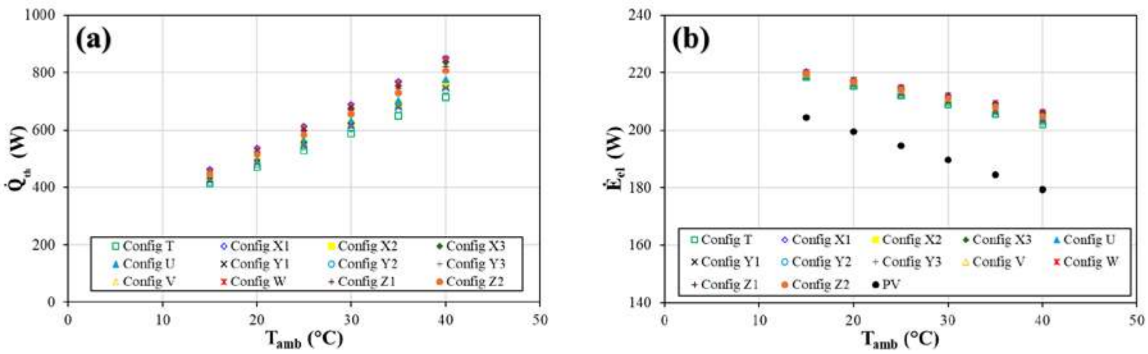

Figure 4.115. Variation of thermal energy production (a) and electrical power (b) of different spiral tube configurations under varying ambient temperature conditions

The thermal and electrical efficiencies which are the key indicators of energy performance for spiral tube PVT collectors exhibited opposing trends with increasing ambient temperature. Thermal efficiency (Figure 4.116a) showed a significant upward trend, reaching its peak value of 0.5464 in Config X1 at the highest ambient temperature of 40 °C. Under the same conditions, the lowest thermal efficiency among spiral tube configurations was observed in Config T, with 0.4597.

In contrast, electrical efficiency (Figure 4.116b) declined with increasing ambient temperature, although the decrease was less pronounced than the corresponding increase in thermal efficiency. When comparing spiral tube PVT collectors with a conventional PV panel, PVT collectors demonstrated 6.92% to 7.76% higher electrical efficiency at the lowest ambient temperature. This performance gap widened further at higher ambient temperatures, reaching 12.66% to 15.18% at 40 °C, depending on the configuration.

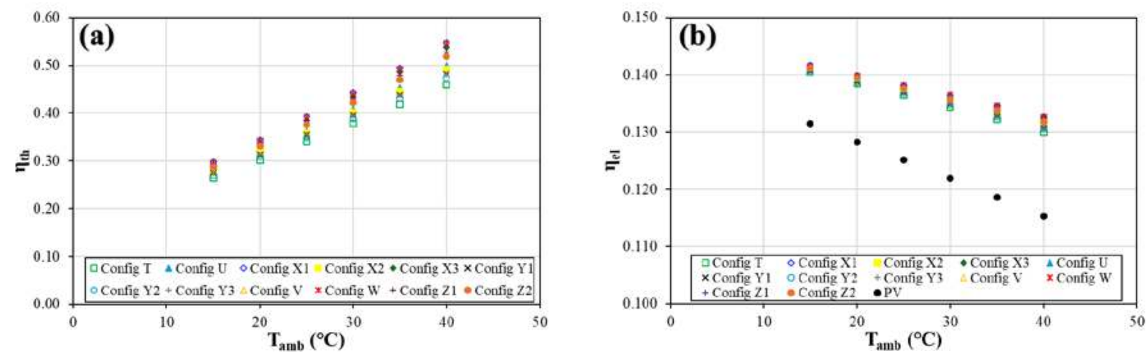

Figure 4.116. Effect of ambient temperature on the thermal (a) and electrical (b) efficiency of spiral tube PVT collectors

The impact of ambient temperature on the exergetic performance parameters namely thermal exergy, electrical exergy, output exergy and exergy destruction is presented in Figure 4.117. Changes in ambient temperature lead to an increase in thermal exergy (Figure 4.117a) for some configurations, while a decline is observed in others due to variations in thermal energy production and Carnot efficiency factor (Eq. 3.43).

Electrical exergy follows the same trend as electrical energy output, showing a consistent decrease with rising ambient temperature (Figure 4.117b). However, the variation in thermal exergy is generally more pronounced than that of electrical exergy. As a result, the behavior of output exergy, which is the sum of thermal and electrical exergy (Eq. 3.41), remains relatively stable for most configurations, although a slight decrease is observed in some cases (Figure 4.117c). Among all spiral tube configurations, Config X1 demonstrates the highest performance across all exergy parameters except exergy destruction (Figure 4.117d), whereas Config T exhibits the highest level of exergy destruction, indicating the least efficient design in terms of exergy utilization.

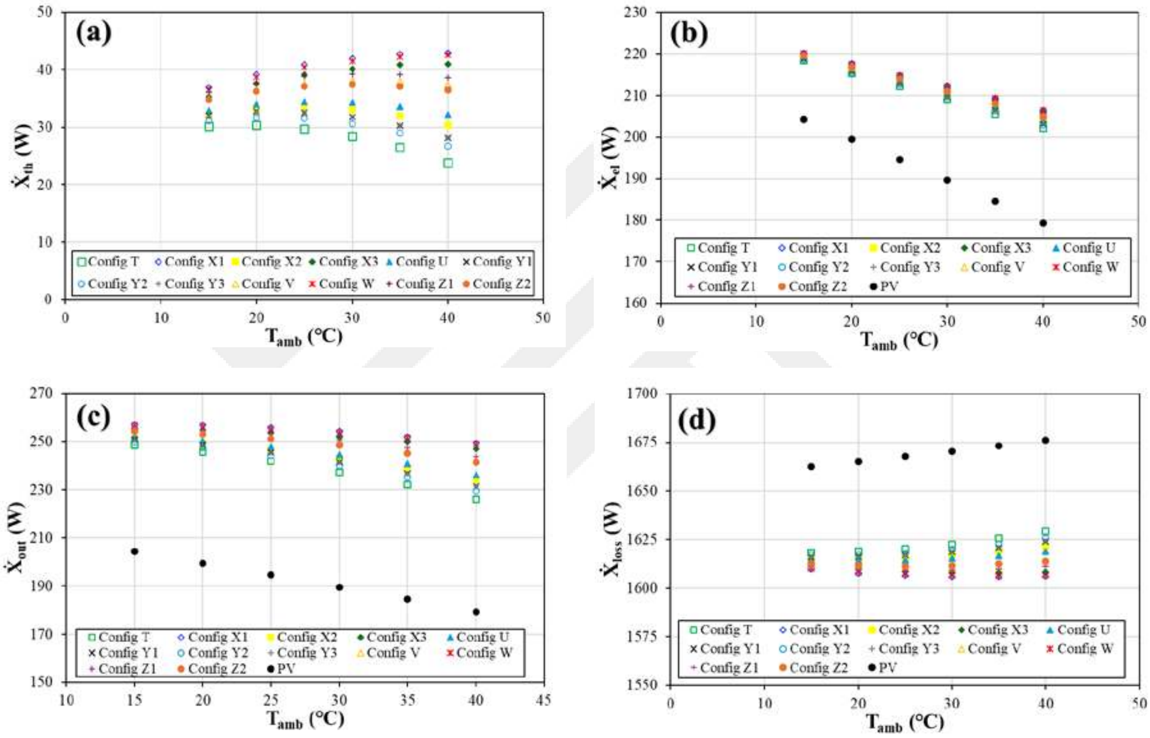

Figure 4.117. Effect of ambient temperature on the thermal (a), electrical (b) and output (c) exergy, and exergy destruction (d) of spiral tube PVT collectors

Figure 4.118 compares the variation in overall efficiency and primary energy saving efficiency both of which are derived from thermal and electrical efficiencies for all spiral tube PVT collectors as a function of ambient temperature. While electrical efficiency exhibits a slight decline with increasing ambient temperature, the substantial increase in thermal efficiency leads to a net improvement in both overall and primary energy saving efficiencies.

At the lowest ambient temperature, overall efficiency (Figure 4.118a) ranges between 0.4053 and 0.4392 across different spiral tube PVT configurations, whereas at the highest ambient temperature, it increases to between 0.5897 and 0.6792. In all cases, Config X1 demonstrates the most effective performance, while Config T consistently ranks lowest across all performance metrics.

A similar trend is observed in primary energy saving efficiency (Figure 4.118b). At 15 °C, values range between 0.6345 and 0.6702, whereas at 40 °C, this range increases to 0.8017-0.8958, depending on the configuration.

Exergy efficiency exhibits a gradual decline as ambient temperature rises, attributed to a slight drop in both exergy input and output, which together contribute to the overall reduction (Figure 4.118c). Nevertheless, the reduction in exergy efficiency is significantly less for PVT collectors than for a conventional PV panel. The highest exergy efficiency, 0.1377, was recorded for Config X1 at an ambient temperature of 15 °C. As ambient temperature rises from minimum to maximum, exergy efficiency in this configuration decreases by only 2.41%, whereas the conventional PV panel experiences a much steeper decline of approximately 11.68%.

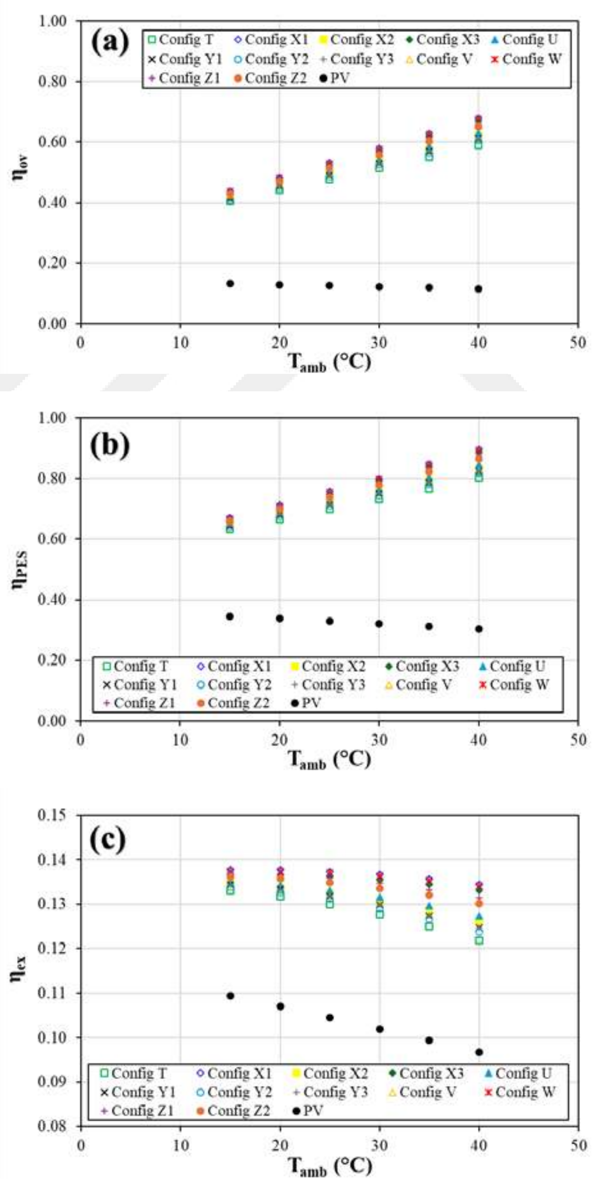

Figure 4.118. Effect of ambient temperature on the overall (a), primary energy saving (b) and exergy (c) efficiency of spiral tube PVT collectors

The effect of ambient temperature on pressure drop and thermal energy produced per unit pressure drop (TEPD) is illustrated in Figure 4.119. As shown in Figure 4.114b, the increase in ambient temperature leads to a rise in fluid outlet temperature, which in turn reduces fluid viscosity and density. This reduction in these fluid properties lowers internal fluid friction and local losses, thereby decreasing the overall pressure drop (Figure 4.119a). At the maximum ambient temperature, the lowest pressure drops are observed across all spiral tube PVT collectors. Specifically, at 40 °C, pressure drop values for double-inlet configurations range between 333 Pa and 354 Pa, while single-inlet configurations, where the fluid travels a longer path, exhibit higher values between 740 Pa and 810 Pa.

Since TEPD (thermal energy produced per unit pressure drop) is a function of both thermal energy output and pressure drop, it increases with rising ambient temperature due to enhanced thermal energy production and reduced hydraulic resistance. The highest TEPD is recorded in Config X1, reaching 2.43 W/Pa at an ambient temperature of 40 °C (Figure 4.119b).

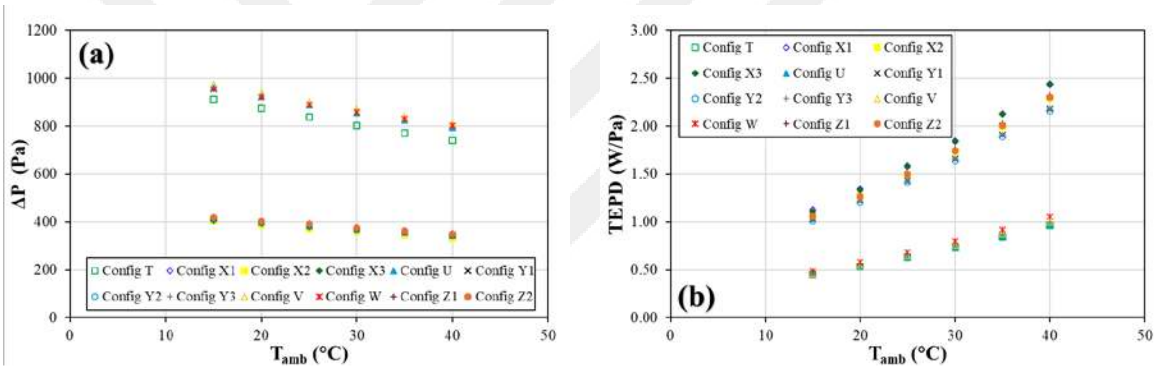

Figure 4.119. Effect of ambient temperature on the pressure drop (a) and TEPD (b) of spiral tube PVT collectors.

4.3.6. Effect of Wind Velocity on the Spiral Tube PVT Collector Configurations

The last operational parameter evaluated in this study is wind velocity, which plays a role in influencing convective heat losses and consequently affects both the energetic and exergetic performance of PVT collectors. In this section, the impact of wind velocity on several performance indicators is examined by systematically varying it from 1 m/s to 5 m/s in 1 m/s increments, while maintaining all other operating parameters such as solar irradiance, fluid flow rate, fluid inlet temperature, and ambient temperature constant, in accordance with the base-case conditions (Table 3.3).

Figure 4.120 illustrates the variation in absorber temperature distributions with wind velocity for the three best-performing spiral tube configurations under base-case conditions (configurations W, X1 and Z1). Meanwhile, Figure 4.121 presents the changes in average PV cell temperatures and fluid outlet temperatures for all spiral tube PVT collectors as a function of wind velocity.

Compared to other operational parameters, the impact of wind velocity on absorber temperature is less pronounced. For all spiral tube three configurations, the maximum absorber temperatures remain below 50 °C, regardless of wind conditions.

A gradual increase in wind velocity enhances convective heat transfer on the absorber surface, thereby lowering the overall temperature levels. This cooling effect results in more uniform temperature distributions across the panel, with reduced thermal energy accumulation.

At the lowest wind velocity (1 m/s), the maximum absorber temperatures are recorded as 47.89 °C for Config W, 48.38 °C for Config X1 and 48.57 °C for Config Z1. Under the highest wind velocity condition (5 m/s), these values decrease to 39.54 °C, 39.99 °C and 40.38 °C, respectively.

As wind velocity increases, convective heat losses to the environment intensify, resulting in a reduction in the average surface temperatures of all spiral tube PVT collectors as well as the conventional PV panel, along with a corresponding decrease in the fluid outlet temperatures of the PVT collectors.

At lower wind velocities, design differences among the PVT collectors become more pronounced, leading to noticeable variation in average PV cell surface and fluid outlet temperatures. However, as wind velocity increases, the temperature values for both parameters begin to close across spiral tube different configurations. Moreover, at low wind velocities, the influence of the absorber plate and embedded tube beneath the PV panel is clearly observed. The average surface temperature of the uncooled PV panel approaches the PV cell temperatures of the PVT collectors with increasing wind velocity.

When wind velocity is at its minimum (1 m/s), the difference in average PV cell temperatures (Figure 4.121a) between the PVT collectors and the PV panel ranges from 16.79 °C to 19.38 °C. At the maximum wind velocity (5 m/s), this gap narrows significantly, ranging from 6.68 °C to 7.47 °C. Similarly, the fluid outlet temperatures (Figure 4.121b) of the spiral tube PVT collectors drop from 42.79 °C to 46.33 °C at 1 m/s to 36.37 °C to 38.36 °C at 5 m/s.

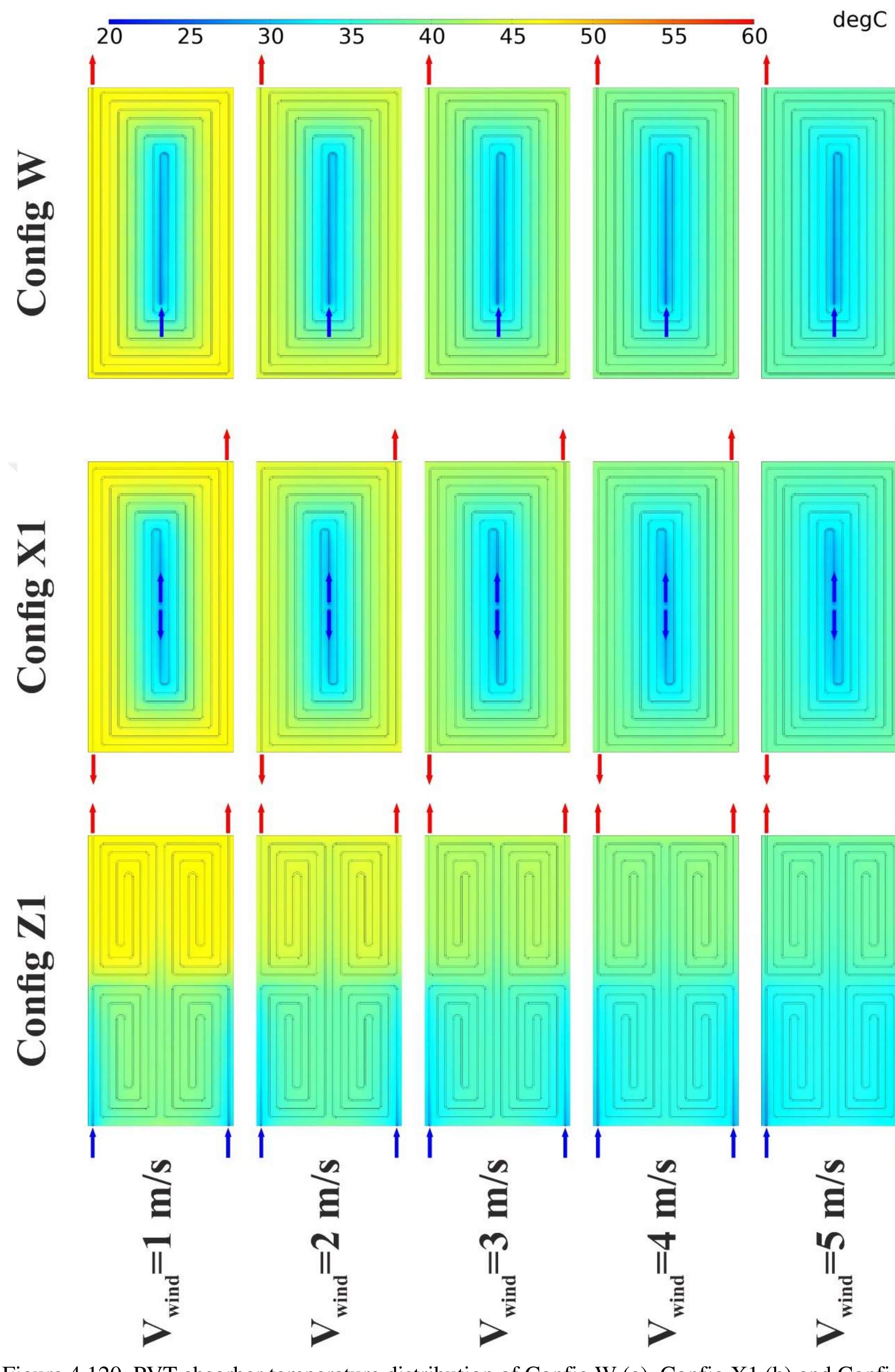

Figure 4.120. PVT absorber temperature distribution of Config W (a), Config X1 (b) and Config Z1 (c) for different wind velocities

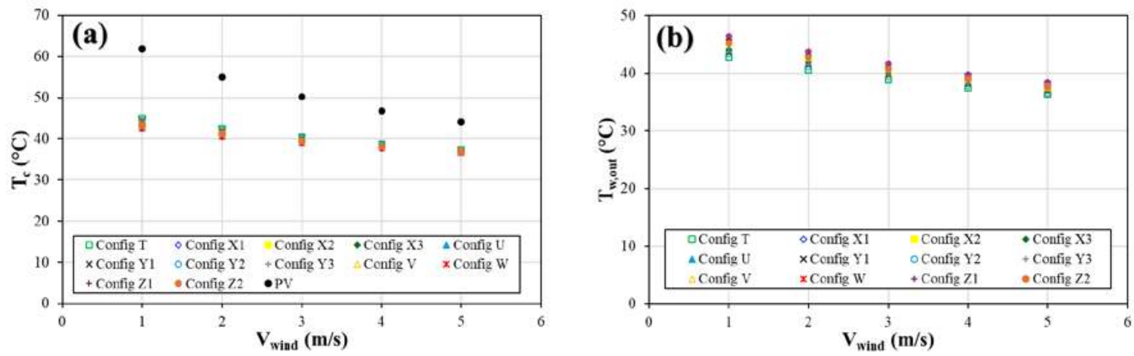

Figure 4.121. Variation of average PV cell (a) and water outlet (b) temperature of different spiral tube configurations under varying wind velocities

Figures 4.122 and 4.123 compare the impact of wind velocity on the thermal and electrical energy outputs of spiral tube PVT collectors, along with their respective efficiencies. As wind velocity increases, convective heat losses rise, resulting in lower fluid outlet temperatures, as also demonstrated in Figure 4.121b. Moreover, thermal energy output also shows a declining tendency with increasing wind velocity due to heat losses.

When analyzing the thermal performance of spiral tube PVT collectors, the influence of the tube arrangement beneath the PV panel is more apparent at lower wind velocities. Among all spiral tube configurations, Config X1 consistently delivers the best thermal performance, whereas Config T shows the lowest performance. At a wind velocity of 1 m/s, Config X1 achieves a thermal energy output of 610.57 W (Figure 4.122a) and a thermal efficiency of 0.3926 (Figure 4.123a), compared to 528.31 W and 0.3397 for Config T. Although the performance gap narrows at higher wind velocities, Config X1 still outperforms Config T by approximately 12% under maximum wind velocity.

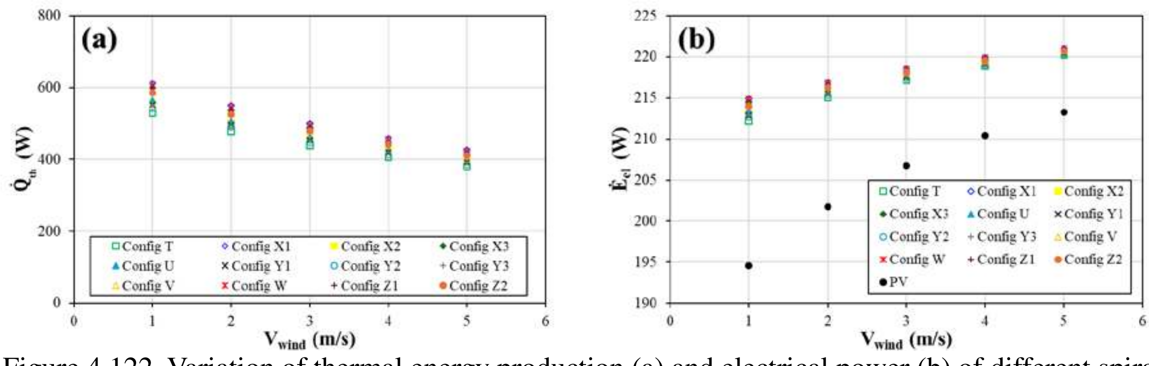

Figure 4.122. Variation of thermal energy production (a) and electrical power (b) of different spiral tube configurations under varying wind velocities

On the other hand, increasing wind velocity leads to increase convective heat losses, which reduces the amount of thermal energy accumulated on the surface of the PVT collector. As a result, PV cell temperatures decrease, thereby improving electrical efficiency and electricity generation (Figure 4.122b). These performance metrics were also compared against those of a conventional

PV panel. At lower wind velocities, the performance gap between spiral tube PVT collectors and the PV panel is substantial; however, as wind velocity increases, this difference gradually diminishes. At the maximum wind velocity (5 m/s), Config X1 achieved the highest values in both metrics, with an electrical output of 221 W and an electrical efficiency of 0.1422 (Figure 4.123b). When compared to the conventional PV panel, the performance advantage of Config X1 was 10.25% at the lowest wind velocity, but this margin decreased to 3.76% at the highest wind velocity.

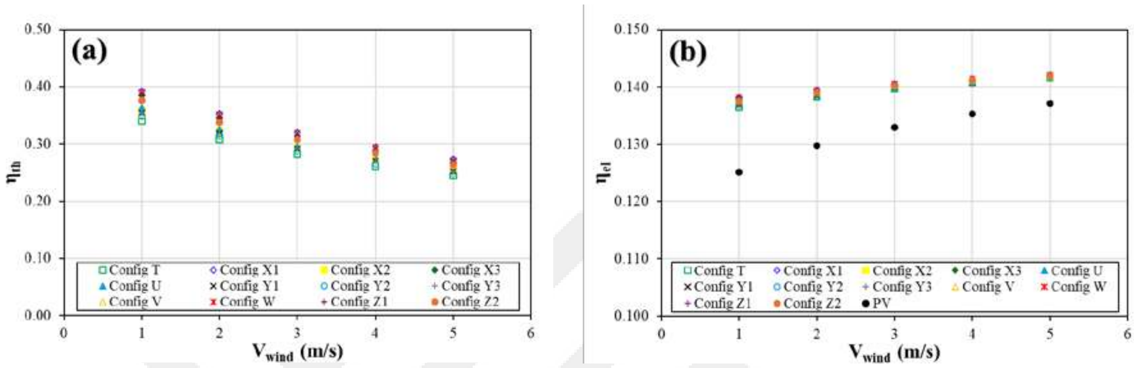

Figure 4.123. Effect of wind velocity on the thermal (a) and electrical (b) efficiency of spiral tube PVT collectors

The influence of wind velocity on the exergetic performance parameters of spiral tube PVT collectors is presented in Figure 4.124. Since the other parameters affecting thermal exergy are kept constant, its variation is directly related to the fluid outlet temperature (Eq. 3.43), which decreases with increasing wind velocity. Consequently, thermal exergy (Figure 4.124a) exhibits a declining trend as wind velocity increases.

Similar to thermal energy production, the highest thermal exergy is observed in Config X1 at a wind velocity of 1 m/s, reaching 40.77 W, which is approximately 37% higher than that of Config T under the same conditions. Since electrical energy is a high-grade energy form, the electrical exergy of PVT collectors is equal to their electricity production and does not exhibit as sharp a variation as thermal exergy (Figure 4.124b). Since the changes in thermal exergy are more pronounced than those in electrical exergy, the output exergy also follows a decreasing trend with increasing wind velocity.

The highest output exergy is recorded in Config X1 at 256 W under the lowest wind velocity, corresponding to a 6% improvement over Config T (Figure 4.124c). As exergy input remains constant for all spiral tube configurations and is unaffected by wind velocity, exergy destruction (Figure 4.124d) displays an inverse trend to that of output exergy. Accordingly, the highest exergy destruction is observed in Config T.

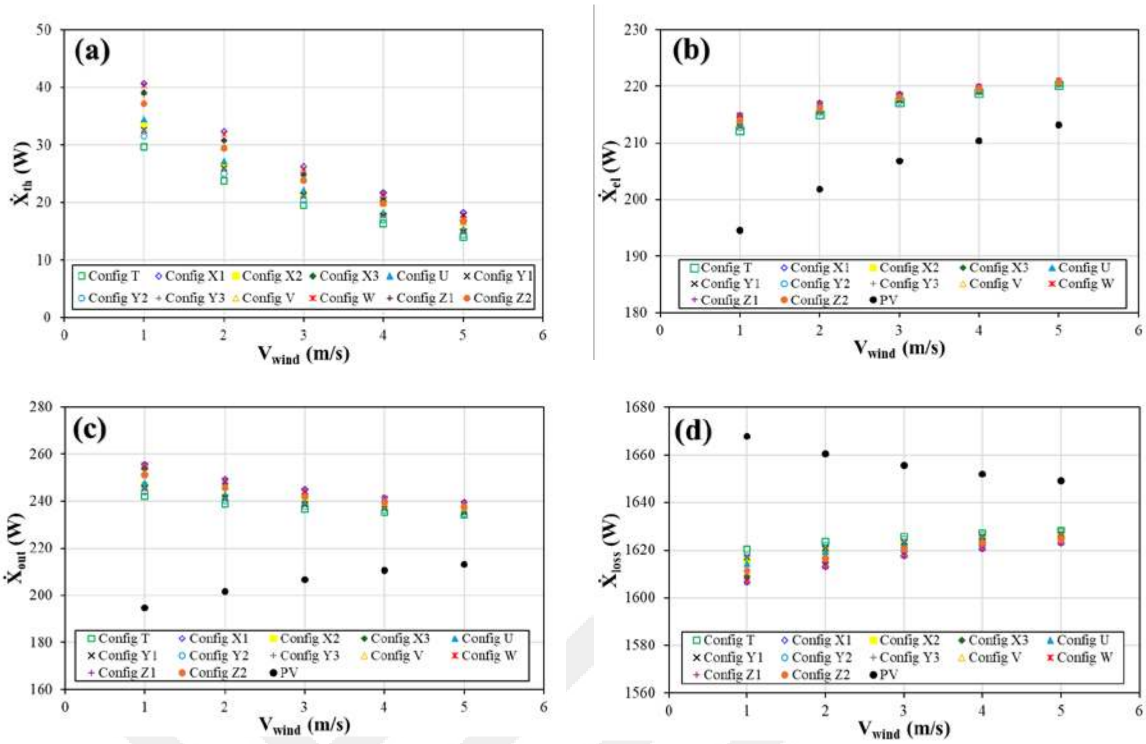

Figure 4.124. Effect of wind velocity on the thermal (a), electrical (b) and output (c) exergy, and exergy destruction (d) of spiral tube PVT collectors

Figure 4.125 presents the variation in overall efficiency, primary energy saving efficiency and exergy efficiency of spiral tube PVT collectors as a function of wind velocity, combining the effects of both thermal and electrical performance parameters.

Although the electrical performance of PVT collectors improves with increasing wind velocity due to reduced PV cell temperatures, the thermal performance deteriorates more significantly as a result of increased convective heat losses. Consequently, both overall efficiency (Figure 4.125a) and primary energy saving (Figure 4.125b) efficiency exhibit a downward trend with increasing wind velocity. For both metrics, the highest values are recorded at a wind velocity of 1 m/s in Config X1, with 0.5308 and 0.7563, respectively. As wind velocity rises to 5 m/s, these values decline to 0.4158 and 0.6478.

On the other hand, when examining exergy efficiency, it is evident that, since exergy input remains constant and is independent of wind velocity, exergy efficiency is directly governed by the output exergy (Eq. 3.45), as previously shown in Figure 4.124c. As wind velocity increases, the decline in output exergy leads to a corresponding reduction in exergy efficiency. The highest exergy efficiency is achieved by Config X1, with a value of 0.1377 at 1 m/s, representing approximately 6% higher performance compared to Config T under the same conditions.

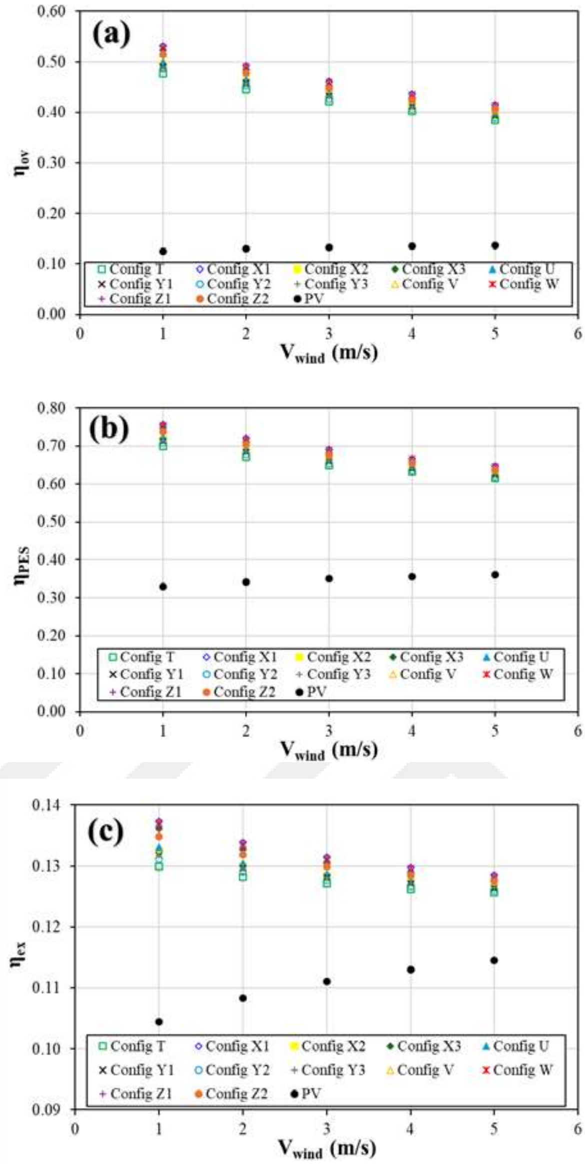

Figure 4.125. Effect of wind velocity on the overall (a), primary energy saving (b) and exergy (c) efficiency of spiral tube PVT collectors

As wind velocity increases, the viscosity and density of the working fluid also rises, leading to higher internal friction and local losses, which in turn amplifies the pressure drop along the tube network. Due to differences in flow distribution across tube bundles, double-inlet configurations generally experience lower pressure drops compared to single-inlet designs (Figure 4.126a).

When wind velocity increases from 1 m/s to 5 m/s, pressure drops rise by approximately 8% to 12%, depending on the configuration. At the same time, convective heat losses rises with increasing wind velocity, which results in a decline in thermal energy production. Coupled with the increase in pressure drop, this causes a reduction in thermal energy produced per unit pressure drop across all spiral tube configurations (Figure 4.126b). The highest TEPD value is recorded at the lowest wind velocity (1 m/s) in Config X1, reaching 1.59 W/Pa.

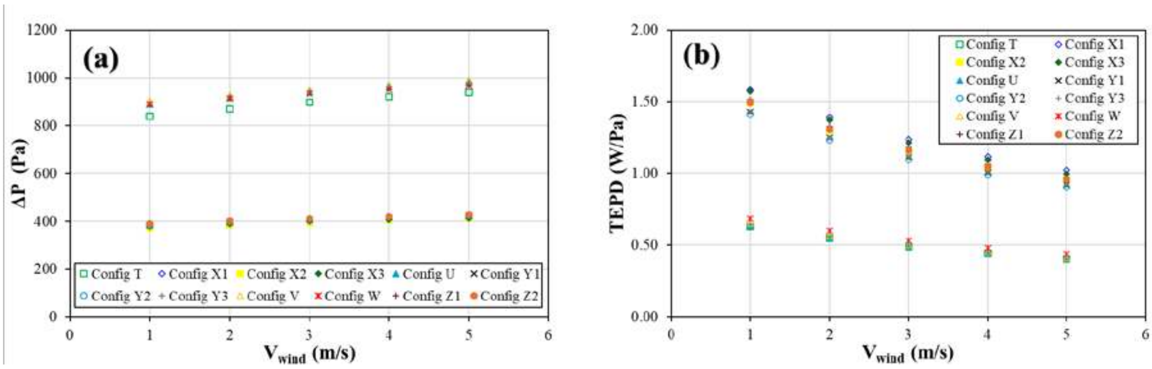

Figure 4.126. Effect of wind velocity on the pressure drop (a) and TEPD (b) of spiral tube PVT collectors

4.4. Comparison of the Top Three Designs of Each Collector Group (Parallel, Serpentine, Spiral)

This section presents a comprehensive comparison of nine PVT configurations, three from each category: parallel, serpentine, and spiral tube designs selected based on their superior performance discussed in previous sections. The analysis focuses on their thermal, electrical and exergetic performance metrics. Specifically, configurations A, E and F represent the top-performing designs among the parallel tube group, while H, R1 and Q stand out in the serpentine tube group. Similarly, W, X1 and Z1 are identified as the most efficient configurations within the spiral tube category. The effects of key operational parameters including solar irradiance, fluid flow rate, fluid inlet temperature, ambient temperature and wind velocity on the performance of these selected configurations are comparatively analyzed in detail.

4.4.1. Effect of Flow Rate on the Best Performing PVT Collector Configurations

In this section, the impact of fluid flow rate on various performance metrics of the nine selected PVT configurations is examined. The flow rate was varied from 5 to 50 L/h in 5 L/h increments, ensuring that the flow conditions remained within the laminar regime throughout the analysis. During this investigation, all other operational parameters namely solar irradiance, water inlet temperature, ambient temperature, and wind velocity were held constant at their base-case values, as detailed in Table 3.3.

Figure 4.127 compares the variation in thermal and electrical efficiencies of the top-performing nine PVT configurations representing parallel, serpentine and spiral tube designs as a function of fluid flow rate. In all configurations, both efficiency metrics exhibit an overall increasing trend with rising flow rate.

At the lowest flow rate of 5 L/h, thermal efficiency (Figure 4.127a) ranged between 0.1328 (Config W, spiral tube) and 0.1524 (Config E, parallel tube). When the flow rate increased to its maximum value of 50 L/h, the highest thermal efficiency was again observed in Config E at

0.6107, followed closely by Config H and R1 (serpentine tube), with only about 0.5% lower efficiency.

Regarding electrical efficiency (Figure 4.127b), the increase in flow rate resulted in enhanced cooling of the PV cells, thereby reducing cell temperature and improving electrical performance. Although the rise in electrical efficiency was not as steep as that of thermal efficiency, an average increase of around 12% was observed across all configurations. The maximum electrical efficiency for all collectors occurred at the highest flow rate, with Config R1 (serpentine tube) reaching 0.1458, which is approximately 1.18% higher than the lowest-performing configuration under the same condition.

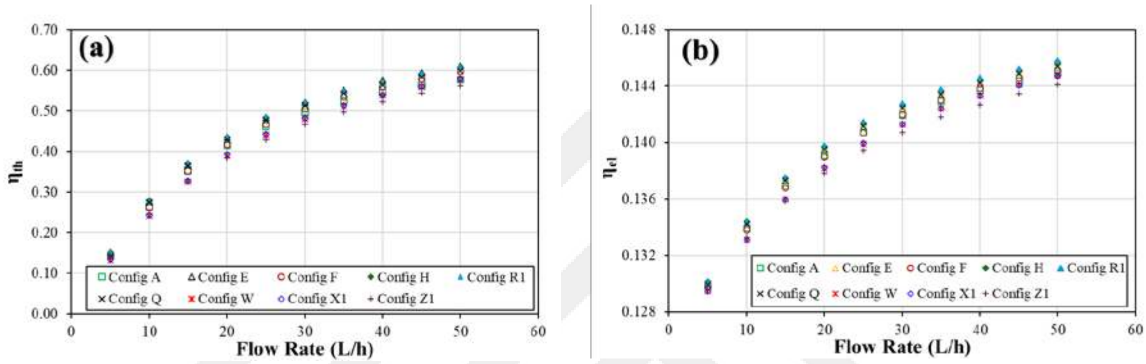

Figure 4.127. Effect of flow rate on the thermal (a) and electrical (b) efficiency of the nine best-performing PVT collectors

Figure 4.128 illustrates the variation of overall efficiency, primary energy saving efficiency and exergy efficiency with fluid flow rate for the top nine PVT configurations. Due to the combined improvement in both thermal and electrical efficiencies with increasing flow rate, overall and primary energy saving efficiencies also exhibit a significant upward trend.

For all configurations, the maximum overall efficiency is observed at the highest flow rate of 50 L/h (Figure 4.128a). Among the configurations, Config E (parallel tube) achieved the highest overall efficiency at 0.7564, followed closely by Config H and R1 (serpentine tube) at 0.7536. These three configurations outperform Config Z1 (spiral tube), the lowest-performing design at this flow rate, by approximately 7%.

Similarly, primary energy saving efficiency (Figure 4.128b) follows a parallel trend with overall efficiency. While the differences between configurations are minimal at lower flow rates, the results begin to diverge as flow rate increases. Beyond 40 L/h, all configurations surpass a primary energy saving efficiency of 0.90. At 50 L/h, Config E, H, and R1 again perform best, exceeding Config Z1 by around 5%. In terms of exergy efficiency (Figure 4.128c), an optimal range is observed between 25 L/h and 30 L/h for configurations. The maximum exergy efficiencies for Config E, H and R1 are recorded as 0.1446, 0.1445 and 0.1448, respectively.

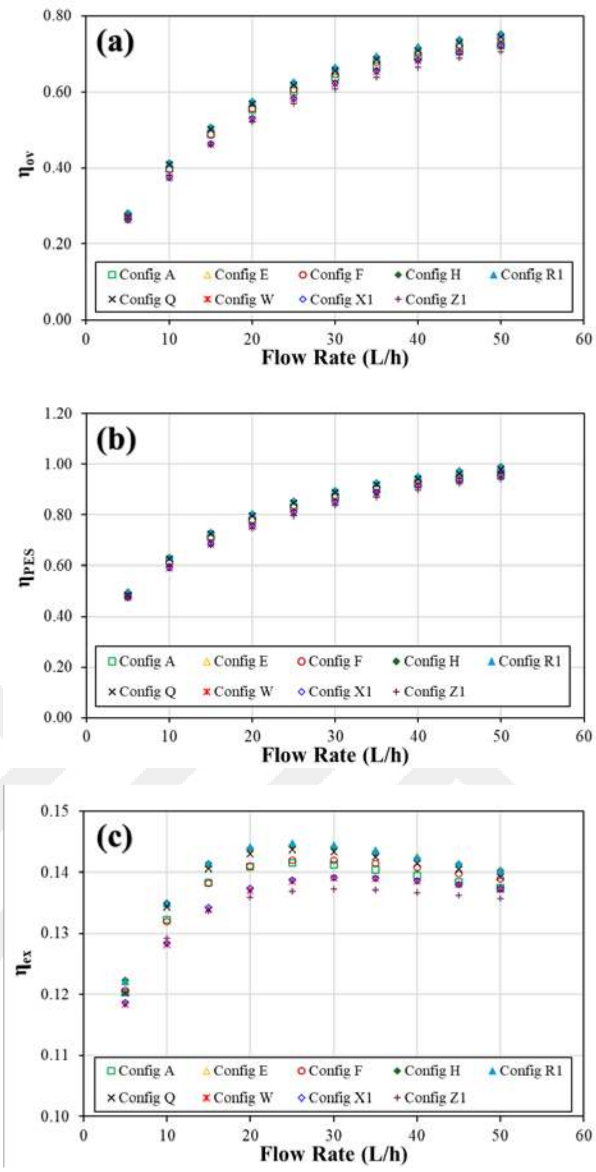

Figure 4.128. Effect of flow rate on the overall (a), primary energy saving (b) and exergy (c) efficiency of the nine best-performing PVT collectors

One of the most significant performance-related differences between parallel, serpentine and spiral tube PVT configurations is their pressure drop behavior under varying flow conditions. As the fluid velocity and density increases, pressure drops rise across all configurations due to enhanced friction between the fluid and tube walls, as well as increased local losses. Among the three collector types, parallel tube configurations (Config A, E and F) exhibit significantly lower pressure drops compared to serpentine (Config H, R1 and Q) and spiral tube designs (Config W, X1 and Z1), owing to their minimal local losses (Figure 4.129a). The highest pressure drop is observed in Config W, a spiral tube design with a single inlet, followed by Config H, a single-inlet serpentine configuration. When considering the thermal energy produced per unit pressure drop (TEPD), it is evident that although thermal energy produced increases with flow rate, the pressure drop increases at a much faster rate. Consequently, TEPD exhibits a decreasing trend with increasing flow rate (Figure 4.129b). The highest TEPD values are achieved in parallel tube configurations (Config A, E and F), while Config W, which experiences the greatest pressure drop, yields the lowest TEPD values among the evaluated designs.

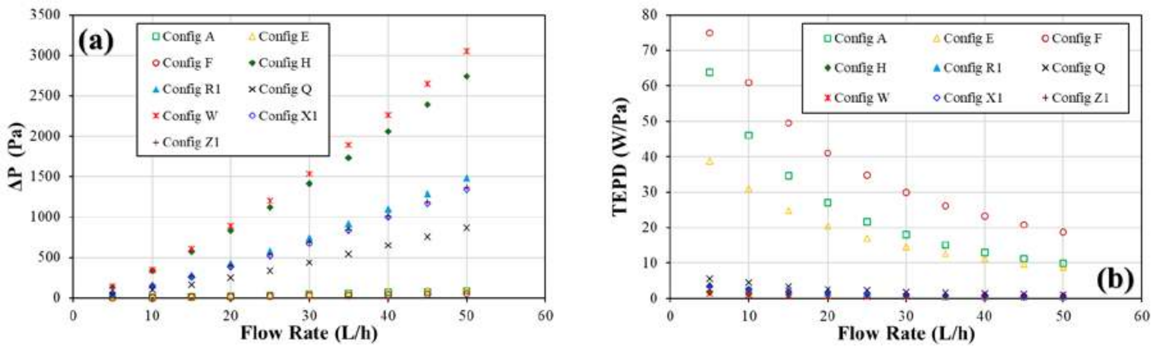

Figure 4.129. Effect of flow rate on the pressure drop (a) and TEPD (b) of the nine best-performing PVT collectors

4.4.2. Effect of Solar Irradiance on the Best Performing PVT Collector Configurations

In this section, the effect of solar irradiance on the thermal, electrical, overall, primary energy saving and exergy efficiencies of parallel, serpentine and spiral tube PVT collectors is comparatively evaluated. In addition, its influence on pressure drop and thermal energy produced per unit pressure drop (TEPD) is also assessed.

Solar irradiance was varied from 200 W/m^2 to 1200 W/m^2 in increments of 200 W/m^2, while other operating parameters were kept constant: fluid flow rate at 20 L/h, fluid inlet temperature at 20 °C, ambient temperature at 25 °C and wind velocity at 1 m/s.

Figure 4.130 presents the variation in thermal and electrical efficiencies of the nine selected PVT configurations as a function of solar irradiance. While thermal efficiency (Figure 4.130a) exhibits only minor changes with increasing irradiance, electrical efficiency (Figure 4.130b) decreases due to the elevated PV cell temperatures caused by higher solar input. Among the evaluated designs, spiral tube configurations show the lowest thermal efficiency, whereas serpentine tube designs particularly Config R1 demonstrate the best thermal performance. Electrical performance was also compared with that of a conventional PV panel. At low irradiance levels, the difference in electrical efficiency between the PVT collectors and the PV panel is relatively small; however, as irradiance increases, the performance gap widens. The highest electrical efficiencies are achieved in Config E (parallel tube) and Config H and R1 (serpentine tube).

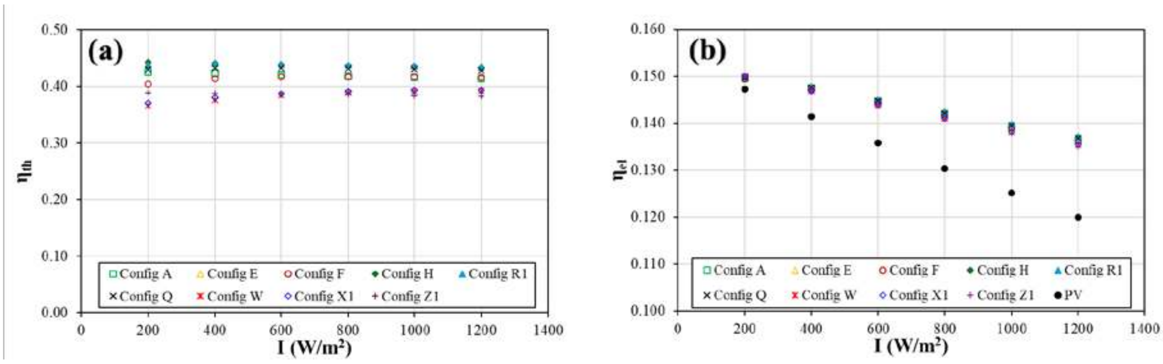

Figure 4.130. Effect of solar irradiance on the thermal (a) and electrical (b) efficiency of the nine best-performing PVT collectors

Figure 4.131 presents the variation of overall efficiency, primary energy saving efficiency, and exergy efficiency with solar irradiance for the nine selected PVT configurations. Since both overall and primary energy saving efficiencies are primarily influenced by thermal efficiency due to their higher values, and given that thermal efficiency exhibits only minor changes with increasing irradiance, the variation in these two metrics remains relatively limited. The highest overall efficiency (Figure 4.131a) is recorded under the lowest solar irradiance condition (200 W/m^2) in Config E at 0.5941, followed by Config H and R1 with 0.5923 and 0.5881, respectively.

In contrast, primary energy saving efficiency, which is more sensitive to electrical efficiency, shows a slight decreasing trend with increasing solar irradiance (Figure 4.131b). At 200 W/m^2, primary energy saving efficiencies are recorded as 0.8385 in Config E, 0.8368 in Config H, and 0.8332 in Config R1. Notably, even the best-performing spiral tube configurations fail to exceed 0.80 in this metric.

As for exergy efficiency (Figure 4.131c), it exhibits a positive trend with increasing solar irradiance, mainly due to the increase in thermal and electrical exergy outputs. While the differences between configurations are negligible at low irradiance levels, they become more pronounced as irradiance increases. The maximum exergy efficiencies are observed in serpentine tube configurations (H, R1 and Q) and parallel tube Config E, all reaching values around 0.147, whereas spiral tube designs remain lower, around 0.140.

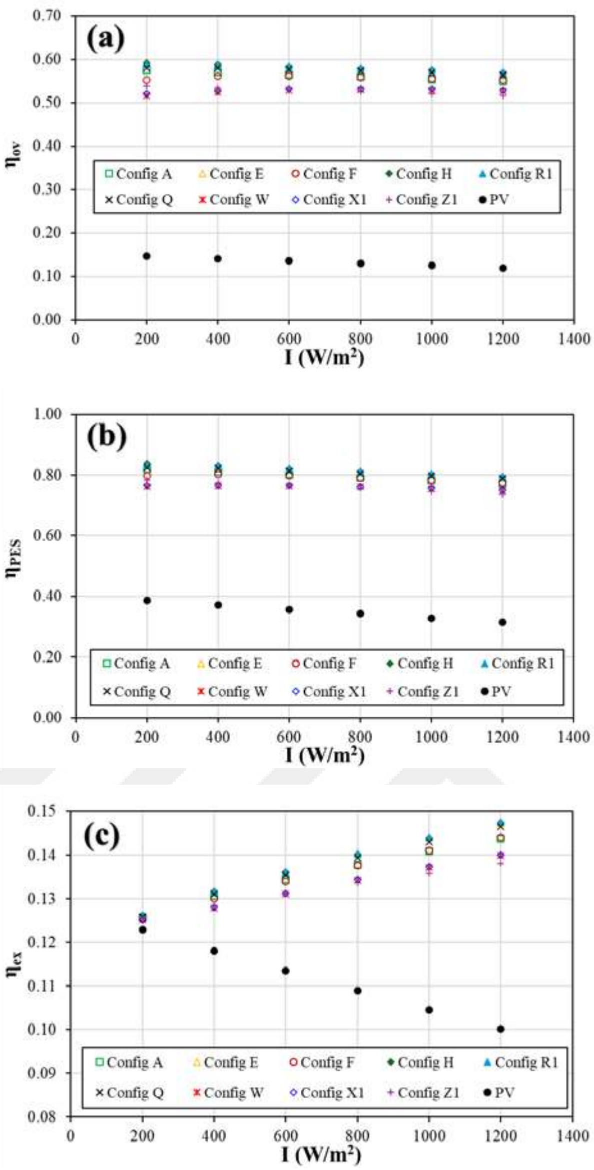

Figure 4.131. Effect of solar irradiance on the overall (a), primary energy saving (b) and exergy (c) efficiency of the nine best-performing PVT collectors

The effect of solar irradiance on pressure drop and thermal energy produced per unit pressure drop (TEPD) for the selected PVT collectors is presented in Figure 4.132. As solar irradiance increases, the outlet temperature of the working fluid rises, leading to a decrease in its viscosity and density. Consequently, a decline in pressure drop is observed across all configurations (Figure 4.132a).

Among the collector types, parallel tube designs exhibit the lowest pressure drops, whereas single-inlet spiral (Config W) and single-inlet serpentine (Config H) configurations experience significantly higher pressure drops due to longer flow paths and elevated local losses. In contrast, double-inlet spiral (Config X1 and Z1) and double-inlet serpentine (Config R1) collectors show comparable and notably reduced pressure drop values. The triple-inlet serpentine configuration

(Config Q) performs better than most other serpentine and spiral designs, and ranks just behind the parallel configurations in terms of minimal pressure drop.

With increasing irradiance, thermal energy production increases, while pressure drop decreases, resulting in a substantial improvement in TEPD (Figure 4.132b). Among all configurations, Config F (parallel tube) delivers the highest TEPD, particularly at high irradiance levels, followed by the other parallel tube designs. Conversely, Config W, which exhibits the highest pressure drop, consistently yields the lowest TEPD values across all irradiance levels.

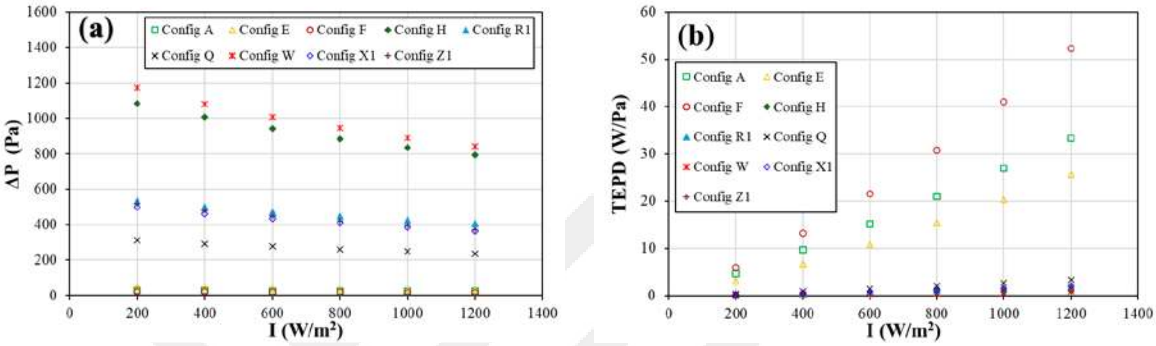

Figure 4.132. Effect of solar irradiance on the pressure drop (a) and TEPD (b) of the nine best-performing PVT collectors

4.4.3. Effect of Fluid Inlet Temperature on the Best Performing PVT Collector Configurations

Fluid inlet temperature is one of the most influential operational parameters affecting the performance of PVT collectors. In this chapter, the inlet temperature was varied from 10 °C to 40 °C in increments of 5 °C, while all other operational parameters were kept constant, as detailed in Table 3.3. A comparative analysis was conducted on nine representative configurations from parallel, serpentine and spiral tube designs, focusing on various efficiency metrics, as well as pressure drop and TEPD.

As shown in Figure 4.133, increasing the fluid inlet temperature leads to a decline in both thermal and electrical efficiencies across all configurations. Although higher inlet temperatures result in higher outlet temperatures, the elevated cell temperature leads to intensified heat dissipation to the surroundings and a reduction in useful heat gain, thereby reducing thermal efficiency. As a result, all configurations achieve their maximum thermal efficiency (Figure 4.133a) when the inlet temperature is at its lowest level (10 °C). At this point, thermal efficiencies range between 0.4755 and 0.5409, with the highest value observed in the serpentine tube Config R1, followed by parallel tube Config E and serpentine tube Config H. In contrast, spiral tube designs demonstrate the poorest thermal performance, with all values falling below 0.50.

A similar trend is observed in electrical efficiency (Figure 4.133b). The best electrical performance is again recorded by Config R1, with an efficiency of 0.1435, while Config E and H follow closely behind. At the lowest inlet temperature, the performance difference between the best and worst configurations in terms of electrical efficiency is 1.77%, whereas this difference narrows to approximately 0.75% when the inlet temperature reaches its maximum level.

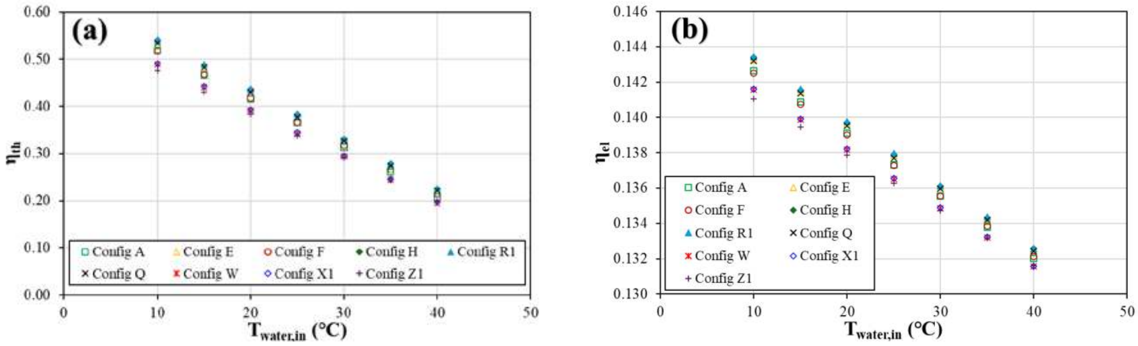

Figure 4.133. Effect of water inlet temperature on the thermal (a) and electrical (b) efficiency of the nine best-performing PVT collectors

As a result of the decreasing thermal and electrical efficiencies, both overall efficiency and primary energy saving efficiency exhibit a significant decline with increasing fluid inlet temperature for all PVT configurations (Figure 4.134). The highest overall efficiency (Figure 4.134a) is observed in Config R1 at an inlet temperature of 10 °C, reaching 0.6843, followed closely by Config H (0.6832) and Config E (0.6821).

In contrast, spiral tube designs perform less efficiently in this metric. Among them, Config Z1 records the lowest value of 0.6166 at the same inlet temperature, approximately 10% lower than Config R1. As inlet temperature increases, the gap between configurations narrows, reducing this difference to around 8% at the maximum inlet temperature.

A similar pattern is observed in primary energy saving efficiency (Figure 4.134b). The maximum value is again achieved by Config R1 at 10 °C with 0.9184, followed by Config H (0.9171) and Config E (0.9159). It is also noteworthy that Config Q, a serpentine tube triple-inlet design, outperforms the parallel tube configurations in this metric, whereas spiral tube designs consistently deliver the lowest performance.

When evaluating exergy efficiency, a decreasing trend is again evident with rising inlet temperature (Figure 4.134c). The differences between configurations are more pronounced at lower inlet temperatures but diminish progressively as the temperature increases. The highest exergy efficiency is recorded at 10 °C for Config R1, reaching 0.1498, followed closely by Config H (0.1496) and E (0.1494).

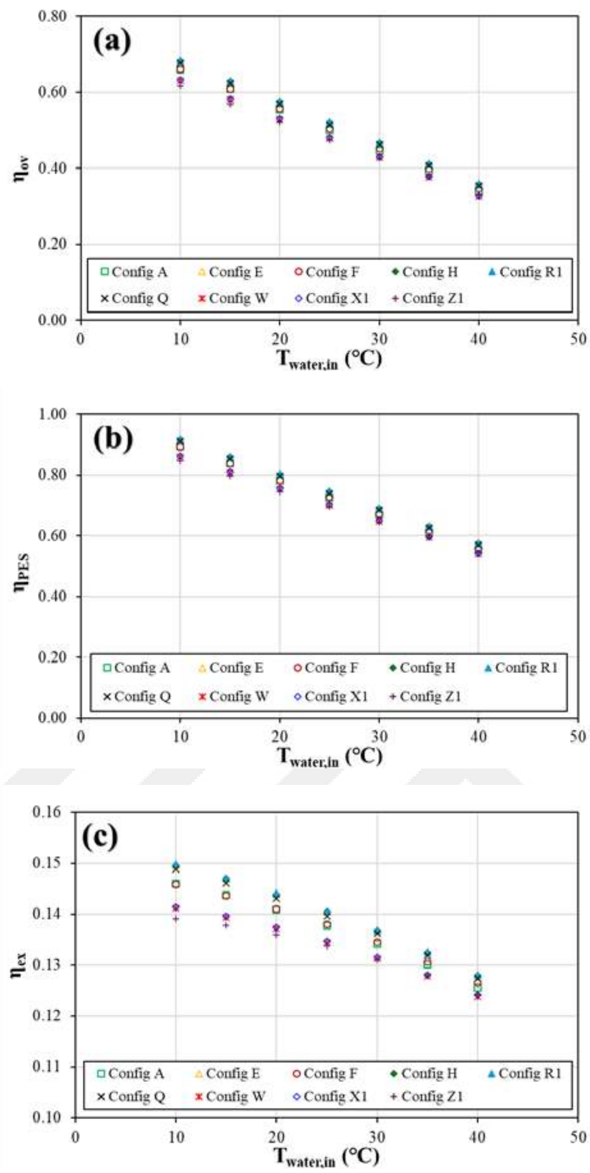

Figure 4.134. Effect of water inlet temperature on the overall (a), primary energy saving (b) and exergy (c) efficiency of the nine best-performing PVT collectors

As the fluid inlet temperature increases, the fluid temperature also rises, leading to a reduction in fluid viscosity and density. This decrease in these fluid properties results in lower internal friction and local losses, thereby reducing the pressure drop across all PVT configurations. Among the designs, parallel tube configurations exhibit the lowest pressure drops (Figure 4.135a), followed by the triple-inlet serpentine design (Config Q) and double-inlet designs. In contrast, the poorest performance in terms of pressure drop is observed in single-inlet configurations, namely Config W (spiral tube) and Config H (serpentine tube).

Regarding the thermal energy produced per unit pressure drop (TEPD), a declining trend is observed with increasing inlet temperature. Although pressure drop decreases, the thermal energy output decreases even more significantly due to the reduced temperature gradient, leading to an overall drop in TEPD. The highest TEPD (Figure 4.135b) values are achieved by parallel tube configurations, particularly Config F, while the lowest performance is consistently delivered by Config W.

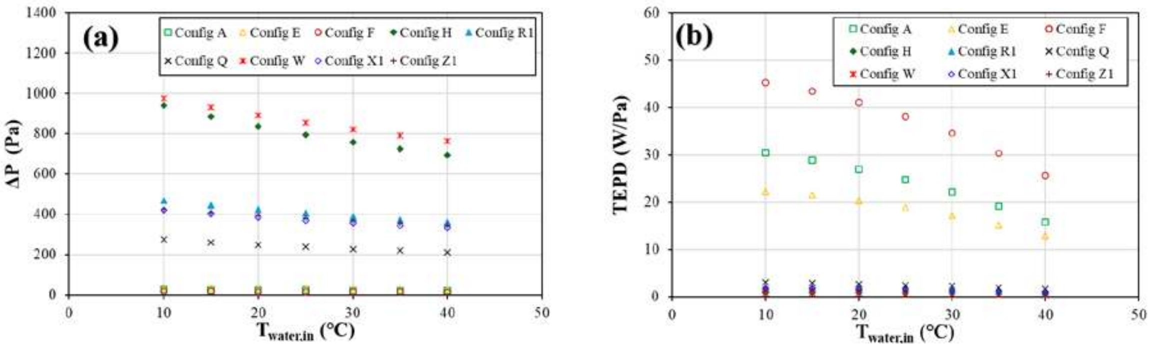

Figure 4.135. Effect of water inlet temperature on the pressure drop (a) and TEPD (b) of the nine best-performing PVT collectors

4.4.4. Effect of Ambient Temperature on the Best Performing PVT Collector Configurations

This section presents a comparative analysis of the impact of ambient temperature on the efficiency metrics and TEPD performance of nine representative PVT configurations from parallel, serpentine and spiral tube designs. The ambient temperature was systematically varied from 15 °C to 40 °C in 5 °C increments, while other operational parameters including solar irradiance (1000 W/m^2), fluid flow rate (20 L/h), fluid inlet temperature (20 °C), and wind velocity (1 m/s) were held constant, as specified under the base-case conditions.

The variation in thermal and electrical efficiencies of the nine selected PVT configurations with respect to ambient temperature is illustrated in Figure 4.136. As ambient temperature increases, heat losses to the environment are reduced, leading to an overall improvement in the thermal efficiency of all PVT collectors (Figure 4.136a). At an ambient temperature of 40 °C, thermal efficiency reaches its maximum for all configurations. The highest performance is recorded in Config R1 with a thermal efficiency of 0.6009, followed closely by Config H and E, with values of 0.5990 each. In contrast, the lowest performance is observed in the spiral tube design Config Z1, with 0.5283, indicating that spiral tube systems generally lag behind serpentine and parallel configurations in terms of thermal performance.

On the other hand, the electrical efficiency (Figure 4.136b) shows a declining trend with increasing ambient temperature, primarily due to the rise in PV cell temperature. However, unlike thermal efficiency, the drop in electrical efficiency is less pronounced. All configurations exhibit their maximum electrical efficiency at the lowest ambient temperature of 15 °C, with values being relatively close across different designs. The highest electrical efficiency of 0.1429 is recorded in Config R1 and H (serpentine tube) and Config E (parallel tube).

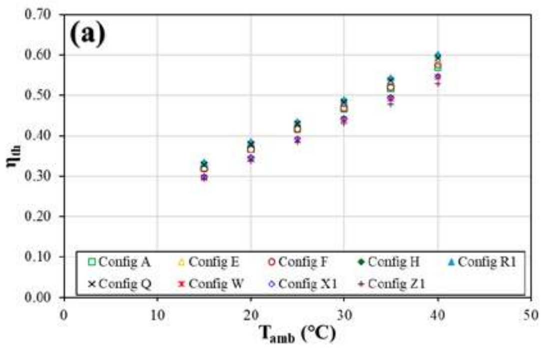

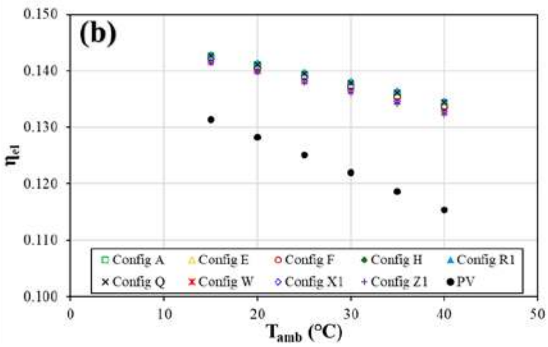

Figure 4.136. Effect of ambient temperature on the thermal (a) and electrical (b) efficiency of the nine best-performing PVT collectors

Given that the variation in thermal efficiency with ambient temperature is significantly greater than that of electrical efficiency, both overall efficiency and primary energy saving efficiency exhibit a clear increasing trend with rising ambient temperature, reaching their maximum values at the highest ambient temperature. In terms of overall efficiency (Figure 4.137a), Config R1 (serpentine tube) demonstrated the best performance with a value of 0.7356, followed closely by Config H (0.7337) and Config E (0.7335). Among the nine configurations evaluated, the three spiral tube designs consistently showed the lowest performance, with overall efficiencies remaining below 0.70.

A similar trend is observed in primary energy saving efficiency (Figure 4.137b). The highest value of 0.9553 is recorded for Config R1, followed by Config H (0.9533) and E (0.9530). As with overall efficiency, the lowest performance is once again exhibited by the spiral tube design Config Z1, confirming that spiral geometries generally fall behind their serpentine and parallel counterparts in terms of energy-saving potential.

When examining exergy efficiency (Figure 4.137c), the top-performing configurations are again Config R1 and H (serpentine tube) and Config E (parallel tube). These three designs deliver very similar results, each reaching approximately 0.1440, further highlighting their superior exergy performance.

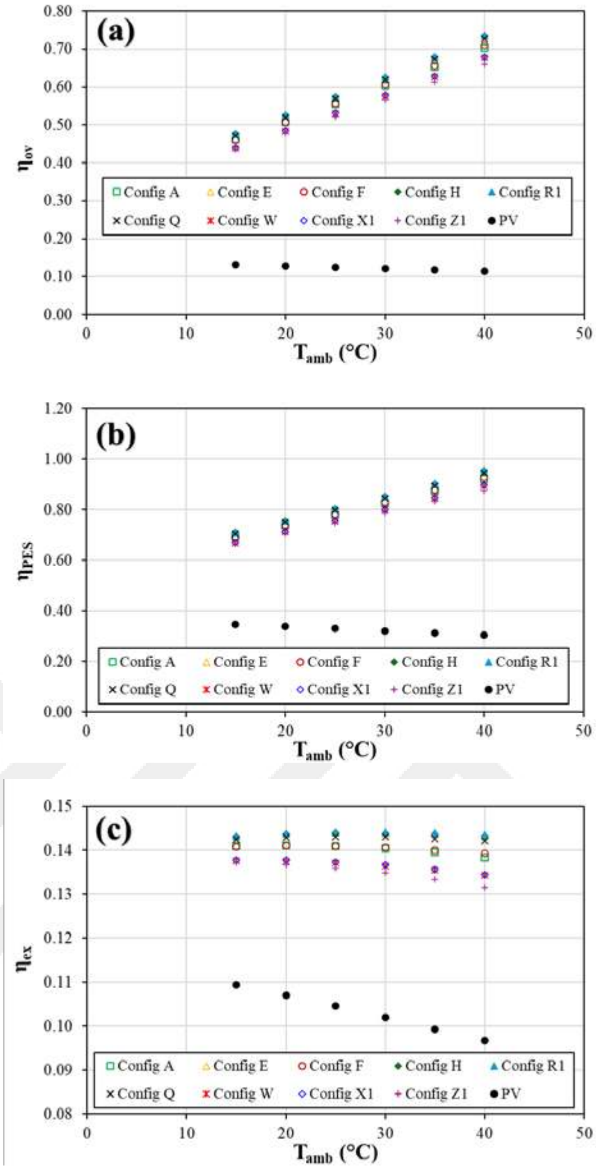

Figure 4.137. Effect of ambient temperature on the overall (a), primary energy saving (b) and exergy (c) efficiency of the nine best-performing PVT collectors

With the increase in ambient temperature, the fluid outlet temperature also rises, leading to a reduction in fluid viscosity and density. The decrease in these fluid properties results in a reduction in pressure drop across all PVT collectors, as illustrated in Figure 4.138. Among the designs evaluated, the parallel tube configurations (Config A, E, and F) exhibit the lowest pressure drops (Figure 4.138a), followed by the triple-inlet serpentine configuration (Config Q) and the double-inlet designs. In contrast, the highest pressure drops are recorded in single-inlet designs, specifically Config W (spiral tube) and Config H (serpentine tube), due to longer flow paths and increased local losses.

Moreover, the combined effect of increased thermal energy production resulting from heat losses and reduced pressure drop leads to a notable improvement in the thermal energy produced per unit pressure drop (TEPD). The parallel tube configurations outperform all others in this metric, primarily due to their significantly lower pressure losses, making them the most effective in terms of TEPD performance (Figure 4.138b).

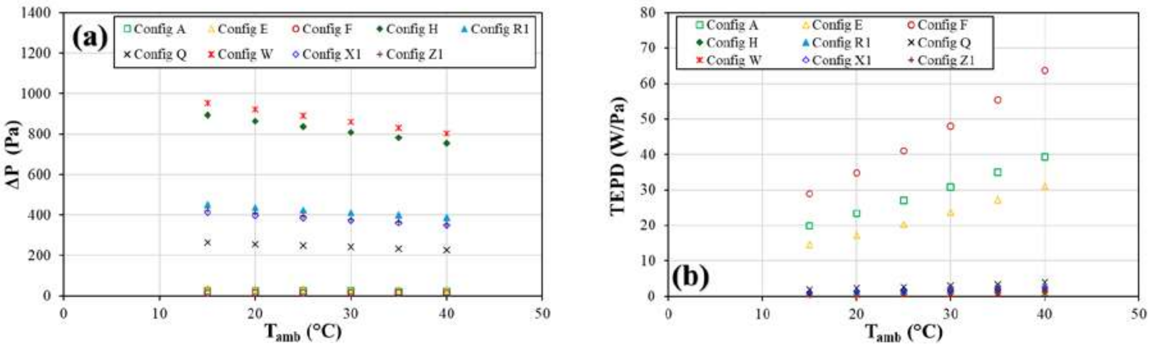

Figure 4.138. Effect of ambient temperature on the pressure drop (a) and TEPD (b) of the nine best-performing PVT collectors

4.4.5. Effect of Wind Velocity on the Best Performing PVT Collector Configurations

Wind velocity is one of the environmental parameters influencing the thermal and electrical performance of PVT collectors due to its effect on convective heat losses. In this section, the wind velocity was varied from 1 m/s to 5 m/s in increments of 1 m/s, and its impact on the performance metrics of nine distinct PVT collector configurations representing the best-performing parallel, serpentine and spiral tube designs was comparatively analyzed.

As wind velocity increases, convective heat losses become more pronounced, leading to a decline in thermal efficiency for all PVT collectors. However, due to the reduced accumulation of thermal energy on the PVT surface, the PV cell temperatures decrease, thereby enhancing electrical efficiency. The highest thermal efficiencies were observed at the lowest wind velocity (1 m/s) across all configurations (Figure 4.139a). At this condition, the serpentine tube Config R1 demonstrated the best thermal performance with an efficiency of 0.4361, while the spiral tube Config Z1 exhibited the lowest with 0.3839. All three spiral tube configurations recorded thermal efficiencies below 0.40, consistently underperforming compared to their parallel and serpentine counterparts.

In contrast, electrical efficiency (Figure 4.139b) showed an increasing trend with rising wind velocity for all PVT collectors, as well as for the conventional PV panel. As wind velocity increases, surface temperatures decrease, reducing thermal energy accumulation on the PV cells and thus improving their electrical performance. Notably, at 5 m/s, the highest electrical efficiency values approximately 0.1427 were recorded for Config R1, H (serpentine tube) and E (parallel tube). Spiral tube designs followed closely, reaching efficiencies around 0.1421, reflecting diminishing performance gaps between configurations as wind velocity increases.

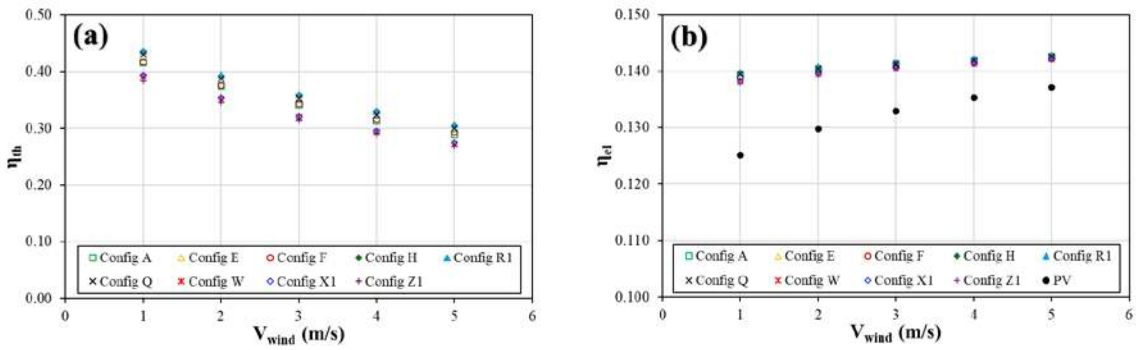

Figure 4.139. Effect of wind velocity on the thermal (a) and electrical (b) efficiency of the nine best-performing PVT collectors

Since thermal efficiency values are much higher than electrical efficiency, it has a more dominant influence on both overall and primary energy saving efficiencies. Therefore, the slight increase in electrical efficiency with rising wind velocity cannot compensate for the significant reduction in thermal efficiency. Consequently, both overall and primary energy saving efficiencies show a declining trend as wind velocity increases. The maximum overall efficiency (Figure 4.140a) is observed at the lowest wind speed (1 m/s) with a value of 0.5758 for the serpentine tube Config R1, followed closely by Config E and H, which recorded efficiencies of 0.5746. Although spiral tube configurations generally performed lower than their parallel and serpentine counterparts, Config X1 achieved the best result among them, with an overall efficiency of 0.5308.

A similar trend is observed for primary energy saving efficiency (Figure 4.140b). The highest value was again obtained at 1 m/s for Config R1, reaching 0.8039, which is approximately 7.66% higher than that of the lowest-performing configuration, the spiral tube Config Z1, under the same wind condition.

On the other hand, when evaluating exergy efficiency, it is noted that increasing wind velocity results in greater convective losses, leading to a decrease in the fluid outlet temperature, and thus a reduction in thermal exergy. Although electrical exergy increases slightly due to enhanced electrical performance, the dominant reduction in thermal exergy causes the total exergy output to decline. Consequently, exergy efficiency (Figure 4.140c) decreases with rising wind velocity. The highest exergy efficiency is again recorded for Config R1 at 1 m/s, with a value of 0.1441, while Config E and H exhibit nearly identical performance. In contrast, the lowest exergy efficiency is found in the spiral tube Config Z1, with a value of 0.1360 under the same wind condition.

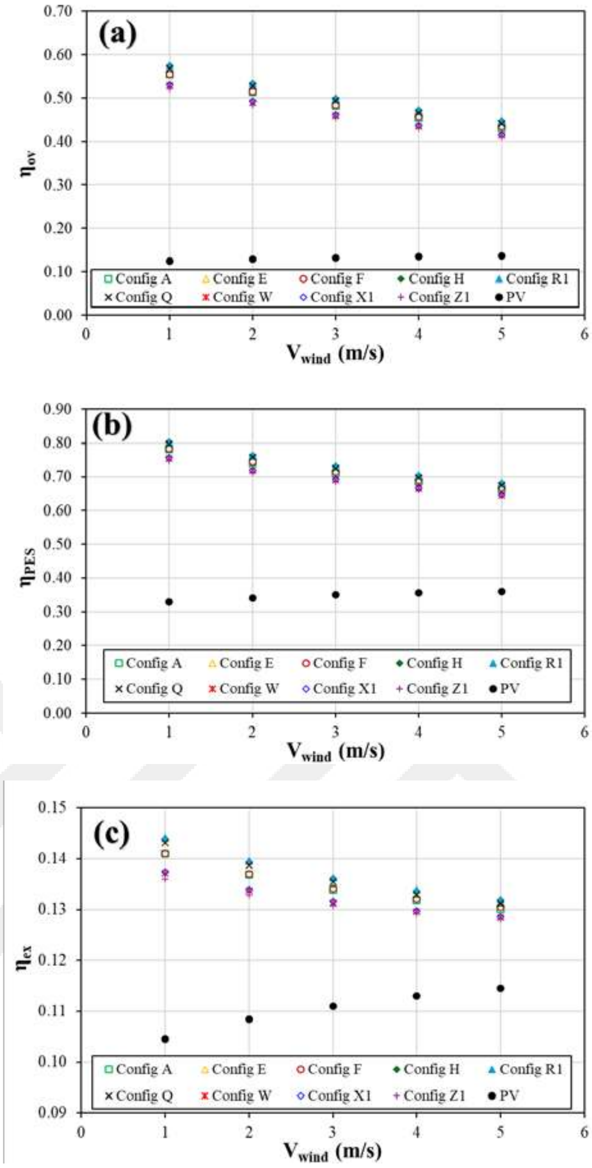

Figure 4.140. Effect of wind velocity on the overall (a), primary energy saving (b) and exergy (c) efficiency of the nine best-performing PVT collectors

As wind velocity increases, the fluid outlet temperature decreases, which leads to an increase in fluid viscosity and density. This rise in these properties results in higher internal friction and local losses, thereby causing an increase in pressure drop across all PVT collectors (Figure 4.141a). Among the designs, parallel tube configurations exhibit significantly lower pressure drops compared to serpentine and spiral tube counterparts. The highest pressure drop is observed in the single-inlet spiral configuration (Config W), followed by the single-inlet serpentine configuration (Config H). After the parallel tube collectors, the triple-inlet serpentine design (Config Q) displays the next lowest pressure drop, while double-inlet serpentine and spiral configurations show comparable results.

When evaluating the TEPD metric, a decreasing trend is observed in all PVT collectors as wind velocity increases (Figure 4.141b). This reduction is attributed to the simultaneous increase in pressure drop and the decline in thermal energy output. Owing to their minimal pressure drops, parallel tube configurations yield significantly higher TEPD values compared to serpentine and spiral tube designs. Among them, Config F demonstrates the best performance, while Config W, with the highest pressure drop, records the lowest TEPD value.

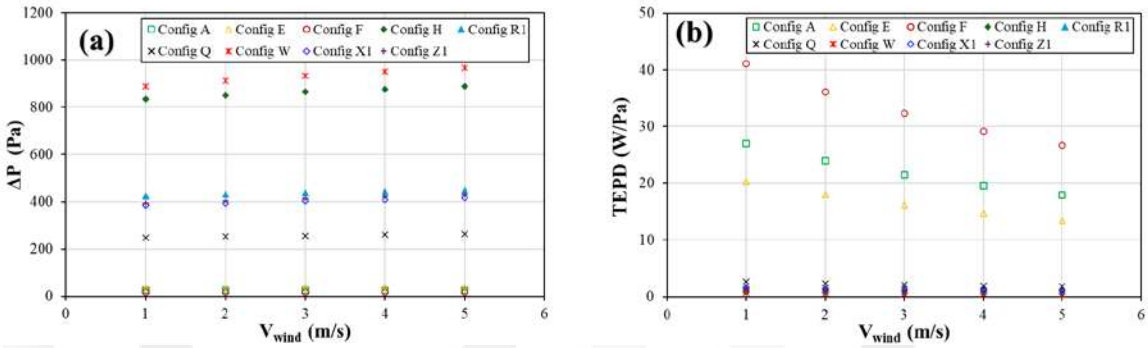

Figure 4.141. Effect of wind velocity on the pressure drop (a) and TEPD (b) of the nine best-performing PVT collectors

4.4.6. Comparison Between the Best-Performing PVT Collectors and Conventional PV Panel

This section presents a comparative analysis of the performance enhancements achieved by the nine top-performing PVT collector configurations over a conventional PV panel, focusing on cell temperature, electrical efficiency, electrical output, overall efficiency, primary energy saving efficiency, and exergy efficiency under different operating conditions. The analysis was conducted using operational parameters of 15 °C, 25 °C and 40 °C for ambient temperature; 200, 800 and 1200 W/m^2 for solar irradiance; 5, 25 and 50 L/h for fluid flow rate; 10 °C, 25 °C and 40 °C for fluid inlet temperature; and 1, 3 and 5 m/s for wind velocity.

Figure 4.142 illustrates the reduction in cell temperatures of the nine PVT collectors compared to a conventional PV panel (Figure 4.142a), along with the corresponding improvements in electrical efficiency (Figure 4.142b) under different flow rates. At low fluid flow rates, since limited heat can be extracted from the PVT surface, cell temperatures are approximately 11% lower than the conventional PV panel. However, as the flow rate increases and heat transfer improves, the cell temperatures become approximately 45-50% lower than that of the uncooled conventional PV panel. Regarding electrical efficiency, which directly depends on cell temperature, PVT collectors show about a 4% improvement over the conventional PV panel at the lowest flow rate. This difference increases with higher flow rates, reaching 15-16.5% at 50 L/h. For both performance metrics, the best performance was observed in the serpentine tube design Config R1, closely followed by Config H (serpentine) and Config E (parallel).

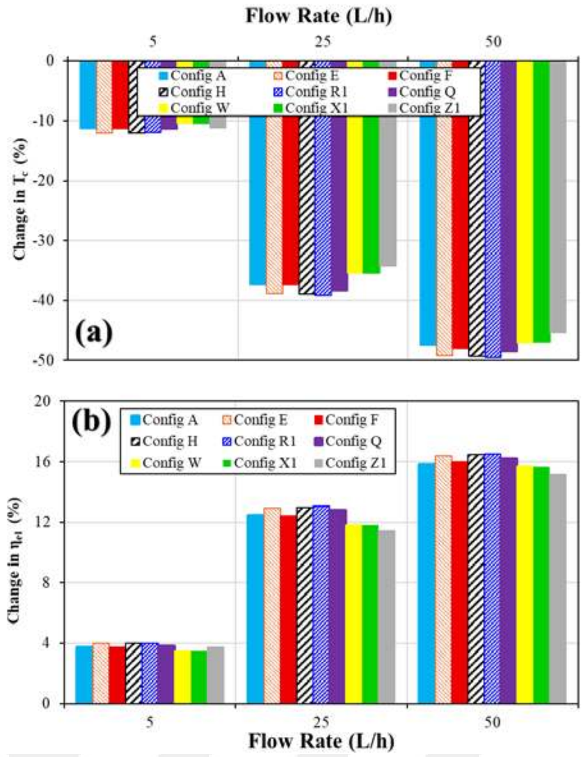

Figure 4.142. Percent change in cell temperature (a) and electrical efficiency (b) of the nine best-performing PVT collectors with respect to PV panel for different flow rates

Figure 4.143 presents the improvements in overall efficiency, primary energy saving efficiency and exergy efficiency of the nine PVT collectors compared to the uncooled conventional PV panel as a function of fluid flow rate. Given that PVT collectors generate both thermal and electrical energy, their overall efficiencies are substantially higher than that of the PV panel, which only produces electricity. At the lowest flow rate, the overall efficiency (Figure 4.143a) of the PVT collectors is between 110% and 125% higher than that of the conventional PV panel. With increasing flow rate, not only does electrical efficiency improve, but thermal efficiency also rises significantly, resulting in an overall efficiency improvement of between 465% and 504% at the highest flow rate.

A similar trend is observed for the primary energy saving efficiency. Since this metric gives greater weight to electrical efficiency compared to overall efficiency, the improvement over the PV panel ranges from 44%-50% at the lowest flow rate, increasing to 186%-201% at the maximum flow rate (Figure 4.143b). In terms of exergy efficiency, PVT collectors exhibit 13%-17% higher exergy efficiency than the PV panel at the lowest flow rate. As discussed in earlier sections, exergy efficiency increases with flow rate, reaching a peak at 25 L/h for all PVT configurations (Figure 4.143c), after which it declines. At the 25 L/h flow rate, the exergy efficiency improvement over the PV panel is between 31% and 38.5%, while at 50 L/h, this improvement is observed to be in the range of 30%-34%. Across all three efficiency metrics, configurations R1, H and E consistently deliver the best performance.

Figure 4.144 demonstrates the reduction in cell temperatures of nine different PVT collectors compared to a conventional PV panel under varying levels of solar irradiance, along with the resulting improvements in electrical efficiency. At the lowest irradiance (200 W/m^2), the PVT collectors exhibit cell temperatures approximately 11.5 % to 14.5 % lower than the conventional PV panel (Figure 4.144a). As irradiance increases, this temperature advantage expands steadily, surpassing 30 % at higher levels. Under maximum irradiance (1200 W/m^2), the largest difference is observed for the serpentine tube design, Config R1, with a 36.5 % lower temperature, followed by Config H and E. In contrast, spiral tube configurations display the smallest temperature differences, with Config Z1 performing the worst at 31.7 %.

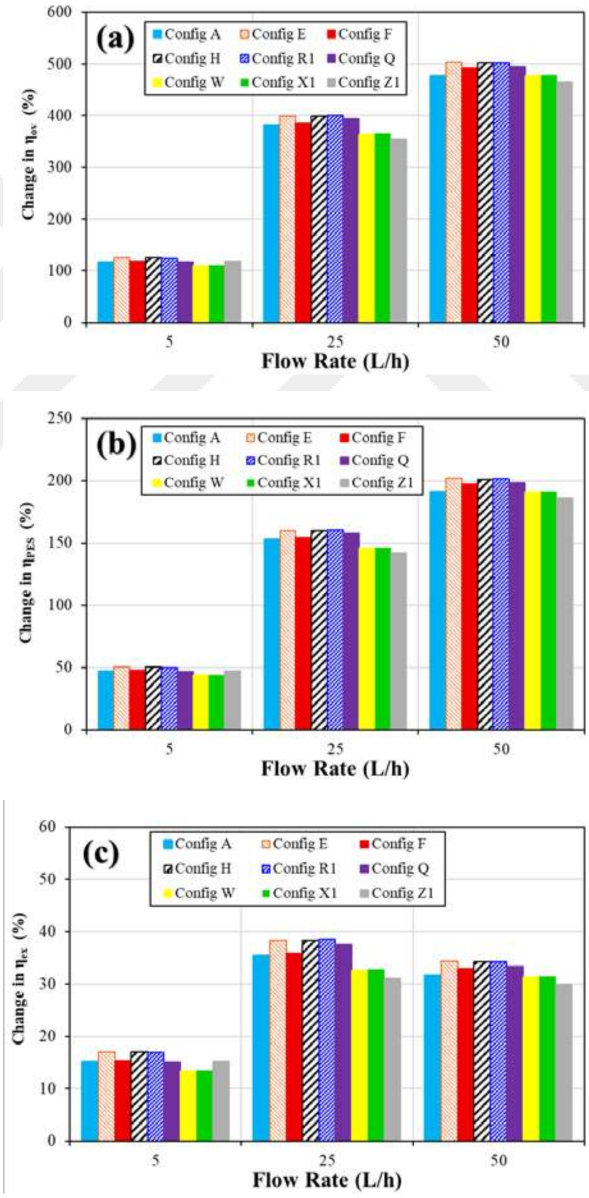

Figure 4.143. Percent change the overall (a), primary energy saving (b) and exergy (c) efficiency of the nine best-performing PVT collectors with respect to PV panel for different flow rates

Regarding electrical efficiency (Figure 4.144b), at 200 W/m^2, the PVT collectors show a modest advantage of about 1.5 % to 1.9 %, led by spiral tube configurations W and X1. As solar irradiance increases, the efficiency gap widens, reaching 12.4 % to 14.3 % at 1200 W/m^2. Notably, while spiral tube designs outperform at lower irradiance, parallel and serpentine designs deliver superior performance under high irradiance conditions. At 1200 W/m^2, the serpentine tube Config R1 achieves the highest efficiency, exceeding the conventional PV panel by 14.3 %.

Figure 4.145 compares the improvements in overall efficiency, primary energy saving efficiency and exergy efficiency of nine different PVT collectors relative to an uncooled conventional PV panel across varying levels of solar irradiance. Since PVT collectors generate both thermal and electrical energy, their overall efficiencies substantially outperform those of conventional PV panels. At the lowest irradiance level, PVT overall efficiency is 250-303% higher than that of the reference PV panel. As irradiance increases, this advantage grows further, reaching 330-376% at maximum irradiance (Figure 4.145a).

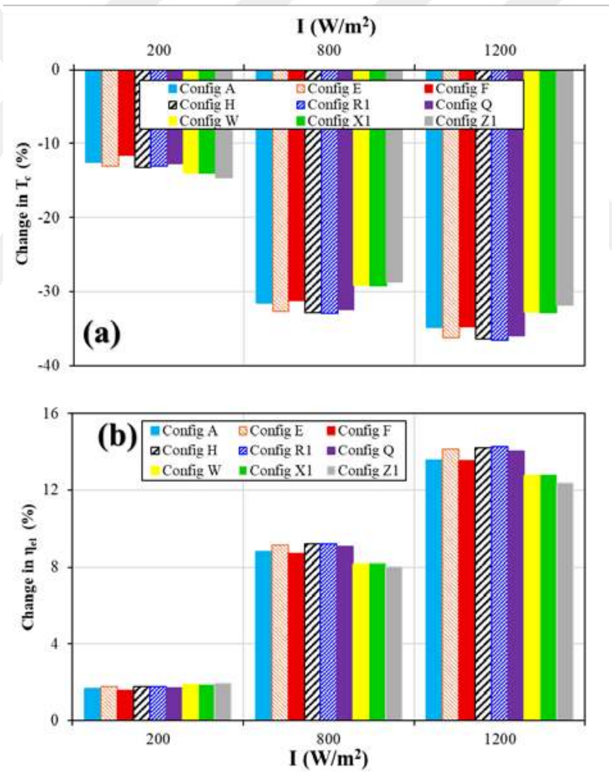

Figure 4.144. Percent change in cell temperature (a) and electrical efficiency of the nine best-performing PVT collectors with respect to PV panel for different solar irradiances

At low irradiance, the highest relative overall efficiency gains are seen in the parallel tube configuration E, followed by the serpentine configurations H and R1. However, at maximum irradiance, the order shifts: Config R1 leads, followed by Config E and Config H. Spiral tube configurations consistently lag behind. At low irradiance, Config Z1 is the best among spiral designs, but it also becomes the worst-performing spiral at maximum irradiance.

Regarding primary energy saving (PES) efficiency, the relative improvement compared to the reference PV panel is less than that observed for overall efficiency. At the lowest irradiance, PES gains range from 96% to 116%; at maximum irradiance, they increase to 133% to 152%. The best low irradiance performer is Config E, and the worst is Config W; at maximum irradiance, Config R1 shows the highest PES improvement, while Config Z1 performs the poorest (Figure 4.145b).

Exergy efficiency improvements also rise with increasing solar irradiance. At low solar irradiance, PVT systems outperform the reference PV panel by around 2%, at maximum solar irradiance, the gains range between 38% and 47%. At high solar irradiance, Config R1 leads in exergy efficiency, closely followed by Config H and Config E (Figure 4.145c).

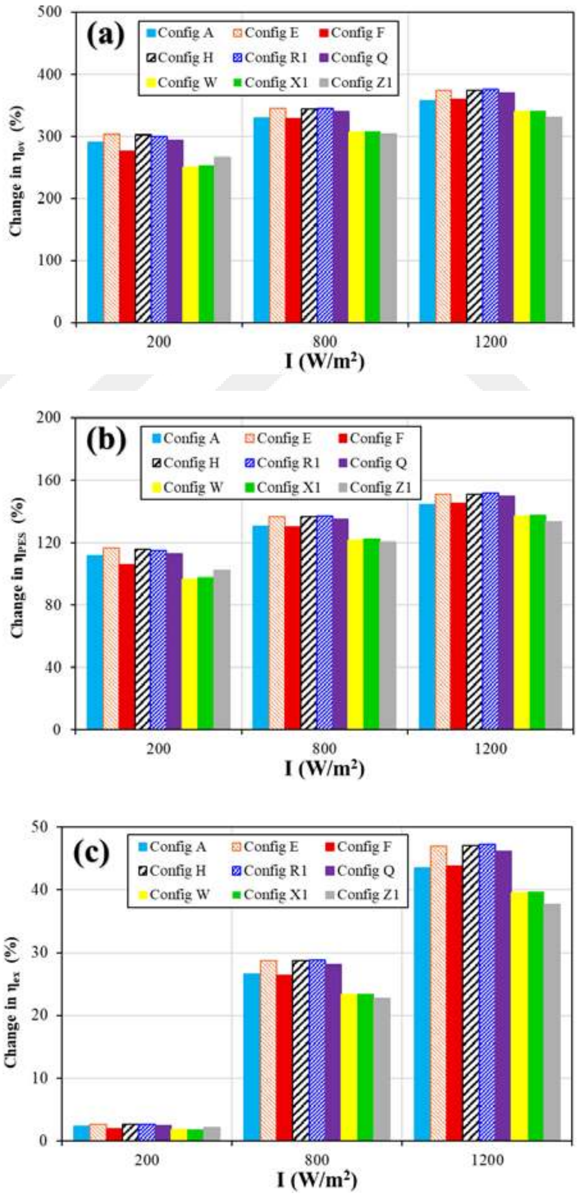

Figure 4.145. Percent change in the overall (a), primary energy saving (b) and exergy (c) efficiency of the nine best-performing PVT collectors with respect to PV panel for different solar irradiances

Figure 4.146 depicts the reduction in cell temperature and the corresponding improvement in electrical efficiency of nine different PVT collectors compared to a conventional PV panel under varying fluid inlet temperatures. When the inlet temperature is 10 °C, the cooling fluid significantly lowers the PV cell temperature, resulting in a 38% to 44% decrease compared to the conventional PV panel (Figure 4.146a). As the inlet temperature increases, the temperature difference between the PVT collectors and the conventional panel diminishes. At 40 °C inlet temperature, the cell temperatures of the PVT collectors are only 15.4% to 17.8% lower than that of the PV panel.

A similar trend is observed in electrical efficiency (Figure 4.146b). At lower fluid inlet temperatures, the PVT collectors exhibit a more pronounced improvement in electrical performance compared to the conventional PV panel, but this advantage decreases as the inlet temperature rises. At 10 °C inlet temperature, the electrical efficiency of PVT collectors is approximately 12.7% to 14.6% higher than that of the PV panel, whereas at 40 °C, this margin drops to around 5% to 6%.

Across all inlet temperatures, the serpentine tube configurations Config R1 and H, along with the parallel tube design Config E, demonstrate the best performance in terms of both cell temperature reduction and electrical efficiency. In contrast, spiral configurations generally lag behind. Among the spiral tube designs, Config Z1 exhibits the poorest performance at the lowest inlet temperature but becomes the best-performing spiral configuration when the inlet temperature reaches its maximum.

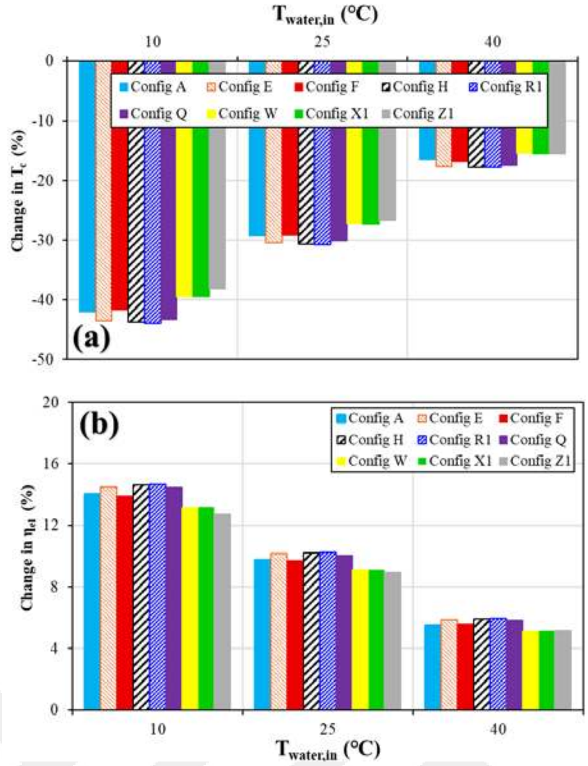

Figure 4.146. Percent change in cell temperature (a) and electrical efficiency of the nine best-performing PVT collectors with respect to PV panel for different water inlet temperatures

Figure 4.147 presents the improvements in overall efficiency, primary energy saving efficiency and exergy efficiency of nine different PVT collectors compared to an uncooled conventional PV panel under varying fluid inlet temperatures. As previously discussed, both thermal and electrical efficiencies of PVT collectors tend to decrease with increasing inlet temperature. Consequently, the overall and primary energy saving efficiencies, which depend on these two parameters, also show a decreasing trend, narrowing the performance gap between the PVT collectors and the conventional PV panel. At the lowest inlet temperature, the overall efficiency of PVT collectors is 392% to 446% higher than that of the conventional PV panel (Figure 4.147a). As the inlet temperature rises, the overall efficiency of the PVT systems decreases, yet still remains significantly higher than the PV panel ranging between 160% and 186% at the highest inlet temperature. Across all inlet temperatures, the serpentine tube configurations R1 and H consistently demonstrate the best improvements over the conventional PV panel, closely followed by the parallel tube configuration E. Spiral tube configurations, on the other hand, generally yield lower performance. Among the spiral designs, Config X1 shows the best performance at the lowest inlet temperature, whereas Config Z1 performs best at the highest inlet temperature.

When examining the primary energy saving efficiency metric, the performance improvement of PVT collectors over the conventional PV panel is generally lower than that observed in overall efficiency (Figure 4.147b). This is mainly due to the higher sensitivity of PES efficiency to electrical performance. At the lowest inlet temperature, the PES efficiency of the PVT collectors is between 157% and 179% higher than that of the conventional PV panel. However, as the inlet temperature increases, this advantage narrows, dropping to a range of 64% to 74% at the highest inlet temperature.

Similar to the trend observed in overall efficiency, the serpentine tube configurations R1 and H exhibit the most significant improvements in PES efficiency compared to the conventional PV panel, followed closely by the parallel tube configuration E. Spiral designs show performance levels closest to the conventional PV panel. Among these, Config Z1 demonstrates the lowest performance at an inlet temperature of 10 °C, but shows the best performance among spiral designs when the inlet temperature reaches its maximum.

It is observed that the exergy efficiencies of the nine different PVT collectors relative to the conventional PV panel decrease with increasing fluid inlet temperature (Figure 4.147c). At an inlet temperature of 10 °C, the exergy efficiencies of the PVT collectors are between 33% and 43% higher than that of the conventional PV panel. However, as the inlet temperature increases to 40 °C, the production of both thermal and electrical exergy declines, resulting in a narrower performance gap, with the PVT collectors performing 18% to 22% better than the conventional PV panel. Across all inlet temperatures, the configurations that show the greatest improvement in exergy efficiency compared to the PV panel are Config E (parallel), Config H (serpentine) and Config R1 (serpentine). At the lowest inlet temperature, the best-performing PVT collectors are Config R1, H and E, respectively. However, at the highest inlet temperature, the ranking slightly shifts to Config E, R1, and H, in that order. While spiral configurations consistently exhibit exergy efficiencies closest to the PV panel across all inlet temperatures, among them, Config X1 shows the best performance at the lowest inlet temperature, whereas Config Z1 delivers the best performance at the highest inlet temperature.

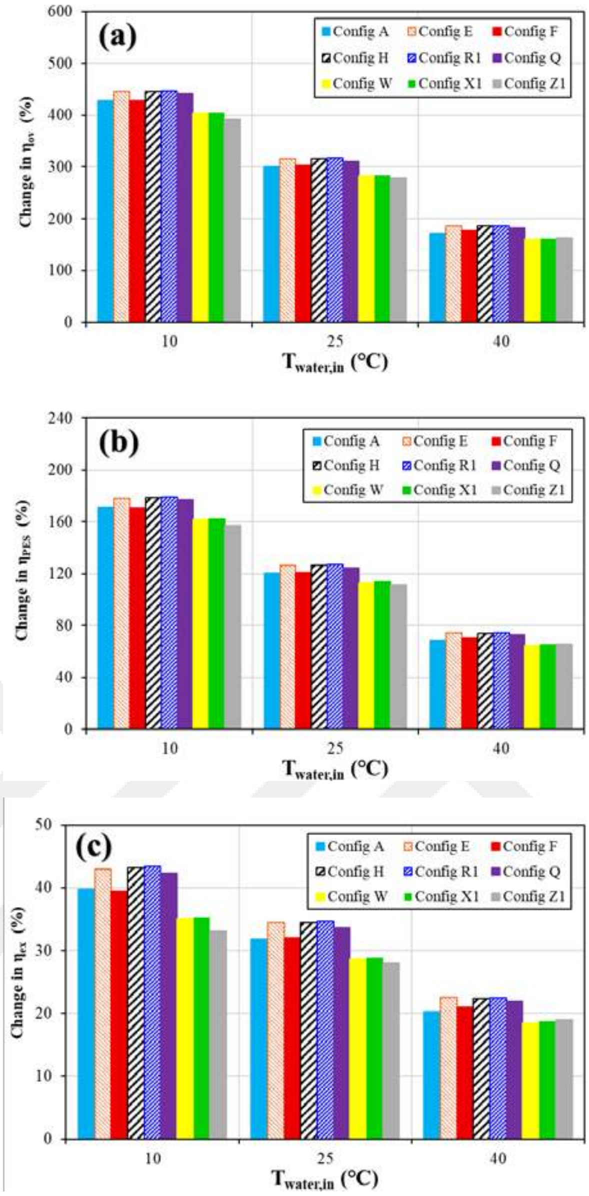

Figure 4.147. Percent change in the overall (a), primary energy saving (b) and exergy (c) efficiency of the nine best-performing PVT collectors with respect to PV panel for different water inlet temperatures

Figure 4.148 displays how varying ambient temperatures influence the cell temperature and electrical efficiency of nine different PVT collectors in comparison to a conventional PV panel. At an ambient temperature of 15 °C, the PVT collectors achieve 28% to 32% lower cell temperatures than the PV panel (Figure 4.148a). As ambient temperature rises, this gap widens, with the PVT collectors maintaining 32.5% to 37.5% lower cell temperatures at 40 °C. While increasing ambient temperature causes a decline in electrical efficiency for both systems, the drop is significantly steeper in the conventional PV panel. Consequently, the relative electrical advantage of the PVT collectors grows with temperature. At 15 °C, their electrical efficiencies are 7.6% to 8.7% higher than those of the PV panel, increasing to 14.5% to 16.7% at 40 °C (Figure 4.148b).

Among all designs, the serpentine configurations R1 and H, and the parallel tube configuration E consistently deliver superior performance in both temperature reduction and electrical efficiency enhancement. On the other hand, spiral tube configurations perform less favorably, with Config X1 standing out slightly ahead of its spiral counterparts, and Config Z1 showing the least improvement across all cases.

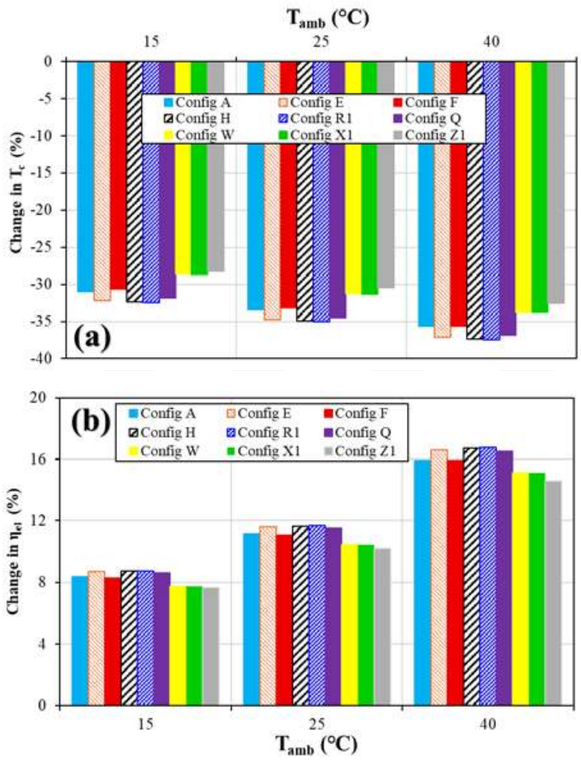

Figure 4.148. Percent change in cell temperature (a) and electrical efficiency of the nine best-performing PVT collectors with respect to PV panel for different ambient temperatures

Figure 4.149 displays the comparative performance of nine different PVT collectors relative to an uncooled conventional PV panel in terms of overall efficiency, primary energy saving efficiency and exergy efficiency across various ambient temperatures. While rising ambient temperatures lead to a decline in electrical efficiency for both systems, the thermal efficiency of the PVT collectors increases due to reduced convective heat losses. This effect causes the overall efficiency (Figure 4.149a) of PVT systems to rise, thereby widening the performance gap between PVT collectors and the PV panel. At 15 °C ambient temperature, the overall efficiency of PVT collectors exceeds that of the conventional PV panel by approximately 231% to 263%. When the ambient temperature reaches 40 °C, this margin expands dramatically, ranging from 472% to 537%. Among all configurations, Config R1 (serpentine tube design), Config E (parallel tube design), and Config H (serpentine tube) stand out as the most effective designs. While Config R1 consistently ranks highest at both low and high ambient temperatures, Config E performs better at lower temperatures, whereas Config H shows stronger results as the ambient temperature increases.

The primary energy saving (PES) efficiency of PVT collectors shows a steady upward trend with increasing ambient temperature when compared to a conventional PV panel. At the lowest ambient temperature, the PES values of the PVT collectors outperform the PV panel by approximately 92% to 105% (Figure 4.149b). As the ambient temperature rises to its maximum level, this advantage becomes more pronounced, reaching between 188% and 215%, depending on the configuration. Among all designs, the most notable differences at low ambient temperatures are observed in the serpentine tube configuration R1, followed by the parallel tube configuration E and the serpentine design H. At the highest ambient temperature, the leading configurations remain R1, H, and E, respectively. In contrast, spiral tube designs consistently exhibit PES values closest to the conventional PV panel, with Config X1 performing best among the spiral tube configurations.

The exergy efficiency of all PVT collectors relative to the conventional PV panel was found to improve as ambient temperature increased. At an ambient temperature of 15 °C, the exergy efficiency of the PVT collectors exceeded that of the PV panel by approximately 25% to 31% (Figure 4.149c). When the ambient temperature reached 40 °C, this margin widened, with exergy efficiencies surpassing the PV baseline by 36% to 48%, depending on the configuration. Across all ambient temperature levels, the most pronounced performance gaps were observed in configurations R1, H and E.

Figure 4.150 illustrates the reduction in cell temperature and the enhancement in electrical efficiency of nine PVT collectors compared to a conventional PV panel under varying wind velocities. As wind velocity increases, convective heat losses become more significant, leading to a decrease in cell temperatures for both PVT collectors and the PV panel (Figure 4.150a). Consequently, the temperature gap between the two narrows with increasing wind velocity. At a wind velocity of 1 m/s, the cell temperatures of PVT collectors are approximately 30% to 35% lower than those of the PV panel, whereas at 5 m/s, this difference decreases to around 16.6% to 19%.

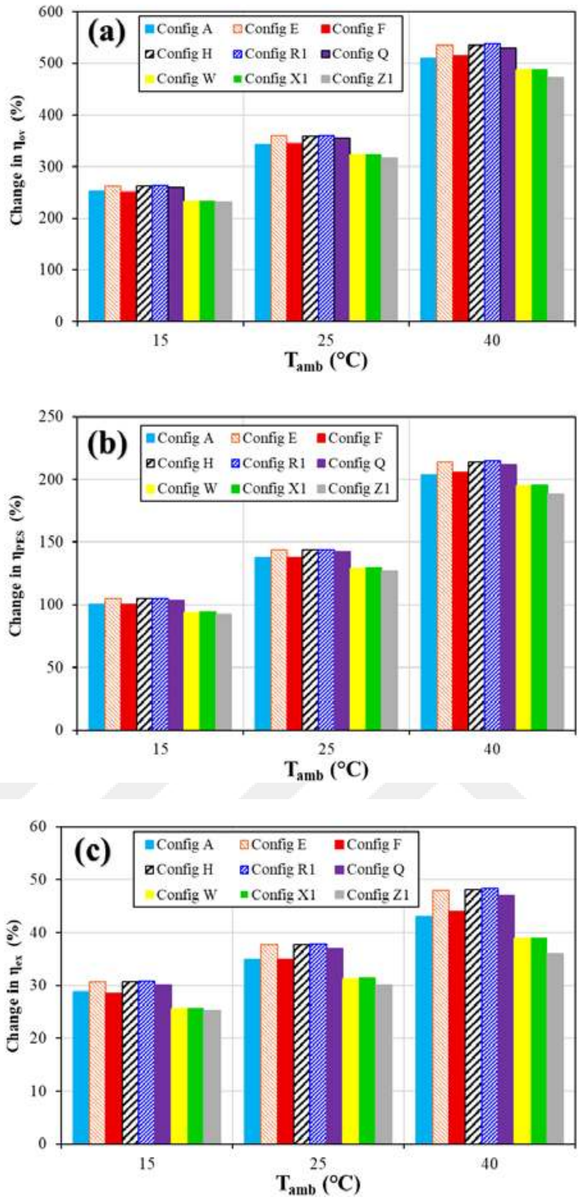

Figure 4.149. Percent change in the overall (a), primary energy saving (b) and exergy (c) efficiency of the nine best-performing PVT collectors with respect to PV panel for different ambient temperatures

When comparing the electrical efficiencies of PVT collectors with a conventional PV panel, it is evident that the performance gap narrows as wind velocity increases (Figure 4.150b). This trend is primarily due to the diminishing difference in cell temperatures between the two systems at higher wind velocities. At a wind velocity of 1 m/s, PVT collectors outperform the PV panel by approximately 10% to 12% in terms of electrical efficiency. However, this advantage decreases to about 3.6% to 4.1% at 5 m/s. Among the evaluated designs, the serpentine tube configurations R1 and H, along with the parallel tube design E, demonstrate the highest electrical efficiency gains at low wind velocites. At the maximum wind velocity, Config R1 continues to lead, followed closely by Configs E and H. In contrast, spiral tube configurations consistently show less favorable results, with Config X1 performing the best within this group and Config Z1 exhibiting the weakest performance overall.

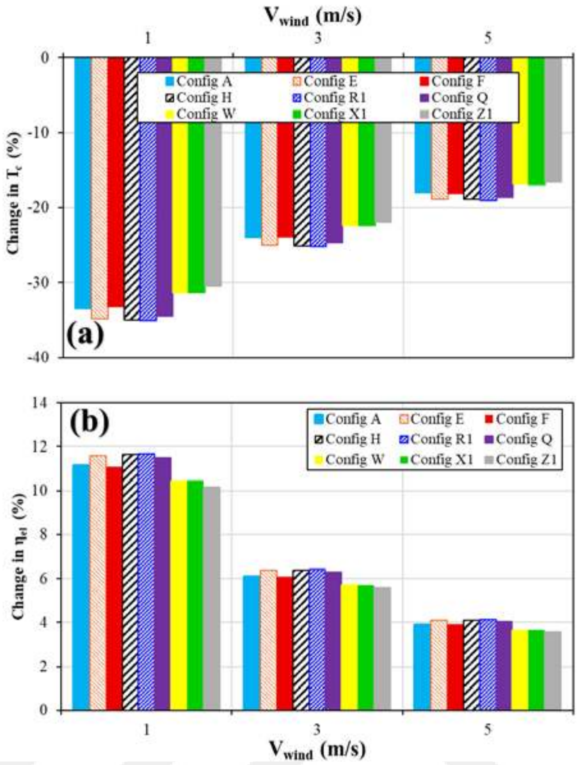

Figure 4.150. Percent change in cell temperature (a) and electrical efficiency of the nine best-performing PVT collectors with respect to PV panel for different wind velocities

Figure 4.151 compares the overall efficiency, primary energy saving efficiency and exergy efficiency of nine PVT collectors relative to a conventional PV panel under varying wind velocities. While the electrical efficiencies of both systems improve with increasing wind velocity due to reduced cell temperatures, the thermal efficiencies of the PVT collectors decline as higher wind velocities intensify convective heat losses. Consequently, the overall efficiency advantage of PVT systems over conventional PV panels diminishes at higher wind velocities (Figure 4.151a). At 1 m/s, the overall efficiency of PVT collectors exceeds that of the PV panel by 317% to 360%, but this margin narrows to 200% to 228% at 5 m/s. At low wind velocity, the best-performing designs are Config R1 and H (serpentine) and Config E (parallel). At higher wind velocities, Config E takes the lead, followed closely by Configs R1 and H.

A similar trend is observed for primary energy saving efficiency (Figure 4.151b). Although PES in PVT collectors decline with increasing wind velocity while improving in conventional PV panels, the PVT collectors still maintain a clear performance advantage. Even under the highest wind velocity, they outperform the PV panel by at least 78%. At 1 m/s, the improvement ranges from 127% to 144%, whereas at 5 m/s it drops to between 78% and 89%. Across all wind conditions, Configs E, H and R1 continue to deliver the strongest performance, following the same ranking trend seen in overall efficiency.

As wind velocity increases, the exergy efficiency of the PVT collectors shows a declining trend, whereas the conventional PV panel exhibits improved exergy performance (Figure 4.151c). At a wind velocity of 1 m/s, the PVT systems achieve 30% to 38% higher exergy efficiency compared to the PV panel. However, this advantage narrows significantly at 5 m/s, where the improvement drops to between 12% and 15%. Among the PVT collectors, the serpentine configurations R1 and H, along with the parallel design Config E, consistently stand out as the top performers. In contrast, spiral configurations lag behind the others, with Config X1 demonstrating the best performance within this group.

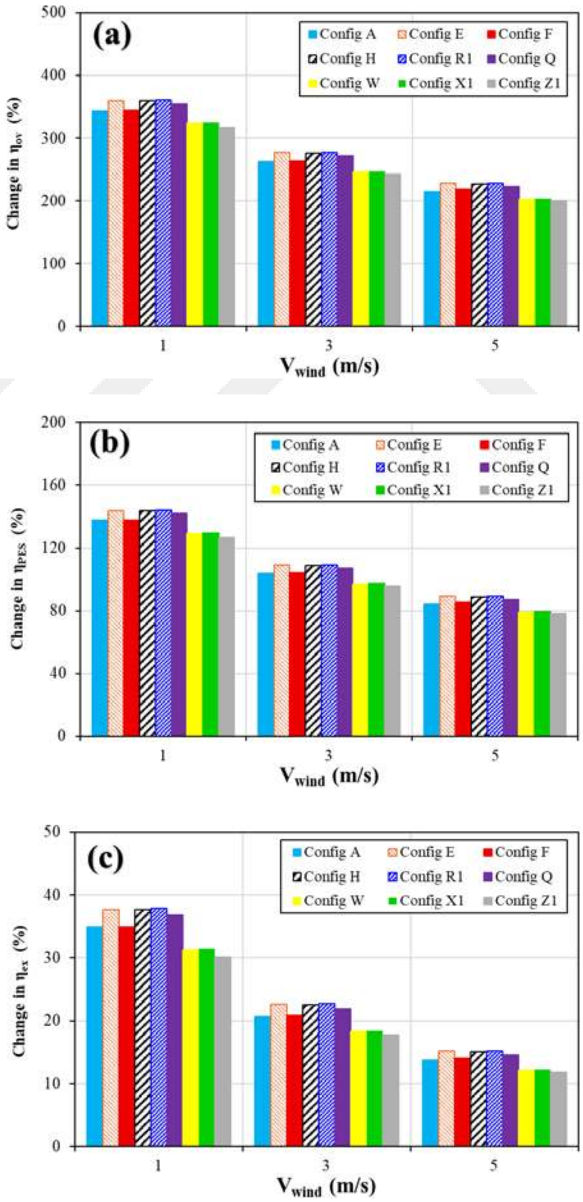

Figure 4.151. Percent change in the overall (a), primary energy saving (b) and exergy (c) efficiency of the nine best-performing PVT collectors with respect to PV panel for different wind velocities

5. CONCLUSION

In this thesis, a comprehensive investigation was conducted on a wide range of PVT collector configurations categorized into three main groups: parallel, serpentine, and spiral tube absorbers. In the first phase, six parallel tube designs (A-F) comprising ten flow configurations were examined, featuring single, double, and multi-inlet designs with both vertical and horizontal orientations. In the second phase, thirteen serpentine tube absorber designs (G-S) and twenty-five configurations were analyzed, incorporating varying inlet numbers and flow directions. The third phase focused on seven spiral tube absorbers (T-Z) with twelve distinct configurations, classified by inlet type (single/double), number of helical turns, inlet positions, and flow paths. Each configuration was analyzed using three-dimensional numerical models in the COMSOL Multiphysics software, and the simulations were carried out through the finite element method. In this context, a total of 1615 simulations were conducted, each requiring approximately two hours on a 40-core workstation.

All configurations were evaluated through both energy and exergy-based performance metrics. A broad set of parameters including temperature distribution, PVT cell and fluid outlet temperatures, thermal and electrical power output, overall and primary energy saving efficiency, pressure drop, thermal energy per unit pressure drop (TEPD), thermal and electrical exergy generation, total exergy output, exergy destruction and exergy efficiency were comprehensively assessed. This multidimensional approach enables a holistic comparison of PVT collector performance from both thermodynamic and hydraulic perspectives.

Additionally, the influence of key operating parameters, namely fluid flow rate, solar irradiance, inlet fluid temperature, ambient temperature, and wind velocity, was systematically investigated. Such an extensive parametric analysis is rarely found in existing literature. The three most efficient designs from each collector category were then compared in detail, followed by a performance benchmarking of the top nine configurations against a conventional PV panel of identical dimensions. These findings provide valuable insight into the real-world operational behavior of PVT systems and serve as a useful reference for both theoretical research and practical implementation.

- Among the parallel tube configurations under base-case operating conditions, Configurations E, F and A exhibited the best performance in terms of thermal and electrical performance metrics as well as exergetic indicators, respectively. When pressure drop and TEPD metrics are considered, Config F stands out as the most hydraulically efficient design.
- In the evaluation of parallel tube configurations under varying operational conditions, the highest thermal energy output and thermal efficiency were obtained at a flow rate of 50 L/h. Config E yielded the maximum thermal output of 949.83 W and the highest thermal

efficiency of 0.6107. Regarding electrical performance, the highest electrical power output was recorded as 255.66 W for Config E under a solar irradiance of 1200 W/m^2. The peak electrical efficiency of 0.1498 was also observed for the same configuration, but under a low irradiance level of 200 W/m^2. Furthermore, Config E exhibited the highest overall and primary energy saving efficiencies at the same flow rate of 50 L/h, with values of 0.7564 and 0.9941, respectively. In terms of TEPD value was achieved at a low flow rate of 5 L/h, where Config F reached 74.91 W/Pa.

- The highest thermal, electrical and total output exergies were observed in Config E among the parallel tube configurations under a solar irradiance of 1200 W/m^2, reaching 73.52 W, 255.66 W, and 329.18 W, respectively. On the other hand, the maximum exergy efficiency was achieved at an inlet fluid temperature of 10 °C, where Config E reached a peak value of 0.1494.
- Among the serpentine tube configurations under base-case operating conditions, configurations H, R1 and Q delivered superior performance in terms of thermal output, electrical generation and exergetic behavior. Notably, Config Q exhibited the lowest pressure drop and the highest TEPD value among this group.
- Thermal and electrical performance of serpentine tube configurations reached their highest levels under a flow rate of 50 L/h, where the system operated at peak efficiency across a wide range of parameters. At this optimal flow condition, configurations H and R1 demonstrated the greatest thermal energy yield of 945 W and a thermal efficiency of 0.6079, indicating excellent heat recovery capabilities. Electrical power output was maximized in Config R1, reaching 255.95 W at a solar irradiance of 1200 W/m^2, while the highest electrical efficiency of 0.1498 was recorded for both H and R1 under low irradiance conditions (200 W/m^2). Overall system efficiency also peaked at 0.7536 under 50 L/h flow in the same configurations. Config R1 further distinguished itself by achieving the top primary energy saving efficiency of 0.9915 under these conditions. On the other hand, Config Q stood out by providing the best pressure-performance balance, recording a TEPD value of 5.55 W/Pa at a low flow rate of 5 L/h.
- Evaluation of exergetic performance in serpentine tube configurations revealed that the highest thermal, electrical and total output exergies were achieved in Config R1 under a solar irradiance of 1200 W/m^2, with values of 73.95 W, 255.95 W and 329.90 W, respectively. Conversely, the maximum exergy efficiency was obtained at an inlet fluid temperature of 10 °C, where Config R1 reached a value of 0.1498.
- Among the spiral tube configurations under base-case operating conditions, configurations W, X1 and Z1 demonstrated superior performance with respect to energetic and exergetic performance indicators. Furthermore, Config X1 achieved the highest TEPD value among

all spiral layouts, highlighting its advantageous balance between thermal output and pressure drop.

- Across all examined operating parameters within the spiral tube configurations, the highest thermal energy output and efficiency were obtained at a flow rate of 50 L/h. Config X1 demonstrated the best thermal performance, reaching a thermal output of 900 W and thermal efficiency of 0.5787. In terms of electrical output, the highest value was again observed in Config X1, producing 252.69 W under a solar irradiance of 1200 W/m^2. As for electrical efficiency, the peak value of 0.1498 was achieved by both Config W and X1 under low irradiance conditions (200 W/m^2). The maximum values for overall efficiency and primary energy saving efficiency were also recorded at 50 L/h, with Config X1 attaining 0.7234 and 0.9595, respectively. Regarding TEPD performance, Config Z1 yielded the highest TEPD among the spiral designs, with a value of 3.65 W/Pa at a low flow rate of 5 L/h.
- When examining the exergetic performance metrics of the spiral tube configurations, Config X1 recorded the highest thermal, electrical and total output exergies under a solar irradiance of 1200 W/m^2, with values of 60.25 W, 252.69 W and 312.94 W, respectively. This was closely followed by Config W, which also demonstrated strong exergetic output. Additionally, the highest exergy efficiency was achieved by Config X1 at an inlet temperature of 10 °C, reaching a value of 0.1414, underscoring its superior second-law performance under optimal thermal conditions.
- Among all 47 configurations evaluated including parallel, serpentine and spiral tube designs, the highest thermal energy output was achieved by the parallel tube configuration Config E, reaching 949.83 W. This was closely followed by the serpentine configurations H (945.39 W) and R1 (945.28 W), both delivering nearly identical thermal outputs. In terms of thermal efficiency, Config E again led with a value of 0.6107, while Config H and R1 followed with 0.6079. Regarding electrical output under a solar irradiance of 1200 W/m^2, the maximum value of 255.95 W was observed in the serpentine configuration Config R1, with Config H (serpentine) and Config E (parallel) trailing closely behind.
- The highest overall efficiency was recorded in the parallel tube configuration E, reaching a value of 0.7564 at a flow rate of 50 L/h among all configurations. This was closely followed by the serpentine configurations H and R1, both exhibiting an overall efficiency of 0.7536. Similarly, the highest primary energy saving efficiency was achieved by Config E under the same flow conditions, with a value of 0.9941. Config R1 and Config H also showed excellent performance, attaining primary energy saving efficiencies of 0.9915 and 0.9914, respectively.
- When the exergetic performance parameters of all configurations are considered, the highest thermal exergy was observed in the serpentine tube configuration R1, reaching

73.95 W under maximum solar irradiance. This was closely followed by the parallel tube configuration E and the serpentine configuration H. In terms of electrical exergy, Config R1 again demonstrated the best performance with a peak value of 255.95 W under the same irradiance condition, with Config H following closely behind. A similar trend was observed for the total output exergy, where Config R1 reached the maximum value of 329.90 W, followed by Config H and E. Regarding exergy efficiency, the highest value was obtained at an inlet fluid temperature of 10 °C. Consistent with other exergetic indicators, Config R1 showed the best performance with an efficiency of 0.1498, followed by Config H at 0.1496 and Config E at 0.1494.

- When comparing the electrical efficiency of PVT collectors to that of a conventional PV panel, the top-performing configurations across parallel, serpentine and spiral tube designs exhibited approximately 4% higher efficiency at low flow rates. This advantage increased significantly with higher flow rates, exceeding 15% at the maximum tested flow rate. Among all designs, the serpentine tube configuration R1 demonstrated the most significant gain, followed closely by Config H and Config E.
- In terms of electrical efficiency under different solar irradiance levels, PVT collectors offer only a slight improvement, less than 2%, over conventional PV panels at low irradiance. However, this efficiency margin widens significantly as irradiance increases, reaching between 12.4% and 14.3% under maximum irradiance conditions. At 1200 W/m^2, the serpentine tube configuration R1 demonstrates the highest efficiency, surpassing the conventional PV panel by 14.3%.
- Lower fluid inlet temperatures led to a more substantial enhancement in the electrical performance of PVT collectors compared to conventional PV panels, whereas this benefit gradually diminishes as the inlet temperature increases. At 10 °C, PVT collectors demonstrate an efficiency improvement of approximately 12.7% to 14.6% over the PV panel, but this margin narrows to around 5% to 6% when the inlet temperature rises to 40 °C. Among all tested configurations, the serpentine tube design Config R1 consistently delivers the highest electrical efficiency across all inlet temperature levels.
- When the electrical efficiency of PVT collectors was evaluated relative to conventional PV panels under varying ambient temperatures, it becomes evident that the relative electrical advantage of PVT collectors becomes more prominent at higher ambient temperatures. At 15 °C, the electrical efficiency of PVT systems is approximately 7.6% to 8.7% higher than that of the PV panel, and this difference increased to 14.5% to 16.7% at maximum ambient temperature.
- In the context of wind velocity, the electrical efficiency advantage of PVT collectors over conventional PV panels diminishes as wind velocity increases. At lowest wind velocity, PVT collectors delivered approximately 10% to 12% higher electrical efficiency, whereas

this margin decreased to around 3.6% to 4.1% at maximum wind velocity due to reduced cell temperature differentials. Across both low and high wind velocities, the serpentine tube Config R1 consistently exhibited the best performance, followed closely by Config H (serpentine) and Config E (parallel).

Future Studies

According to the findings and limitations observed in this study, the following suggestions are presented for future research.

- All simulations in this study were conducted using water as the working fluid. The use of air, nano fluids or alternative heat transfer fluids (e.g., ethylene glycol mixtures) can be explored to enhance thermal performance.
- The effect of partial shading and dust accumulation on both thermal and electrical efficiency was not considered in this work. These real-world conditions can be incorporated into future modeling studies.
- Experimental prototypes based on the best-performing configurations should be developed to validate numerical results and assess manufacturability.
- An enviro-economic analysis comparing the environmental benefits and cost-effectiveness of different PVT configurations would help identify the most sustainable options.
- The incorporation of phase change materials (PCMs) into the absorber or back layer of PVT collectors can enhance thermal storage capacity and improve temperature regulation. Future studies could investigate the effects of PCM integration on thermal stabilization and energy efficiency under varying solar irradiance and ambient conditions.

REFERENCES

Abdalla, A. N., and Shahsavar, A., 2023. An experimental comparative assessment of the energy and exergy efficacy of a ternary nanofluid-based photovoltaic/thermal system equipped with a sheet-and-serpentine tube collector. Journal of Cleaner Production, 395:136460. https://doi.org/10.1016/j.jclepro.2023.136460

Abdollahi, S. A., Faramarz Ranjbar, S., and Jafari, M., 2024. Numerical investigation of increasing the efficiency of thermal photovoltaic system by changing the level of heat transfer distribution. Case Studies in Thermal Engineering, 54:103989. https://doi.org/10.1016/j.csite.2024.103989

Abdul-Ganiyu, S., Quansah, D. A., Ramde, E. W., Seidu, R., and Adaramola, M. S., 2021. Study effect of flow rate on flat-plate water-based photovoltaic-thermal (PVT) system performance by analytical technique. Journal of Cleaner Production, 321:128985. https://doi.org/10.1016/j.jclepro.2021.128985

Abo-Zahhad, E. M., Hachicha, A. A., Radwan, A., Said, Z., Rahman, S. M. A., and Haridy, S., 2024. Comprehensive Performance Evaluation of New Photovoltaic/Serpentine Collectors using Response Surface Methodology: Energy, Exergy, and Environmental Perspectives. Solar Energy, 268:112258. https://doi.org/10.1016/j.solener.2023.112258

Aghakhani, S., Afrand, M., Karimipour, A., Kalbasi, R., and Razzaghi, M. M., 2022. Numerical study of the cooling effect of a PVT on its thermal and electrical efficiency using a Cu tube of different diameters and lengths. Sustainable Energy Technologies and Assessments, 52:102044. https://doi.org/10.1016/j.seta.2022.102044

Ahmadinejad, M., and Moosavi, R., 2023. Energy and exergy evaluation of a baffled-nanofluid-based photovoltaic thermal system (PVT). International Journal of Heat and Mass Transfer, 203:123775. https://doi.org/10.1016/j.ijheatmasstransfer.2022.123775

Ahmadinejad, M., Soleimani, A., and Gerami, A., 2022. The effects of a novel baffle-based collector on the performance of a photovoltaic/thermal system using SWCNT/Water nanofluid. Thermal Science and Engineering Progress, 34:101443. https://doi.org/10.1016/j.tsep.2022.101443

Al-Shamani, A. N., Sopian, K., Mat, S., Hasan, H. A., Abed, A. M., and Ruslan, M. H., 2016. Experimental studies of rectangular tube absorber photovoltaic thermal collector with various types of nanofluids under the tropical climate conditions. Energy Conversion and Management, 124: 528-542. https://doi.org/10.1016/j.enconman.2016.07.052

Alhamayani, A., 2024. Numerical analysis and deep learning algorithm for photovoltaic-thermal systems using various nanofluids and volume fractions at Riyadh, Saudi Arabia. Case Studies in Thermal Engineering, 54:103974. https://doi.org/10.1016/j.csite.2024.103974

Alous, S., Kayfeci, M., and Uysal, A., 2019. Experimental investigations of using MWCNTs and graphene nanoplatelets water-based nanofluids as coolants in PVT systems. Applied Thermal Engineering, 162:114265. https://doi.org/10.1016/j.applthermaleng.2019.114265

Alsharifi, T., Mahdi, J. M., Togun, H., Al-Najjar, H. M. T., Khedher, N. B., Cairns, A., and Talebizadehsardari, P., 2024. Design and optimization of a household photovoltaic/thermal collector with serpentine tube: Energy and exergy analysis. Applied Thermal Engineering, 246:122983. https://doi.org/10.1016/j.applthermaleng.2024.122983

Arslan, E., Aktaş, M., and Can, Ö. F., 2020. Experimental and numerical investigation of a novel photovoltaic thermal (PV/T) collector with the energy and exergy analysis. Journal of Cleaner Production, 276:123255. https://doi.org/10.1016/j.jclepro.2020.123255

Attia, M. E. H., Zayed, M. E., Kabeel, A. E., Khelifa, A., Arıcı, M., and Abdelgaied, M., 2024. Design and performance optimization of a novel zigzag channeled solar photovoltaic thermal system: Numerical investigation and parametric analysis. Journal of Cleaner Production, 434:140220. https://doi.org/10.1016/j.jclepro.2023.140220

Badescu, V., 2008. Unified upper bound for photothermal and photovoltaic conversion efficiency. Journal of Applied Physics, 103(5). https://doi.org/10.1063/1.2890145

Badescu, V., 2015. Maximum reversible work extraction from a blackbody radiation reservoir. A way to closing the old controversy. Europhysics Letters, 109(4):40008. https://doi.org/10.1209/0295-5075/109/40008

Bayrak, F., Abu-Hamdeh, N., Alnefaie, K. A., and Öztop, H. F., 2017. A review on exergy analysis of solar electricity production. Renewable and Sustainable Energy Reviews, 74:755-770. https://doi.org/10.1016/j.rser.2017.03.012

Büyükalaca, O., Kılıç, H. M., Olmuş, U., Güzelel, Y. E., and Çerçi, K. N., 2023. Numerical investigation and ANN modeling of performance for hexagonal boron Nitride-water nanofluid PVT collectors. Thermal Science and Engineering Progress, 43:101997. https://doi.org/10.1016/j.tsep.2023.101997

Ceylan, İ., Gürel, A. E., Demircan, H., and Aksu, B., 2014. Cooling of a photovoltaic module with temperature controlled solar collector. Energy and Buildings, 72:96-101. https://doi.org/10.1016/j.enbuild.2013.12.058

Chen, J. F., Zhang, L., and Dai, Y. J., 2018. Performance analysis and multi-objective optimization of a hybrid photovoltaic/thermal collector for domestic hot water application. Energy, 143:500-516. https://doi.org/10.1016/j.energy.2017.10.143

Çerçi, K. N., Saydam, D. B., Hürdoğan, E., and Ozalp, C., 2024. Experimental investigation and artificial neural networks (ANNs) based prediction of thermal performance of solar air heaters with different surface geometry. Solar Energy, 273:112499. https://doi.org/10.1016/j.solener.2024.112499

Dehghan, M., Vajedi, H., Rahgozar, S., and Karimi, N., 2024. Energy, economic, and environmental analysis of converging air-based photovoltaic-thermal (air/PV-T) systems: A yearly benchmarking. Journal of Cleaner Production, 434:139871. https://doi.org/10.1016/j.jclepro.2023.139871

Dong, S., Long, H., Guan, J., Jiang, L., Zhuang, C., Gao, Y., and Di, Y., 2024. Performance investigation of a hybrid PV/T collector with a novel trapezoidal fluid channel. Energy, 288:129594. https://doi.org/10.1016/j.energy.2023.129594

Dubey, S., Sandhu, G. S., and Tiwari, G. N., 2009. Analytical expression for electrical efficiency of PV/T hybrid air collector. Applied Energy, 86(5):697-705. https://doi.org/10.1016/j.apenergy.2008.09.003

Eisapour, M., Eisapour, A. H., Hosseini, M. J., and Talebizadehsardari, P., 2020. Exergy and energy analysis of wavy tubes photovoltaic-thermal systems using microencapsulated PCM nano-slurry coolant fluid. Applied Energy, 266:114849. https://doi.org/10.1016/j.apenergy.2020.114849

Evola, G., and Marletta, L., 2014. Exergy and thermoeconomic optimization of a water-cooled glazed hybrid photovoltaic/thermal (PVT) collector. Solar Energy, 107:12-25. https://doi.org/10.1016/j.solener.2014.05.041

Fayaz, H., Nasrin, R., Rahim, N. A., and Hasanuzzaman, M., 2018. Energy and exergy analysis of the PVT system: Effect of nanofluid flow rate. Solar Energy, 169:217-230. https://doi.org/10.1016/j.solener.2018.05.004

Fayaz, H., Rahim, N. A., Hasanuzzaman, M., Rivai, A., and Nasrin, R., 2019. Numerical and outdoor real time experimental investigation of performance of PCM based PVT system. Solar Energy, 179:135-150. https://doi.org/10.1016/j.solener.2018.12.057

Hamada, A., Emam, M., Refaey, H. A., Moawed, M., Abdelrahman, M. A., and Elsayed, M. E. A., 2024. Identification of a different design of a photovoltaic thermal collector based on fuzzy logic control and the ARMAX model. Thermal Science and Engineering Progress, 48:102395. https://doi.org/10.1016/j.tsep.2024.102395

Herrando, M., Ramos, A., Zabalza, I., and Markides, C. N., 2019. A comprehensive assessment of alternative absorber-exchanger designs for hybrid PVT-water collectors. Applied Energy, 235:1583-1602. https://doi.org/10.1016/j.apenergy.2018.11.024

Herrando, M., Wang, K., Huang, G., Otanicar, T., Mousa, O. B., Agathokleous, R. A., Ding, Y., Kalogirou, S., Ekins-Daukes, N., Taylor, R. A., and Markides, C. N., 2023. A review of solar hybrid photovoltaic-thermal (PV-T) collectors and systems. Progress in Energy and Combustion Science, 97:101072. https://doi.org/10.1016/j.pecs.2023.101072

Hosseinzadeh, M., Salari, A., Sardarabadi, M., and Passandideh-Fard, M., 2018. Optimization and parametric analysis of a nanofluid based photovoltaic thermal system: 3D numerical model with experimental validation. Energy Conversion and Management, 160:93-108. https://doi.org/10.1016/j.enconman.2018.01.006

IEA (International Energy Agency), 2024a. World Energy Outlook 2024. IEA Publications, Paris, France. https://www.iea.org/reports/world-energy-outlook-2024 [Son erişim tarihi: 09.10.2025]

IEA (International Energy Agency), 2024b. Renewables 2024: Analysis and Forecast to 2030. IEA Publications, Paris, France. https://www.iea.org/reports/renewables-2024 [Son erişim tarihi: 09.10.2025]

Kalogirou, S. A., 2001. Use of TRNSYS for modelling and simulation of a hybrid pv–thermal solar system for Cyprus. Renewable Energy, 23(2): 247-260. https://doi.org/10.1016/S0960-1481(00)00176-2

Kazem, H. A., Al-Waeli, A. H. A., Chaichan, M. T., Al-Waeli, K. H., Al-Aasam, A. B., and Sopian, K., 2020. Evaluation and comparison of different flow configurations PVT systems in Oman: A numerical and experimental investigation. Solar Energy, 208:58-88. https://doi.org/10.1016/j.solener.2020.07.078

Kazem, H. A., Chaichan, M. T., Al-Waeli, A. H. A., and Sopian, K., 2021. Comparison and evaluation of solar photovoltaic thermal system with hybrid collector: An experimental study. Thermal Science and Engineering Progress, 22:100845. https://doi.org/10.1016/j.tsep.2021.100845

Kazemian, A., Parcheforosh, A., Salari, A., and Ma, T., 2021. Optimization of a novel photovoltaic thermal module in series with a solar collector using Taguchi based grey relational analysis. Solar Energy, 215: 492-507. https://doi.org/10.1016/j.solener.2021.01.006

Kazemian, A., Ma, T., and Hongxing, Y., 2024. Evaluation of various collector configurations for a photovoltaic thermal system to achieve high performance, low cost, and lightweight. Applied Energy, 357:122422. https://doi.org/10.1016/j.apenergy.2023.122422

Khan, S. Y., Waqas, A., Kumar, M., Liu, S., Shen, Y., Chen, T., Shoaib, M., and Khan, M. O., 2024. Experimental, numerical, and 4E assessment of photovoltaic module using macro-encapsulation of pure and nano phase change material: A comparative analysis. Energy, 290:130162. https://doi.org/10.1016/j.energy.2023.130162

Khanjari, Y., Pourfayaz, F., and Kasaeian, A. B., 2016. Numerical investigation on using of nanofluid in a water-cooled photovoltaic thermal system. Energy Conversion and Management, 122:263-278. https://doi.org/10.1016/j.enconman.2016.05.083

Landsberg, P., and Mallinson, J., 1976. Thermodynamic constraints, effective temperatures and solar cells. International Conference on Solar Electricity, Toulouse, France.

Maadi, S. R., Sabzali, H., Kolahan, A., and Wood, D., 2020. Improving the performance of PV/T systems by using conical-leaf inserts in the coolant tubes. Solar Energy, 212:84-100. https://doi.org/10.1016/j.solener.2020.10.011

Maseer, M. M., Ismail, F. B., Kazem, H. A., Wai, L. C., and Al-Gburi, K. A. H., 2024. Optimal evaluation of photovoltaic-thermal solar collectors cooling using a half-tube of different diameters and lengths. Solar Energy, 267:112193. https://doi.org/10.1016/j.solener.2023.112193

McAdams, W., 1954. Heat Transmission. McGraw-Hill, New York, 532p.

Michael, J. J., Selvarasan, I., and Goic, R., 2016. Fabrication, experimental study and testing of a novel photovoltaic module for photovoltaic thermal applications. Renewable Energy, 90:95-104. https://doi.org/10.1016/j.renene.2015.12.064

Mosa, M., Labat, M., and Lorente, S., 2019. Role of flow architectures on the design of radiant cooling panels, a constructal approach. Applied Thermal Engineering, 150:1345-1352. https://doi.org/10.1016/j.applthermaleng.2018.12.107

Nahar, A., Hasanuzzaman, M., and Rahim, N. A. (2017). Numerical and experimental investigation on the performance of a photovoltaic thermal collector with parallel plate flow channel under different operating conditions in Malaysia. Solar Energy, 144:517-528. https://doi.org/10.1016/j.solener.2017.01.041

Nahar, A., Hasanuzzaman, M., Rahim, N. A., and Parvin, S., 2019. Numerical investigation on the effect of different parameters in enhancing heat transfer performance of photovoltaic thermal systems. Renewable Energy, 132: 284-295. https://doi.org/10.1016/j.renene.2018.08.008

Nasrin, R., Hasanuzzaman, M., and Rahim, N. A., 2018a. Effect of high irradiation and cooling on power, energy and performance of a PVT system. Renewable Energy, 116:552-569. https://doi.org/10.1016/j.renene.2017.10.004

Nasrin, R., Rahim, N. A., Fayaz, H., and Hasanuzzaman, M. 2018b. Water/MWCNT nanofluid based cooling system of PVT: Experimental and numerical research. Renewable Energy, 121:286-300. https://doi.org/10.1016/j.renene.2018.01.014

Olmuş, U., Güzelel, Y. E., Pınar, E., Özbek, A., and Büyükalaca, O., 2022. Performance assessment of a desiccant air-conditioning system combined with dew-point indirect evaporative cooler and PV/T. Solar Energy, 231:566-577. https://doi.org/10.1016/j.solener.2021.12.004

Olmuş, U., Güzelel, Y. E., and Büyükalaca, O., 2023. Seasonal analysis of a desiccant air-conditioning system supported by water-cooled PV/T units. Energy and Buildings, 291:113111. https://doi.org/10.1016/j.enbuild.2023.113101

Olmuş, U., Güzelel, Y. E., and Büyükalaca, O., 2025a. Comparative numerical investigation of different PVT collector configurations: Energy and exergy analysis. Energy, 316:134500. https://doi.org/10.1016/j.energy.2025.134500

Olmuş, U., Güzelel, Y. E., Çerçi, K. N., and Büyükalaca, O., 2025b. Numerical analysis and comparison of different serpentine-based photovoltaic-thermal collectors. Renewable Energy, 241:122196. https://doi.org/10.1016/j.renene.2024.122196

Park, S. S., Kim, Y.-J., Kang, E.-C., Lee, E.-J., and Entchev, E., 2022. Numerical investigations of a solar energy heat transfer performances with experimental validations in a water-based serpentine photovoltaic-thermal (PVT) collector. Journal of Thermal Analysis and Calorimetry, 148(5):2149-2169. https://doi.org/10.1007/s10973-022-11861-z

Parthiban, A., Reddy, K. S., Pesala, B., and Mallick, T. K., 2020. Effects of operational and environmental parameters on the performance of a solar photovoltaic-thermal collector. Energy Conversion and Management, 205:112428. https://doi.org/10.1016/j.enconman.2019.112428

Petela, R., 1964. Exergy of heat radiation. Journal of Heat Transfer, 86(2):187-192. https://doi.org/10.1115/1.3687092

Poredoš, P., Tomc, U., Petelin, N., Vidrih, B., Flisar, U., and Kitanovski, A., 2020. Numerical and experimental investigation of the energy and exergy performance of solar thermal, photovoltaic and photovoltaic-thermal modules based on roll-bond heat exchangers. Energy Conversion and Management, 210:112674. https://doi.org/10.1016/j.enconman.2020.112674

Prakash, K. B., Chinnasamy, S., Manimuthu, C., and Manoj Kumar, P., 2024. Assimilation of a novel thermal collector and phase change material in photovoltaic/thermal system - An energy and exergy based comparative study. Journal of Energy Storage, 81:110461. https://doi.org/10.1016/j.est.2024.110461

Preet, S., Bhushan, B., and Mahajan, T., 2017. Experimental investigation of water based photovoltaic/thermal (PV/T) system with and without phase change material (PCM). Solar Energy, 155:1104-1120. https://doi.org/10.1016/j.solener.2017.07.040

Press, W. H., 1976. Theoretical maximum for energy from direct and diffuse sunlight. Nature, 264:734-735. https://doi.org/10.1038/264734a0

Rahman, M. M., Hasanuzzaman, M., and Rahim, N. A., 2015. Effects of various parameters on PV-module power and efficiency. Energy Conversion and Management, 103:348-358. https://doi.org/10.1016/j.enconman.2015.06.067

Rajamony, R. K., Pandey, A. K., Samykano, M., Siaw Paw, J. K., Kareri, T., Laghari, I. A., and Tyagi, V. V., 2024. Heat transfer and energy performance analysis of photovoltaic thermal system using functionalized carbon nanotubes enhanced phase change material. Applied Thermal Engineering, 243:122544. https://doi.org/10.1016/j.applthermaleng.2024.122544

Rubbi, F., Habib, K., Saidur, R., Aslfattahi, N., Yahya, S. M., and Das, L., 2020. Performance optimization of a hybrid PV/T solar system using Soybean oil/MXene nanofluids as A new class of heat transfer fluids. Solar Energy, 208:124-138. https://doi.org/10.1016/j.solener.2020.07.060

Sardarabadi, M., and Passandideh-Fard, M., 2016. Experimental and numerical study of metal-oxides/water nanofluids as coolant in photovoltaic thermal systems (PVT). Solar Energy Materials and Solar Cells, 157:533-542. https://doi.org/10.1016/j.solmat.2016.07.008

Shen, C., Zhang, Y., Zhang, C., Pu, J., Wei, S., and Dong, Y., 2021a. A numerical investigation on optimization of PV/T systems with the field synergy theory. Applied Thermal Engineering, 185:116381. https://doi.org/10.1016/j.applthermaleng.2020.116381

Shen, C., Liu, F., Qiu, S., Liu, X., Yao, F., and Zhang, Y., 2021b. Numerical study on the thermal performance of photovoltaic thermal (PV/T) collector with different parallel cooling channels. Sustainable Energy Technologies and Assessments, 45:101101. https://doi.org/10.1016/j.seta.2021.101101

Sheshpoli, A. Z., Jahanian, O., Nikzadfar, K., and Delavar, M. A, 2021. Numerical and experimental investigation on the performance of hybrid PV/thermal systems in the north of Iran. Solar Energy, 215:108-120. https://doi.org/10.1016/j.solener.2020.12.036

Shi, Q., Lv, J., Guo, C., and Zheng, B., 2017. Experimental and simulation analysis of a PV/T system under the pattern of natural circulation. Applied Thermal Engineering, 121:828-837. https://doi.org/10.1016/j.applthermaleng.2017.04.140

Shyam, Tiwari, G. N., and Al-Helal, I. M., 2015. Analytical expression of temperature dependent electrical efficiency of N-PVT water collectors connected in series. Solar Energy, 114:61-76. https://doi.org/10.1016/j.solener.2015.01.026

Si, Y., Brumercik, F., Yang, C., Glowacz, A., Ma, Z., Siarry, P., Sulowicz, M., Gupta, M. K., and Li, Z., 2023. Prediction and evaluation of energy and exergy efficiencies of a nanofluid-based photovoltaic-thermal system with a needle finned serpentine channel using random forest machine learning approach. Engineering Analysis with Boundary Elements, 151:328-343. https://doi.org/10.1016/j.enganabound.2023.03.009

Song, Z., Ji, J., Zhang, Y., Li, Y., Li, J., and Zhao, X., 2023. Annual analysis of the photovoltaic direct-expansion heat pump assisted by double condensing equipment for secondary power generation. Renewable Energy, 209: 169-183. https://doi.org/10.1016/j.renene.2023.03.059

Sreekumar, S., Shah, N., Mondol, J. D., Hewitt, N., and Chakrabarti, S., 2022. Numerical investigation and feasibility study on MXene/water nanofluid based photovoltaic/thermal system. Cleaner Energy Systems, 2:100010. https://doi.org/10.1016/j.cles.2022.100010

Swinbank, W. C., 1963. Long-wave radiation from clear skies. Quarterly Journal of the Royal Meteorological Society, 89:339-348. https://doi.org/10.1002/qj.49708938105

Teymori-omran, M., Motevali, A., Reza Mousavi Seyedi, S., and Montazeri, M., 2021. Numerical simulation and experimental validation of a photovoltaic/thermal system: Performance comparison inside and outside greenhouse. Sustainable Energy Technologies and Assessments, 46:101271. https://doi.org/10.1016/j.seta.2021.101271

Tian, M.W., Khetib, Y., Yan, S.R., Rawa, M., Sharifpur, M., Cheraghian, G., and Melaibari, A. A., 2021. Energy, exergy and economics study of a solar/thermal panel cooled by nanofluid. Case Studies in Thermal Engineering, 28:101481. https://doi.org/10.1016/j.csite.2021.101481

Tripanagnostopoulos, Y., Nousia, T., Souliotis, M., and Yianoulis, P., 2002. Hybrid photovoltaic/thermal solar systems. Solar Energy, 72(3):217-234. https://doi.org/10.1016/S0038-092X(01)00096-2

Tyagi, P. K., and Kumar, R., 2024. Thermodynamic modeling and performance optimization of nanofluid-based photovoltaic/thermal system using central composite design scheme of response surface methodology. Renewable Energy, 225:120341. https://doi.org/10.1016/j.renene.2024.120341

Yan, B., Wu, Q., Chi, X., Wu, C., Luo, P., Luo, Y., and Zeng, P., 2022. Numerical and Experimental Investigation of Photovoltaic/Thermal Systems: Parameter Analysis and Determination of Optimum Flow. Sustainability, 14(16):10156. https://doi.org/10.3390/su141610156

Yu, Q., Romagnoli, A., Yang, R., Xie, D., Liu, C., Ding, Y., and Li, Y., 2019. Numerical study on energy and exergy performances of a microencapsulated phase change material slurry based photovoltaic/thermal module. Energy Conversion and Management, 183:708-720. https://doi.org/10.1016/j.enconman.2019.01.029

Zhou, J., Ke, H., and Deng, X., 2018. Experimental and CFD investigation on temperature distribution of a serpentine tube type photovoltaic/thermal collector. Solar Energy, 174:735-742. https://doi.org/10.1016/j.solener.2018.09.063

Zou, W., Yu, G., and Du, X., 2024. Energy and exergy analysis of photovoltaic thermal collectors: Comprehensive investigation of operating parameters in different dynamic models. Renewable Energy, 221:119710. https://doi.org/10.1016/j.renene.2023.119710

CURRICULUM VITAE

Umutcan OLMUŞ graduated from Çukurova University, Mechanical Engineering Department in July 2015. In September 2016, he started his Master of Science education at the same university and graduated in 2019. In the same year, he began his Doctor of Philosophy education within the Mechanical Engineering Main Science Brance at Çukurova University. He has been working as a Research Assistant at Çukurova University, Department of Mechanical Engineering since 2018.